

Dissertation zur Erlangung des Doktorgrades  
der Fakultät für Chemie und Pharmazie  
der Ludwig-Maximilians-Universität München

**Synthesis, Characterization  
and Quantum-Chemical Analysis  
of  $\{\text{FeNO}\}^7$  and  $\{\text{Fe}(\text{NO})_2\}^9$  Compounds**

Markus Wolf

aus

Radolfzell am Bodensee, Deutschland

2016

### Erklärung

Diese Dissertation wurde im Sinne von § 7 der Promotionsordnung vom 28. November 2011 von Herrn Prof. Dr. Peter Klüfers betreut.

### Eidesstattliche Versicherung

Diese Dissertation wurde eigenständig und ohne unerlaubte Hilfe erarbeitet.

München, 29. April 2016

Markus Wolf

Dissertation eingereicht am 29. April 2016

1. Gutachter: Prof. Dr. Peter Klüfers
2. Gutachter: Prof. Dr. Hans-Christian Böttcher

Mündliche Prüfung am 10. Juni 2016

# Contents

<b>List of Figures</b>	<b>v</b>
<b>List of Tables</b>	<b>vii</b>
<b>Abbreviations</b>	<b>ix</b>
<b>Overview of numbered compounds</b>	<b>xi</b>
Iminodiacetate derivatives used as chelating ligands . . . . .	xi
Quartet- $\{\text{FeNO}\}^7$ compounds with aminocarboxylato ligands . . . . .	xii
Iron(II) aminocarboxylates . . . . .	xiii
Halogenidonitrosylferrates . . . . .	xiv
<b>1 Introduction</b>	<b>1</b>
1.1 Physical and chemical properties of nitric oxide . . . . .	1
1.2 Relevance of nitrosyl-iron compounds . . . . .	2
1.3 Photoinduced linkage isomerism . . . . .	3
1.4 Aim of this work . . . . .	4
<b>2 Results</b>	<b>5</b>
2.1 Synthesis of new iminodiacetic acid derivatives . . . . .	5
2.1.1 Disodium <i>N</i> -phenyliminodiacetate ( $\text{Na}_2\text{phida}$ ) . . . . .	5
2.1.2 <i>N</i> -( <i>p</i> -Bromobenzyl)iminodiacetic acid ( $\text{H}_2\text{brbnida}$ ) and <i>N</i> -phenylethyliminodiacetic acid ( $\text{H}_2\text{pheida}$ ) . . . . .	6
2.1.3 Dipotassium <i>N</i> -(1,3-dihydroxypropane-2-yl)iminodiacetate ( $\text{K}_2\text{dhpida}$ ) and tripotassium <i>N</i> -[4-(carboxymethoxy)phenyl]iminodiacetate ( $\text{K}_3\text{cpida}$ ) . . . . .	6
2.2 Quartet- $\{\text{FeNO}\}^7$ compounds with aminocarboxylato ligands . . . . .	6
2.2.1 $[\text{Fe}(\text{ida})(\text{NO})(\text{OH}_2)_2]$ . . . . .	8
2.2.2 $[\text{Fe}(\text{heida})(\text{NO})(\text{OH}_2)]$ . . . . .	10
2.2.3 $[\text{Fe}(\text{dhpida})(\text{NO})]$ . . . . .	12
2.2.4 $[\text{Fe}(\text{NO})(\text{OH}_2)_2(\text{oda})]$ . . . . .	14
2.2.5 $[\text{Fe}(\text{NO})(\text{OH}_2)_2(\text{phida})] \cdot \text{H}_2\text{O}$ . . . . .	16
2.2.6 $[\text{Fe}(\text{bnida})(\text{NO})(\text{OH}_2)_2]$ . . . . .	18
2.2.7 $[\text{Fe}(\text{brbnida})(\text{NO})(\text{OH}_2)_2]$ . . . . .	20

---

2.2.8	[Fe(NO)(OH <sub>2</sub> ) <sub>2</sub> (pheidate)] . . . . .	22
2.2.9	[Fe(dipic)(NO)(OH <sub>2</sub> ) <sub>2</sub> ] . . . . .	23
2.3	Iron(II) aminocarboxylates . . . . .	25
2.3.1	[Fe(dhpida)(OH <sub>2</sub> ) <sub>2</sub> ] · 2 H <sub>2</sub> O . . . . .	25
2.3.2	[Fe(dipic)(OH <sub>2</sub> ) <sub>3</sub> ] · 2 H <sub>2</sub> O . . . . .	27
2.3.3	[Fe(ca)(OH <sub>2</sub> ) <sub>3</sub> ] · 0.5 H <sub>2</sub> O . . . . .	29
2.3.4	[Fe <sub>3</sub> (cpida) <sub>2</sub> (OH <sub>2</sub> ) <sub>8</sub> ] · 2 H <sub>2</sub> O . . . . .	31
2.4	Halogenidonitrosylferrates . . . . .	33
2.4.1	{PPN}[FeCl <sub>3</sub> (NO)] . . . . .	34
2.4.2	{PPN}[FeBr <sub>3</sub> (NO)] . . . . .	35
2.4.3	{{PPN}[FeI <sub>2</sub> (NO) <sub>2</sub> ]}{{PPN}[I <sub>3</sub> ]} . . . . .	36
2.4.4	{PPN}[Fe(N <sub>3</sub> ) <sub>2</sub> (NO) <sub>2</sub> ] . . . . .	37
2.4.5	{PPN}[FeCl <sub>2</sub> (NO) <sub>2</sub> ] . . . . .	37
2.5	IR spectroscopy . . . . .	38
2.6	UV-VIS spectroscopy . . . . .	40
2.7	SQUID magnetometry . . . . .	42
2.8	Quantum-chemical calculations . . . . .	43
2.8.1	Structural optimizations of complexes with aminocarboxylato ligands . . . . .	43
2.8.2	Structural optimizations of halogenidonitrosylferrates . . . . .	48
2.8.3	Electronic description of the Fe–N–O moiety . . . . .	48
2.8.4	CASSCF calculations . . . . .	54
2.8.5	TDDFT calculations . . . . .	60
2.9	The Fe–N–O bond angle . . . . .	60
2.10	Iron mono- and dinitrosyls and their corresponding nitrosyl-free compounds . . . . .	63
2.11	PLI measurements . . . . .	64
2.11.1	PLI of quartet-{FeNO} <sup>7</sup> compounds with aminocarboxylato ligands . . . . .	66
2.11.2	PLI experiment on {PPN}[FeCl <sub>3</sub> (NO)] . . . . .	66
<b>3</b>	<b>Discussion</b> . . . . .	<b>71</b>
3.1	Quartet-{FeNO} <sup>7</sup> compounds with aminocarboxylato ligands . . . . .	71
3.2	Halogenidonitrosylferrates . . . . .	72
3.3	Structural correlations . . . . .	74
3.4	The oxidation state of Fe and NO . . . . .	75
3.4.1	Spectroscopic evidence . . . . .	76
3.4.2	Quantum-chemical evidence . . . . .	77
3.5	PLI measurements . . . . .	79
3.6	UV-VIS spectra and TDDFT . . . . .	80
3.7	The brown ring . . . . .	81

---

---

<b>4</b>	<b>Summary</b>	<b>83</b>
<b>5</b>	<b>Experimental Part</b>	<b>87</b>
5.1	Common working techniques . . . . .	87
5.2	Analytical methods . . . . .	87
5.2.1	NMR spectroscopy . . . . .	87
5.2.2	IR spectroscopy . . . . .	88
5.2.3	Mass spectrometry . . . . .	88
5.2.4	Elemental analysis . . . . .	88
5.2.5	UV-VIS spectroscopy . . . . .	88
5.2.6	X-Ray diffraction . . . . .	88
5.2.7	Magnetic Susceptibilities . . . . .	89
5.3	Reagents and solvents . . . . .	90
5.4	Synthesis of ligands and PPN salts . . . . .	92
5.4.1	Dipotassium <i>N</i> -(1,3-dihydroxypropane-2-yl)iminodiacetate ( <b>K<sub>2</sub>2c</b> ) . . . . .	92
5.4.2	<i>N</i> -Phenyldiethyliminodiacetate . . . . .	93
5.4.3	Disodium <i>N</i> -phenyliminodiacetate ( <b>Na<sub>2</sub>2e</b> ) . . . . .	94
5.4.4	<i>N</i> - <i>p</i> -Bromobenzyliminodiacetic acid ( <b>H<sub>2</sub>2g</b> ) . . . . .	95
5.4.5	<i>N</i> -Phenylethyliminodiacetic acid ( <b>H<sub>2</sub>2h</b> ) . . . . .	96
5.4.6	Tripotassium <i>N</i> -[4-(carboxymethoxy)phenyl]iminodiacetate ( <b>K<sub>3</sub>2k</b> ) . . . . .	97
5.4.7	Bis(triphenylphosphane)iminium bromide, (PPN)Br . . . . .	98
5.4.8	Bis(triphenylphosphane)iminium iodide, (PPN)I . . . . .	99
5.4.9	Bis(triphenylphosphane)iminium azide, (PPN)N <sub>3</sub> . . . . .	100
5.4.10	Bis(triphenylphosphane)iminium nitrite, (PPN)NO <sub>2</sub> . . . . .	101
5.5	Synthesis of quartet- $\{\text{FeNO}\}^7$ compounds with aminocarboxylato ligands . . . . .	102
5.5.1	[Fe(ida)(NO)(OH <sub>2</sub> ) <sub>2</sub> ] ( <b>3a</b> ) . . . . .	102
5.5.2	[Fe(heida)(NO)(OH <sub>2</sub> ) <sub>2</sub> ] ( <b>3b</b> ) . . . . .	103
5.5.3	[Fe(dhpida)(NO)] ( <b>3c</b> ) . . . . .	104
5.5.4	[Fe(NO)(OH <sub>2</sub> ) <sub>2</sub> (oda)] ( <b>3d</b> ) . . . . .	105
5.5.5	[Fe(NO)(OH <sub>2</sub> ) <sub>2</sub> (phida)] · H <sub>2</sub> O ( <b>3e</b> ) . . . . .	106
5.5.6	[Fe(bnida)(NO)(OH <sub>2</sub> ) <sub>2</sub> ] ( <b>3f</b> ) . . . . .	107
5.5.7	[Fe(brbnida)(NO)(OH <sub>2</sub> ) <sub>2</sub> ] ( <b>3g</b> ) . . . . .	108
5.5.8	[Fe(NO)(OH <sub>2</sub> ) <sub>2</sub> (pheida)] ( <b>3h</b> ) . . . . .	109
5.5.9	[Fe(dipic)(NO)(OH <sub>2</sub> ) <sub>2</sub> ] ( <b>3i</b> ) . . . . .	110
5.6	Synthesis of iron(II) aminocarboxylates . . . . .	111
5.6.1	[Fe(dhpida)(OH <sub>2</sub> ) <sub>2</sub> ] · 2 H <sub>2</sub> O ( <b>4c</b> ) . . . . .	111
5.6.2	[Fe(dipic)(OH <sub>2</sub> ) <sub>3</sub> ] · 2 H <sub>2</sub> O ( <b>4i</b> ) . . . . .	112
5.6.3	[Fe(ca)(OH <sub>2</sub> ) <sub>3</sub> ] · 0.5 H <sub>2</sub> O ( <b>4j</b> ) . . . . .	113
5.6.4	[Fe <sub>3</sub> (cpida) <sub>2</sub> (OH <sub>2</sub> ) <sub>8</sub> ] · 2 H <sub>2</sub> O ( <b>4k</b> ) . . . . .	114

---

5.7	Synthesis of halogenidonitrosylferrates . . . . .	115
5.7.1	{PPN}[FeCl <sub>3</sub> (NO)] ((PPN) <b>5a</b> ) . . . . .	115
5.7.2	{PPN}[FeBr <sub>3</sub> (NO)] ((PPN) <b>5b</b> ) . . . . .	116
5.7.3	{{PPN}[FeI <sub>2</sub> (NO) <sub>2</sub> ]}{{PPN}[I <sub>3</sub> ]} ((PPN) <sub>2</sub> <b>5c</b> (I <sub>3</sub> )) . . . . .	117
5.7.4	{PPN}[Fe(N <sub>3</sub> ) <sub>2</sub> (NO) <sub>2</sub> ] ((PPN) <b>5d</b> ) . . . . .	118
5.7.5	{PPN}[Fe(CO) <sub>3</sub> (NO)] . . . . .	119
5.7.6	{PPN}[Fe(NO) <sub>2</sub> (ONO) <sub>2</sub> ] . . . . .	120
5.7.7	{PPN}[FeCl <sub>2</sub> (NO) <sub>2</sub> ] ((PPN) <b>5e</b> ) . . . . .	121
5.8	Computational methods . . . . .	122
<b>6</b>	<b>Appendix</b> . . . . .	<b>123</b>
6.1	Packing diagrams of the crystal structures . . . . .	123
6.2	Crystallographic tables . . . . .	141
<b>7</b>	<b>Bibliography</b> . . . . .	<b>149</b>

# List of Figures

1.1	MO diagram of NO . . . . .	2
1.2	Various M–N–O bonding modes . . . . .	3
2.1	Synthesis of new ligands . . . . .	5
2.2	Synthesis of octahedral quartet- $\{\text{FeNO}\}^7$ compounds . . . . .	7
2.3	Plot of the complex $[\text{Fe}(\text{ida})(\text{NO})(\text{OH}_2)_2]$ in crystals of <b>3a</b> . . . . .	9
2.4	Plot of the complex $[\text{Fe}(\text{heida})(\text{NO})(\text{OH}_2)]$ in crystals of <b>3b</b> . . . . .	11
2.5	Plot of the complex $[\text{Fe}(\text{dhpida})(\text{NO})]$ in crystals of <b>3c</b> . . . . .	12
2.6	Plot of the zigzag chain of $[\{\text{Fe}(\text{dhpida})(\text{NO})\}_n]$ in crystals of <b>3c</b> . . . . .	14
2.7	Plot of the complex $[\text{Fe}(\text{NO})(\text{OH}_2)_2(\text{oda})]$ in crystals of <b>3d</b> . . . . .	15
2.8	Plot of the compound $[\text{Fe}(\text{NO})(\text{OH}_2)_2(\text{phida})] \cdot \text{H}_2\text{O}$ in crystals of <b>3e</b> . . . . .	17
2.9	Plot of the complex $[\text{Fe}(\text{bnida})(\text{NO})(\text{OH}_2)_2]$ in crystals of <b>3f</b> . . . . .	19
2.10	Plot of the complex $[\text{Fe}(\text{brbnida})(\text{NO})(\text{OH}_2)_2]$ in crystals of <b>3g</b> . . . . .	21
2.11	Plot of the complex $[\text{Fe}(\text{NO})(\text{OH}_2)_2(\text{pheida})]$ in crystals of <b>3h</b> . . . . .	22
2.12	Plot of the complex $[\text{Fe}(\text{dipic})(\text{NO})(\text{OH}_2)_2]$ in crystals of <b>3i</b> . . . . .	24
2.13	Plot of the compound $[\text{Fe}(\text{dhpida})(\text{OH}_2)_2] \cdot 2\text{H}_2\text{O}$ in crystals of <b>4c</b> . . . . .	26
2.14	Plot of the compound $[\text{Fe}(\text{dipic})(\text{OH}_2)_3] \cdot 2\text{H}_2\text{O}$ in crystals of <b>4i</b> . . . . .	28
2.15	Plot of the compound $[\text{Fe}(\text{ca})(\text{OH}_2)_3] \cdot 0.5\text{H}_2\text{O}$ in crystals of <b>4j</b> . . . . .	30
2.16	Plot of the compound $[\text{Fe}_3(\text{cpida})_2(\text{OH}_2)_8] \cdot 2\text{H}_2\text{O}$ in crystals of <b>4k</b> . . . . .	32
2.17	Plot of the anion $[\text{FeCl}_3(\text{NO})]^-$ in crystals of (PPN) <b>5a</b> . . . . .	34
2.18	Plot of the anion $[\text{FeBr}_3(\text{NO})]^-$ in crystals of (PPN) <b>5b</b> . . . . .	35
2.19	Plot of the anion $[\text{FeI}_2(\text{NO})_2]^-$ in crystals of (PPN) <b>5c(I<sub>3</sub>)</b> . . . . .	36
2.20	Plot of the anion $[\text{FeCl}_2(\text{NO})_2]^-$ in crystals of (PPN) <b>5e</b> . . . . .	38
2.21	IR spectra in solution . . . . .	40
2.22	UV-VIS spectra . . . . .	41
2.23	SQUID measurements of <b>3a</b> and <b>3f</b> . . . . .	43
2.24	OPDOS between Fe and NO of <b>3a</b> . . . . .	51
2.25	LUMO – LUMO+6 and corresponding occupied orbitals of <b>3a</b> . . . . .	52
2.26	Natural orbitals of <b>3a</b> . . . . .	53
2.27	Natural orbitals of <b>5e</b> . . . . .	55
2.28	Spin density of <b>5e</b> , <b>3a</b> and <b>5a</b> . . . . .	55

---

2.29	Active space in the CASSCF calculations of <b>3a</b> and <b>5a</b> . . . . .	58
2.30	Active space in the CASSCF calculation of <b>5e</b> . . . . .	59
2.31	UV-VIS spectra with calculated excitations . . . . .	61
2.32	Temperature dependence of ADPs of <b>3e</b> and <b>3f</b> . . . . .	62
2.33	Fe–N–O bending potential and corresponding $\nu(\text{NO})$ . . . . .	63
2.34	Walsh diagram of <b>3a</b> . . . . .	64
2.35	PLI experiment on <b>3e</b> . . . . .	66
2.36	PLI experiment on (PPN) <b>5a</b> . . . . .	67
2.37	PLI experiment on (PPN) <b>5a</b> . . . . .	68
2.38	DFT calculation on the oxidation of <b>5a</b> . . . . .	69
3.1	Plot of Fe–N–O angle <i>vs.</i> $\nu(\text{NO})$ . . . . .	74
4.1	Plot of the complex $[\text{Fe}(\text{ida})(\text{NO})(\text{OH}_2)_2]$ in crystals of <b>3a</b> . . . . .	84
6.1	Packing diagram of <b>3a</b> . . . . .	124
6.2	Packing diagram of <b>3b</b> . . . . .	125
6.3	Packing diagram of <b>3c</b> . . . . .	126
6.4	Packing diagram of <b>3d</b> . . . . .	127
6.5	Packing diagram of <b>3e</b> . . . . .	128
6.6	Packing diagram of <b>3f</b> . . . . .	129
6.7	Packing diagram of <b>3g</b> . . . . .	130
6.8	Packing diagram of <b>3h</b> . . . . .	131
6.9	Packing diagram of <b>3i</b> . . . . .	132
6.10	Packing diagram of <b>4c</b> . . . . .	133
6.11	Packing diagram of <b>4i</b> . . . . .	134
6.12	Packing diagram of <b>4j</b> . . . . .	135
6.13	Packing diagram of <b>4k</b> . . . . .	136
6.14	Packing diagram of <b>5a</b> . . . . .	137
6.15	Packing diagram of <b>5b</b> . . . . .	138
6.16	Packing diagram of <b>5c</b> . . . . .	139
6.17	Packing diagram of <b>5e</b> . . . . .	140

# List of Tables

2.1	Hydrogen bonds in <b>3a</b> . . . . .	10
2.2	Hydrogen bonds in <b>3b</b> . . . . .	11
2.3	Hydrogen bonds in <b>3c</b> . . . . .	13
2.4	Hydrogen bonds in <b>3d</b> . . . . .	16
2.5	Hydrogen bonds in <b>3e</b> . . . . .	16
2.6	Hydrogen bonds in <b>3f</b> . . . . .	18
2.7	Hydrogen bonds in <b>3g</b> . . . . .	20
2.8	Hydrogen bonds in <b>3h</b> . . . . .	23
2.9	Hydrogen bonds in <b>3i</b> . . . . .	25
2.10	Hydrogen bonds in <b>4c</b> . . . . .	27
2.11	Hydrogen bonds in <b>4i</b> . . . . .	29
2.12	Hydrogen bonds in <b>4j</b> . . . . .	31
2.13	Hydrogen bonds in <b>4k</b> . . . . .	33
2.14	IR-spectroscopic data . . . . .	39
2.15	UV-VIS-spectroscopic data . . . . .	41
2.16	DFT results on <b>3a</b> . . . . .	45
2.17	DFT results on <b>3</b> . . . . .	46
2.18	DFT results on different coordination isomers. . . . .	47
2.19	DFT results on <b>5</b> . . . . .	49
2.20	MPA and NPA analysis . . . . .	56
2.21	CDA analysis . . . . .	56
2.22	Mulliken analysis on CASSCF wave function. . . . .	58
2.23	Oxidation states from the localized CASSCF orbitals. . . . .	59
2.24	TDDFT calculations. . . . .	61
2.25	Comparison of {FeNO} <sup>7</sup> compounds with nitrosyl-free compounds . . . . .	65
3.1	Comparison of N–O bond lengths and $\nu(\text{NO})$ stretching vibration bands . . . . .	76
3.2	Comparison of nitrosyl-iron compounds in literature . . . . .	77
6.1	Crystallographic data of <b>3a</b> , <b>3b</b> and <b>3c</b> . . . . .	142
6.2	Crystallographic data of <b>3d</b> , <b>3e</b> and <b>3f</b> . . . . .	143

6.3	Crystallographic data of <b>3g</b> , <b>3h</b> and <b>3i</b> . . . . .	144
6.4	Crystallographic data of <b>4c</b> , <b>4i</b> and <b>4j</b> . . . . .	145
6.5	Crystallographic data of <b>4k</b> , <b>5a</b> and <b>5b</b> . . . . .	146
6.6	Crystallographic data of <b>5c</b> and <b>5e</b> . . . . .	147

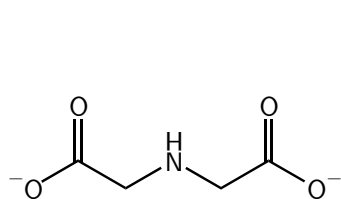
# Abbreviations

ATR	attenuated total reflection
Bn	benzyl
bnida	<i>N</i> -benzyliminodiacetate
br	broad
brbnida	<i>N</i> -( <i>p</i> -bromobenzyl)iminodiacetate
ca	4-hydroxypyridine-2,6-dicarboxylate
calcd	calculated
CASSCF	complete active space self consistent field
CDA	charge decomposition analysis
cpida	<i>N</i> -[4-(carboxymethoxy)phenyl]iminodiacetate
CShM	continous shape measurement
d	doublet
DCM	dichloromethane
DEI	desorption electron ionization
DFT	density functional theory
dhpida	<i>N</i> -(1,3-dihydroxypropane-2-yl)iminodiacetate
dipic	pyridine-2,6-dicarboxylate
Et	ethyl
FAB	fast atom bombardment
heida	<i>N</i> -(2-hydroxyethyl)iminodiacetate
HOMO	highest occupied molecular orbital
ida	iminodiacetate
IR	infrared
L	ligand
LUMO	lowest unoccupied molecular orbital
m	medium (IR spectroscopy) / multiplet (NMR spectroscopy)
Me	methyl
MO	molecular orbital
MS	mass spectrometry
NMR	nuclear magnetic resonance
oda	oxodiacetate

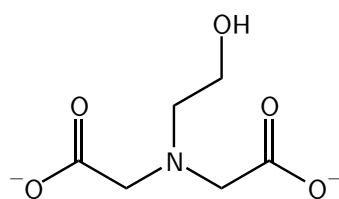
OPDOS	overlap population density of states
<i>p</i>	<i>para</i>
Ph	phenyl
pheida	<i>N</i> -(2-phenylethyl)iminodiacetate
phida	<i>N</i> -phenyliminodiacetate
PLI	photoinduced linkage isomerism
ppm	parts per million
PPN	bis(triphenylphosphane)iminium
q	quartet
s	strong (IR spectroscopy) / singlet (NMR spectroscopy)
t	triplet
TDDFT	time dependent density functional theory
THF	tetrahydrofuran
UV-VIS	ultraviolet-visible
vs	very strong
vw	very weak
w	weak

# Overview of numbered compounds

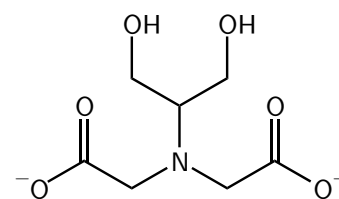
## Iminodiacetate derivatives used as chelating ligands



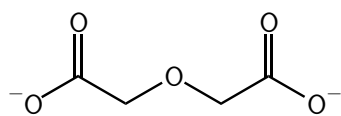
ida (2a)



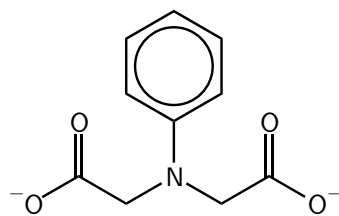
heida (2b)



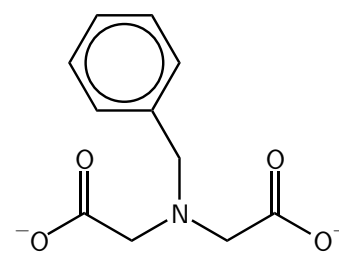
dhpida (2c)



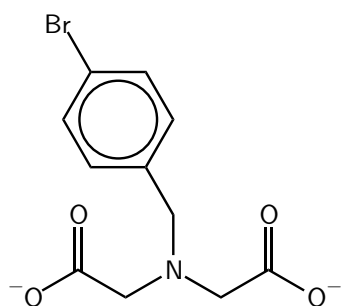
oda (2d)



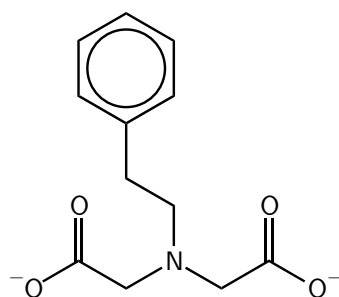
phida (2e)



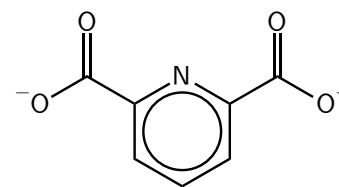
bnida (2f)



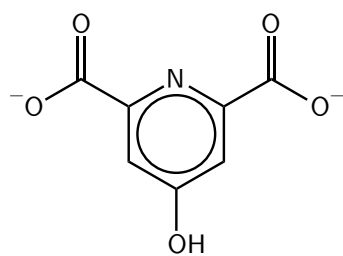
brbnida (2g)



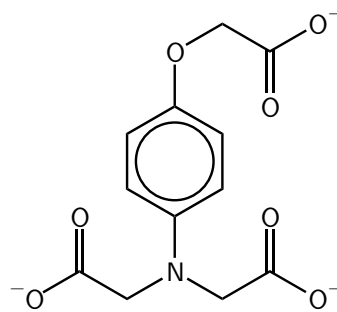
pheida (2h)



dipic (2i)

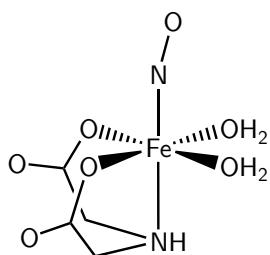


ca (2j)

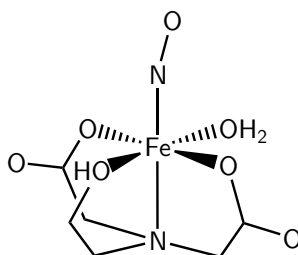


cpida (2k)

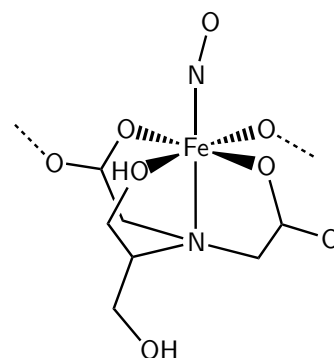
### Quartet- $\{FeNO\}^7$ compounds with aminocarboxylato ligands



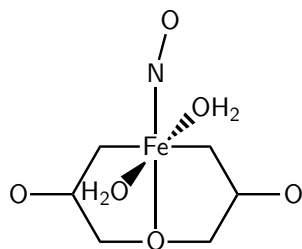
[Fe(ida)(NO)(OH<sub>2</sub>)<sub>2</sub>]  
(3a)



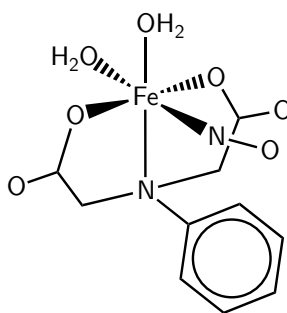
[Fe(heida)(NO)(OH<sub>2</sub>)<sub>2</sub>]  
(3b)



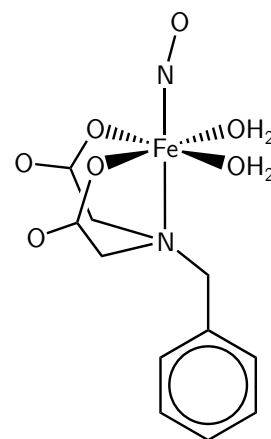
[Fe(dhpida)(NO)(OH<sub>2</sub>)<sub>2</sub>]  
(3c)



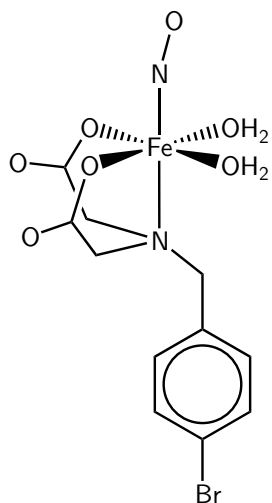
[Fe(NO)(OH<sub>2</sub>)<sub>2</sub>(oda)]  
(3d)



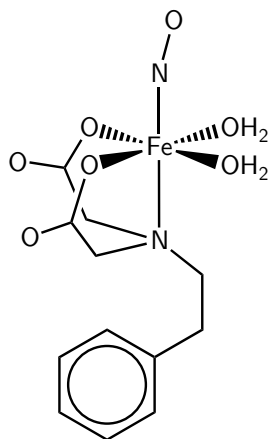
[Fe(NO)(OH<sub>2</sub>)<sub>2</sub>(phida)]  
(3e)



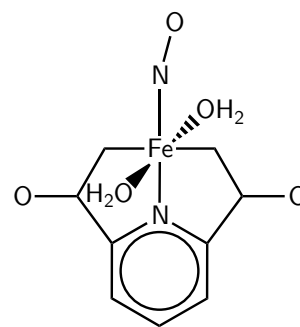
[Fe(bnida)(NO)(OH<sub>2</sub>)<sub>2</sub>]  
(3f)



[Fe(brbnida)(NO)(OH<sub>2</sub>)<sub>2</sub>]  
(3g)

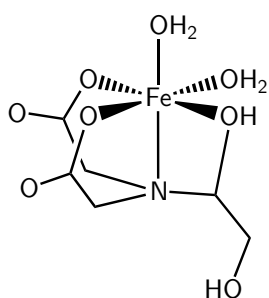


[Fe(NO)(OH<sub>2</sub>)<sub>2</sub>(pheida)]  
(3h)

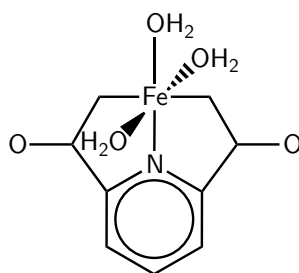


[Fe(dipic)(NO)(OH<sub>2</sub>)<sub>2</sub>]  
(3i)

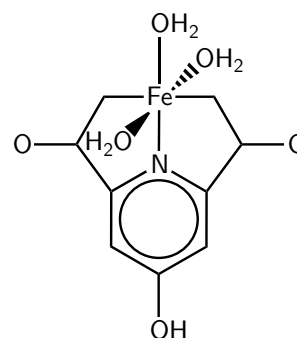
## Iron(II) aminocarboxylates



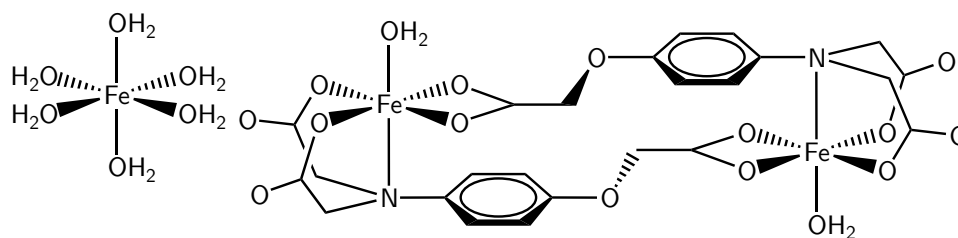
[Fe(dhpida)(OH<sub>2</sub>)<sub>2</sub>]  
(4c)



[Fe(dipic)(OH<sub>2</sub>)<sub>3</sub>]  
(4i)

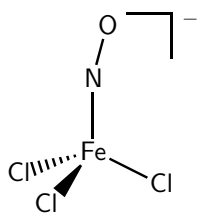


[Fe(ca)(OH<sub>2</sub>)<sub>3</sub>]  
(4j)

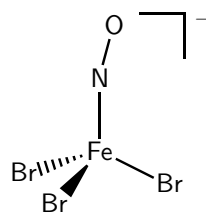


[Fe<sub>3</sub>(cpida)<sub>2</sub>(OH<sub>2</sub>)<sub>8</sub>]  
(4k)

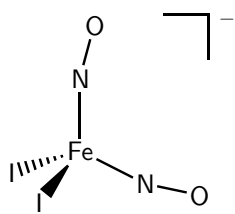
## Halogenidonitrosylferrates



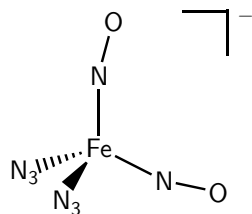
[FeCl<sub>3</sub>NO]<sup>-</sup> (5a)



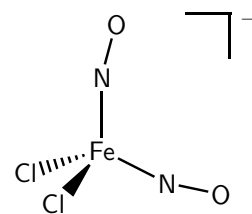
[FeBr<sub>3</sub>NO]<sup>-</sup> (5b)



[FeI<sub>2</sub>(NO)<sub>2</sub>]<sup>-</sup> (5c)



[Fe(N<sub>3</sub>)<sub>2</sub>(NO)<sub>2</sub>]<sup>-</sup> (5d)



[FeCl<sub>2</sub>(NO)<sub>2</sub>]<sup>-</sup> (5e)

# 1 Introduction

In 1992 nitric oxide was announced “molecule of the year” by the magazine *Science*.<sup>[1,2]</sup> Infamous for years for being responsible for acid rain,<sup>[3]</sup> causing cancer<sup>[4,5]</sup> and destroying the ozone layer,<sup>[6–8]</sup> nitric oxide suddenly gained much attention for acting as a secondary messenger,<sup>[9]</sup> regulating the blood pressure,<sup>[10]</sup> assisting the immune system<sup>[11]</sup> and being an anti-tumor agent.<sup>[5]</sup> Subsequently more and more research was done, focusing on nitric oxide and its role in organisms. In 1996, the “Nitric Oxide Society” was founded and in 1998 the Nobel Prize in Physiology or Medicine was awarded to Furchgott, Ignarro and Murad “for their discoveries concerning nitric oxide as a signalling molecule in the cardiovascular system”.

## 1.1 Physical and chemical properties of nitric oxide

Nitric oxide is the most simple reaction product of nitrogen and oxygen. Its formation is highly endothermic:<sup>[12]</sup>



It is a colorless, paramagnetic, toxic gas with a characteristic smell.<sup>[12]</sup> Its bond order is 2.5, its bond length is 1.15 Å<sup>[13]</sup> and its stretching vibration band is found at 1875 cm<sup>-1</sup>. As a free radical, nitric oxide carries an unpaired electron and can be described by the following Lewis formulas:



From the MO diagram (see Figure 1.1) the different possibilities for NO to react and to coordinate metal ions become evident. The 5σ orbital with its larger lobe on the nitrogen atom can form σ bonds with empty metal orbitals. The 2π orbitals, again with larger lobes on the nitrogen atom, can act as electron-donating and electron-accepting orbitals and form either two π bonds with linear coordination of a metal ion or one σ bond and one π bond with a strongly bent coordination. In any case the coordination *via* the nitrogen atom is favored (κN). Upon coordination an electron transfer from or to the nitrosyl ligand is possible (reductive or oxidative nitrosylation). Hence, nitric oxide is called a non-innocent ligand.

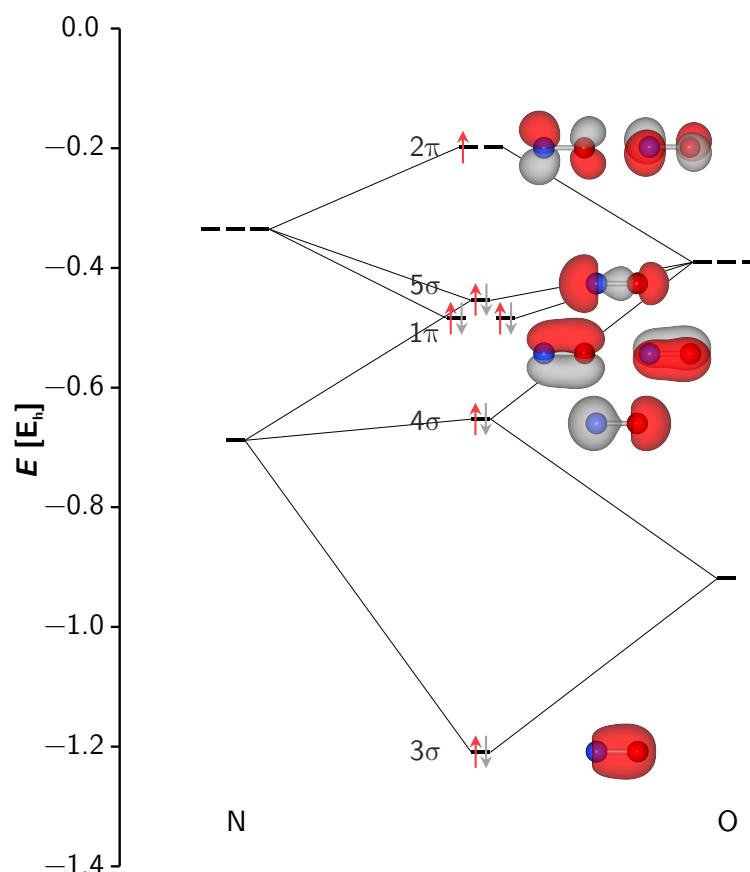


**Figure 1.1:** MO diagram of nitric oxide. Calculated using TPSSh, def2-TZVP, dispersion correction and D-COSMO-RS.

Possible formal oxidation states and resulting coordination figures of nitric oxide are: (1)  ${}^1\text{NO}^+$  with linear coordination, (2)  ${}^1\text{NO}^-$  with strongly bent ( $120^\circ$ ) coordination, (3)  ${}^2\text{NO}^0$  with a less bent ( $140^\circ$ ) coordination and (4)  ${}^3\text{NO}^-$  with slightly bent ( $160^\circ$ – $180^\circ$ ) coordination of the metal ion (see Figure 1.2).<sup>[14,15]</sup>

Of course, all these configurations also allow assignments of formal oxidation states. A  $\text{M}^{1+}\text{-NO}^+$  moiety can also be described as  $\text{M}^{2+}\text{-NO}^0$  or  $\text{M}^{3+}\text{-NO}^-$ . To circumvent such confusion, Enemark and Feltham developed a special notation for nitrosyl metal complexes, denoting them as  $\{\text{M}(\text{NO})_x\}^n$  with  $x$  being the number of nitrosyl ligands and  $n$  being the sum of electrons in metal  $d$ - and NO  $\pi^*$ -orbitals.<sup>[16]</sup>

## 1.2 Relevance of nitrosyl-iron compounds

Enzymes containing heme and non-heme iron active sites play an important role in nitric oxide metabolism.<sup>[17–19]</sup> Important examples are NO synthases,<sup>[20–22]</sup> NO reductases,<sup>[23–28]</sup>

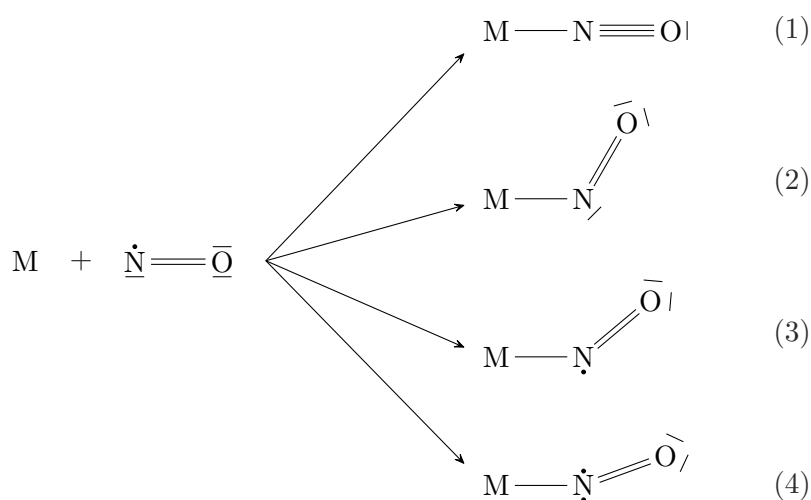
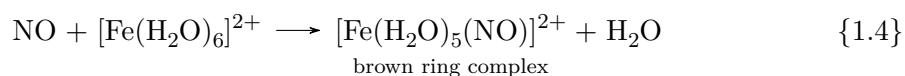


**Figure 1.2:** Formation of various M–N–O bonding modes. The assignment of formal charges was omitted.

NO carriers<sup>[29,30]</sup> or NO receptors in neural signaling.<sup>[31,32]</sup> Furthermore, NO is often used as a paramagnetic probe to analyze otherwise EPR-silent active centers that usually bind O<sub>2</sub>.<sup>[33,34]</sup> Thus, it is not surprising that there is an ongoing interest in and research on nitrosyl-iron compounds. Generally they can be divided into mono- and dinitrosyl-iron compounds (MNICs and DNICs), lately also tri- and tetranitrosyl-iron compounds have been described.<sup>[35–38]</sup> Further classification is possible in respect to the total spin state and oxidation state of particular compounds. Most important are ( $S = 0$ ) $\{\text{Fe}(\text{NO})\}^6$ , ( $S = 1/2$ ) $\{\text{FeNO}\}^7$ , ( $S = 3/2$ ) $\{\text{FeNO}\}^7$  and ( $S = 1/2$ ) $\{\text{Fe}(\text{NO})_2\}^9$ .<sup>[14,39]</sup> From a chemical point of view, the use of iron complexes for NO detection is noteworthy<sup>[40–42]</sup> and, last but not least, the so-called “brown ring test” must be mentioned.<sup>[43]</sup> It is the long-known test reaction for nitrate in aqueous solution, performed regularly in undergraduate education. Its details, however, are still not fully understood.



### 1.3 Photoinduced linkage isomerism

As stated above, the  $\kappa\text{N}$  coordination is common to nitrosyl metal complexes. For some of them it is, however, possible to obtain  $\kappa\text{O}$  or  $\kappa(\text{N},\text{O})$  isomers by irradiation with light in the range of  $\lambda = 350\text{--}580\text{ nm}$ ,<sup>[44,45]</sup> a phenomenon called photoinduced linkage isomerism (PLI). If these excited states are metastable below a certain temperature, they can be identified by

IR spectroscopy, differential scanning calorimetry and photocrystallography.<sup>[46,47]</sup> Sodium nitroprusside was the first compound for which this behavior was detected.<sup>[48]</sup> Since then many other nitrosyl metal complexes, showing a PLI, have been identified.<sup>[49–60]</sup> They represent interesting objects of research in several respects: they allow insight into the electronic structure of the ground state as well as the excited state. These insights help in developing experiments to alter the electronic structure, for example, switching between different states by excitation with different wavelengths. If such experiments are successful, the application of such compounds as optical data storage might become possible.

## 1.4 Aim of this work

As of January, 2011, the Cambridge Structural Database listed 622 nitrosyl-iron compounds of which 440 are MNICs. Only 24, however, belong to the group of octahedral quartet- $\{\text{FeNO}\}^7$  compounds.<sup>[42,61–78]</sup> Their electronic configuration is the subject of ongoing discussion and, so far, no PLI has been reported for any of them. Between 2001 and 2002, the group of van Eldik reported investigations of the reactivity of nitric oxide in aqueous solutions of iron(II) aminocarboxylates.<sup>[79–81]</sup> Inspired by their work, Kästele from the Klüfers group succeeded in crystallizing the quartet- $\{\text{FeNO}\}^7$  compound  $[\text{Fe}(\text{ida})(\text{NO})(\text{OH}_2)_2]$  (**3a**). This compound was the starting point of the present thesis. The aim was to crystallize a series of MNICs with iminodiacetic acid ( $\text{H}_2\text{ida}$ , **2a**) derivatives as chelating ligands. They were to be subsequently analyzed with respect to a possible PLI and their electronic configuration investigated by means of quantum-chemical calculations.

A second starting point for this thesis were still open questions, regarding simple halogenidinitrosylferrates. In 1983 the Beck group reported the crystal structure of the quartet- $\{\text{FeNO}\}^7$  compound  $[\text{AsPh}_4][\text{FeCl}_3(\text{NO})]$ .<sup>[82]</sup> Yet they obtained their crystals from a solution that consisted mainly of  $[\text{AsPh}_4][\text{FeCl}_2(\text{NO})_2]$  – a compound of which no disorder-free crystal structure could be obtained to this day. Also, the red-brown color of the crystals they described, is in contrast to the otherwise dark green color of quartet- $\{\text{FeNO}\}^7$  compounds. Later attempts by our group to reproduce Beck’s findings, resulted in disordered crystals in which the chlorido and nitrosyl positions interchanged. So second the aim of this work was to obtain disorder-free crystals of both the  $[\text{FeCl}_3(\text{NO})]^-$  and the  $[\text{FeCl}_2(\text{NO})_2]^-$  anion and to subject them to PLI and quantum-chemical investigations.

## 2 Results

### 2.1 Synthesis of new iminodiacetic acid derivatives

Most of the ligands used for the complexation of iron(II) were commercially available. However, the ligands disodium *N*-phenyliminodiacetate (Na<sub>2</sub>phida, **2e**), *N*-phenylethyliminodiacetic acid (H<sub>2</sub>pheida, **2h**), *N*-(*p*-bromobenzyl)iminodiacetic acid (H<sub>2</sub>brbnida, **2g**), dipotassium *N*-(1,3-dihydroxypropane-2-yl)iminodiacetate (K<sub>2</sub>dhpida, **2c**) and tripotassium *N*-[4-(carboxymethoxy)phenyl]iminodiacetate (K<sub>3</sub>cpida, **2k**) had to be synthesized. The general approach was the same for all these ligands: The desired amine is reacted with two equivalents of chloroacetic acid or ethyl bromoacetate in the presence of base. The ligand is isolated either as alkaline salt or as free acid.

#### 2.1.1 Disodium *N*-phenyliminodiacetate (Na<sub>2</sub>phida)

The synthesis of Na<sub>2</sub>phida (Na<sub>2</sub>**2e**) followed a simple route developed by Gould *et al.*<sup>[83]</sup> Ethyl bromoacetate and aniline are refluxed for six days in acetonitrile using potassium iodide as catalyst and potassium carbonate as base. Distillation of the crude product *in vacuo* yields 43 % of diethyl (*N*-phenylimino)-diacetate. Subsequent alkaline hydrolysis with sodium hydroxide in a mixture of water, ethanol and THF gives Na<sub>2</sub>**2e** in 53 % yield. <sup>1</sup>H-NMR, <sup>13</sup>C{<sup>1</sup>H}-NMR and mass spectrometry confirm the successful synthesis.

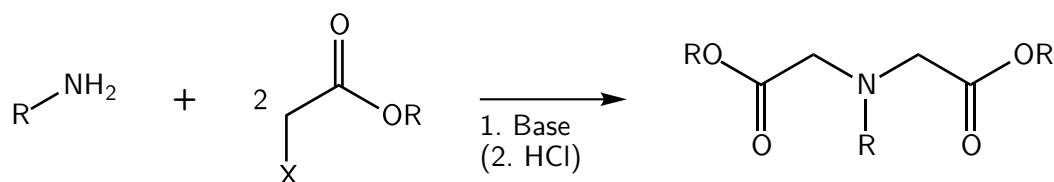


**Figure 2.1:** General procedure for the synthesis of new aminocarboxylato ligands.

### 2.1.2 *N*-(*p*-Bromobenzyl)iminodiacetic acid (H<sub>2</sub>brbnida) and *N*-phenylethyliminodiacetic acid (H<sub>2</sub>pheida)

The synthesis of H<sub>2</sub>brbnida (H<sub>2</sub>**2g**) and H<sub>2</sub>pheida (H<sub>2</sub>**2h**) followed a route developed by Smrečki *et al.*<sup>[84]</sup> An ice-cooled solution of chloroacetic acid in water is slowly neutralized with an aqueous solution of sodium hydroxide. Afterwards, phenylethylamine or *p*-bromobenzylamine is slowly added. The resulting solution is refluxed and an aqueous solution of sodium hydroxide is added during a one-hour period. The refluxing is continued for another hour, then diluted hydrochloric acid is added until the solution reaches pH  $\approx$  2. After several hours the desired products H<sub>2</sub>**2g** or H<sub>2</sub>**2h** precipitate in good yield (82 % and 85 % respectively). They are washed with ice water and can be used without further purification as confirmed by by <sup>1</sup>H-NMR, <sup>13</sup>C{<sup>1</sup>H}-NMR and mass spectrometry.

### 2.1.3 Dipotassium *N*-(1,3-dihydroxypropane-2-yl)iminodiacetate (K<sub>2</sub>dhpida) and tripotassium *N*-[4-(carboxymethoxy)phenyl]iminodiacetate (K<sub>3</sub>cpida)

K<sub>2</sub>dhpida (K<sub>2</sub>**2c**) and K<sub>3</sub>cpida (K<sub>3</sub>**2k**) were synthesized following a patent by Miralles *et al.*<sup>[85]</sup> The synthesis is quite similar to that of **2g** and **2h**. Potassium hydroxide is used as base and the product is not acidified after its formation but extracted with dichloromethane and precipitated as potassium salt. K<sub>2</sub>**2c** and K<sub>3</sub>**2k** are obtained in 38 % yield and 22 % yield respectively and characterized by <sup>1</sup>H-NMR, <sup>13</sup>C{<sup>1</sup>H}-NMR, and mass spectrometry.

## 2.2 Quartet-{FeNO}<sup>7</sup> compounds with aminocarboxylato ligands

{FeNO}<sup>7</sup> compounds with iminodiacetic acid derivatives (**2**) as ligands were obtained by the following general procedure which was derived from work of the group of van Eldik.<sup>[79]</sup> In a Schlenk tube with inert gas atmosphere an iron(II) salt is dissolved in a polar solvent. Ligand **2** is added and dissolved. To assist solution, up to two equivalents of sodium or potassium hydroxide can be added. A nearly colorless solution results. Nitric oxide is bubbled through the solution. Meanwhile the solution turns dark green. The product can be crystallized by the slow diffusion of acetone into the solution yielding black-green crystals.

Water, methanol or ethanol are the best solvents. Other solvents like acetone, acetonitrile or dimethyl sulfoxide result in either poor solubility of the reactants or fast decomposition of the products. As the reaction system is very sensitive towards oxygen, all solvents have to be degassed properly. With one exception, crystalline products were obtained only from aqueous solutions, therefore water is the solvent of choice.

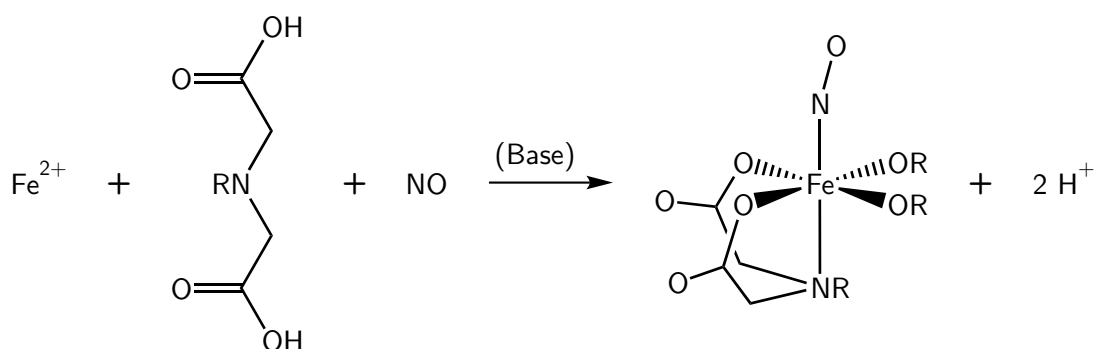


**Figure 2.2:** General procedure for the synthesis of quartet- $\{FeNO\}^7$  compounds with aminocarboxylato ligands.

As an iron source, basically any iron(II) salt soluble in the solvents mentioned before is appropriate. The used anion should be weakly coordinating and the salt should show a certain air stability for better handling. These considerations lead to the choice of  $FeSO_4 \cdot 7 H_2O$  and  $Fe(OTf)_2 \cdot 3 CH_3CN$  as the best suited iron(II) salts.  $FeSO_4 \cdot 7 H_2O$  is usually used in aqueous solutions due to its higher air stability.  $Fe(OTf)_2 \cdot 3 CH_3CN$  is used in methanol and ethanol due to its better solubility in those solvents.  $FeCl_2 \cdot 4 H_2O$  and  $Fe(OAc)_2$  were also tested, however, they show no advantage over  $FeSO_4 \cdot 7 H_2O$  and  $Fe(OTf)_2 \cdot 3 CH_3CN$  but lack their air stability.

Ligand **2** can be added in its acidic form or as the disodium and dipotassium salt respectively. Using the alkaline salts results in a much better solubility of the ligand but sometimes leads to quick amorphous precipitation of the final  $\{FeNO\}^7$  compounds. A better solubility of the ligands can also be achieved by the gentle heating of the solutions.

Nitric oxide is added to the reaction system by slowly bubbling the gas through the solution. Almost immediately the colorless solutions start to turn green. First a light yellow-green color intensifying with every bubble of nitric oxide and quickly turning into an opaque black-green color.

The concentration of the prepared solutions is limited mainly by the solubility of the ligands. In their acidic form most ligands show a solubility of up to  $200 \text{ mmol L}^{-1}$ , rendering this the preferred concentration. The ratio of iron-to-ligand can be kept at 1:1 as any significant influence could not be determined.

Crystallization can be induced by the slow diffusion of acetone into the dark green solutions. As said above the use of alkaline ligand salts also accelerates the precipitation but usually leads to the formation of amorphous solids. Some products crystallize within days to weeks without the addition of acetone or the use of alkaline ligand salts. A correlation between different chelating ligands and the tendency to crystallize could not be established.

Following the procedures described above, opaque black-green solutions are obtained. Under inert conditions these solutions are stable for several years at room temperature. Towards oxygen they show high sensitivity and decompose in a period from several minutes to hours. If low pressure or heat is applied, or if the solutions are purged with argon or nitrogen, they lose nitric oxide quite rapidly. The original, colorless iron(II) aminocarboxylate solutions are obtained which can again be reacted with nitric oxide. If  $\text{FeSO}_4 \cdot 7\text{H}_2\text{O}$  is used as the iron source, the slow diffusion of acetone leads quite often to the formation of large crystals of  $\text{FeSO}_4 \cdot 7\text{H}_2\text{O}$ . In many cases, especially if the solutions are kept in a nitric oxide atmosphere, they feature a dark brown color indicating the presence of NO. Throughout this thesis they will be referred to as “brown  $\text{FeSO}_4$ ” (**1**). When crystalline  $\{\text{FeNO}\}^7$  compounds are obtained, they are often accompanied by “brown  $\text{FeSO}_4$ ” crystals. If the solutions are covered or mixed directly with acetone, nitric oxide is lost and only colorless, amorphous powders are obtained. Crystalline  $\{\text{FeNO}\}^7$  compounds are usually obtained as small dark-green blocks, platelets or needles. Viewed in a transmitted-light microscope they usually appear opaque, sometimes showing a blueish glint. The crystals are stable against oxygen and moisture. They cannot be dissolved again in common solvents and start to decompose at temperatures around 150 °C. The products obtained were characterized by single-crystal X-ray diffraction, IR spectroscopy and UV-VIS spectroscopy.

### Other synthetic methods

Several other methods to synthesize the desired products were investigated but did not yield any results:

- Oversaturated solutions were heated in a sealed tube after the addition of nitric oxide. Unfortunately nitric oxide got lost during the process and nearly colorless solutions resulted.
- At  $-160\text{ °C}$  nitric oxide was condensed in a Schlenk tube loaded with  $\text{FeSO}_4 \cdot 7\text{H}_2\text{O}$  and ligand **2**. After stirring for 15 min the mixture was warmed to room temperature. No reaction was observed.
- A mixture of  $\text{FeCl}_2 \cdot 4\text{H}_2\text{O}$  and ligand **2** was heated to 700 °C to obtain a melt but the ligand started to decompose around 250 °C.

#### 2.2.1 $[\text{Fe}(\text{ida})(\text{NO})(\text{OH}_2)_2]$

When iminodiacetate (ida, **2a**) is used as ligand in the reaction described above, *OC*-6-22-diaquaminodiacetatonitrosyliron (**3a**) is obtained after one week as dark green crystalline

blocks in 25 % yield. If no acetone is added by diffusion, crystals can be obtained after three weeks in comparable yield. This compound had already been isolated by Kästele. It is the leading structure for all other  $\{FeNO\}^7$  compounds with aminocarboxylato ligands, therefore it will be described in detail in this thesis.

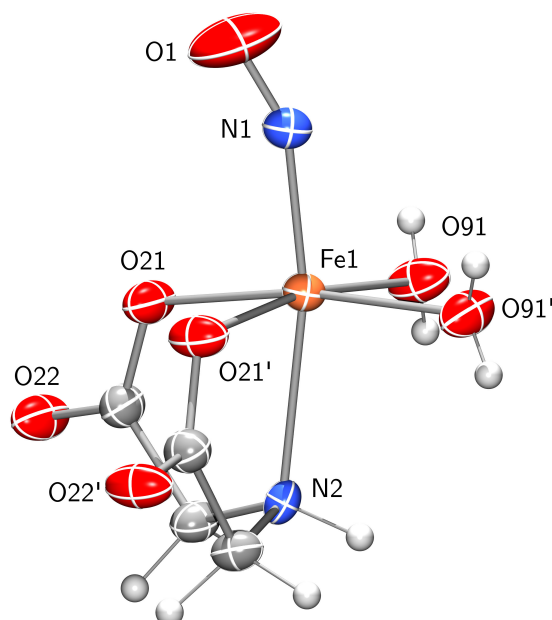


**Figure 2.3:**

Plot of the complex  $[Fe(ida)(NO)(OH_2)_2]$  in crystals of **3a**. Space group:  $Cmc2_1$ .  $CShM_{OC-6}$ : 0.617. The thermal ellipsoids are drawn at 50 % probability. Interatomic distances ( $\text{\AA}$ ) and angles ( $^\circ$ ), the standard deviation of the last decimal place is given in parentheses:

Fe1–N1 1.783(5), Fe1–N2 2.269(4), Fe1–O21 2.050(3), Fe1–O91 2.063(2), N1–O1 1.111(7).  
 Fe1–N1–O1 155.2(5), N1–Fe1–O21 93.22(13), N1–Fe1–O91 96.79(14), N1–Fe1–N2 168.15(19),  
 O21–Fe1–O21<sup>i</sup> 91.20(16), O21–Fe1–O91 90.40(11), O91–Fe1–O91<sup>i</sup> 86.28(14), O21–Fe1–O91<sup>i</sup>  
 169.76(11), O21–Fe1–N2 78.57(10), O91–Fe1–N2 91.84(12).

Symmetry code: <sup>i</sup>  $1 - x, y, z$ .

**3a** crystallizes from water/acetone in the orthorhombic space group  $Cmc2_1$  with four formula units in the primitive cell. The molecule consists of one iron atom coordinated octahedrally by one nitrosyl ligand, ida and two aqua ligands. ida coordinates facially as a tridentate ligand, forming two nearly planar five-membered chelate rings twisted on Fe1–N2. The nitrosyl ligand coordinates *trans* to the nitrogen atom of ida. The molecule contains a mirror plane, spanned by Fe, NO and the nitrogen atom of ida, therefore the asymmetric unit consists of one-half molecule of  $[Fe(ida)(NO)(OH_2)_2]$  (**3a**). The Fe–N–O moiety has a bond angle of  $155^\circ$  with the oxygen atom pointing in between the two acetate groups. The whole nitrosyl ligand is pointing in that direction with a  $N_{NO}$ –Fe– $N_{ida}$ -angle of  $168^\circ$ . The thermal ellipsoid of the nitrosyl-oxygen atom is quite large but flat, having the form of a discus. When the axial

**Table 2.1:** Distances [ $\text{\AA}$ ] and angles [ $^\circ$ ] of hydrogen bonds in **3a**, the standard deviation of the last decimal place is given in parentheses.

Donor	Hydrogen Atom	Acceptor	$d(\text{D-H})$	$d(\text{H}\cdots\text{A})$	$d(\text{D}\cdots\text{A})$	$\alpha(\text{D-H}\cdots\text{A})$
O91	H911	O22 <sup>ii</sup>	0.77(3)	1.85(3)	2.613(4)	171(6)
O91	H912	O22 <sup>iii</sup>	0.76(3)	1.90(3)	2.637(4)	163(5)

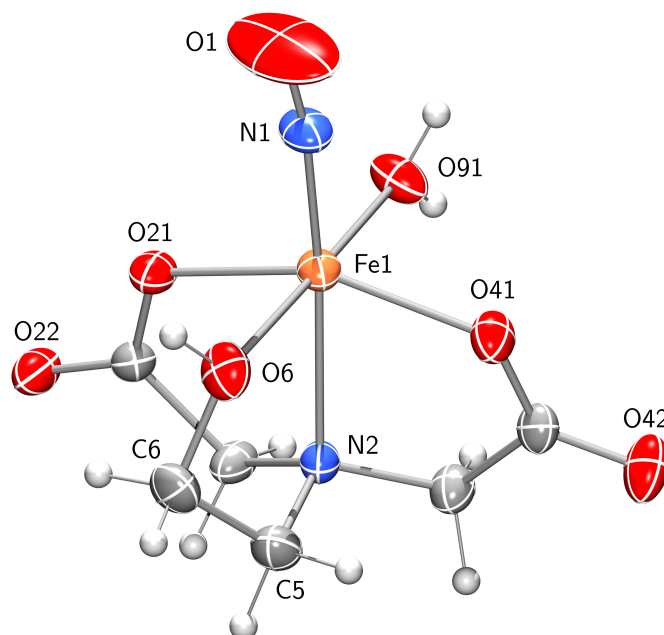
Symmetry code: <sup>ii</sup>  $3/2 - x, 1/2 + y, z$ ; <sup>iii</sup>  $3/2 - x, 1/2 - y, -1/2 + z$ .

direction is defined along the two nitrogen atoms, it is obvious that all equatorial ligands tilt away from the nitrosyl ligand, resulting in an average  $\text{N}_{\text{NO}}\text{-Fe-L}_{\text{eq}}$ -angle of  $95^\circ$ . Both aqua ligands form hydrogen bonds to the carbonyl-oxygen atoms of neighboring molecules, thus forming a three-dimensional network (see Table 2.6). All nitrosyl groups are aligned in  $[00\bar{1}]$ -direction.

### 2.2.2 [Fe(heida)(NO)(OH<sub>2</sub>)]

When the nitrogen atom in iminodiacetate is substituted with a hydroxyethyl group, the tetradentate ligand *N*-(2-hydroxyethyl)iminodiacetate (heida, **2b**) is obtained. Together with  $\text{FeSO}_4 \cdot 7\text{H}_2\text{O}$  and nitric oxide, a dark-green aqueous solution is gained. After the diffusion of acetone for three weeks, crystals of *OC*-6-13-aqua-*N*-(2-hydroxyethyl)iminodiacetatonitrosyliron (**3b**) separate as dark green blocks in 27% yield.

**3b** crystallizes from water/acetone in the monoclinic space group *Cc* with four formula units in the primitive cell. The asymmetric unit contains one molecule of  $[\text{Fe}(\text{heida})(\text{NO})(\text{OH}_2)]$  (**3b**). The molecule consists of one iron atom coordinated octahedrally by one nitrosyl ligand, heida and one aqua ligand. heida coordinates facially as a tetradentate ligand with the nitrogen atom at the apical position. Three five-membered chelate rings are formed. The one formed by O21 has an envelope conformation on N2, the other rings are twisted on C5–C6 and on Fe1–N2 respectively. The two acetate groups coordinate *trans* to each other, the nitrosyl ligand coordinates *trans* to the nitrogen atom of heida. The Fe–N–O moiety has a bond angle of  $171^\circ$  with the oxygen atom pointing in between the hydroxyethyl group and one acetate group. The whole nitrosyl ligand is pointing in that direction with a  $\text{N}_{\text{NO}}\text{-Fe-N}_{\text{heida}}$ -angle of  $171^\circ$ . The thermal ellipsoid of the nitrosyl-oxygen atom is quite large but flat, having a cigar-like form. Again the equatorial ligands tilt away from the nitrosyl group, the average  $\text{N}_{\text{NO}}\text{-Fe-L}_{\text{eq}}$ -angle is  $97^\circ$ . Hydrogen bonds from O6 to O42 and from O91 to O22 connect different molecules to form a two-dimensional double-layer parallel to (010) (see Table 2.2). Different double layers are connected by non-classical hydrogen bonds from C5 and C6. Again all nitrosyl groups are oriented identically in the direction  $[\bar{1}0\bar{1}]$ .

**Figure 2.4:**

Plot of the complex  $[Fe(heida)(NO)(OH_2)]$  in crystals of **3b**. Space group:  $Cc$ .  $CShM_{OC-6}$ : 1.238. The thermal ellipsoids are drawn at 50% probability. Interatomic distances ( $\text{\AA}$ ) and angles ( $^\circ$ ), the standard deviation of the last decimal place is given in parentheses:

Fe1–N1 1.761(3), Fe1–O21 2.055(2), Fe1–O41 2.054(2), Fe1–O6 2.101(3), Fe1–O91 2.083(2), Fe1–N2 2.223(3), N1–O1 1.107(5).

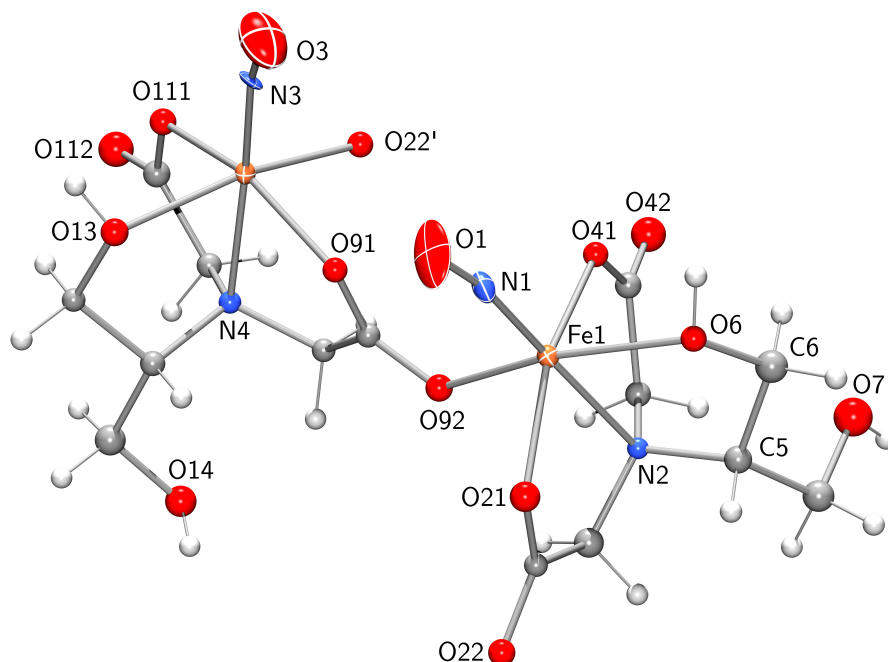
Fe1–N1–O1 170.9(4), N1–Fe1–O21 102.45(13), N1–Fe1–O41 103.14(13), N1–Fe1–O6 91.05(13), N1–Fe1–O91 92.93(12), N1–Fe1–N2 170.03(13), O21–Fe1–O6 87.66(10), O6–Fe1–O41 93.18(11), O41–Fe1–O91 90.08(11), O91–Fe1–O21 87.29(10), O21–Fe1–O41 154.37(10), O6–Fe1–O91 174.16(10), O21–Fe1–N2 77.94(10), O41–Fe1–N2 77.10(10), O6–Fe1–N2 78.99(11), O91–Fe1–N2 97.04(10).

**Table 2.2:** Distances [ $\text{\AA}$ ] and angles [ $^\circ$ ] of hydrogen bonds in **3b**, the standard deviation of the last decimal place is given in parentheses.

Donor	Hydrogen Atom	Acceptor	$d(D-H)$	$d(H\cdots A)$	$d(D\cdots A)$	$\alpha(D-H\cdots A)$
O6	H86	O42 <sup>i</sup>	0.84	1.78	2.588(4)	160.6
O91	H911	O22 <sup>ii</sup>	0.82(3)	1.83(3)	2.649(4)	173(4)
O91	H912	O22 <sup>iii</sup>	0.83(3)	1.80(3)	2.621(4)	171(5)
C5	H51	O41 <sup>iv</sup>	0.99	2.64	3.277(4)	122.5
C6	H62	O6 <sup>iv</sup>	0.99	2.54	3.468(4)	155.5

Symmetry code: <sup>i</sup>  $-1 + x, y, z$ ; <sup>ii</sup>  $x, y, -1 + z$ ; <sup>iii</sup>  $1/2 + x, 1/2 - y, -1/2 + z$ ; <sup>iv</sup>  $x, 1 - y, 1/2 + z$ .

## 2.2.3 [Fe(dhpida)(NO)]

**Figure 2.5:**

Plot of the complex [Fe(dhpida)(NO)] in crystals of **3c**. Space group:  $P2_12_12_1$ .  $CShM_{OC-6}$ : 0.794 (Fe1), 0.910 (Fe2). The thermal ellipsoids are drawn at 50 % probability. Interatomic distances (Å) and angles (°), the standard deviation of the last decimal place is given in parentheses:

Fe1–N1 1.752(8), Fe1–N2 2.232(8), Fe1–O21 2.037(7), Fe1–O41 2.059(7), Fe1–O6 2.130(7), Fe1–O92 2.082(7), N1–O1 1.148(11), Fe2–N3 1.765(8), Fe2–N4 2.226(8), Fe2–O111 2.056(7), Fe2–O91 2.036(6), Fe2–O13 2.112(7), Fe2–O22<sup>i</sup> 2.075(7), N3–O3 1.130(12).

Fe1–N1–O1 169.9(9), N1–Fe1–O21 98.2(4), N1–Fe1–O41 105.6(3), N1–Fe1–O6 95.1(3), N1–Fe1–O92 103.3(4), N1–Fe1–N2 173.0(4), O21–Fe1–O92 86.9(3), O92–Fe1–O41 85.9(3), O41–Fe1–O6 85.1(3), O6–Fe1–O21 94.7(3), O21–Fe1–O41 156.2(3), O6–Fe1–O92 161.1(3), O21–Fe1–N2 77.9(3), O41–Fe1–N2 78.6(3), O6–Fe1–N2 79.5(3), O92–Fe1–N2 82.5(3), Fe2–N3–O3 161.6(9), N3–Fe2–O91 96.0(4), N3–Fe2–O111 107.8(3), N3–Fe2–O13 92.4(3), N3–Fe2–O22<sup>i</sup> 104.7(3), N3–Fe2–N4 169.2(4), O91–Fe2–O13 94.4(3), O13–Fe2–O111 86.7(3), O111–Fe2–O22<sup>i</sup> 85.6(3), O22<sup>i</sup>–Fe2–O91 86.5(3), O91–Fe2–O111 156.1(3), O13–Fe2–O22<sup>i</sup> 162.7(3), O91–Fe2–N4 77.9(3), O111–Fe2–N4 78.9(3), O13–Fe2–N4 79.4(3), O22<sup>i</sup>–Fe2–N4 84.0(3).

Symmetry code: <sup>i</sup>  $-1 + x, y, z$ .

*N*-(1,3-Dihydroxypropane-2-yl)iminodiacetate (dhpida, **2c**) is a derivative of heida (**2b**). It is obtained by substituting the hydroxyethyl group in heida by a 1,3-dihydroxypropyl group, thus gaining a pentadentate ligand. It was synthesized in order to obtain {FeNO}<sup>7</sup>

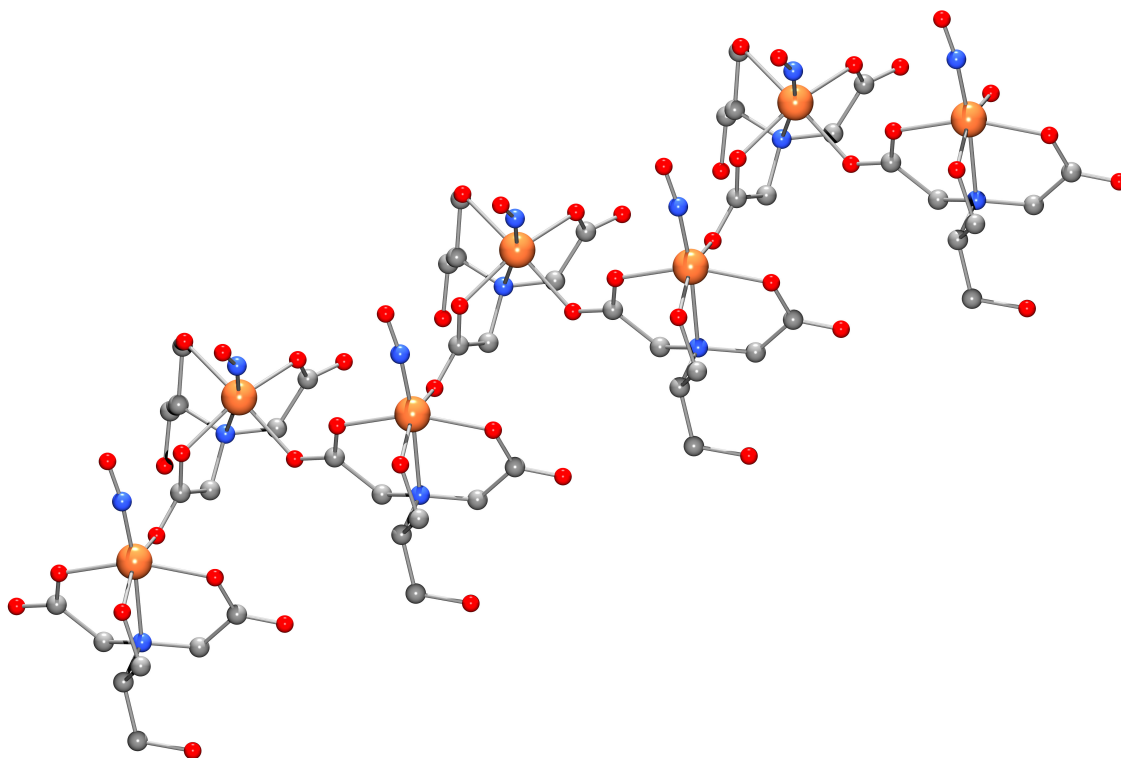
compounds without aqua ligands. Following the general procedures, only  $[Fe(dhpida)(OH_2)_2] \cdot 2H_2O$  (**4c**) was obtained (see page 25). It lacks the nitrosyl ligand and **2c** coordinates only as tetradentate ligand. Therefore the preparation was repeated in ethanol to prevent the coordination of aqua ligands,  $Fe(OTf)_2$  was used as iron source. After bubbling nitric oxide through the ethanolic solution, it turns dark green, as the aqueous solutions do. Diffusion of acetone for two weeks results in the formation of dark green crystals of *OC*-6-13-*N*-(1,3-dihydroxypropane-2-yl)iminodiacetonitrosyliron (**3c**) in 12 % yield.

**3c** crystallizes from ethanol/acetone in the orthorhombic space group  $P2_12_12_1$  with sixteen formula units in the primitive cell. Due to bad crystal quality, only the iron atom and the nitrosyl moiety were refined anisotropically. The molecule consists of one iron atom coordinated octahedrally by one nitrosyl ligand and dhpida. The pentadentate ligand dhpida coordinates facially with only four donor atoms in the same fashion as heida does: with its nitrogen atom, both acetate groups and one of its hydroxy groups. Three five-membered chelate rings are formed, two of them twisted on Fe1–N2, one twisted on C5–C6. The two acetate groups coordinate *trans* to each other, the nitrosyl ligand coordinates *trans* to the nitrogen atom of dhpida. The second hydroxy group bends away from the iron atom and forms a hydrogen bond to a neighboring molecule. Hence one position at the iron atom remains unoccupied and is coordinated by a carbonyl-oxygen atom of dhpida of an adjacent complex, thus a zigzag chain of  $[Fe(dhpida)(NO)]_n$  is formed. The molecule shows no intramolecular symmetry, the asymmetric unit consists of two molecules  $[Fe(dhpida)(NO)]$  (**3c**). The Fe–N–O moiety has an average bond angle of  $166^\circ$  with the oxygen atom pointing towards the acetate group coordinating the adjacent iron atom. When the axial direction is defined along the two nitrogen atoms, it is obvious that all equatorial ligands tilt away from the nitrosyl ligand, resulting in an average  $N_{NO}-Fe-L_{eq}$ -angle of  $100^\circ$ . Both hydroxy groups form hydrogen bonds to acetate groups of neighboring molecules, thus forming a three-dimensional network (see Table 2.3). It is quite surprising that the pentadentate coordination of dhpida is so disfavored. Obviously, the intramolecular strain is too heavy, so that, rather, a polymer chain is formed.

**Table 2.3:** Distances [ $\text{\AA}$ ] and angles [ $^\circ$ ] of hydrogen bonds in **3c**, the standard deviation of the last decimal place is given in parentheses.

Donor	Hydrogen Atom	Acceptor	$d(D-H)$	$d(H\cdots A)$	$d(D\cdots A)$	$\alpha(D-H\cdots A)$
O6	H86	O111 <sup>i</sup>	0.84	1.80	2.631(9)	172.3
O7	H87	O42 <sup>ii</sup>	0.84	1.90	2.739(11)	174.4
O13	H813	O41 <sup>iii</sup>	0.84	1.74	2.577(10)	175.0
O14	H814	O112 <sup>iv</sup>	0.84	1.90	2.727(11)	166.4

Symmetry code: <sup>i</sup>  $1 - x, -1/2 + y, 1/2 - z$ ; <sup>ii</sup>  $1/2 + x, 1/2 - y, 1 - z$ ; <sup>iii</sup>  $1 - x, 1/2 + y, 1/2 - z$ ; <sup>iv</sup>  $1 + x, y, z$ .

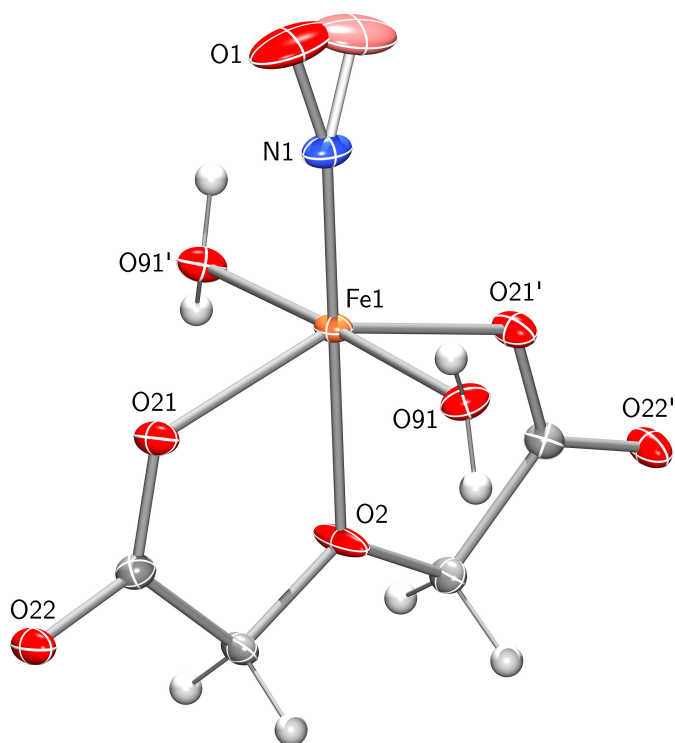


**Figure 2.6:** Plot of the zigzag chain of  $[\{\text{Fe}(\text{dhpida})(\text{NO})\}_n]$  in crystals of **3c**.

#### 2.2.4 $[\text{Fe}(\text{NO})(\text{OH}_2)_2(\text{oda})]$

Oxodiacetate (oda, **2d**) is a derivative of iminodiacetate (**2a**), obtained by replacing the nitrogen atom by an oxygen atom. Using it as a ligand for  $\{\text{FeNO}\}^7$  compounds, a dark-green aqueous solution is gained. Crystals of *OC*-6-14-diaquanitrosyloxodiacetatoiron (**3d**) are obtained in 21 % yield as dark green blocks, by the diffusion of acetone into the aqueous solution for two weeks.

**3d** crystallizes from water/acetone in the orthorhombic space group *Aba2* with four formula units in the primitive cell. The molecule consists of one iron atom coordinated octahedrally by one nitrosyl ligand, oda and two aqua ligands. oda coordinates meridionally as a tridentate ligand, forming two planar five-membered chelate rings. The nitrosyl ligand coordinates *trans* to the central oxygen atom of oda, thus defining the axial direction. The equatorial coordination sphere is completed by the two aqua ligands coordinating *trans* to each other. The molecule contains an intramolecular two-fold axis defined by N1–Fe1–O2, hence the asymmetric unit contains one-half molecule of  $[\text{Fe}(\text{NO})(\text{OH}_2)_2(\text{oda})]$  (**3d**). The two-fold axis results in a disordering of the nitrosyl-oxygen atom with two equally occupied positions. The Fe–N–O moiety has a bond angle of  $165^\circ$  with the oxygen atom pointing in the direction of one acetate group. The thermal ellipsoids of the nitrosyl-oxygen atom are quite large

**Figure 2.7:**

Plot of the complex  $[\text{Fe}(\text{NO})(\text{OH}_2)_2(\text{oda})]$  in crystals of **3d**. Space group:  $Aba2$ .  $\text{CShM}_{\text{OC-6}}$ : 1.464. The thermal ellipsoids are drawn at 50% probability. Interatomic distances ( $\text{\AA}$ ) and angles ( $^\circ$ ), the standard deviation of the last decimal place is given in parentheses:

$\text{Fe1-N1}$  1.769(4),  $\text{Fe1-O2}$  2.123(4),  $\text{Fe1-O21}$  2.0663(13),  $\text{Fe1-O91}$  2.0757(11),  $\text{N1-O1}$  1.146(5).  
 $\text{Fe1-N1-O1}$  164.6(4),  $\text{N1-Fe1-O21}$  105.76(4),  $\text{N1-Fe1-O91}$  91.49(5),  $\text{N1-Fe1-O2}$  180.00,  $\text{O21-Fe1-O91}$  90.25(5),  $\text{O91-Fe1-O21}^i$  88.94(5),  $\text{O21-Fe1-O21}^i$  148.48(7),  $\text{O91-Fe1-O91}^i$  177.02(7),  $\text{O21-Fe1-O2}$  74.24(4),  $\text{O91-Fe1-O2}$  88.51(5).

Symmetry code:  $^i 1 - x, 1 - y, z$ .

but flat, having a discus-like form. Yet they are smaller than in complexes **3a** and **3b** due to the disordering of the oxygen atom. In contrast to complexes **3a**, **3b** and **3c** only the acetato ligands tilt away from the nitrosyl group, with a  $\text{N}_{\text{NO}}\text{-Fe-O}_{\text{Ac}}$ -angle of  $106^\circ$ . The  $\text{N}_{\text{NO}}\text{-Fe-O}_{\text{H}_2\text{O}}$ -angle is  $91^\circ$ . The aqua ligands form hydrogen bonds to the carbonyl-oxygen atoms of neighboring molecules, thus forming a three-dimensional network (see Table 2.4). All nitrosyl groups point in the direction  $[00\bar{1}]$ .

What makes **3d** special, is the fact that so far only two crystalline single-core and two crystalline multi-core quartet- $\{\text{FeNO}\}^7$  compounds with only oxo ligands are known in the literature.<sup>[68,69,74]</sup>

**Table 2.4:** Distances [ $\text{\AA}$ ] and angles [ $^\circ$ ] of hydrogen bonds in **3d**, the standard deviation of the last decimal place is given in parentheses.

Donor	Hydrogen Atom	Acceptor	$d(\text{D-H})$	$d(\text{H}\cdots\text{A})$	$d(\text{D}\cdots\text{A})$	$\alpha(\text{D-H}\cdots\text{A})$
O91	H911	O22 <sup>ii</sup>	0.81(2)	1.88(2)	2.676(2)	170(3)
O91	H912	O21 <sup>iii</sup>	0.82(2)	2.60(2)	3.124(2)	123(2)
O91	H912	O22 <sup>iii</sup>	0.82(2)	1.83(2)	2.647(2)	178(3)

Symmetry code: <sup>ii</sup>  $1 - x, 1/2 - y, -1/2 + z$ ; <sup>iii</sup>  $-1/2 + x, 1/2 - y, z$ .

### 2.2.5 [Fe(NO)(OH<sub>2</sub>)<sub>2</sub>(phida)] · H<sub>2</sub>O

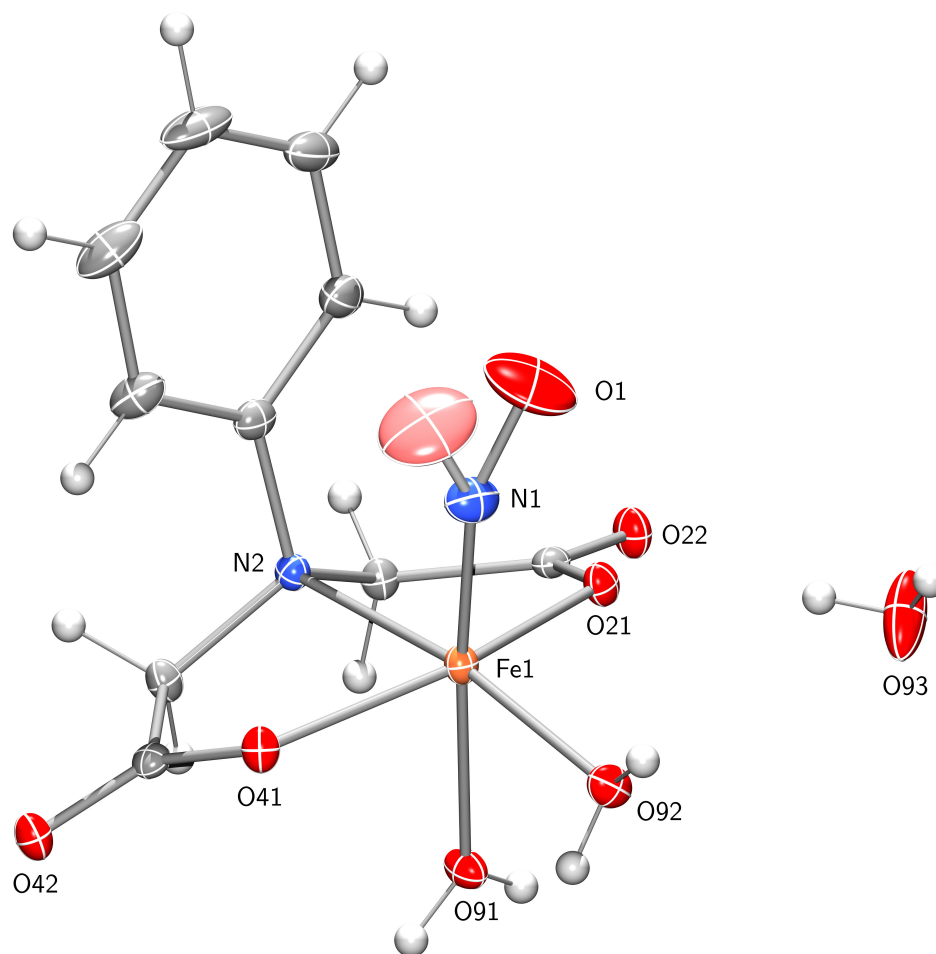
*N*-Phenyliminodiacetate (phida, **2e**) is obtained by substituting the nitrogen atom of ida with a phenyl group. The aromatic iminodiacetic acid derivative can act as a tridentate ligand to build {FeNO}<sup>7</sup> compounds. By the diffusion of acetone into the brown-green aqueous solutions, large brown-green crystals of *OC*-6-14-diaquanitrosyl-*N*-phenyliminodiacetatoiron hydrate (**3e**) are obtained in 40% yield.

**Table 2.5:** Distances [ $\text{\AA}$ ] and angles [ $^\circ$ ] of hydrogen bonds in **3e**, the standard deviation of the last decimal place is given in parentheses.

Donor	Hydrogen Atom	Acceptor	$d(\text{D-H})$	$d(\text{H}\cdots\text{A})$	$d(\text{D}\cdots\text{A})$	$\alpha(\text{D-H}\cdots\text{A})$
O91	H911	O22 <sup>i</sup>	0.80(1)	1.94(1)	2.720(2)	168(2)
O91	H912	O42 <sup>ii</sup>	0.81(1)	1.99(1)	2.774(2)	163(2)
O92	H921	O93 <sup>i</sup>	0.80(1)	1.79(1)	2.578(2)	170(2)
O92	H922	O42 <sup>iii</sup>	0.81(1)	1.86(1)	2.663(2)	175(2)
O93	H931	O22 <sup>iv</sup>	0.80(1)	1.99(2)	2.733(2)	154(3)
O93	H932	O21	0.79(1)	1.99(1)	2.780(2)	172(3)

Symmetry code: <sup>i</sup>  $1/2 + x, y, 1/2 - z$ ; <sup>ii</sup>  $-1/2 + x, y, 1/2 - z$ ; <sup>iii</sup>  $3/2 - x, 1/2 + y, z$ ; <sup>iv</sup>  $1/2 - x, 1/2 + y, z$ .

**3e** crystallizes from water/acetone in the orthorhombic space group *Pbca* with eight formula units in the primitive cell. The molecule consists of one iron atom coordinated distorted octahedrally by one nitrosyl ligand, phida and two aqua ligands. phida coordinates meridionally as a tridentate ligand, defining the equatorial plane. Two five-membered chelate rings are formed, both with a twist conformation, twisted on Fe1–N2. The nitrosyl ligand coordinates axial, the two aqua ligands occupy the remaining axial and equatorial positions. **3e** contains no intramolecular symmetry. It crystallizes as a hydrate, the asymmetric unit contains one molecule of [Fe(NO)(OH<sub>2</sub>)<sub>2</sub>(phida)] (**3e**) and one water molecule. The nitrosyl-

**Figure 2.8:**

Plot of the compound  $[Fe(NO)(OH_2)_2(phida)] \cdot H_2O$  in crystals of **3e**. Space group: *Pbca*.  $CShM_{OC-6}$ : 1.349. The thermal ellipsoids are drawn at 50% probability. Interatomic distances (Å) and angles (°), the standard deviation of the last decimal place is given in parentheses:

Fe1–N1 1.7834(17), Fe1–N2 2.3194(16), Fe1–O21 2.0271(12), Fe1–O41 2.0241(12), Fe1–O91 2.1849(13), Fe1–O92 2.0223(13), N1–O1 1.169(4).

Fe1–N1–O1<sup>a</sup> 148.4(2), Fe1–N1–O1<sup>b</sup> 150.9(3), N1–Fe1–O21 95.45(6), N1–Fe1–O41 99.36(6), N1–Fe1–O91 175.97(6), N1–Fe1–O92 94.55(7), N1–Fe1–N2 98.10(7), O21–Fe1–O91 82.73(5), O91–Fe1–O41 83.75(5), O21–Fe1–O41 152.42(5), O21–Fe1–O92 100.72(5), O41–Fe1–O92 101.15(5), O91–Fe1–O92 82.29(5), O21–Fe1–N2 77.33(5), O41–Fe1–N2 77.64(5), O91–Fe1–N2 85.04(5), O92–Fe1–N2 167.33(6).

oxygen atom is disordered and occupies two positions nearly equally (59% and 41%), the Fe–N–O bond angle is 148° and 151° respectively with the oxygen atoms pointing towards the acetate groups. The thermal ellipsoids of the nitrosyl-oxygen atom are quite large but flat, having a disc-like form. Yet they are smaller than in complexes **3a** and **3b** due to the disordering of the oxygen atom. All equatorial ligands again tilt away from the nitrosyl group with an average  $N_{NO}\text{--}Fe\text{--}O/N$ -angle of 97°. The structure of **3e** is unique with respect

to several properties. It is the only structure with the nitrosyl group coordinating *cis* to the central heteroatom of the diacetic acid ligand. At the same time it has the smallest Fe–N–O bond angle. However, the Fe–N<sub>NO</sub> bond length of 1.78 Å lies within the range found for all other structures. Furthermore **3e** features the shortest Fe–O<sub>ac</sub> bond length (2.02 Å) and the shortest and longest Fe–O<sub>H<sub>2</sub>O</sub> bond lengths (2.02 Å for H<sub>2</sub>O<sub>eq</sub> and 2.19 Å for H<sub>2</sub>O<sub>ax</sub>). The aqua ligands and the water of crystallization form hydrogen bonds to acetate groups of neighboring molecules (see Table 2.5). Thus a two-dimensional double-layer parallel to (001) is formed with the phenyl rings pointing away from that layer on both sides. Through  $\pi$ – $\pi$ -interactions neighboring double-layers are connected to each other.

### 2.2.6 [Fe(bnida)(NO)(OH<sub>2</sub>)<sub>2</sub>]

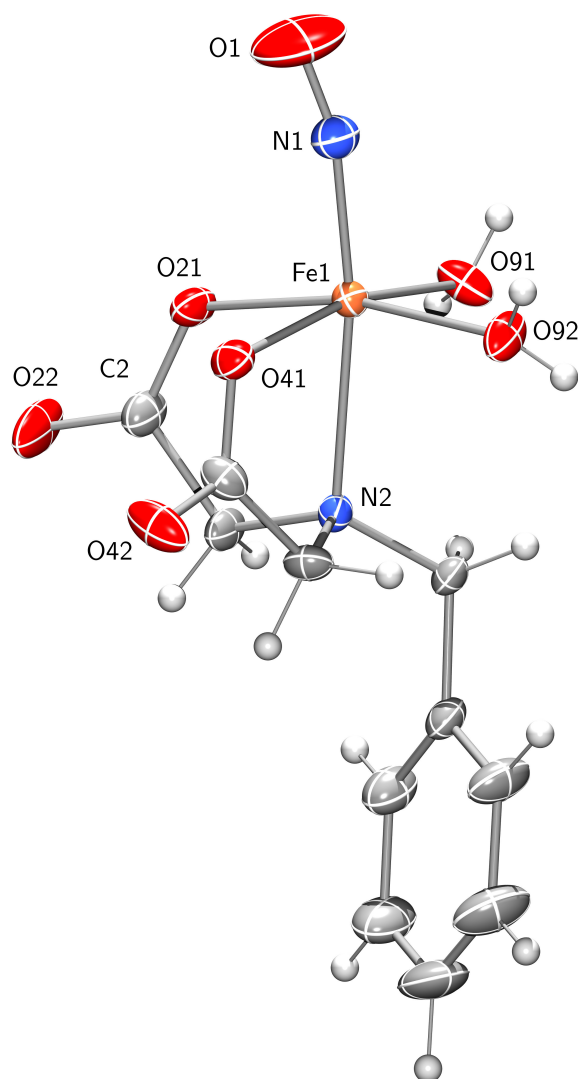
*N*-Benzyliminodiacetate (bnida, **2f**) can be derived from *N*-phenyliminodiacetate (**2e**) by inserting a methylene group between the nitrogen atom and the phenyl substituent. Used as a ligand in the synthesis of {FeNO}<sup>7</sup> compounds, dark-green aqueous solutions are obtained. After four weeks of diffusion of acetone into the solution, dark-green crystals of *OC*-6-22-diaqua-*N*-benzyliminodiacetatonitrosyliron (**3f**) are obtained in 15 % yield.

**Table 2.6:** Distances [Å] and angles [°] of hydrogen bonds in **3f**, the standard deviation of the last decimal place is given in parentheses.

Donor	Hydrogen Atom	Acceptor	$d(\text{D-H})$	$d(\text{H}\cdots\text{A})$	$d(\text{D}\cdots\text{A})$	$\alpha(\text{D-H}\cdots\text{A})$
O91	H911	O21 <sup>i</sup>	0.79(2)	1.89(3)	2.649(3)	162(4)
O91	H912	O42 <sup>ii</sup>	0.79(3)	1.89(3)	2.647(3)	160(5)
O92	H921	O41 <sup>iii</sup>	0.79(3)	1.89(3)	2.680(3)	178(4)
O92	H922	O22 <sup>iv</sup>	0.79(2)	1.87(3)	2.638(4)	168(5)

Symmetry code: <sup>i</sup>  $1 - x, 1/2 + y, 1 - z$ ; <sup>ii</sup>  $-1 + x, y, z$ ; <sup>iii</sup>  $2 - x, 1/2 + y, 1 - z$ ; <sup>iv</sup>  $x, 1 + y, z$ .

**3f** crystallizes from water/acetone in the monoclinic space group  $P2_1$  with two formula units in the primitive cell. The molecule consists of one iron atom coordinated octahedrally by one nitrosyl ligand, bnida and two aqua ligands. bnida coordinates facially as a tridentate ligand, forming two five-membered chelate rings with envelope conformation on C2 and N2 respectively. The nitrosyl ligand coordinates *trans* to the nitrogen atom of bnida. The molecule contains no intramolecular symmetry, the asymmetric unit consists of one molecule of [Fe(bnida)(NO)(OH<sub>2</sub>)<sub>2</sub>] (**3f**). The Fe–N–O moiety has a bond angle of 165° with the oxygen atom pointing in between the two acetate groups. The whole nitrosyl ligand is pointing in that direction with a N<sub>NO</sub>–Fe–N<sub>ida</sub>-angle of 171°. The thermal ellipsoid of the nitrosyl-oxygen atom is quite large but flat, having the form of a discus. When the axial direction is defined along the two nitrogen atoms, it is obvious that all equatorial ligands

**Figure 2.9:**

Plot of the complex  $[\text{Fe}(\text{bnida})(\text{NO})(\text{OH}_2)_2]$  in crystals of **3f**. Space group:  $P2_1$ .  $\text{CShM}_{\text{OC-6}}$ : 0.427. The thermal ellipsoids are drawn at 50% probability. Interatomic distances ( $\text{\AA}$ ) and angles ( $^\circ$ ), the standard deviation of the last decimal place is given in parentheses:

$\text{Fe1-N1}$  1.780(3),  $\text{Fe1-N2}$  2.322(2),  $\text{Fe1-O21}$  2.052(2),  $\text{Fe1-O41}$  2.067(2),  $\text{Fe1-O91}$  2.039(2),  $\text{Fe1-O92}$  2.056(2),  $\text{N1-O1}$  1.129(4).

$\text{Fe1-N1-O1}$  164.8(4),  $\text{N1-Fe1-O21}$  96.10(16),  $\text{N1-Fe1-O41}$  94.20(10),  $\text{N1-Fe1-O91}$  99.40(10),  $\text{N1-Fe1-O92}$  96.89(16),  $\text{N1-Fe1-N2}$  170.51(14),  $\text{O21-Fe1-O41}$  85.80(9),  $\text{O41-Fe1-O92}$  89.90(10),  $\text{O92-Fe1-O91}$  89.83(12),  $\text{O91-Fe1-O21}$  91.37(10),  $\text{O21-Fe1-O92}$  166.58(9),  $\text{O41-Fe1-O91}$  166.34(9),  $\text{O21-Fe1-N2}$  78.16(11),  $\text{O41-Fe1-N2}$  77.97(8),  $\text{O91-Fe1-N2}$  88.37(9),  $\text{O92-Fe1-N2}$  88.51(11).

tilt away from the nitrosyl ligand, resulting in an average  $\text{N}_{\text{NO}}\text{-Fe-L}_{\text{eq}}$ -angle of  $97^\circ$ . Both aqua ligands form hydrogen bonds to acetate groups of neighboring molecules (see Table 2.6). Thus a two-dimensional double-layer is formed, parallel to (001) with the phenyl rings

pointing away from that layer on both sides similar to the crystal structure of **3e**. Through  $\pi$ - $\pi$ -interactions neighboring double-layers are connected to each other. The nitrosyl groups point in the directions [001] and [00 $\bar{1}$ ].

### 2.2.7 [Fe(brbnida)(NO)(OH<sub>2</sub>)<sub>2</sub>]

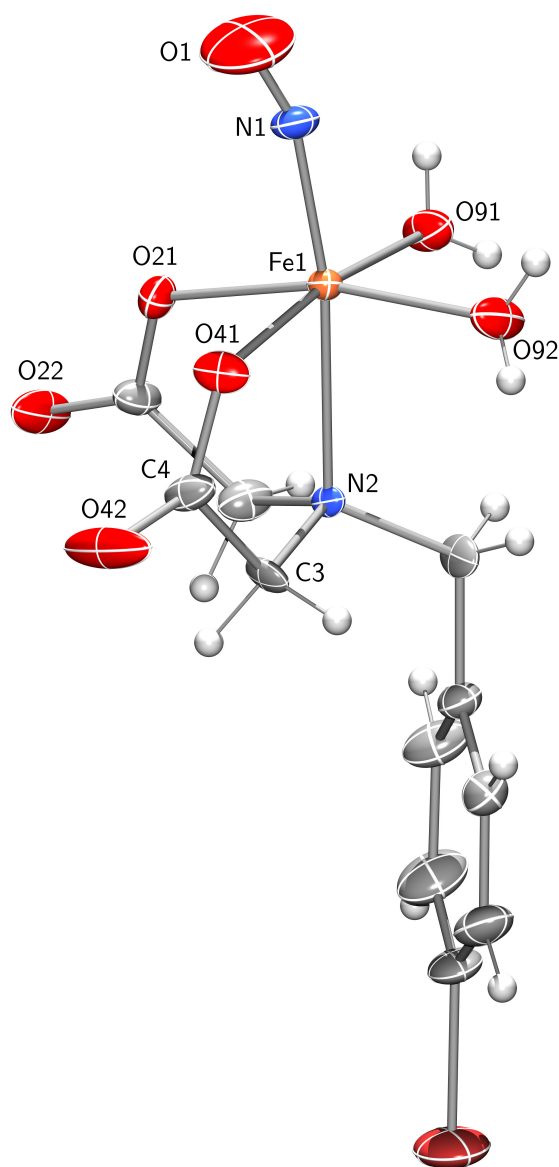
*N*-(*p*-Bromobenzyl)iminodiacetate (brbnida, **2g**) is a direct derivative of bnida (**2f**). Used as a ligand in the synthesis of {FeNO}<sup>7</sup> compounds, dark-green aqueous solutions are obtained. After one week of diffusion of acetone into the solution, dark-green crystals of *OC*-6-22-di-aqua-*N*-*p*-bromobenzyliminodiacetatonitrosyliron (**3g**) are obtained in 13% yield.

**Table 2.7:** Distances [Å] and angles [°] of hydrogen bonds in **3g**, the standard deviation of the last decimal place is given in parentheses.

Donor	Hydrogen Atom	Acceptor	$d(\text{D-H})$	$d(\text{H}\cdots\text{A})$	$d(\text{D}\cdots\text{A})$	$\alpha(\text{D-H}\cdots\text{A})$
O91	H911	O42 <sup>i</sup>	0.78(3)	1.84(4)	2.590(6)	163(6)
O91	H912	O21 <sup>ii</sup>	0.78(3)	1.97(4)	2.729(5)	165(7)
O92	H921	O22 <sup>iii</sup>	0.77(3)	1.90(3)	2.665(6)	174(6)
O92	H922	O41 <sup>iv</sup>	0.78(3)	1.91(4)	2.654(5)	160(7)

Symmetry code: <sup>i</sup>  $x, 1 + y, z$ ; <sup>ii</sup>  $-x, 1/2 + y, 1 - z$ ; <sup>iii</sup>  $1 + x, y, z$ ; <sup>iv</sup>  $1 - x, 1/2 + y, 1 - z$ .

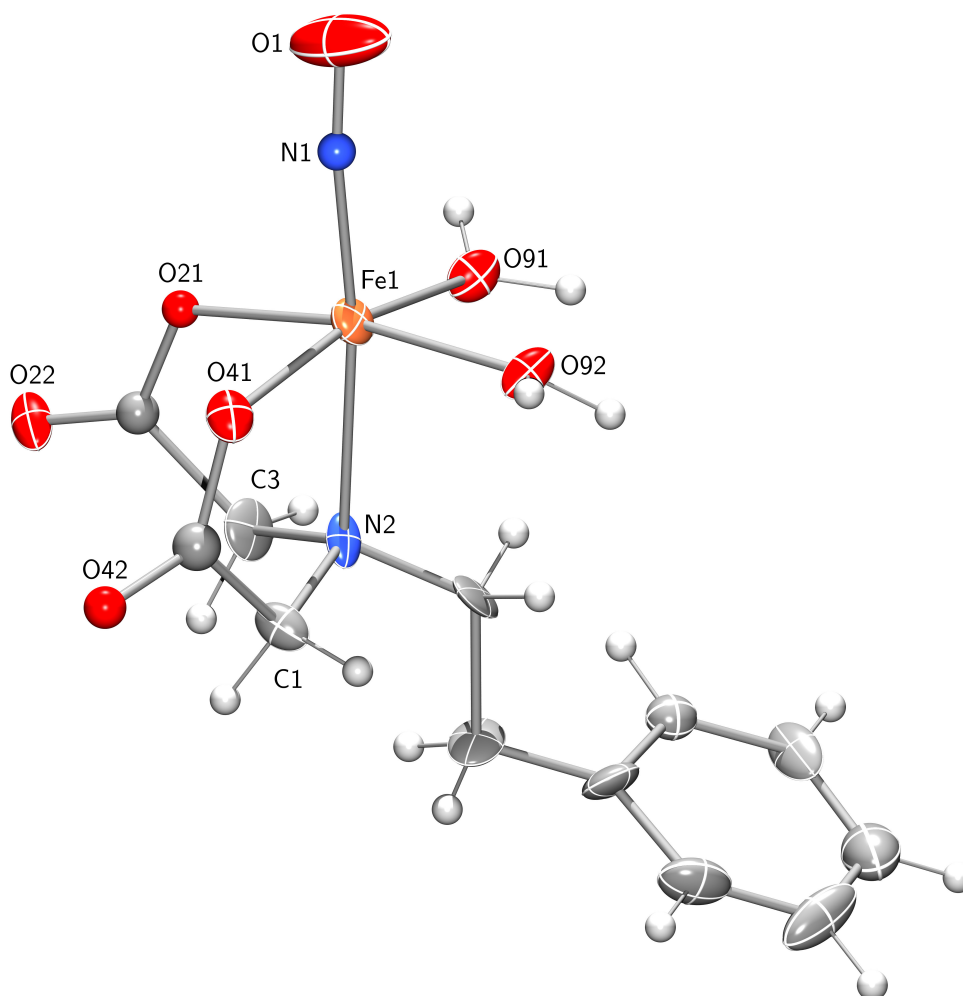
**3g** crystallizes from water/acetone in the monoclinic space group  $P2_1$  with two formula units in the primitive cell. The crystal structure is isomorphous to that of **3f**. The molecule consists of one iron atom coordinated octahedrally by one nitrosyl ligand, brbnida and two aqua ligands. brbnida coordinates facially as a tridentate ligand. Two five-membered chelate rings are formed. One is twisted on C3-C4, the other one has an envelope conformation on N2. The nitrosyl ligand coordinates *trans* to the nitrogen atom of brbnida. The molecule contains no intramolecular symmetry, the asymmetric unit consists of one molecule of [Fe(brbnida)(NO)(OH<sub>2</sub>)<sub>2</sub>] (**3g**). The Fe-N-O moiety has a bond angle of 158° with the oxygen atom pointing in the direction of one acetate group. The whole nitrosyl ligand is pointing in that direction with a N<sub>NO</sub>-Fe-N<sub>ida</sub>-angle of 171°. The thermal ellipsoid of the nitrosyl-oxygen atom is quite large but flat, having the form of a discus. When the axial direction is defined along the two nitrogen atoms, it is obvious that all equatorial ligands tilt away from the nitrosyl ligand, resulting in an average N<sub>NO</sub>-Fe-L<sub>eq</sub>-angle of 96°. Both aqua ligands form hydrogen bonds to acetate groups of neighboring molecules (see Table 2.7). A two-dimensional double-layer is formed, parallel to (001) with the phenyl rings pointing away from that layer on both sides. Through  $\pi$ - $\pi$ -interactions neighboring double-layers are connected to each other. The nitrosyl groups point in the directions [001] and [00 $\bar{1}$ ].

**Figure 2.10:**

Plot of the complex  $[Fe(brbnida)(NO)(OH_2)_2]$  in crystals of **3g**. Space group:  $P2_1$ .  $CShM_{OC-6}$ : 0.452. The thermal ellipsoids are drawn at 50% probability. Interatomic distances ( $\text{\AA}$ ) and angles ( $^\circ$ ), the standard deviation of the last decimal place is given in parentheses:

Fe1–N1 1.798(5), Fe1–N2 2.331(3), Fe1–O21 2.053(4), Fe1–O41 2.038(4), Fe1–O91 2.062(4), Fe1–O92 2.044(4), N1–O1 1.094(7).

Fe1–N1–O1 158.0(5), N1–Fe1–O21 95.88(18), N1–Fe1–O41 94.00(19), N1–Fe1–O91 96.8(2), N1–Fe1–O92 98.0(2), N1–Fe1–N2 170.6(2), O21–Fe1–O41 86.49(16), O41–Fe1–O92 91.24(19), O92–Fe1–O91 89.6(2), O91–Fe1–O21 90.02(19), O21–Fe1–O92 166.02(15), O41–Fe1–O91 168.95(15), O21–Fe1–N2 77.87(14), O41–Fe1–N2 78.76(15), O91–Fe1–N2 90.26(18), O92–Fe1–N2 88.15(17).

2.2.8 [Fe(NO)(OH<sub>2</sub>)<sub>2</sub>(pheida)]**Figure 2.11:**

Plot of the complex [Fe(NO)(OH<sub>2</sub>)<sub>2</sub>(pheida)] in crystals of **3h**. Space group: *Pbca*. CShM<sub>OC-6</sub>: 0.404. The thermal ellipsoids are drawn at 50% probability. Interatomic distances (Å) and angles (°), the standard deviation of the last decimal place is given in parentheses:

Fe1–N1 1.776(13), Fe1–N2 2.287(13), Fe1–O21 2.059(10), Fe1–O41 2.023(11), Fe1–O91 2.082(12), Fe1–O92 2.065(11), O1–N1 1.097(19).

Fe1–N1–O1 167.6(13), N1–Fe1–O21 94.8(5), N1–Fe1–O41 97.8(5), N1–Fe1–O91 97.7(5), N1–Fe1–O92 96.7(5), N1–Fe1–N2 172.8(5), O21–Fe1–O41 86.5(4), O41–Fe1–O92 91.9(4), O92–Fe1–O91 89.7(4), O91–Fe1–O21 88.9(4), O21–Fe1–O92 168.5(4), O41–Fe1–O91 164.1(4), O21–Fe1–N2 79.1(4), O41–Fe1–N2 78.3(4), O91–Fe1–N2 85.9(4), O92–Fe1–N2 89.4(4).

*N*-(2-Phenylethyl)iminodiacetate (pheida, **2h**) can be derived from *N*-phenyliminodiacetate (**2e**) by inserting an ethylene group between the nitrogen atom and the phenyl substituent.

Used as a ligand in the synthesis of  $\{\text{FeNO}\}^7$  compounds, dark-green aqueous solutions are obtained. After four weeks of diffusion of acetone into the solution, dark-green crystals of *OC*-6-22-diaquanitrosyl-*N*-(2-phenylethyl)iminodiacetatoiron (**3h**) are obtained in 9% yield.

**3h** crystallizes from water/acetone in the orthorhombic space group *Pbca* with eight formula units in the primitive cell. The molecule consists of one iron atom coordinated octahedrally by one nitrosyl ligand, pheida and two aqua ligands. pheida coordinates facially as a tridentate ligand. Two five-membered chelate rings are formed with an envelope conformation on C1 and C3 respectively. The nitrosyl ligand coordinates *trans* to the nitrogen atom of pheida. The molecule contains no intramolecular symmetry, the asymmetric unit consists of one molecule of  $[\text{Fe}(\text{NO})(\text{OH}_2)_2(\text{pheida})]$  (**3h**). The Fe–N–O moiety has a bond angle of  $168^\circ$  with the oxygen atom pointing in the direction of one aqua ligand. The thermal ellipsoid of the nitrosyl-oxygen atom is quite large but flat, having the form of a cigar. When the axial direction is defined along the two nitrogen atoms, it is obvious that all equatorial ligands tilt away from the nitrosyl ligand, resulting in an average  $\text{N}_{\text{NO}}\text{--Fe--L}_{\text{eq}}$ -angle of  $97^\circ$ . Both aqua ligands form hydrogen bonds to acetate groups of neighboring molecules, thus forming a three-dimensional network.

**Table 2.8:** Distances [ $\text{\AA}$ ] and angles [ $^\circ$ ] of hydrogen bonds in **3h**, the standard deviation of the last decimal place is given in parentheses.

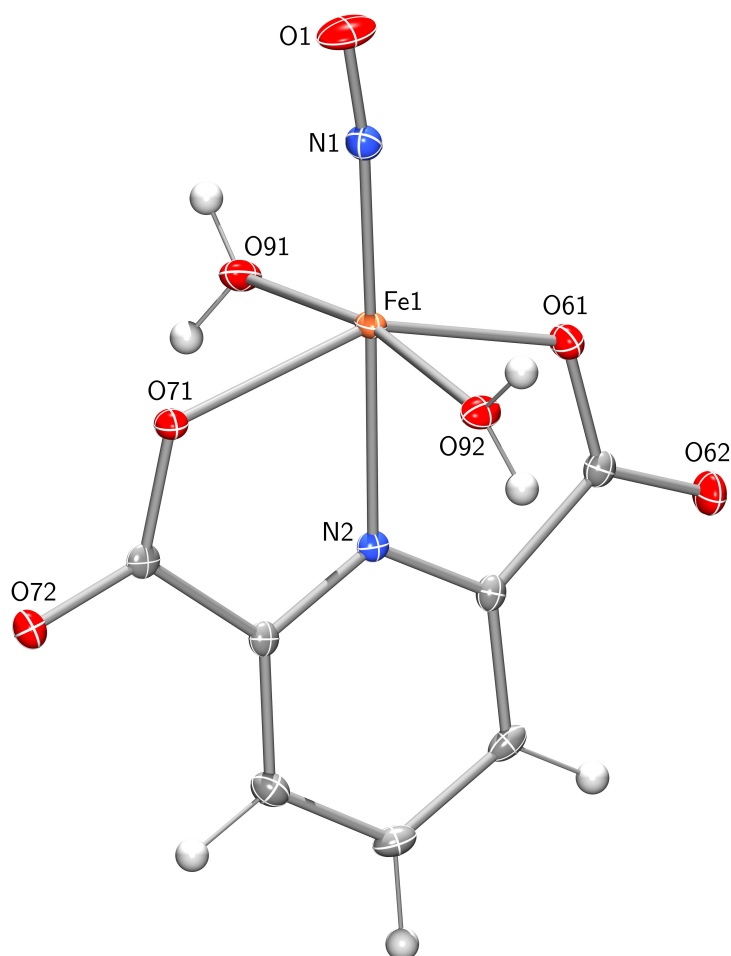
Donor	Hydrogen Atom	Acceptor	$d(\text{D--H})$	$d(\text{H}\cdots\text{A})$	$d(\text{D}\cdots\text{A})$	$\alpha(\text{D--H}\cdots\text{A})$
O91	H911	O41 <sup>i</sup>	0.95(7)	1.76(7)	2.711(15)	175(14)
O91	H912	O21 <sup>ii</sup>	0.95(7)	1.87(11)	2.679(14)	142(13)
O92	H921	O22 <sup>iii</sup>	0.88(7)	1.85(10)	2.639(15)	149(15)
O92	H922	O42 <sup>i</sup>	0.95(7)	1.69(7)	2.630(15)	169(15)

Symmetry code: <sup>i</sup>  $3/2 - x, 1/2 + y, z$ ; <sup>ii</sup>  $1 - x, 1 - y, 1 - z$ ; <sup>iii</sup>  $1 + x, y, z$ .

### 2.2.9 $[\text{Fe}(\text{dipic})(\text{NO})(\text{OH}_2)_2]$

Pyridine-2,6-dicarboxylate (dipicolinate, dipic, **2i**) can be seen as a derivative of iminodiacetate (**2a**). Used as a ligand in the synthesis of  $\{\text{FeNO}\}^7$  compounds, dark-green aqueous solutions are obtained. After one day of diffusion of acetone into the solution, dark-green crystals of *OC*-6-12-diaquadipicolinatinitrosyliron (**3i**) are obtained in 38% yield.

**3i** crystallizes from water/acetone in the orthorhombic space group  $P2_12_12_1$  with eight formula units in the primitive cell. The molecule consists of one iron atom coordinated octahedrally by one nitrosyl ligand, dipic and two aqua ligands. dipic coordinates meridionally

**Figure 2.12:**

Plot of the complex  $[\text{Fe}(\text{dipic})(\text{NO})(\text{OH}_2)_2]$  in crystals of **3i**. Space group:  $P2_12_12_1$ .  $\text{CShM}_{\text{OC-6}}$ : 1.278. The thermal ellipsoids are drawn at 50% probability. Interatomic distances ( $\text{\AA}$ ) and angles ( $^\circ$ ), the standard deviation of the last decimal place is given in parentheses:

$\text{Fe1-N1}$  1.765(2),  $\text{Fe1-N2}$  2.0957(19),  $\text{Fe1-O61}$  2.1122(18),  $\text{Fe1-O71}$  2.1466(18),  $\text{Fe1-O91}$  2.1278(19),  $\text{Fe1-O92}$  2.1043(19),  $\text{N1-O1}$  1.142(3).

$\text{Fe1-N1-O1}$  170.9(2),  $\text{N1-Fe1-O61}$  107.69(9),  $\text{N1-Fe1-O71}$  102.41(9),  $\text{N1-Fe1-O91}$  95.46(9),  $\text{N1-Fe1-O92}$  93.34(10),  $\text{N1-Fe1-N2}$  176.42(10),  $\text{O61-Fe1-O91}$  91.13(7),  $\text{O91-Fe1-O71}$  86.03(7),  $\text{O71-Fe1-O92}$  86.33(7),  $\text{O92-Fe1-O61}$  91.81(7),  $\text{O61-Fe1-O71}$  149.91(7),  $\text{O91-Fe1-O92}$  169.41(7),  $\text{O61-Fe1-N2}$  75.24(7),  $\text{O71-Fe1-N2}$  74.69(7),  $\text{O91-Fe1-N2}$  86.49(7),  $\text{O92-Fe1-N2}$  84.43(7).

**Table 2.9:** Distances [ $\text{\AA}$ ] and angles [ $^\circ$ ] of hydrogen bonds in **3i**, the standard deviation of the last decimal place is given in parentheses.

Donor	Hydrogen Atom	Acceptor	$d(\text{D-H})$	$d(\text{H}\cdots\text{A})$	$d(\text{D}\cdots\text{A})$	$\alpha(\text{D-H}\cdots\text{A})$
O91	H911	O141 <sup>i</sup>	0.78(2)	1.96(2)	2.736(3)	174(4)
O91	H912	O142 <sup>ii</sup>	0.78(2)	1.95(2)	2.729(3)	172(3)
O92	H921	O61 <sup>iii</sup>	0.80(2)	2.00(2)	2.774(3)	164(3)
O92	H922	O132	0.78(2)	1.92(2)	2.702(3)	173(3)
O93	H931	O71 <sup>iv</sup>	0.79(2)	1.91(2)	2.699(3)	174(3)
O93	H932	O72 <sup>v</sup>	0.79(2)	1.93(2)	2.702(3)	167(3)
O94	H941	O131 <sup>vi</sup>	0.79(2)	2.53(3)	3.027(2)	123(3)
O94	H941	O132 <sup>vi</sup>	0.79(2)	1.98(2)	2.761(3)	176(3)
O94	H942	O62 <sup>vii</sup>	0.79(2)	1.99(2)	2.761(3)	168(3)

Symmetry code: <sup>i</sup>  $-1 + x, -1 + y, z$ ; <sup>ii</sup>  $1 - x, -1/2 + y, 1/2 - z$ ; <sup>iii</sup>  $1/2 + x, 1/2 - y, 1 - z$ ;  
<sup>iv</sup>  $x, 1 + y, z$ ; <sup>v</sup>  $1 - x, 1/2 + y, 1/2 - z$ ; <sup>vi</sup>  $1/2 + x, 3/2 - y, 1 - z$ ; <sup>vii</sup>  $1 + x, y, z$ .

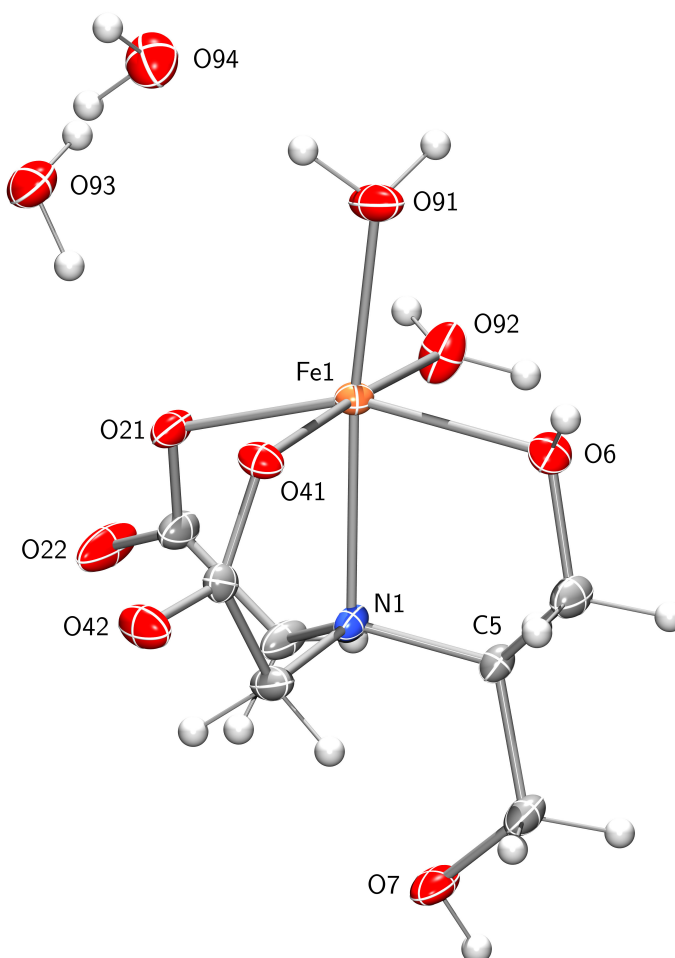
as a tridentate ligand, the nitrosyl ligand coordinates *trans* to the nitrogen atom of dipic. Two planar five-membered chelate rings are formed. The molecule contains no intramolecular symmetry, the asymmetric unit consists of two molecules of  $[\text{Fe}(\text{dipic})(\text{NO})(\text{OH}_2)_2]$  (**3i**). The Fe–N–O moiety has an average bond angle of  $174^\circ$  with the oxygen atom pointing in between one acetate group and one aqua ligand. The thermal ellipsoid of the nitrosyl-oxygen atom is quite small, compared to all other structures obtained. When the axial direction is defined along the two nitrogen atoms, it is obvious that all equatorial ligands tilt away from the nitrosyl ligand, resulting in an average  $\text{N}_{\text{NO}}\text{-Fe-L}_{\text{eq}}$ -angle of  $99^\circ$ . Both aqua ligands form hydrogen bonds to acetate groups of neighboring molecules, thus forming a three-dimensional network (see Table 2.9).

## 2.3 Iron(II) aminocarboxylates

With the aminocarboxylato ligands **2c,i-k**, iron(II) complexes without bearing a nitrosyl group were obtained. These complexes are of some relevance to compare bond lengths and angles and how they are influenced by the coordination of the nitrosyl ligand.

### 2.3.1 $[\text{Fe}(\text{dhpida})(\text{OH}_2)_2] \cdot 2\text{H}_2\text{O}$

The pentadentate ligand *N*-(1,3-dihydroxypropane-2-yl)iminodiacetate (dhpida, **2c**) has already been described above (see page 12). After preparing the dark-green aqueous  $\{\text{FeNO}\}^7$

**Figure 2.13:**

Plot of the compound  $[\text{Fe}(\text{dhpida})(\text{OH}_2)_2] \cdot 2 \text{H}_2\text{O}$  in crystals of **4c**. Space group:  $P2_1/c$ .  $\text{CShM}_{\text{OC-6}}$ : 1.434. The thermal ellipsoids are drawn at 50 % probability. Interatomic distances ( $\text{\AA}$ ) and angles ( $^\circ$ ), the standard deviation of the last decimal place is given in parentheses:

$\text{Fe1-N1}$  2.2354(16),  $\text{Fe1-O21}$  2.1306(15),  $\text{Fe1-O41}$  2.0933(15),  $\text{Fe1-O6}$  2.1474(15),  $\text{Fe1-O91}$  2.0541(17),  $\text{Fe1-O92}$  2.0886(16).

$\text{N1-Fe1-O21}$  77.35(6),  $\text{N1-Fe1-O41}$  79.51(6),  $\text{N1-Fe1-O6}$  79.06(6),  $\text{N1-Fe1-O92}$  96.02(6),  $\text{N1-Fe1-O91}$  167.60(7),  $\text{O21-Fe1-O41}$  91.63(6),  $\text{O41-Fe1-O6}$  90.79(6),  $\text{O6-Fe1-O92}$  89.98(6),  $\text{O92-Fe1-O21}$  85.74(6),  $\text{O21-Fe1-O6}$  155.42(6),  $\text{O41-Fe1-O92}$  175.23(6),  $\text{O21-Fe1-O91}$  112.87(6),  $\text{O41-Fe1-O91}$  92.81(6),  $\text{O6-Fe1-O91}$  91.43(6),  $\text{O92-Fe1-O91}$  91.88(6).

**Table 2.10:** Distances [Å] and angles [°] of hydrogen bonds in **4c**, the standard deviation of the last decimal place is given in parentheses.

Donor	Hydrogen Atom	Acceptor	$d(\text{D-H})$	$d(\text{H}\cdots\text{A})$	$d(\text{D}\cdots\text{A})$	$\alpha(\text{D-H}\cdots\text{A})$
O6	H86	O41 <sup>i</sup>	0.84	1.83	2.674(2)	177.4
O7	H87	O22 <sup>ii</sup>	0.84	1.83	2.656(2)	169.0
O91	H911	O42 <sup>iii</sup>	0.89(1)	1.85(2)	2.733(2)	168(3)
O91	H912	O94	0.91(2)	1.75(2)	2.650(2)	174(3)
O92	H921	O22 <sup>iv</sup>	0.89(1)	1.84(2)	2.720(2)	175(3)
O92	H922	O93 <sup>v</sup>	0.88(2)	1.79(2)	2.665(2)	172(3)
O93	H931	O21	0.89(2)	1.92(2)	2.790(2)	167(3)
O93	H932	O7 <sup>vi</sup>	0.89(2)	1.89(2)	2.773(2)	173(3)
O94	H941	O6 <sup>vii</sup>	0.89(2)	2.53(3)	3.086(2)	121(2)
O94	H941	O93	0.89(2)	2.16(2)	2.925(3)	144(3)
O94	H942	O42 <sup>viii</sup>	0.89(2)	1.88(2)	2.760(2)	168(3)

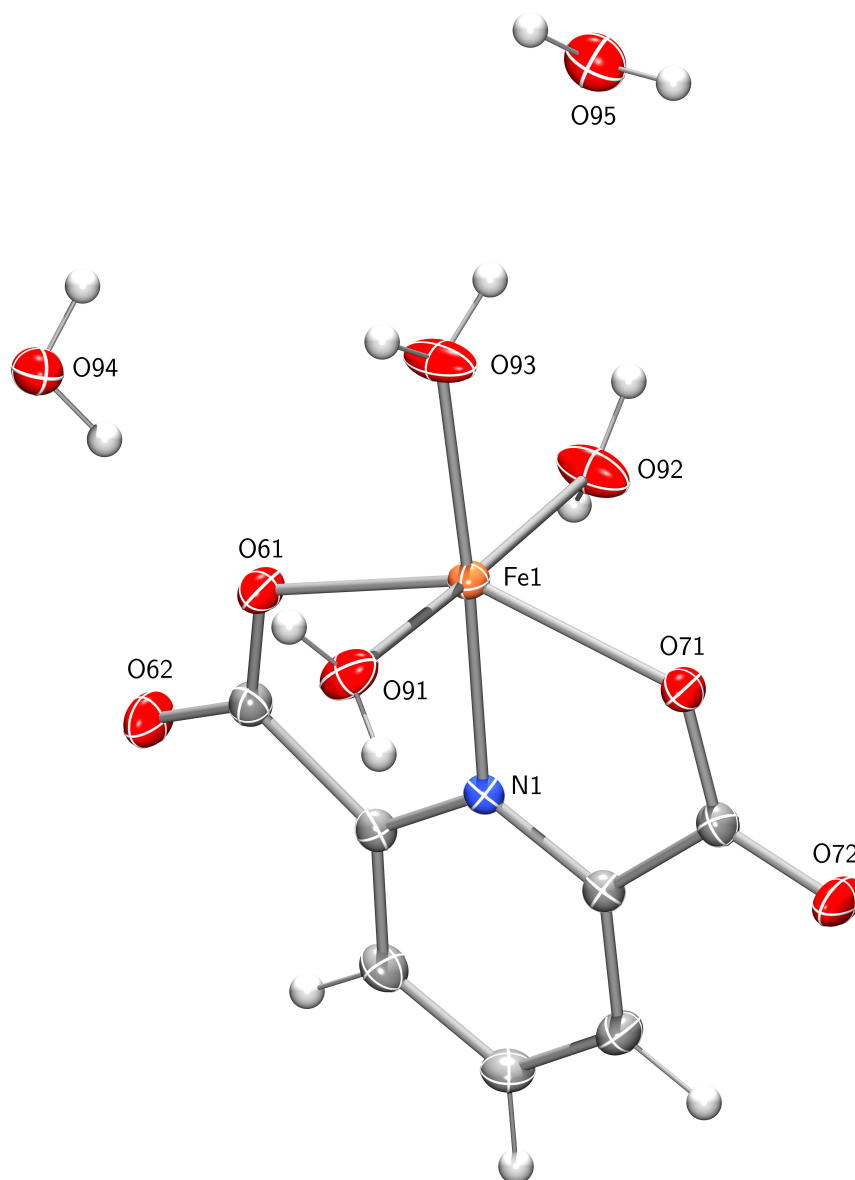
Symmetry code: <sup>i</sup>  $-x, 1-y, -z$ ; <sup>ii</sup>  $1+x, 1/2-y, 1/2+z$ ; <sup>iii</sup>  $x, y, -1+z$ ; <sup>iv</sup>  $x, 1/2-y, -1/2+z$ ; <sup>v</sup>  $1+x, y, z$ ; <sup>vi</sup>  $-1+x, y, -1+z$ ; <sup>vii</sup>  $-1+x, y, z$ ; <sup>viii</sup>  $-1-x, 1-y, -z$ .

solution in the usual way, nearly colorless crystals of *OC*-6-32-diaqua-*N*-(1,3-dihydroxypropane-2-yl)iminodiacetatoiron dihydrate (**4c**) are obtained after the diffusion of acetone in 25 % yield.

**4c** crystallizes from water/acetone in the monoclinic space group  $P2_1/c$  with four formula units in the primitive cell. The molecule consists of one iron atom coordinated octahedrally by dhpida and two aqua ligands. As in compound **3c**, dhpida coordinates facially as a tetradentate ligand with its nitrogen atom, both acetate groups and one of its hydroxy groups, forming three five-membered chelate rings with envelope conformation on C5, twisted on Fe1–O41 and twisted on Fe1–N1. In contrast to **3c** both acetate groups coordinate *cis* to each other. The second hydroxy group bends away from the iron atom and builds a hydrogen bond to a neighboring molecule. The molecule contains no intramolecular symmetry and crystallizes as a hydrate. The asymmetric unit consists of one molecule of  $[\text{Fe}(\text{dhpida})(\text{OH}_2)_2]$  (**4c**) and two water molecules. Every hydrogen atom bound to an oxygen atom forms hydrogen bonds to acetate groups of neighboring molecules or to neighboring water molecules, thus forming a three-dimensional network (see Table 2.10).

### 2.3.2 $[\text{Fe}(\text{dipic})(\text{OH}_2)_3] \cdot 2\text{H}_2\text{O}$

From an aqueous solution of equal amounts of  $\text{FeSO}_4 \cdot 7\text{H}_2\text{O}$  and dipicolinic acid, ( $\text{H}_2\mathbf{2i}$ ), red crystals of *OC*-6-13-triaquadipicolinatoiron dihydrate (**4i**) can be obtained after five days. They are fairly air stable and dissolve quickly in water; the aqueous solution oxidize

**Figure 2.14:**

Plot of the compound  $[\text{Fe}(\text{dipic})(\text{OH}_2)_3] \cdot 2\text{H}_2\text{O}$  in crystals of **4i**. Space group:  $P2_1/n$ .  $\text{CShM}_{\text{OC-6}}$ : 2.100. The thermal ellipsoids are drawn at 50% probability. Interatomic distances ( $\text{\AA}$ ) and angles ( $^\circ$ ), the standard deviation of the last decimal place is given in parentheses:

$\text{Fe1-N1}$  2.0848(10),  $\text{Fe1-O61}$  2.1576(9),  $\text{Fe1-O71}$  2.1689(9),  $\text{Fe1-O91}$  2.1333(10),  $\text{Fe1-O92}$  2.1064(11),  $\text{Fe1-O93}$  2.0584(10).

$\text{N1-Fe1-O61}$  74.75(4),  $\text{N1-Fe1-O71}$  74.51(4),  $\text{N1-Fe1-O91}$  94.71(4),  $\text{N1-Fe1-O92}$  89.64(4),  $\text{N1-Fe1-O93}$  174.33(4),  $\text{O61-Fe1-O91}$  92.97(4),  $\text{O91-Fe1-O71}$  88.44(3),  $\text{O71-Fe1-O92}$  90.98(4),  $\text{O92-Fe1-O61}$  89.92(4),  $\text{O61-Fe1-O71}$  149.24(3),  $\text{O91-Fe1-O92}$  175.29(4),  $\text{O61-Fe1-O93}$  100.11(4),  $\text{O71-Fe1-O93}$  110.66(4),  $\text{O91-Fe1-O93}$  87.86(4),  $\text{O92-Fe1-O93}$  87.97(4).

**Table 2.11:** Distances [Å] and angles [°] of hydrogen bonds in **4i**, the standard deviation of the last decimal place is given in parentheses.

Donor	Hydrogen Atom	Acceptor	$d(\text{D-H})$	$d(\text{H}\cdots\text{A})$	$d(\text{D}\cdots\text{A})$	$\alpha(\text{D-H}\cdots\text{A})$
O91	H911	O71 <sup>i</sup>	0.82(1)	1.93(1)	2.744(1)	174(2)
O91	H912	O95 <sup>ii</sup>	0.82(1)	1.99(1)	2.805(1)	170(2)
O92	H921	O62 <sup>iii</sup>	0.83(1)	1.85(1)	2.680(1)	172(2)
O92	H922	O94 <sup>iii</sup>	0.83(1)	2.00(1)	2.820(1)	170(2)
O93	H931	O95	0.82(1)	2.07(1)	2.862(1)	161(2)
O93	H932	O72 <sup>i</sup>	0.83(1)	1.84(1)	2.670(1)	175(2)
O94	H941	O61	0.82(1)	2.04(1)	2.823(1)	160(2)
O94	H942	O72 <sup>iv</sup>	0.82(1)	1.90(1)	2.712(1)	173(2)
O95	H951	O62 <sup>v</sup>	0.83(1)	2.04(1)	2.846(1)	165(2)
O95	H952	O94 <sup>vi</sup>	0.83(1)	1.98(1)	2.796(1)	169(2)

Symmetry code: <sup>i</sup>  $1/2 - x, 1/2 + y, 1/2 - z$ ; <sup>ii</sup>  $-1/2 + x, 1/2 - y, -1/2 + z$ ; <sup>iii</sup>  $3/2 - x, -1/2 + y, 1/2 - z$ ; <sup>iv</sup>  $1/2 + x, 1/2 - y, 1/2 + z$ ; <sup>v</sup>  $-1/2 + x, 1/2 - y, 1/2 + z$ ; <sup>vi</sup>  $1 - x, 1 - y, 1 - z$ .

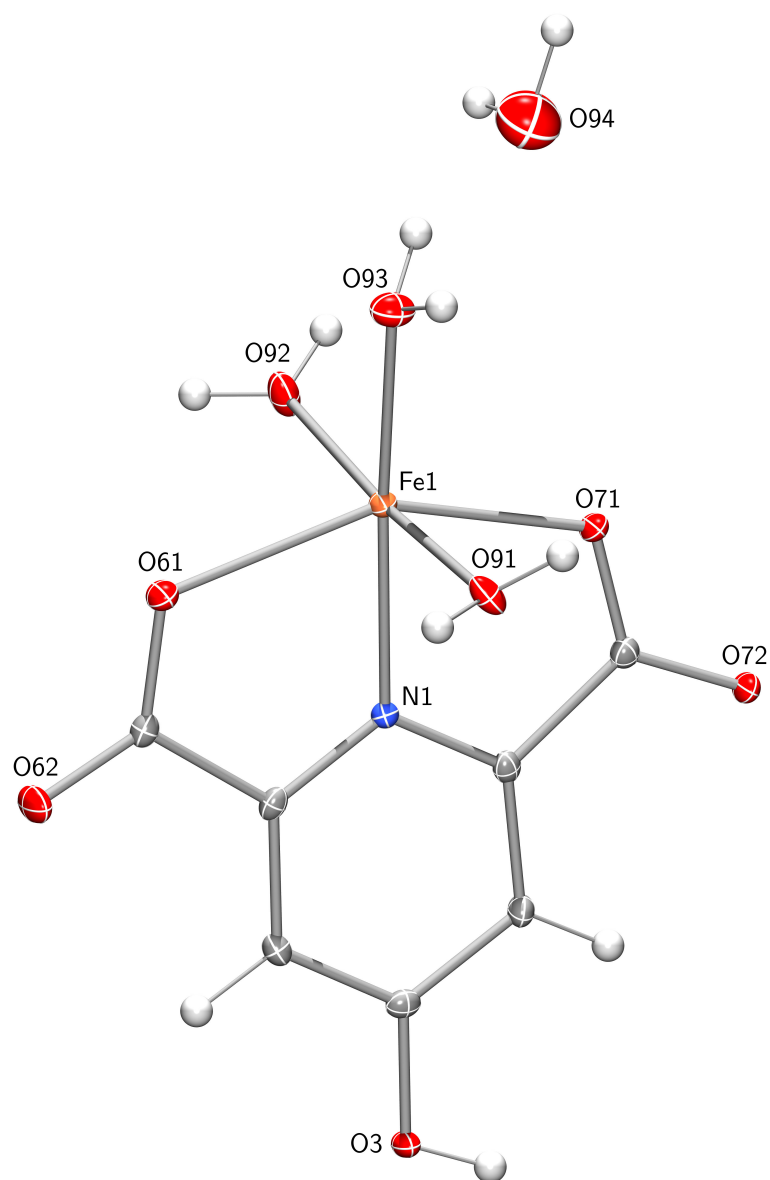
quite quickly. Crystals of  $[\text{Fe}(\text{dipic})(\text{OH}_2)_3]$  have already been published<sup>[86]</sup>, however, not in the dihydrate form.

**4i** crystallizes from water/acetone in the monoclinic space group  $P2_1/n$  with four formula units in the primitive cell. The molecule consists of one iron atom coordinated octahedrally by dipic and three aqua ligands. dipic coordinates meridionally as a tridentate ligand, forming two planar five-membered chelate rings. The remaining three positions are occupied by aqua ligands. The molecule contains no intramolecular symmetry and crystallizes as a dihydrate. The asymmetric unit consists of one molecule of  $[\text{Fe}(\text{dipic})(\text{OH}_2)_3]$  (**4i**) and two water molecules. Hydrogen bonds from aqua ligands to acetate groups of neighboring molecules form two-dimensional layers parallel to (001). The water of crystallization connects the separate layers by hydrogen bonds to form a three-dimensional network (see Table 2.11).

### 2.3.3 $[\text{Fe}(\text{ca})(\text{OH}_2)_3] \cdot 0.5 \text{H}_2\text{O}$

4-Hydroxypyridine-2,6-dicarboxylate (ca, **2j**) is a derivative of dipic (**2i**). From an aqueous solution of equal amounts of  $\text{FeSO}_4 \cdot 7 \text{H}_2\text{O}$  and  $\text{H}_2\text{ca}$ , orange crystals of *OC-6-13*-triaqua-chelidaminatoiron hemihydrate (**4j**) can be obtained after five weeks. They are fairly air stable and dissolve quickly in water; the aqueous solution oxidize quite quickly.

**4j** crystallizes from water/acetone in the monoclinic space group  $P2_1/c$  with four formula units in the primitive cell. The molecule consists of one iron atom coordinated octahedrally by ca and three aqua ligands. ca coordinates meridionally as a tridentate ligand. Two

**Figure 2.15:**

Plot of the compound  $[\text{Fe}(\text{ca})(\text{OH}_2)_3] \cdot 0.5 \text{H}_2\text{O}$  in crystals of **4j**. Space group:  $P2_1/c$ .  $\text{CShM}_{\text{OC-6}}$ : 2.728. The thermal ellipsoids are drawn at 50% probability. Interatomic distances ( $\text{\AA}$ ) and angles ( $^\circ$ ), the standard deviation of the last decimal place is given in parentheses:

$\text{Fe1-N1}$  2.0986(18),  $\text{Fe1-O61}$  2.2397(15),  $\text{Fe1-O71}$  2.2006(16),  $\text{Fe1-O91}$  2.0850(17),  $\text{Fe1-O92}$  2.1369(17),  $\text{Fe1-O93}$  2.0637(16).

$\text{N1-Fe1-O61}$  73.51(6),  $\text{N1-Fe1-O71}$  74.15(6),  $\text{N1-Fe1-O91}$  100.82(7),  $\text{N1-Fe1-O92}$  86.32(7),  $\text{N1-Fe1-O93}$  171.17(7),  $\text{O61-Fe1-O91}$  87.19(6),  $\text{O91-Fe1-O71}$  93.84(7),  $\text{O71-Fe1-O92}$  87.81(7),  $\text{O92-Fe1-O61}$  95.18(6),  $\text{O61-Fe1-O71}$  147.24(6),  $\text{O91-Fe1-O92}$  172.86(7),  $\text{O61-Fe1-O93}$  106.64(6),  $\text{O71-Fe1-O93}$  106.12(7),  $\text{O91-Fe1-O93}$  87.99(7),  $\text{O92-Fe1-O93}$  84.87(7).

**Table 2.12:** Distances [Å] and angles [°] of hydrogen bonds in **4j**, the standard deviation of the last decimal place is given in parentheses.

Donor	Hydrogen Atom	Acceptor	$d(\text{D-H})$	$d(\text{H}\cdots\text{A})$	$d(\text{D}\cdots\text{A})$	$\alpha(\text{D-H}\cdots\text{A})$
O3	H83	O61 <sup>i</sup>	0.82	1.79	2.601(2)	170.9
O91	H911	O72 <sup>ii</sup>	0.83(2)	1.95(2)	2.774(2)	177(3)
O91	H912	O62 <sup>iii</sup>	0.83(2)	1.87(2)	2.695(2)	172(3)
O92	H921	O71 <sup>iv</sup>	0.83(2)	1.95(2)	2.737(2)	159(3)
O92	H922	O3 <sup>v</sup>	0.83(2)	2.03(2)	2.792(2)	153(3)
O93	H931	O72 <sup>iv</sup>	0.83(2)	2.01(2)	2.830(2)	172(3)
O93	H932	O72 <sup>vi</sup>	0.82(2)	2.04(2)	2.855(2)	172(3)
O94	H941	O72 <sup>ii</sup>	0.84(2)	2.16(3)	2.935(5)	153(6)
O94	H941	O93 <sup>vii</sup>	0.84(2)	2.49(7)	3.050(5)	124(6)
O94	H942	O62 <sup>viii</sup>	0.84(2)	1.97(2)	2.806(5)	170(8)

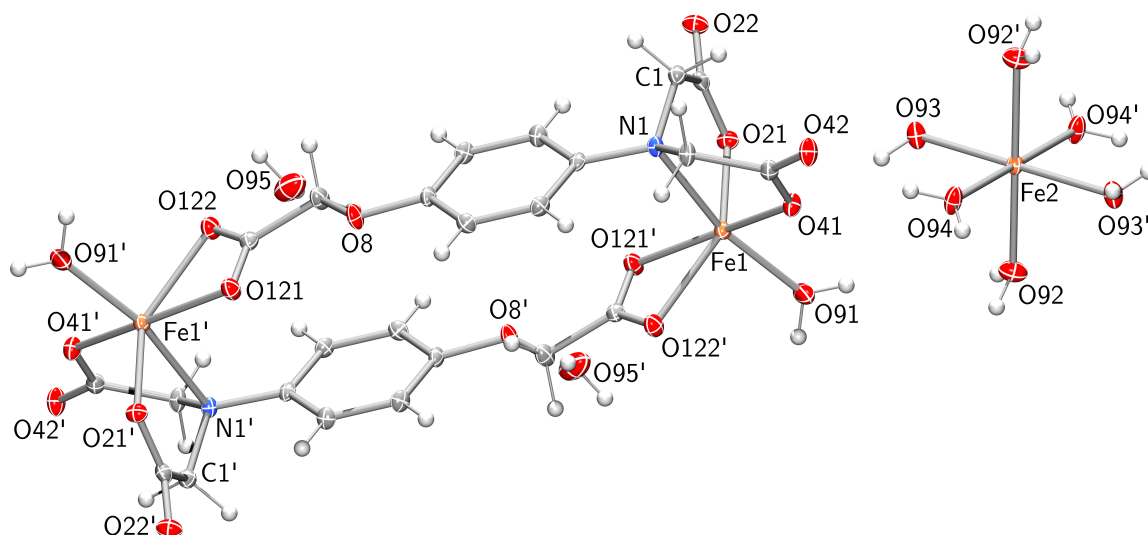
Symmetry code: <sup>i</sup>  $x, 3/2 - y, 1/2 + z$ ; <sup>ii</sup>  $1 - x, 2 - y, 1 - z$ ; <sup>iii</sup>  $-x, 1/2 + y, 1/2 - z$ ; <sup>iv</sup>  $1 - x, 1 - y, 1 - z$ ; <sup>v</sup>  $-x, 1 - y, 1 - z$ ; <sup>vi</sup>  $x, 3/2 - y, -1/2 + z$ ; <sup>vii</sup>  $1 - x, 1/2 + y, 1/2 - z$ ; <sup>viii</sup>  $1 + x, y, z$ .

planar five-membered chelate rings are formed. The remaining three positions are occupied by aqua ligands. The molecule contains no intramolecular symmetry and crystallizes as semihydrate. The asymmetric unit consists of one molecule of  $[\text{Fe}(\text{ca})(\text{OH}_2)_3]$  (**4j**) and one-half water molecule. Every hydrogen atom bonded to an oxygen atom forms hydrogen bonds to acetate groups of neighboring molecules or to neighboring water molecules, thus forming a three-dimensional network (see Table 2.12).

### 2.3.4 $[\text{Fe}_3(\text{cpida})_2(\text{OH}_2)_8] \cdot 2\text{H}_2\text{O}$

*N*-[4-(Carboxymethoxy)phenyl]iminodiacetate (cpida, **2k**) is a derivative of *N*-phenyliminodiacetate (phida, **2e**). It is obtained by substituting phida with a carboxymethoxy group at the *para*-position. The use of **2k** as a ligand was inspired by crystal structures published by Liu *et al.*<sup>[87]</sup> The authors presented nickel(II) and cobalt(II) complexes with cpida as the ligand. Both cations form dinuclear complexes of  $[\text{Co}_2(\text{cpida})_2(\text{OH}_2)_2]^{2-}$  and  $[\text{Ni}_2(\text{cpida})_2(\text{OH}_2)_6]^{2-}$  respectively which are bridged by  $[\text{Co}(\text{OH}_2)_6]^{2+}$  or  $[\text{Ni}(\text{OH}_2)_6]^{2+}$  counterions. The intention was to obtain similar complexes with iron(II) with one or several aqua ligands substituted by nitric oxide. Unfortunately only light brown crystals of **4k** are obtained six months after preparing the dark-green aqueous  $\{\text{FeNO}\}^7$  solution in the usual way.

**4k** crystallizes from water/acetone in the triclinic space group  $P\bar{1}$  with one formula unit in the primitive cell. The crystal structure is isomorphous to that which Liu *et al.* obtained with cobalt(II) and cpida: one iron atom is coordinated tridentate facially by the iminodiacetato moiety of one ligand molecule and bidentate by the carboxymethoxy moiety of a second ligand

**Figure 2.16:**

Plot of the compound  $[\text{Fe}_3(\text{cpida})_2(\text{OH}_2)_8] \cdot 2\text{H}_2\text{O}$  in crystals of **4k**. Space group:  $P\bar{1}$ .  $\text{CShM}_{\text{OC-6}}$ : 4.387 (Fe1), 0.031 (Fe2). The thermal ellipsoids are drawn at 50% probability. Interatomic distances ( $\text{\AA}$ ) and angles ( $^\circ$ ), the standard deviation of the last decimal place is given in parentheses: Fe1–N1 2.3328(14), Fe1–O21 2.0410(12), Fe1–O41 2.0426(12), Fe1–O121<sup>i</sup> 2.2185(12), Fe1–O122<sup>i</sup> 2.1836(12), Fe1–O91 2.0504(13), Fe1–Fe1<sup>i</sup> 10.756, Fe2–O92 2.1209(13), Fe2–O93 2.1244(12), Fe2–O94 2.1165(12).

N1–Fe1–O21 79.55(5), N1–Fe1–O41 76.47(5), N1–Fe1–O121<sup>i</sup> 98.01(5), N1–Fe1–O122<sup>i</sup> 95.99(5), N1–Fe1–O91 165.38(6), O21–Fe1–O41 103.63(5), O41–Fe1–O122<sup>i</sup> 112.00(5), O122<sup>i</sup>–Fe1–O121<sup>i</sup> 59.68(5), O121<sup>i</sup>–Fe1–O21 83.39(5), O21–Fe1–O122<sup>i</sup> 142.01(5), O41–Fe1–O121<sup>i</sup> 169.90(5), O21–Fe1–O91 100.10(5), O41–Fe1–O91 89.52(6), O121<sup>i</sup>–Fe1–O91 96.45(6), O122<sup>i</sup>–Fe1–O91 93.10(5), O92–Fe2–O93 91.44(5), O92–Fe2–O94 91.96(5), O93–Fe2–O94 90.50(5), O92–Fe2–O92<sup>ii</sup> 180.00, O92–Fe2–O93<sup>iii</sup> 88.56(5), O92–Fe2–O94<sup>ii</sup> 88.04(5), O93–Fe2–O93<sup>iii</sup> 180.00, O93–Fe2–O94<sup>ii</sup> 89.50(5), O94–Fe2–O94<sup>ii</sup> 180.00.

Symmetry code: <sup>i</sup>  $1 - x, -y, 1 - z$ ; <sup>ii</sup>  $1 - x, 2 - y, -z$ .

**Table 2.13:** Distances [Å] and angles [°] of hydrogen bonds in **4k**, the standard deviation of the last decimal place is given in parentheses.

Donor	Hydrogen Atom	Acceptor	$d(\text{D-H})$	$d(\text{H}\cdots\text{A})$	$d(\text{D}\cdots\text{A})$	$\alpha(\text{D-H}\cdots\text{A})$
O91	H911	O22 <sup>ii</sup>	0.80(2)	2.05(2)	2.842(2)	169(2)
O91	H912	O22 <sup>iii</sup>	0.80(2)	1.84(2)	2.639(2)	171(2)
O92	H921	O22 <sup>ii</sup>	0.80(2)	2.01(2)	2.815(2)	175(2)
O92	H922	O95 <sup>iv</sup>	0.81(2)	1.94(2)	2.744(2)	176(2)
O93	H931	O21 <sup>ii</sup>	0.81(2)	1.97(2)	2.776(2)	173(2)
O93	H932	O41	0.80(2)	1.91(2)	2.714(2)	175(2)
O94	H941	O121 <sup>iv</sup>	0.80(2)	2.03(2)	2.802(2)	163(2)
O94	H942	O42	0.80(2)	1.99(2)	2.776(2)	171(2)
O95	H951	O8	0.81(2)	2.26(2)	3.030(2)	159(2)
O95	H952	O92 <sup>v</sup>	0.80(1)	2.61(2)	3.303(2)	145(3)
O95	H952	O93 <sup>vi</sup>	0.81(2)	2.52(2)	3.214(2)	144(3)

Symmetry code: <sup>ii</sup>  $1 - x, 1 - y, -z$ ; <sup>iii</sup>  $1 + x, y, z$ ; <sup>iv</sup>  $1 - x, 1 - y, 1 - z$ ; <sup>v</sup>  $-1 + x, -1 + y, 1 + z$ ;  
<sup>vi</sup>  $-x, 1 - y, 1 - z$ .

molecule. Two five-membered chelate rings are formed, with a twisted conformation on C1–N1 and an envelope conformation on N1. The octahedral coordination sphere is completed by one aqua ligand *trans* to the nitrogen atom. Both cpida ligands coordinate a second iron atom in the same manner to form a dinuclear  $[\text{Fe}_2(\text{cpida})_2(\text{OH}_2)_2]^{2-}$  entity with a Fe–Fe distance of 10.76 Å. A third iron atom is present as nearly perfectly octahedral  $[\text{Fe}(\text{OH}_2)_6]^{2+}$  (CShM<sub>OC-6</sub>: 0.031.). Chains of alternating  $[\text{Fe}_2(\text{cpida})_2(\text{OH}_2)_2]^{2-}$  and  $[\text{Fe}(\text{OH}_2)_6]^{2+}$  fragments, connected by hydrogen bonds are formed in the direction  $[02\bar{1}]$ . These chains, again, are connected among each other by hydrogen bonds (see Table 2.13). The compound crystallizes as a dihydrate. Due to the inversion center, the asymmetric unit consists of one-half of an  $[\text{Fe}_2(\text{cpida})_2(\text{OH}_2)_2]^{2-}$  fragment, one-half of an  $[\text{Fe}(\text{OH}_2)_6]^{2+}$  fragment and one water molecule.

## 2.4 Halogenidonitrosylferrates

Simple halogenidonitrosyl anions of iron like  $[\text{FeCl}_3(\text{NO})]^-$ ,  $[\text{FeCl}_2(\text{NO})_2]^-$  and  $[\text{FeI}_2(\text{NO})_2]^-$  are well known compounds and have been described thoroughly in literature.<sup>[42,82,88–108]</sup> Kohlschütter and Manchot were first to describe these compounds.<sup>[88–92]</sup> Later Connelly and Gardner gave an extensive characterization of five different ferrates.<sup>[97]</sup> Steimann *et al.* published the crystal structure of  $[\text{Ph}_4\text{As}][\text{FeCl}_3(\text{NO})]$ .<sup>[82]</sup> Wah *et al.* and Akutsu *et al.* published crystal structures of  $[\text{Fe}(\text{bpy})_3][\text{FeCl}_2(\text{NO})_2]$  and  $[\text{PPh}_4][\text{FeCl}_2(\text{NO})_2]$  respectively, unfortunately of rather poor quality in the first case and disordered in the second case.<sup>[103,107]</sup>

A crystal structure of  $\{\text{PPN}\}[\text{FeI}_2(\text{NO})_2]$  was published by Bryar *et al.*<sup>[104]</sup> Most recently Wilfer<sup>[109]</sup> as well as Böttcher<sup>[110]</sup> obtained new crystal structures of  $[\text{FeCl}_3(\text{NO})]^-$  and  $[\text{FeBr}_3(\text{NO})]^-$ .

These compounds can be seen as key structures in the quartet- $\{\text{FeNO}\}^7$  and doublet- $\{\text{Fe}(\text{NO})_2\}^9$  chemistry. Therefore, new and easier syntheses were searched for and the crystallization, especially of  $[\text{FeCl}_2(\text{NO})_2]^-$ , was attempted to obtain a better quality crystal structure.

### 2.4.1 $\{\text{PPN}\}[\text{FeCl}_3(\text{NO})]$

By known syntheses  $[\text{FeCl}_3(\text{NO})]^-$  can be obtained in several ways: by the addition of chlorine in  $\text{CH}_2\text{Cl}_2$  to a solution of  $\{\text{PPN}\}[\text{Fe}(\text{CO})_3(\text{NO})]$ ,<sup>[97]</sup> by the addition of HCl to a solution of  $[\text{AsPh}_4][\text{Fe}_2(\text{NO})_4\text{S}_2]$ <sup>[99]</sup> or by the addition of NO to a solution of  $\text{AsPh}_4\text{Cl}$  and  $\text{FeCl}_2$  in half-concentrated hydrochloric acid.<sup>[109]</sup>

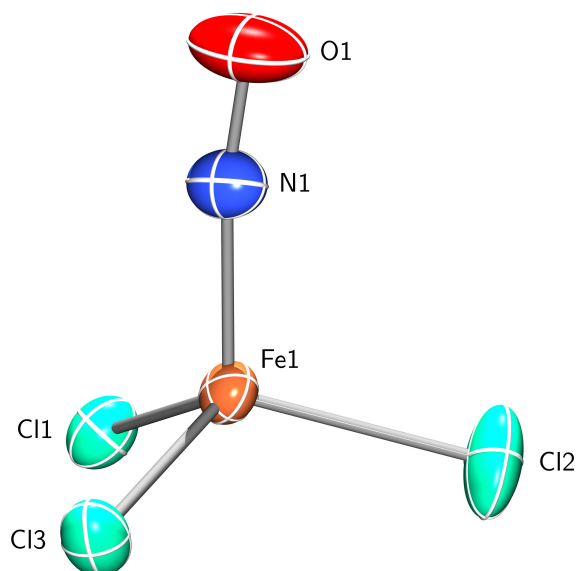


**Figure 2.17:**

Plot of the anion  $[\text{FeCl}_3(\text{NO})]^-$  in crystals of  $(\text{PPN})\mathbf{5a}$ . Space group:  $C2/c$ .  $\text{CShM}_{T-4}$ : 0.925. The thermal ellipsoids are drawn at 50 % probability. Interatomic distances ( $\text{\AA}$ ) and angles ( $^\circ$ ), the standard deviation of the last decimal place is given in parentheses: Fe1–N1 1.7394(19), Fe1–Cl1 2.2354(9), Fe1–Cl2 2.2154(9), Fe1–Cl3 2.2346(8), N1–O1 1.140(3). Fe1–N1–O1 170.88(19), N1–Fe1–Cl1 110.16(8), N1–Fe1–Cl2 105.20(7), N1–Fe1–Cl3 109.88(7), Cl1–Fe1–Cl2 111.37(3), Cl2–Fe1–Cl3 111.35(4), Cl3–Fe1–Cl1 108.84(3).

A new and simple method for the synthesis of  $\{\text{PPN}\}[\text{FeCl}_3(\text{NO})]$  has now been developed: to a solution of  $\text{Fe}(\text{OTf})_2$  in methanol,  $(\text{PPN})\text{Cl}$  is added in excess. Subsequently, NO gas is

bubbled through the solution. Immediately green crystals of bis(triphenylphosphane)iminium trichloridonitrosylferrate ((PPN)**5a**) form in high yield (81 %) and suitable for X-Ray diffraction.

The crystal structure of (PPN)**5a** is identical to that which Böttcher obtained, by reaction of {PPN}[Fe(CO)<sub>3</sub>(NO)] with appropriate amounts of SO<sub>2</sub>Cl<sub>2</sub> in dichloromethane at room temperature. (PPN)**5a** crystallizes from methanol in the monoclinic space group *C2/c* with eight formula units in the primitive cell. The anion [FeCl<sub>3</sub>(NO)]<sup>−</sup> consists of one iron atom which is coordinated in slightly distorted tetrahedral conformation by three chlorido ligands and one nitrosyl ligand. The Fe–N–O-angle is nearly linear (171°). Compared to the octahedral nitrosyl-iron compounds **3**, the thermal ellipsoid of the nitrosyl-oxygen atom is quite small. The cation (PPN)<sup>+</sup> does not form any contacts to the anion. The asymmetric unit contains one formula unit of {PPN}[FeCl<sub>3</sub>(NO)] ((PPN)**5a**).

#### 2.4.2 {PPN}[FeBr<sub>3</sub>(NO)]

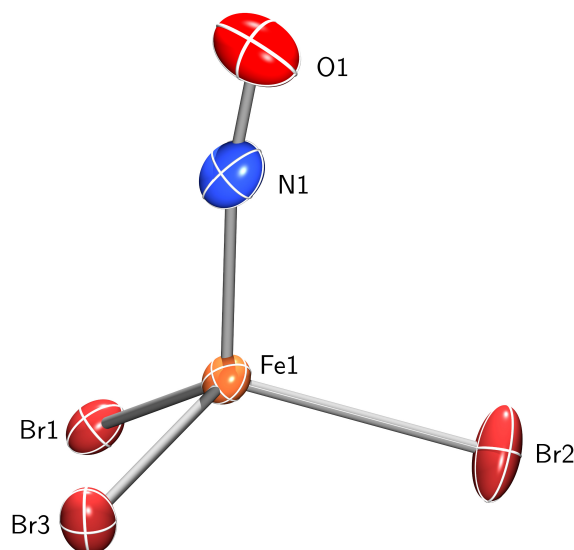


**Figure 2.18:**

Plot of the anion [FeBr<sub>3</sub>(NO)]<sup>−</sup> in crystals of (PPN)**5b**. Space group: *C2/c*. CShM<sub>T-4</sub>: 1.240. The thermal ellipsoids are drawn at 50 % probability. Interatomic distances (Å) and angles (°), the standard deviation of the last decimal place is given in parentheses: Fe1–N1 1.760(3), Fe1–Br1 2.3692(5), Fe1–Br2 2.3498(5), Fe1–Br3 2.3571(5), N1–O1 1.085(4). Fe1–N1–O1 170.5(3), N1–Fe1–Br1 111.63(10), N1–Fe1–Br2 103.79(11), N1–Fe1–Br3 110.25(9), Br1–Fe1–Br2 111.83(2), Br2–Fe1–Br3 111.36(2), Br3–Fe1–Br1 107.99(2).

The [FeBr<sub>3</sub>(NO)]<sup>−</sup>-anion has been crystallized by Wilfer as [PPh<sub>4</sub>][FeBr<sub>3</sub>(NO)] earlier, using FeBr<sub>2</sub> and half concentrated hydrobromic acid.<sup>[109]</sup> The method now developed to synthesize (PPN)**5a** is tested with (PPN)Br to obtain {PPN}[FeBr<sub>3</sub>(NO)] ((PPN)**5b**). This time,

however, only one equivalent of (PPN)Br is used, to avoid an excess of (PPN)<sup>+</sup> cations. The remaining two equivalents of Br<sup>-</sup> needed, are added as HBr to the methanolic solution of Fe(OTf)<sub>2</sub>. Bubbling of NO gas results in a dark green solution from which green crystals of bis(triphenylphosphane)iminium tribromidonitrosylferrate ((PPN)**5b**) separate in 52 % yield after five weeks.

The crystal structure of (PPN)**5b** is isomorphous to that of (PPN)**5a**. It crystallizes from methanol in the monoclinic space group *C2/c* with eight formula units in the primitive cell. The anion [FeBr<sub>3</sub>(NO)]<sup>-</sup> consists of one iron atom which is coordinated in slightly distorted tetrahedral conformation by three bromido ligands and one nitrosyl ligand. The Fe–N–O-angle is nearly linear (171°). Compared to the octahedral nitrosyl-iron compounds **3**, the thermal ellipsoid of the nitrosyl-oxygen atom is quite small. The cation (PPN)<sup>+</sup> does not form any contacts to the anion. The asymmetric unit contains one formula unit of {PPN}[FeBr<sub>3</sub>(NO)] ((PPN)**5b**).

### 2.4.3 {{PPN}[FeI<sub>2</sub>(NO)<sub>2</sub>]}{{PPN}[I<sub>3</sub>]}

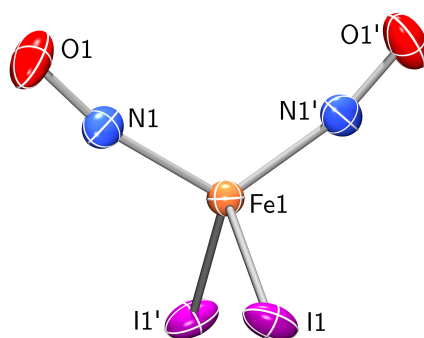


**Figure 2.19:**

Plot of the anion [FeI<sub>2</sub>(NO)<sub>2</sub>]<sup>-</sup> in crystals of (PPN)<sub>2</sub>**5c**(I<sub>3</sub>). Space group: *lbca*. CShM<sub>T-4</sub>: 4.186. The thermal ellipsoids are drawn at 25 % probability. Interatomic distances (Å) and angles (°), the standard deviation of the last decimal place is given in parentheses:

Fe1–N1 1.693(2), Fe1–I1 2.5847(3), N1–O1 1.164(3).

Fe1–N1–O1 166.6(2), N1–Fe1–N1<sup>i</sup> 116.0(2), I1–Fe1–I1<sup>i</sup> 113.05(2), I1–Fe1–N1 106.02(7), I1–Fe1–N1<sup>i</sup> 108.00(7).

Symmetry code: <sup>i</sup> 3/2 – x, y, 1 – z.

The crystal structure of [FeI<sub>3</sub>(NO)]<sup>-</sup> is so far unknown. In the attempt to adopt the method presented above to synthesize {PPN}[FeI<sub>3</sub>(NO)], (PPN)I is used together with Fe(OTf)<sub>2</sub> and NO. Brown crystals of bis(triphenylphosphane)iminium diiodidodinitrosylferrate(I)-triiodide ((PPN)<sub>2</sub>**5c**(I<sub>3</sub>)) are obtained in 22 % yield. The crystals obtained initially are of very poor quality. Later In-Iam obtained similar crystals of high quality by the same procedure.<sup>[111]</sup> Therefore, relevant data discussed in this thesis are taken from her crystals.

(PPN)<sub>2</sub>**5c**(I<sub>3</sub>) crystallizes from methanol in the orthorhombic space group *Ibca* with eight formula units in the primitive cell. It is a cocrystal of {PPN}[FeI<sub>2</sub>(NO)<sub>2</sub>] and {PPN}I<sub>3</sub> with a ratio of 1:1. The anion [FeI<sub>2</sub>(NO)<sub>2</sub>]<sup>−</sup> consists of one iron atom coordinated by two nitrosyl ligands and two iodido ligands in slightly distorted tetrahedral conformation. It contains a two-fold axis, the Fe–N–O-angle is 167°. The two nitrosyl ligands point toward each other. Compared to the octahedral nitrosyl-iron compounds **3**, the thermal ellipsoids of the nitrosyl-oxygen atoms are quite small. The two anions form discrete layers that are separated by layers of (PPN)<sup>+</sup>. The asymmetric unit contains one-half formula unit of [FeI<sub>2</sub>(NO)<sub>2</sub>]<sup>−</sup>, one-half formula unit of I<sub>3</sub><sup>−</sup> and two half formula units of (PPN)<sup>+</sup>.

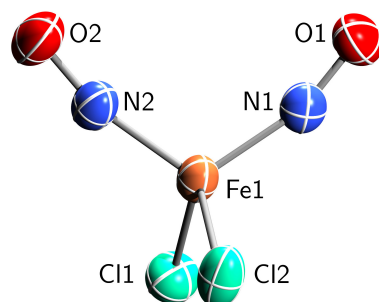
#### 2.4.4 {PPN}[Fe(N<sub>3</sub>)<sub>2</sub>(NO)<sub>2</sub>]

The anion [Fe(N<sub>3</sub>)<sub>3</sub>(NO)]<sup>−</sup> is completely unknown to literature. The reaction of (PPN)N<sub>3</sub> with Fe(OTf)<sub>2</sub> and NO in methanol yields a red amorphous powder. IR-spectroscopy shows two vibration bands at 1757 cm<sup>−1</sup> and 1698 cm<sup>−1</sup>, assigned to two nitrosyl ligands as symmetric and antisymmetric stretching vibrations and another two vibration bands at 2061 cm<sup>−1</sup> and 2035 cm<sup>−1</sup>, assigned to two azide ligands as symmetric and antisymmetric stretching vibrations. Together these vibration bands indicate the formation of {PPN}[Fe(N<sub>3</sub>)<sub>2</sub>(NO)<sub>2</sub>] ((PPN)**5d**). The synthesis and crystal structure of (PPN)**5d** have already been published<sup>[102,112]</sup>, however, with far more complicated synthetic routes.

#### 2.4.5 {PPN}[FeCl<sub>2</sub>(NO)<sub>2</sub>]

The known syntheses of [FeCl<sub>2</sub>(NO)<sub>2</sub>]<sup>−</sup> involve either the addition of 2,2'-bipyridine to a solution of [{FeCl(NO)<sub>2</sub>}]<sub>2</sub><sup>[113]</sup> or the addition of a solution of NOCl in CH<sub>2</sub>Cl<sub>2</sub> to a solution of {PPN}[Fe(CO)<sub>3</sub>(NO)].<sup>[97]</sup> The method to prepare (PPN)<sub>2</sub>**5c**(I<sub>3</sub>) and (PPN)**5d** does not yield [FeCl<sub>2</sub>(NO)<sub>2</sub>]<sup>−</sup>. Therefore, a different synthesis had to be developed: it starts also with {PPN}[Fe(CO)<sub>3</sub>(NO)]<sup>[114]</sup> which is converted to {PPN}[Fe(NO)<sub>2</sub>(ONO)<sub>2</sub>] following a procedure of Tsai *et al.*<sup>[115]</sup> {PPN}[Fe(NO)<sub>2</sub>(ONO)<sub>2</sub>] is then suspended in ethanol together with (PPN)Cl. After filtration and diffusion of petroleum ether, brown crystals of bis(triphenylphosphane)iminium dichloridodinitrosylferrate ((PPN)**5e**) are obtained in 38 % yield.

(PPN)**5e** crystallizes from ethanol/petroleum ether in the triclinic space group *P* $\bar{1}$  with two formula units in the primitive cell. The anion [FeCl<sub>2</sub>(NO)<sub>2</sub>]<sup>−</sup> consists of one iron atom which is coordinated in slightly distorted tetrahedral conformation, by two chlorido ligands and two nitrosyl ligands. The two Fe–N–O-angles are nearly identical with 161° and 166°. The two nitrosyl ligands point toward each other. Compared to the octahedral nitrosyl-iron

**Figure 2.20:**

Plot of the anion  $[\text{FeCl}_2(\text{NO})_2]^-$  in crystals of (PPN)**5e**. Space group:  $P\bar{1}$ .  $C_{\text{ShM}_{T-4}}$ : 1.575. The thermal ellipsoids are drawn at 50 % probability. Interatomic distances ( $\text{\AA}$ ) and angles ( $^\circ$ ), the standard deviation of the last decimal place is given in parentheses:

Fe1–N1 1.696(2), Fe1–N2 1.687(2), Fe1–Cl1 2.2692(7), Fe1–Cl2 2.2651(8), N1–O1 1.161(3), N2–O2 1.169(3).

Fe1–N1–O1 161.3(2), Fe1–N2–O2 165.7(2), N1–Fe1–N2 110.71(10), N1–Fe1–Cl1 113.00(8), N1–Fe1–Cl2 105.15(8), N2–Fe1–Cl1 107.33(8), N2–Fe1–Cl2 111.06(8), Cl1–Fe1–Cl2 109.64(3).

compounds **3**, the thermal ellipsoids of the nitrosyl-oxygen atoms are quite small. The cation  $(\text{PPN})^+$  does not form any contacts to the anion. The asymmetric unit contains one formula unit of  $\{\text{PPN}\}[\text{FeCl}_2(\text{NO})_2]$ .

## 2.5 IR spectroscopy

Besides single-crystal X-Ray diffraction, IR spectroscopy is the most useful method to analyze nitrosyl-iron compounds. Yet some drawbacks had to be taken into account. The stretching vibration band of nitric oxide in  $\{\text{FeNO}\}^7$  and  $\{\text{Fe}(\text{NO})_2\}^9$  compounds is usually found in the region of  $1750\text{ cm}^{-1}$  to  $1850\text{ cm}^{-1}$ . This is also the region of a strong absorption of water due to its deformation vibration. Thus the observation of the stretching vibration band of nitric oxide is hardly possible if  $\text{H}_2\text{O}$  is used as solvent. The easiest answer to this problem is the use of  $\text{D}_2\text{O}$  as solvent. Here the deformation vibration band is found in the region of  $1200\text{ cm}^{-1}$  to  $1300\text{ cm}^{-1}$ .

Quite unexpected was the observation that  $200\text{ mmol L}^{-1}$   $\text{D}_2\text{O}$  solutions of equal amounts of  $\text{FeSO}_4 \cdot 7\text{H}_2\text{O}$  and aminocarboxylato ligand **2**, mixed with nitric oxide, do not show their nitric-oxide-stretching vibration band at or close to the value found for the respective crystalline products (Figure 2.21, black dotted line) but always at  $1810\text{ cm}^{-1}$ , the value also detected for penta-aquanitrosyliron(2+) solutions (Figure 2.21, black solid line). Meanwhile, the vibration bands of the ligand remain completely unaffected by the addition of iron(II) and are found at the same values and the same intensity as they are in solutions without

**Table 2.14:** IR-spectroscopic data of compounds **3a–i** and **5a–e**. ( $\tilde{\nu}/\text{cm}^{-1}$ , vs = very strong, s = strong, m = medium, w = weak, vw = very weak.)

Compound	$\nu(\text{NO})$	$\nu(\text{NN})$
$[\text{Fe}(\text{NO})(\text{OH}_2)_5]^{2+}$ / “brown $\text{FeSO}_4$ ” ( <b>1</b> )	1810 (m)	
$[\text{Fe}(\text{ida})(\text{NO})(\text{OH}_2)_2]$ ( <b>3a</b> )	1772 (s)	
$[\text{Fe}(\text{heida})(\text{NO})(\text{OH}_2)]$ ( <b>3b</b> )	1782 (m)	
$[\text{Fe}(\text{dhpida})(\text{NO})]$ ( <b>3c</b> )	{ 1788 (m) 1804 (w)	
$[\text{Fe}(\text{NO})(\text{OH}_2)_2(\text{oda})]$ ( <b>3d</b> )	1799 (m)	
$[\text{Fe}(\text{NO})(\text{OH}_2)_2(\text{phida})] \cdot \text{H}_2\text{O}$ ( <b>3e</b> )	1764 (s)	
$[\text{Fe}(\text{bnida})(\text{NO})(\text{OH}_2)_2]$ ( <b>3f</b> )	1803 (m)	
$[\text{Fe}(\text{brbnida})(\text{NO})(\text{OH}_2)_2]$ ( <b>3g</b> )	1800 (m)	
$[\text{Fe}(\text{NO})(\text{OH}_2)_2(\text{pheida})]$ ( <b>3h</b> )	{ 1793 (m) 1814 (m)	
$[\text{Fe}(\text{dipic})(\text{NO})(\text{OH}_2)_2]$ ( <b>3i</b> )	1806 (m)	
$\{\text{PPN}\}[\text{FeCl}_3(\text{NO})]$ ((PPN) <b>5a</b> )	1791 (m)	
$\{\text{PPN}\}[\text{FeBr}_3(\text{NO})]$ ((PPN) <b>5b</b> )	1772 (w)	
$\{\{\text{PPN}\}[\text{FeI}_2(\text{NO})_2]\}\{\{\text{PPN}\}[\text{I}_3]\}$ ((PPN) <b>5c</b> ( $\text{I}_3$ ))	{ 1712 (m) 1762 (w)	
$\{\text{PPN}\}[\text{Fe}(\text{N}_3)_2(\text{NO})_2]$ ((PPN) <b>5d</b> )	{ 1698 (w) 2034 (vw) 1757 (vw) 2061 (vw)	
$\{\text{PPN}\}[\text{FeCl}_2(\text{NO})_2]$ ((PPN) <b>5e</b> )	{ 1697 (m) 1773 (w)	

iron(II) (Figure 2.21, black dashed lines). When sodium or potassium hydroxide is added, the nitric-oxide-stretching vibration band shifts in the direction of the value found for the corresponding crystalline products but does not get close to it. Also, the vibration bands of the ligand are affected by the addition of base (Figure 2.21, colored lines).

All crystalline  $\{\text{FeNO}\}^7$  compounds show one single  $\nu(\text{NO})$  stretching vibration band. The only exceptions are  $[\text{Fe}(\text{dhpida})(\text{NO})]$  and  $[\text{Fe}(\text{NO})(\text{OH}_2)_2(\text{pheida})]$  for which two bands close to each other are found, possibly due to the two different molecules in the asymmetric unit of the crystal structures. The lowest value for  $\nu(\text{NO})$  is found at  $1764\text{ cm}^{-1}$  for  $[\text{Fe}(\text{NO})(\text{OH}_2)_2(\text{phida})] \cdot \text{H}_2\text{O}$ , the highest value is found for  $[\text{Fe}(\text{NO})(\text{OH}_2)_2(\text{pheida})]$  at  $1814\text{ cm}^{-1}$ . The three  $\{\text{Fe}(\text{NO})_2\}^9$  compounds show two stretching vibration bands between

1697  $\text{cm}^{-1}$  (antisymmetric) and 1773  $\text{cm}^{-1}$  (symmetric). For  $\{\text{PPN}\}[\text{Fe}(\text{N}_3)_2(\text{NO})_2]$  two characteristic  $\nu(\text{NN})$  vibration bands are detected at 2035  $\text{cm}^{-1}$  (antisymmetric) and 2061  $\text{cm}^{-1}$  (symmetric).

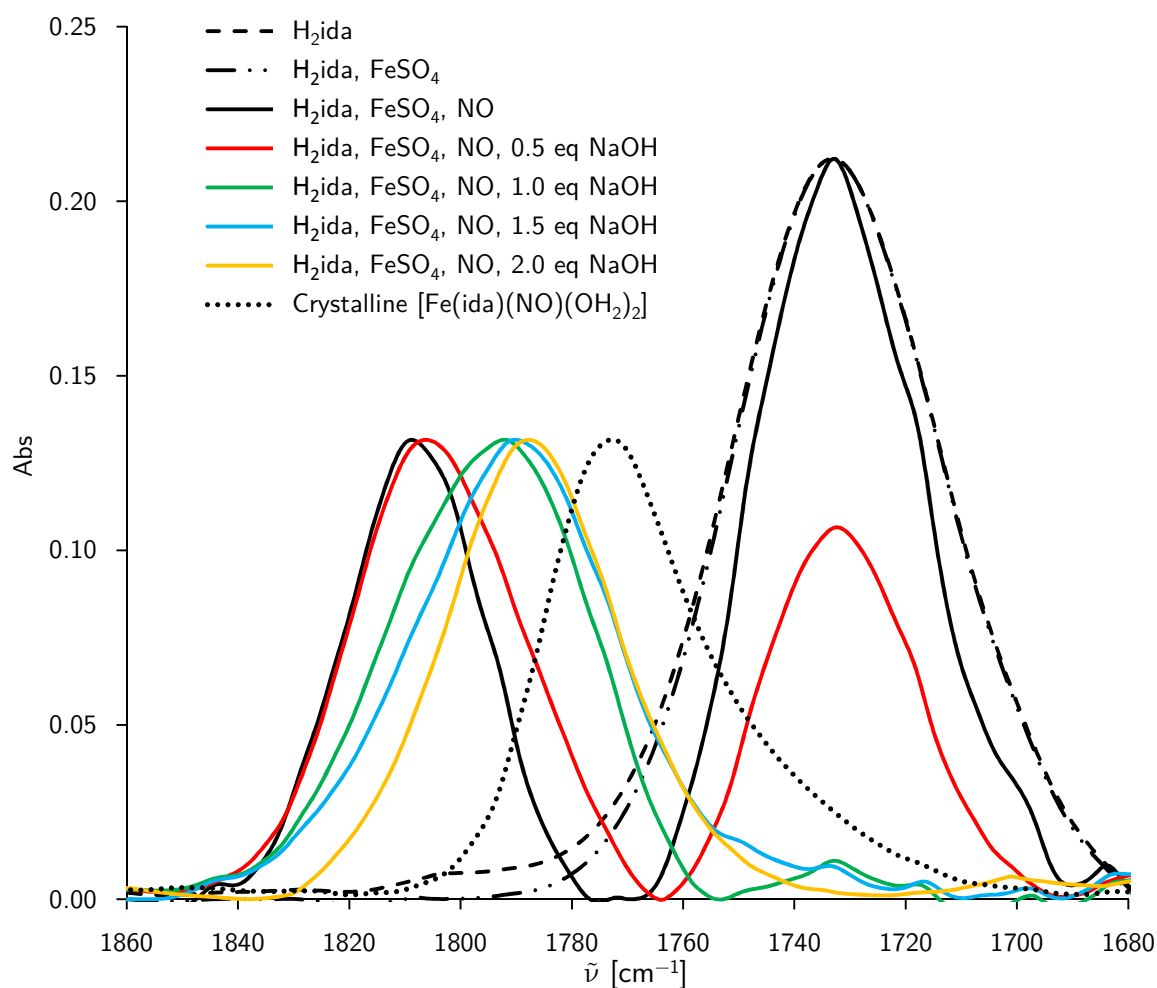


**Figure 2.21:** IR spectra of **3a** in  $\text{D}_2\text{O}$  solution:  $\text{H}_2\text{ida}$  alone,  $\text{H}_2\text{ida}$  with  $\text{FeSO}_4$ ,  $\text{H}_2\text{ida}$  with  $\text{FeSO}_4$  and nitric oxide and  $\text{H}_2\text{ida}$  with  $\text{FeSO}_4$ , nitric oxide and different amounts of  $\text{NaOH}$ .

On page 8 the frequent formation of brown  $\text{FeSO}_4$  crystals (**1**) was reported. Their IR spectrum agrees with that of commercially available  $\text{FeSO}_4 \cdot 7\text{H}_2\text{O}$ . But in some cases, if the brown color of these crystals is very strong, a tiny absorption band around 1810  $\text{cm}^{-1}$  is observed, corresponding to the value found for the penta-aquanitrosyliron(2+) solution.

## 2.6 UV-VIS spectroscopy

Due to the dark green color of  $\{\text{FeNO}\}^7$  compounds, UV-VIS spectra were recorded from solid samples and from solutions. Figure 2.22 and Table 2.15 show the relevant results.

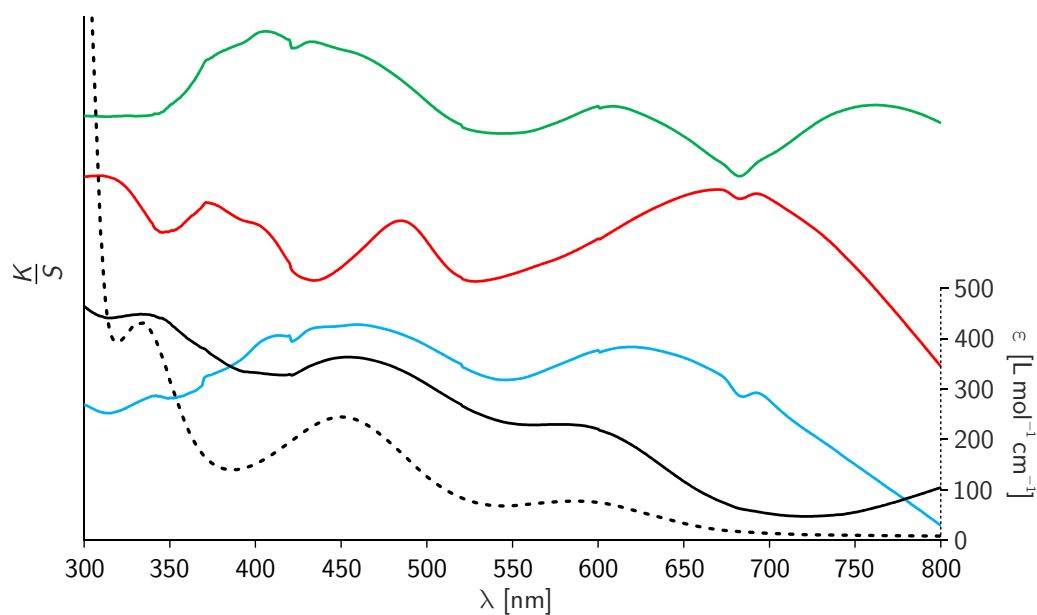


**Figure 2.22:** UV-VIS spectra of the pentaquanitrosyliron(2+) solution (black, dotted) in  $\text{L mol}^{-1} \text{cm}^{-1}$  and of solid samples of **1** (black), **3a** (blue), (PPN)**5a** (red) and (PPN)**25c**(I<sub>3</sub>) (green) in  $\text{K S}^{-1}$ .

**Table 2.15:** UV-VIS-spectroscopic data of compounds **3a-d,f-h** and **5a-c**.

Compound	$\lambda/\text{nm}$				
$[\text{Fe}(\text{NO})(\text{OH}_2)_5]^{2+}$	333	451	584		
“brown $\text{FeSO}_4$ ” ( <b>1</b> )	333	453	579		
$[\text{Fe}(\text{ida})(\text{NO})(\text{OH}_2)_2]$ ( <b>3a</b> )	340	414	459	618	692
$[\text{Fe}(\text{heida})(\text{NO})(\text{OH}_2)]$ ( <b>3b</b> )	341	402	457	625	691
$[\text{Fe}(\text{dhpida})(\text{NO})]$ ( <b>3c</b> )	341	412	457	625	690
$[\text{Fe}(\text{NO})(\text{OH}_2)_2(\text{oda})]$ ( <b>3d</b> )	340	407	459	571	693
$[\text{Fe}(\text{bnida})(\text{NO})(\text{OH}_2)_2]$ ( <b>3f</b> )	341	408	459	596	692
$[\text{Fe}(\text{brbnida})(\text{NO})(\text{OH}_2)_2]$ ( <b>3g</b> )	371	402	459	595	691
$[\text{Fe}(\text{NO})(\text{OH}_2)_2(\text{pheida})]$ ( <b>3h</b> )	340	420	459	596	693
$\{\text{PPN}\}[\text{FeCl}_3(\text{NO})]$ ((PPN) <b>5a</b> )	309	371	485	670	692
$\{\text{PPN}\}[\text{FeBr}_3(\text{NO})]$ ((PPN) <b>5b</b> )	326	382	500	673	696
$\{\{\text{PPN}\}[\text{FeI}_2(\text{NO})_2]\}\{\{\text{PPN}\}[\text{I}_3]\}$ ((PPN) <b>25c</b> (I <sub>3</sub> ))	302	406	433	608	762

Solid samples of **3** show absorptions around 340 nm, 410 nm, 460 nm, 600 nm and 690 nm. All compounds **3** give very similar spectra. The only significant change is observed for the absorption band around 600 nm. It is detected between 571 nm for **3d** and 625 nm for **3b** and **3c**. Due to technical reasons the absorption band around 340 nm could not be measured properly for solid samples, as the spectrometer performs a change of the light source at that wavelength. Compounds **5a** and **5b** show spectra comparable to those of **3**, the dinitrosyl **5c**, which is of a more brownish color, shows a quite different spectrum.

Samples in solution show the same behavior as in IR spectroscopy, only the absorption bands of penta-aquanitrosyliron(2+) are detected at 333 nm, 451 nm and 584 nm. It is obvious, that the spectrum lacks the absorption bands around 410 nm and 690 nm. A solid sample of the brown FeSO<sub>4</sub> crystals (**1**) (see page 8) shows a spectrum nearly identical to that of the penta-aquanitrosyliron(2+) solution.

## 2.7 SQUID magnetometry

For samples of high purity, the superconducting quantum interference device (SQUID) magnetometry measurements represent an effective method to determine the spin state of a given compound. Using the equation 2.1, the magnetic moment  $\mu_{\text{eff}}$  is calculated from  $\chi_{\text{M}}T$ , the result of SQUID measurements. The value obtained is compared to expected results, calculated by using the spin-only equation for  $\mu_{\text{s.o.}}$  (2.2). Figure 2.23 shows the results of SQUID measurements on complexes **3a** and **3f**. Both compounds show nearly perfect *Curie* behavior, the drop at low temperatures is probably due to zero-field splitting. Using equation 2.1, values of  $\mu_{\text{eff}} = 3.95 \mu_B$  and  $\mu_{\text{eff}} = 4.13 \mu_B$  are obtained for **3a** and **3f** respectively. These values lie in the expected range for quartet compounds, the spin-only equation calculates  $\mu_{\text{s.o.}} = 3.88 \mu_B$ .

$$\mu_{\text{eff}} = \sqrt{\frac{3k_B}{N_a \mu_B^2}} \cdot \sqrt{\chi_{\text{M}}T} \cdot \mu_B \quad (2.1)$$

$$\mu_{\text{s.o.}} = g \cdot \sqrt{S(S+1)} \cdot \mu_B \quad (2.2)$$

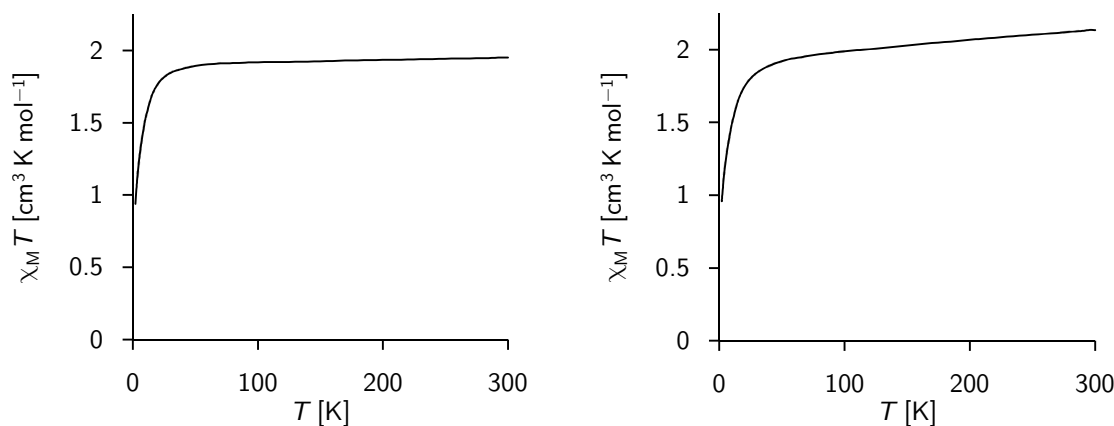


Figure 2.23:  $\chi_M T$  vs.  $T$  plots of **3a** (left) and **3f** (right).

## 2.8 Quantum-chemical calculations

Quantum-chemical calculations, based on DFT, were carried out to gain better insight into the electronic properties of the crystallized nitrosyl-iron compounds. Furthermore, a better understanding of Fe–N–O bond angles and corresponding  $\nu(\text{NO})$  stretching vibration energies was to be achieved. Additionally different possible coordination isomers of nitrosyl-iron compounds with aminocarboxylato ligands were to be compared.

### 2.8.1 Structural optimizations of complexes with aminocarboxylato ligands

The biggest challenge for all calculations on complexes with aminocarboxylato ligands was the correct prediction of the iron–oxygen bond lengths for aqua, acetato and hydroxyethyl ligands. When a simple structural optimization on **3a** is performed, using BP-86<sup>[116,117]</sup> as the functional and def2-TZVP<sup>[118]</sup> as the basis set, a pentagonal bipyramidal coordination figure is obtained with only one coordinating aqua ligand left. This problem can easily be overcome using the COSMO solvation model,<sup>[119]</sup> yet the prediction of the bond lengths is still very poor: the acetato ligands bind too close to the iron atom and the aqua ligands move much too far away. The reason is the embedding of the complexes in a strong hydrogen bond network. In all crystal structures each aqua ligand and each acetate group form at least two hydrogen bonds which have a significant impact on the Fe–O bond lengths. This hydrogen bond network cannot be described appropriately by the COSMO model which takes only electrostatic and *van-der-Waals* interactions into account. There are several possibilities to deal with this problem: (1) using periodic DFT to calculate real crystal structures; (2) using the supermolecule approach or QM/MM methods to model the hydrogen bond network by hand; (3) using the D-COSMO-RS model<sup>[120,121]</sup> which is an extension of the COSMO model and can also describe hydrogens bonds without knowing the explicit position of all

molecules in space. The periodic DFT is computationally very expensive while, on the other hand, the gain in accuracy is negligible. The same is true for the QM/MM methods. For the supermolecule approach, each hydrogen-bond donor and acceptor has to be added by hand from the crystal structure. Acetate groups are inserted as acetic acid. This gives very promising results and describes the Fe–O bond lengths very accurately. The biggest problem is the very slow convergence of structural optimizations and the high computational cost. Nearly equally good results are obtained using the D-COSMO-RS model. The accuracy of Fe–O bond lengths is a bit inferior to the supermolecule approach, but structural optimizations converge a lot faster and the computational cost is lower. Therefore, all structural optimizations and frequency calculations were carried out, using the D-COSMO-RS model.

All computational results show a rather weak dependence on the basis set. It is not very surprising that using a triple-zeta basis with polarized and diffuse functions is necessary to receive a satisfying agreement of calculation and experiment. A lot more pronounced is the dependence on the functional: pure density functionals like BP-86 or TPSS<sup>[122,123]</sup> calculate slightly longer aqua–iron distances and shorter acetate–iron distances than hybrid functionals like B3-LYP<sup>[116,124,125]</sup> or TPSSh.<sup>[122,123,126]</sup> The differences become more obvious regarding the Fe–N–O moiety: pure density functionals calculate a 10° to 25° more acute Fe–N–O bond angle, the calculated  $\nu(\text{NO})$  stretching vibration energies lie approximately 80 cm<sup>-1</sup> lower. Regarding only bond distances, the best overall agreement of computational and experimental results is obtained using the hybrid density functional TPSSh with def2-TZVP as the basis set. The best description of the Fe–N–O moiety is obtained using the dispersion-corrected functional B97-D.<sup>[127]</sup> A comparison of results on **3a** with different computational methods can be found in Table 2.16 results on compounds **3a–i** using the functionals B97-D and TPSSh can be found in Table 2.17.

### Comparison of coordination isomers

For most chelating ligands **2** different coordination isomers are possible. For **2a,d–h** facial and meridional coordination of the iron atom is possible. For the coordination with **2b** and **2c** different isomers regarding the position of the aqua ligand are possible. For **2c** also the pentadentate coordination isomer is possible. Additionally, for all compounds **3** the nitrosyl ligand can coordinate in different positions.

To verify whether the coordination isomers found in the crystalline structures represent the energetic minimum also in solution, different isomers were calculated by DFT. Table 2.18 summarizes the results of these calculations. In most cases all isomers lie energetically close to each other within a range of at most 15 kJ mol<sup>-1</sup>. Not always does the isomer found in the crystalline structure represent the energetic minimum in solution. For [Fe(NO)(OH<sub>2</sub>)<sub>2</sub>(phida)]

**Table 2.16:** DFT results on **3a** using different computational methods.

	Crystal	BP-86		BP-86		BP-86		B97-D		TPSS		TPSSh		TPSSh	
		BP-86	BP-86	COSMO	COSMO-RS	Supermolecule									
Fe1-O91 [Å]	2.06	2.40	2.24	2.20	2.20	2.20	2.20	2.20	2.20	2.19	2.17	2.17	2.17	2.10	2.10
Fe1-O91 <sup>i</sup> [Å]	2.06	2.40	2.24	2.19	2.20	2.20	2.20	2.20	2.20	2.18	2.16	2.16	2.16	2.10	2.10
Fe1-O21 [Å]	2.05	1.96	1.99	2.05	2.07	2.07	2.07	2.07	2.07	2.04	2.06	2.06	2.06	2.04	2.04
Fe1-O21 <sup>i</sup> [Å]	2.05	1.96	1.99	2.04	2.07	2.07	2.07	2.07	2.07	2.04	2.06	2.06	2.06	2.04	2.04
Fe1-N2 [Å]	2.27	2.20	2.18	2.17	2.21	2.21	2.21	2.21	2.21	2.17	2.20	2.20	2.20	2.25	2.25
Fe1-N1 [Å]	1.78	1.72	1.73	1.74	1.78	1.78	1.78	1.78	1.78	1.74	1.78	1.78	1.78	1.78	1.78
N1-O1 [Å]	1.11	1.17	1.17	1.17	1.16	1.16	1.16	1.16	1.16	1.17	1.16	1.16	1.16	1.16	1.16
Fe1-N1-O1 [°]	155	150	147	146	151	151	151	151	151	148	164	164	164	154	154
O1-N1-Fe1-O21 [°]	46	59	49	49	48	48	48	48	48	48	51	51	51	44	44
O1-N1-Fe1-O21 <sup>i</sup> [°]	46	59	49	45	48	48	48	48	48	46	43	43	43	44	44
$\nu(\text{NO})$ [cm <sup>-1</sup> ]	1772	1792	1728	1730	1781	1781	1781	1781	1781	1743	1845	1845	1845	1820	1820

Symmetry code: <sup>i</sup> 1 -  $x, y, z$ . All calculations were performed using def2-TZVP basis sets and dispersion correction (D3).<sup>[128,129]</sup> For the supermolecule approach, four water molecules and four acetic acid molecules were added and COSMO was used.

**Table 2.17:** DFT results on **3** using the functionals B97-D (B) and TPSSh (T), def2-TZVP, D-COSMO-RS and dispersion correction (D3). Distances in Å, angles in °,  $\nu(\text{NO})$  energies and  $J$  coupling constants in  $\text{cm}^{-1}$ .

	<b>3a</b>			<b>3b</b>			<b>3c</b>		
	exp.	B	T	exp.	B	T	exp.	B	T
Fe1-OH <sub>2</sub> /OR <sup>a</sup>	2.06	2.20	2.17	2.08	2.20	2.16	2.08	2.20	2.13
Fe1-OH <sub>2</sub> /OHR <sup>b</sup>	2.06	2.20	2.16	2.10	2.18	2.14	2.12	2.16	2.13
Fe1-OAc	2.05	2.07	2.06	2.05	2.08	2.06	2.04	2.06	2.05
Fe1-OAc	2.05	2.07	2.06	2.05	2.07	2.05	2.06	2.07	2.05
Fe1-N2	2.27	2.21	2.20	2.22	2.25	2.23	2.23	2.27	2.25
Fe1-N1	1.78	1.78	1.78	1.76	1.77	1.77	1.76	1.77	1.77
N1-O1 <sup>c</sup>	1.11	1.16	1.16	1.11	1.16	1.16	1.14	1.16	1.15
Fe1-N1-O1	155	151	164	171	178	175	166	160	175
$\nu(\text{NO})^{\text{d}}$	1772	1781	1845	1782	1799	1858	1796	1807	1870
$J$		2268	2057		2235	2071		2293	2131
	<b>3d</b>			<b>3e</b>			<b>3f</b>		
	exp.	B	T	exp.	B	T	exp.	B	T
Fe1-OH <sub>2</sub>	2.08	2.21	2.16	2.19	2.23	2.19	2.06	2.21	2.16
Fe1-OH <sub>2</sub>	2.08	2.17	2.14	2.02	2.13	2.10	2.04	2.17	2.14
Fe1-OAc	2.07	2.08	2.05	2.03	2.05	2.04	2.07	2.09	2.07
Fe1-OAc	2.07	2.07	2.05	2.02	2.04	2.04	2.06	2.06	2.05
Fe1-N2/O2 <sup>e</sup>	2.12	2.17	2.14	2.32	2.38	2.32	2.32	2.27	2.26
Fe1-N1	1.77	1.77	1.77	1.78	1.78	1.78	1.78	1.79	1.78
N1-O1 <sup>c</sup>	1.15	1.16	1.15	1.17	1.16	1.16	1.13	1.16	1.16
Fe1-N1-O1	165	169	180	148	153	166	165	149	160
$\nu(\text{NO})$	1799	1838	1877	1764	1792	1855	1803	1777	1837
$J$		2313	2160		2205	2057		2240	2051
	<b>3g</b>			<b>3h</b>			<b>3i</b>		
	exp.	B	T	exp.	B	T	exp.	B	T
Fe1-OH <sub>2</sub>	2.06	2.20	2.16	2.09	2.22	2.16	2.11	2.20	2.15
Fe1-OH <sub>2</sub>	2.04	2.17	2.14	2.06	2.19	2.13	2.10	2.18	2.15
Fe1-OAc	2.05	2.09	2.07	2.06	2.08	2.05	2.14	2.15	2.11
Fe1-OAc	2.04	2.06	2.05	2.02	2.05	2.05	2.10	2.15	2.11
Fe1-N2	2.33	2.28	2.26	2.29	2.27	2.30	2.09	2.10	2.10
Fe1-N1	1.80	1.79	1.78	1.77	1.79	1.78	1.76	1.77	1.77
N1-O1 <sup>c</sup>	1.09	1.16	1.16	1.10	1.16	1.16	1.14	1.16	1.15
Fe1-N1-O1	158	149	160	167	148	159	167	167	180
$\nu(\text{NO})^{\text{d}}$	1800	1779	1840	1803	1776	1739	1806	1832	1873
$J$		2252	2064		2247	2080		2316	2159

<sup>a</sup> Valid for **3c**. <sup>b</sup> Valid for **3b** and **3c**. <sup>c</sup> Libration corrected. <sup>d</sup> For **3c** and **3h** the mean value of experimental  $\nu(\text{NO})$  energies is quoted. <sup>e</sup> Valid for **3d**.

**Table 2.18:** DFT results on different coordination isomers with aminocarboxylato ligands.

Isomer	Coordination of chelating ligand	Orientation of nitrosyl ligand <sup>a</sup>	B97-D [kJ mol <sup>-1</sup> ] <sup>b</sup>	TPSSh [kJ mol <sup>-1</sup> ] <sup>b</sup>
[Fe(ida)(NO)(OH <sub>2</sub> ) <sub>2</sub> ]				
OC-6-22	facial	<i>trans</i>	0.00	0.00
OC-6-12	meridional	<i>trans</i>	3.33	3.69
OC-6-32	facial	<i>cis</i>	-5.89	-5.51
OC-6-14	meridional	<i>cis</i>	-1.65	-0.12
[Fe(NO)(oda)(OH <sub>2</sub> ) <sub>2</sub> ]				
OC-6-14	meridional	<i>trans</i>	0.00	0.00
OC-6-33	facial	<i>trans</i>	-0.79	0.87
OC-6-13	meridional	<i>cis</i>	4.95	7.64
OC-6-43	facial	<i>cis</i>	5.88	10.03
[Fe(bnida)(NO)(OH <sub>2</sub> ) <sub>2</sub> ]				
OC-6-22	facial	<i>trans</i>	0.00	0.00
OC-6-12	meridional	<i>trans</i>	6.91	5.20
OC-6-32	facial	<i>cis</i>	-0.20	-0.36
OC-6-14	meridional	<i>cis</i>	-3.35	-3.05
OC-6-14	meridional	<i>cis</i>	7.54	9.38
[Fe(NO)(OH <sub>2</sub> ) <sub>2</sub> (phida)]				
OC-6-14	meridional	<i>cis</i>	0.00	0.00
OC-6-14	meridional	<i>cis</i>	24.16	27.70
OC-6-32	facial	<i>cis</i>	15.01	16.86
OC-6-12	meridional	<i>trans</i>	13.62	13.61
OC-6-22	facial	<i>trans</i>	16.29	18.24
[Fe(dipic)(NO)(OH <sub>2</sub> ) <sub>2</sub> ]				
OC-6-12	meridional	<i>trans</i>	0.00	0.00
OC-6-14	meridional	<i>cis</i>	-4.24	-0.14
[Fe(heida)(NO)(OH <sub>2</sub> ) <sub>2</sub> ]				
OC-6-13	facial	<i>trans</i>	0.00	0.00
OC-6-32	facial	<i>trans</i>	-0.67	2.07
OC-6-14	facial	<i>cis</i>	1.46	6.35
OC-6-42	facial	<i>cis</i>	10.41	14.74
[Fe(dhpida)(OH <sub>2</sub> ) <sub>2</sub> ]				
[Fe(dhpida)(OH <sub>2</sub> ) <sub>2</sub> ] · H <sub>2</sub> O	pentadentate	<i>trans</i>	30.34	26.58
[Fe(dhpida)(NO)(OH <sub>2</sub> ) <sub>2</sub> ]	facial	<i>trans</i>	0.00	0.00
[Fe(dhpida)(NO)] · H <sub>2</sub> O	pentadentate	<i>trans</i>	21.17	16.18
[Fe(dhbida)(NO)(OH <sub>2</sub> ) <sub>2</sub> ]	facial	<i>trans</i>	0.00	0.00
[Fe(dhbida)(NO)] · H <sub>2</sub> O	pentadentate	<i>trans</i>	37.08	33.63

All calculations were performed using def2-TZVP basis sets, dispersion correction and D-COSMO-RS. <sup>a</sup> Orientation of the nitrosyl ligand relative to the central hetero atom of the chelating ligand. <sup>b</sup>  $\Delta E$  relative to the isomer of the crystal structure.

and  $[\text{Fe}(\text{bnida})(\text{NO})(\text{OH}_2)_2]$  two different *OC*-6-14 isomers are distinguished: with the nitrosyl ligand pointing in the direction of the aromatic substituent or in the opposite direction. In the case of  $[\text{Fe}(\text{NO})(\text{OH}_2)_2(\text{phida})]$  this accounts for a difference of  $25 \text{ kJ mol}^{-1}$ .

dhpida (**2c**) had been synthesized to obtain a pentadentate ligand and to circumvent the coordination of aqua ligands. However, compounds **3c** and **4c** show only a tetradentate coordination by **2c**. A possible explanation is the intramolecular strain that may be too heavy. The desired pentadentate isomers were calculated by DFT and support this hypothesis. They are found to be up to  $30 \text{ kJ mol}^{-1}$  higher in energy. This result leads to the assumption that the ligand *N*-(1,4-dihydroxybutane-2-yl)iminodiacetate (dhbida) might favor the pentadentate coordination due to its longer alkyl chain. But DFT calculations show that the energetic difference to the tetradentate isomer is even higher.

### 2.8.2 Structural optimizations of halogenidonitrosylferrates

The best description of the structure of halogenidonitrosylferrates is obtained using the hybrid density functional TPSSh in combination with the COSMO solvation model which takes into account the negative charge of the ferrates. However, the  $\nu(\text{NO})$  stretching vibration energies are calculated much too high. They can be predicted very well using the functionals BP-86 for **5a** and **5b** and B97-D for **5c** and **5e**. Table 2.19 gives an overview of computational results on halogenidonitrosylferrates.

### 2.8.3 Electronic description of the Fe–N–O moiety

All calculations were performed using spin-unrestricted open-shell systems with three unpaired electrons. Hence separate orbitals for spin-up and spin-down electrons were obtained. The electronic description of the Fe–N–O moiety is the same for all quartet- $\{\text{FeNO}\}^7$  compounds, presented in this thesis. It is influenced minimally by the different chelating or halogenido ligands. Also, the density functional (B97-D or TPSSh) does not affect the description significantly.

The Fe–NO bond is dominated by the antiferromagnetic coupling of both spin-down NO  $\pi^*$  orbitals with the Fe  $d_{xz}$  and Fe  $d_{yz}$  orbitals, representing HOMO–1 and HOMO–2. The orbitals possess a 30 % to 40 % Fe  $d$  character, up to a 2 % Fe  $p$  character and a 50 % to 60 % NO  $p$  character. For spin-up orbitals this interaction is difficult to find but is detected at much lower energies with a 60 % to 70 % Fe  $d$  character and only up to a 5 % NO  $p$  character. The interaction is supported by the energetically low lying interactions of the NO  $\pi$ ,  $5\sigma$  and  $4\sigma$  orbitals with corresponding Fe orbitals for both spin-up and spin-down electrons. Only small antibonding interactions between Fe and NO are detected, the most important one being

**Table 2.19:** DFT results on **5** using the functionals B97-D (B), BP-86 (BP) and TPSSh (T), def2-TZVP and COSMO. Distances in Å, angles in °,  $\nu(\text{NO})$  energies and  $J$  coupling constants in  $\text{cm}^{-1}$ .

	<b>5a</b>				<b>5b</b>			
	exp.	B	BP	T	exp.	B	BP	T
Fe1–N1	1.74	1.74	1.71	1.74	1.76	1.74	1.70	1.74
N1–O1 <sup>a</sup>	1.14	1.16	1.17	1.15	1.09	1.16	1.16	1.15
Fe1–X1	2.22	2.28	2.25	2.26	2.35	2.44	2.40	2.41
Fe1–X2	2.23	2.28	2.26	2.26	2.36	2.44	2.40	2.41
Fe1–X3	2.24	2.28	2.26	2.26	2.37	2.44	2.41	2.41
Fe1–N1–O1	171	178	178	179	171	179	180	180
$\nu(\text{NO})$	1791	1809	1788	1857	1772	1808	1785	1857
$J$		2233	2515	2157		2318	2591	2210

	<b>5c</b>				<b>5e</b>			
	exp.	B	BP	T	exp.	B	BP	T
Fe1–N1	1.69	1.69	1.66	1.70	1.69	1.70	1.67	1.72
N1–O1 <sup>a</sup>	1.16	1.17	1.18	1.17	1.17	1.17	1.18	1.17
Fe1–N2	1.69	1.69	1.66	1.70	1.70	1.70	1.67	1.72
N2–O2 <sup>a</sup>	1.16	1.17	1.18	1.17	1.16	1.17	1.18	1.17
Fe1–X1	2.58	2.69	2.63	2.64	2.27	2.33	2.29	2.30
Fe1–X2	2.58	2.69	2.63	2.64	2.27	2.33	2.29	2.30
Fe1–N1–O1	167	164	165	168	166	161	162	164
Fe1–N2–O2	167	164	165	168	161	161	162	164
$\nu(\text{NO})$	1712	1706	1685	1734	1697	1694	1674	1723
	1762	1775	1755	1825	1773	1780	1763	1826
$J$		2667	3002	2470		2518	2883	2267

<sup>a</sup> Libration corrected.

that with the NO  $5\sigma$  orbital. It is interacting with the spin-up Fe  $d_{z^2}$  orbital which is, in turn, antibonding with respect to the heteroatom *trans* to NO. This MO represents the HOMO and possesses a 25 % to 35 % Fe  $d$  character, no Fe  $p$  character and a 5 % to 10 % NO character. The same interaction is found again with lower energy and a bonding interaction of the Fe  $d_{z^2}$  orbital and the heteroatom *trans* to NO. For the tetrahedral halogenidonitrosylferrates, there is, of course, no interaction with an atom *trans* to NO. The Fe–NO antibond, however, remains unaffected with a 35 % Fe  $d$  character, no Fe  $p$  character and a 9 % NO character. Figure 2.24 illustrates the overlap population density of states (OPDOS) between Fe and NO of **3a** and relevant occupied molecular orbitals. It is representative for all investigated

$\{\text{FeNO}\}^7$  compounds.

The occupied orbitals, relevant to describe the interactions of Fe and NO, are strongly mixed due to spin polarization and sometimes difficult to identify. An alternative approach to depict the Fe–NO bonding, is to look at the unoccupied antibonding orbitals. They reflect the uncompensated occupied counterparts which are involved in bonding.<sup>[34,130–133]</sup> The  $\beta$  orbitals LUMO and LUMO+5,6 comprise mainly an Fe  $d$  character and are assigned to the three unpaired Fe electrons responsible for the quartet state of the  $\{\text{FeNO}\}^7$  compounds. As LUMO+1 – LUMO+4 two  $\beta$  Fe  $d$  orbitals and two  $\alpha$  NO  $\pi^*$  orbitals are identified. Thereby the Fe orbitals show strong NO contributions and the NO orbitals show small Fe contributions. Figure 2.25 shows the seven lowest unoccupied orbitals of **3a** as well as their occupied counterparts. Another and often more convenient method to visualize the Fe–NO bonding is to calculate natural orbitals. They combine  $\alpha$  and  $\beta$  spin density in one orbital and their occupation numbers can take any value between 0 and 2. Figure 2.26 shows the relevant natural orbitals of **3a**. The three unpaired electrons reside nearly exclusively on the Fe atom. The bonding Fe  $d$ –NO  $\pi^*$  interaction is occupied by a total of 3.66 electrons which are strongly delocalized between Fe and NO with a majority of 68 % on the Fe atom. There is also some occupation of the antibonding Fe  $d$ –NO  $\pi^*$  interaction with 0.34 electrons which are distributed nearly equally between Fe, N and O.

To estimate the strength of the antiferromagnetic coupling, broken symmetry calculations were done with all  $\{\text{FeNO}\}^7$  complexes.<sup>[134,135]</sup> They allow the calculation of the Heisenberg coupling constant  $J$  which is derived from the Heisenberg spin Hamiltonian (see equation 2.3) by using the Yamaguchi formalism<sup>[136]</sup> (see equation 2.4).

$$H = -2JS_{\text{A}} \cdot S_{\text{B}} \quad (2.3)$$

$$J = -\frac{E_{\text{HS}} - E_{\text{BS}}}{\langle \text{S}^2 \rangle_{\text{HS}} - \langle \text{S}^2 \rangle_{\text{BS}}} \quad (2.4)$$

The wave functions, obtained by using the broken symmetry formalism, are identical to those, obtained by directly applying the quartet spin. The calculated values for  $J$  vary between  $-2205 \text{ cm}^{-1}$  and  $-2318 \text{ cm}^{-1}$  for the B97-D functional and between  $-2051 \text{ cm}^{-1}$  and  $-2210 \text{ cm}^{-1}$  for the TPSSh functional, indicating a strong antiferromagnetic coupling, which could almost be described as a covalent bond. The overlap integral  $S_{ab}$  is calculated to 0.82 to 0.84 for the B97-D functional and to 0.76 to 0.80 for the TPSSh functional.

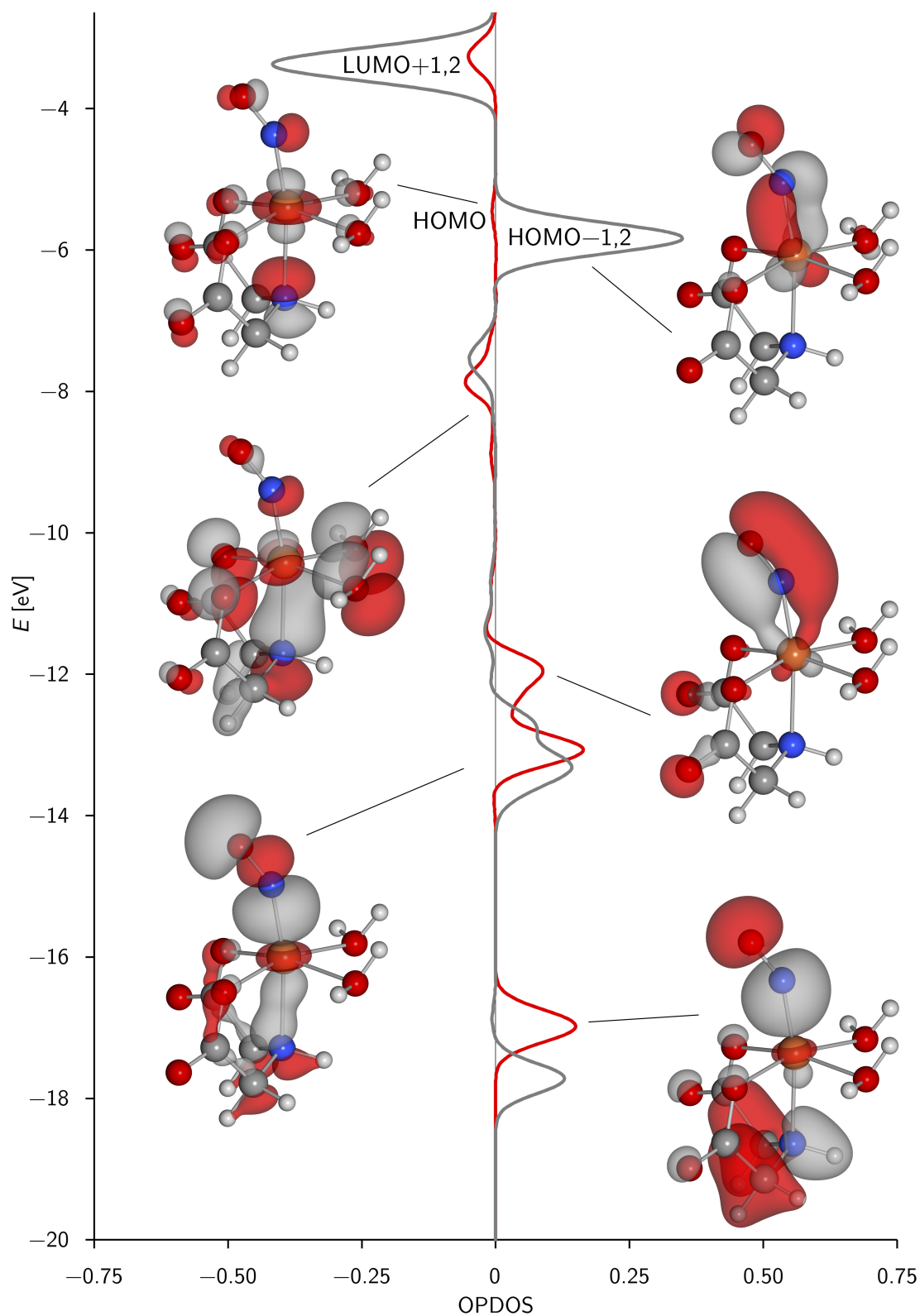


**Figure 2.24:** Plot of the overlap population density of states between Fe and NO of **3a** together with relevant bonding and antibonding molecular orbitals. Spin-up OPDOS in red, spin-down OPDOS in grey. Calculated using B97-D, def2-TZVP, D-COSMO-RS and dispersion correction (D3).

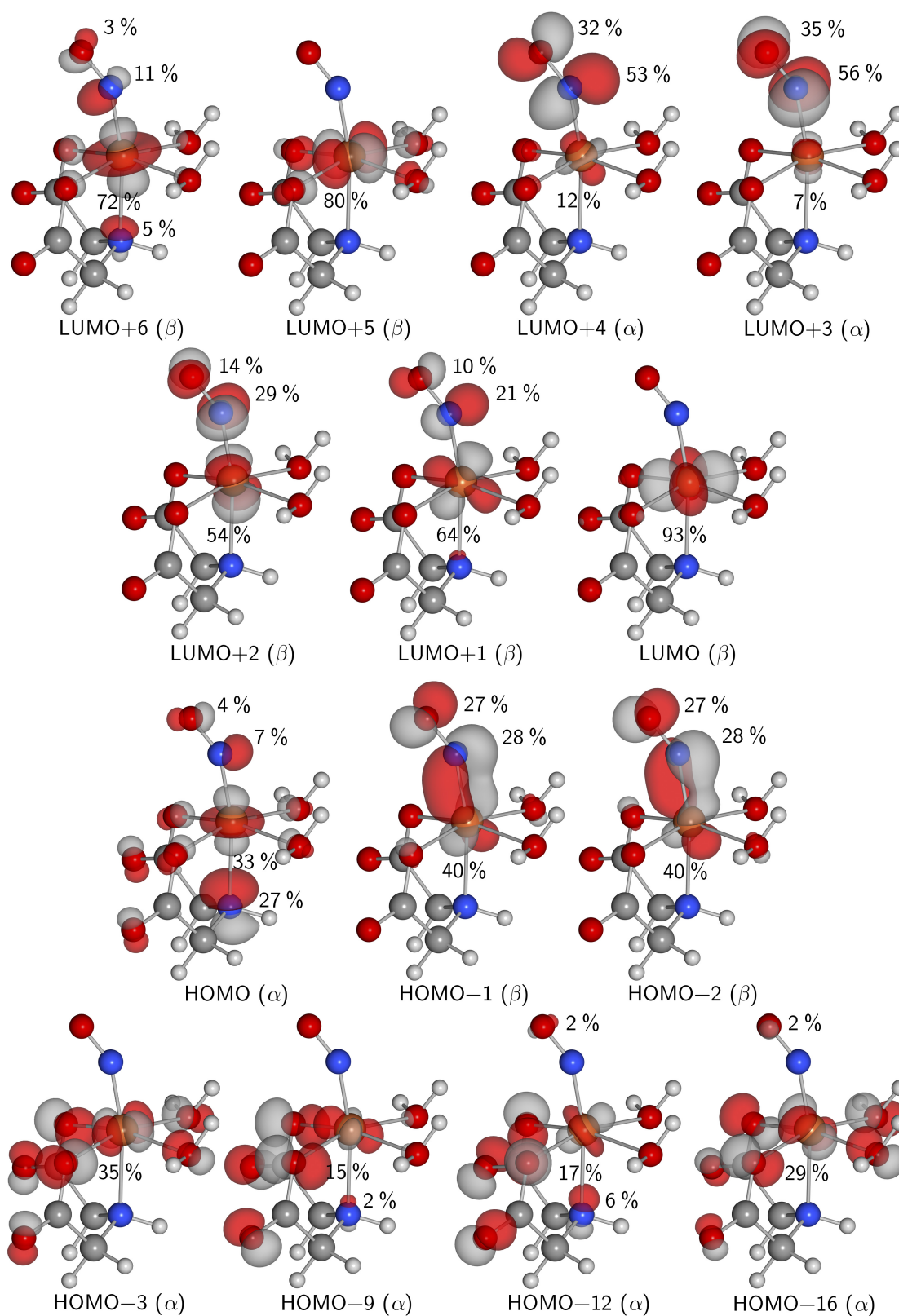


**Figure 2.25:** Contours of the seven lowest unoccupied orbitals of **3a** and their occupied counterparts. Calculated using B97-D, def2-TZVP, D-COSMO-RS and dispersion correction (D3). Individual contributions are derived from Mulliken population analyses.

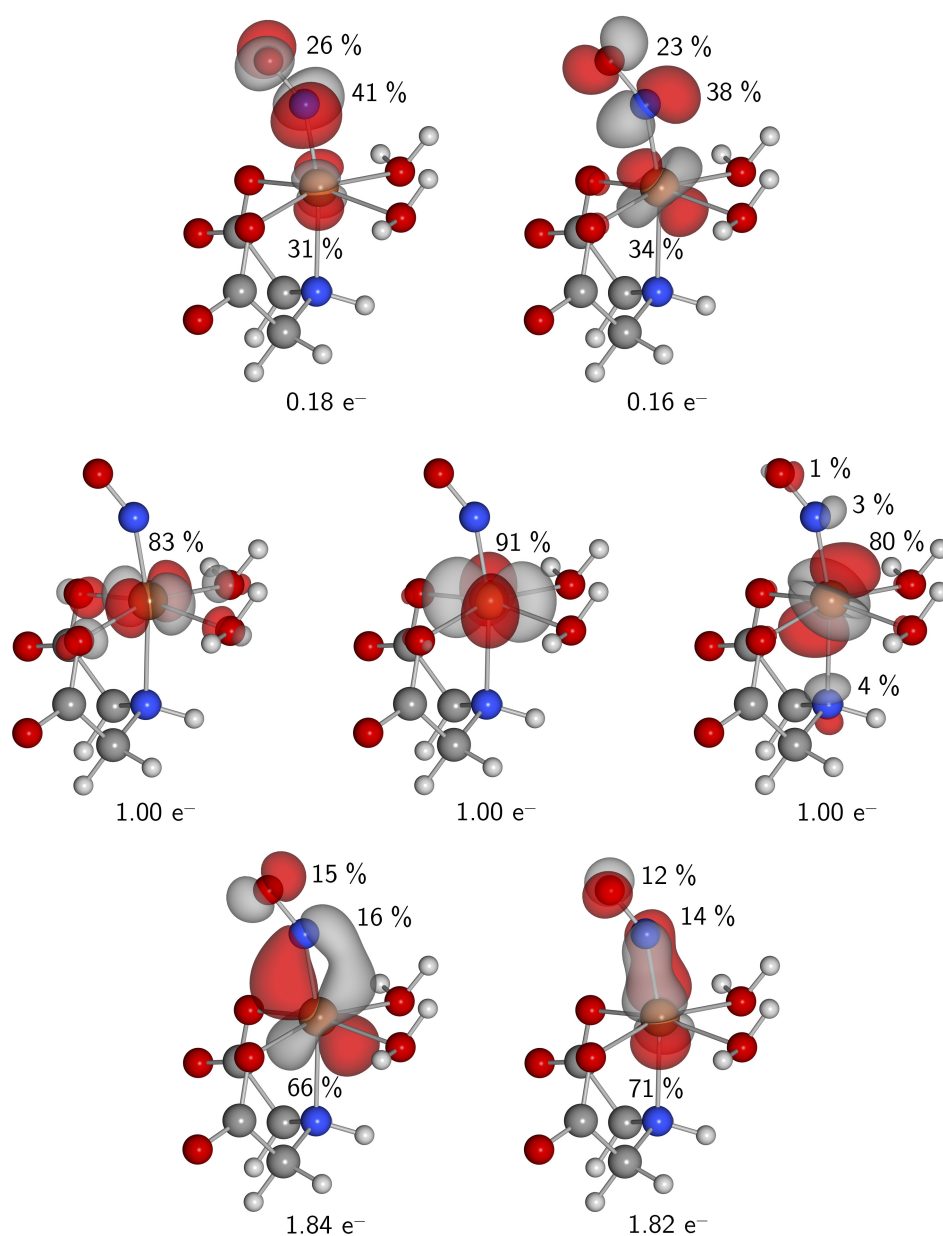


**Figure 2.26:** Contours of the seven relevant natural orbitals of **3a** together with their occupation numbers and individual atomic contributions. Calculated using B97-D, def2-TZVP, D-COSMO-RS and dispersion correction (D3). Individual contributions are derived from Mulliken populations analyses.

For the  $\{\text{Fe}(\text{NO})_2\}^9$  compounds **5c** and **5e**, the electronic description is basically the same as for the  $\{\text{FeNO}\}^7$  compounds. The dominating bonding interactions are those of the four spin-down NO  $\pi^*$  orbitals with all Fe  $d$  orbitals but Fe  $d_{z^2}$ . In the case of **5e**, the orbitals possess a 25% to 40% Fe  $d$  character, up to a 3% Fe  $p$  character and a 40% to 60% NO  $p$  character. In the case of **5c** they possess only a 15% to 30% Fe  $d$  character, up to a 5% Fe  $p$  character and a 15% to 45% NO  $p$  character due to large iodine contributions. The

HOMO represents again the spin-up Fe  $d_{z^2}$  orbital, where, however, no antibonding interaction with the NO  $5\sigma$  orbitals is observed. Figure 2.27 shows the relevant natural orbitals of **5e**. There is no big difference to the natural orbitals of **3a**, only the occupation of the virtual orbitals is a bit smaller. In summary, 7.63 electrons reside in the Fe–NO bonding orbitals and 0.37 electrons reside in the corresponding antibonding orbitals. The calculated Heisenberg coupling constants  $J$  are somewhat higher than for the mononitrosyl compounds.

Mulliken population analysis (MPA),<sup>[137]</sup> natural population analysis (NPA)<sup>[138]</sup> and AOMix-FO charge decomposition analyses (CDA)<sup>[139,140]</sup> were performed to gain insight into the charge and spin distribution between the iron atom and the nitrosyl ligand (see Tables 2.20 and 2.21). As before, the different chelating ligands hardly affect the results. For the mononitrosyl compounds, all population analyses assign neutral charge to the nitrosyl ligand. The calculated charge for the iron atom varies depending on the method. MPA calculates elementary charges between +0.5 and +0.6, NPA assigns +1.4 to compounds **3** and +1 to **5a** and **5b**. For the dinitrosyl species all charges are a bit lower. The spin densities show only a small dependence on the method but quite some dependence on the functional, with TPSSh calculating more spin polarized solutions. For **3**, **5a** and **5b** a  $\beta$  spin between  $-0.8$  and  $-1.1$  is calculated for the nitrosyl ligand and an  $\alpha$  spin between  $+3.3$  and  $+3.8$  is calculated for the iron atom. **5c** and **5e** have smaller spin densities on both iron atom and nitrosyl ligand. Figure 2.28 shows the spin densities on **3a**, **5a** and **5e**. The AOMix-FO analyses were performed using the fragments  ${}^2\text{NO}^0$  and  $\text{Fe}^{\text{II}}\text{L}$  (L = all ligands but NO). The analyses show that hardly any charge transfer occurs. The only exception are the  $\{\text{Fe}(\text{NO})_2\}^9$  compounds. Here, a charge transfer of 0.2  $\alpha$  electrons from the iron atom to each nitrosyl occurs.

#### 2.8.4 CASSCF calculations

To gain further insight into the Fe–N–O bond, CASSCF calculations were performed for **3a**, **5a** and **5e**. In contrast to DFT calculations, a CASSCF calculation can take into account several electronic configurations at one time and thus draw a much more elaborate picture of a given system. The minimum active space to describe the Fe–N–O moiety has to consist of seven electrons in five orbitals (three Fe  $d$  orbitals and two Fe  $d - \text{NO} \pi^*$  orbitals) for **3a** and **5a** and nine electrons in five orbitals (one Fe  $d$  orbital and four Fe  $d - \text{NO} \pi^*$  orbitals) for **5e**. However, to properly describe the compounds, a larger active space is required, taking into account the Fe–NO  $\sigma$  bond, unoccupied antibonding Fe–NO  $\pi$  interactions and double  $d$ -shells for Fe. For **3a** and **5a**, an active space of 9 electrons in 13 orbitals was chosen, for **5e** 13 electrons in 16 orbitals. Figures 2.29 and 2.30 show the relevant natural orbitals representing the active space for **3a**, **5a** and **5e** (without the double-shells) and their occupations. The result of the CASSCF calculations is similar for all three compounds. The dominant configuration of the CAS wave function corresponds to the DFT result: the

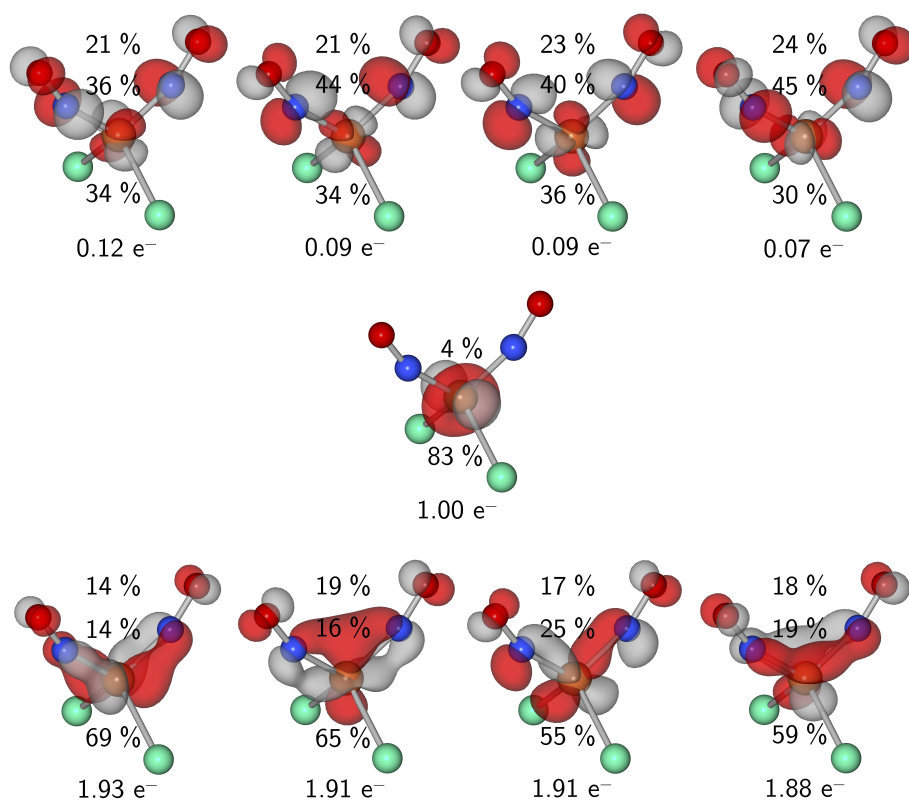


**Figure 2.27:** Contours of the nine relevant natural orbitals of **5e** together with their occupation number and individual atomic contributions. Calculated using B97-D, def2-TZVP and COSMO. Individual contributions are derived from Mulliken population analyses. Contributions from nitrogen and oxygen are identical for both nitrosyl ligands and are summarized.

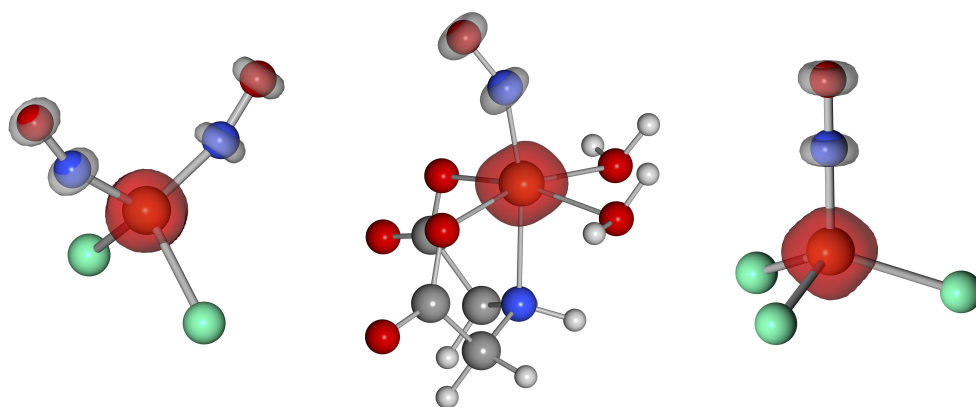


**Figure 2.28:** Spin density of **5e**, **3a** and **5a**. Calculated using B97-D, def2-TZVP, COSMO (**5e**, **5a**) or D-COSMO-RS (**3a**) and dispersion correction (D3) (only **3a**).

**Table 2.20:** MPA and NPA analysis on **3** and **5**. All values are elementary charges.

			Charge				Spin			
			Fe	N	O	NO	Fe	N	O	NO
<b>3</b>	MPA	B	0.57	0.18	-0.11	0.07	3.57	-0.51	-0.42	-0.93
		T	0.59	0.20	-0.12	0.08	3.78	-0.59	-0.48	-1.08
	NPA	B	1.35	0.08	-0.15	-0.06	3.51	-0.53	-0.37	-0.91
		T	1.41	0.08	-0.15	-0.07	3.69	-0.61	-0.43	-1.04
<b>5a</b>	MPA	B	0.56	0.12	-0.09	0.04	3.36	-0.47	-0.40	-0.88
		T	0.58	0.16	-0.10	0.06	3.54	-0.53	-0.45	-0.98
	NPA	B	0.99	0.06	-0.15	-0.09	3.42	-0.47	-0.37	-0.84
		T	1.07	0.06	-0.15	-0.09	3.55	-0.49	-0.41	-0.90
<b>5b</b>	MPA	B	0.47	0.14	-0.08	0.06	3.30	-0.45	-0.40	-0.85
		T	0.48	0.18	-0.09	0.09	3.49	-0.50	-0.43	-0.93
	NPA	B	0.88	0.07	-0.15	-0.08	3.34	-0.42	-0.35	-0.78
		T	0.95	0.07	-0.14	-0.07	3.48	-0.44	-0.39	-0.83
<b>5c</b>	MPA	B	0.30	0.05	-0.16	-0.11	2.09	-0.36	-0.29	-0.64
		T	0.29	0.08	-0.17	-0.09	2.69	-0.52	-0.41	-0.93
	NPA	B	0.56	0.06	-0.21	-0.16	2.00	-0.31	-0.26	-0.57
		T	0.67	0.03	-0.22	-0.19	2.50	-0.42	-0.37	-0.79
<b>5e</b>	MPA	B	0.45	0.03	-0.16	-0.13	2.31	-0.42	-0.33	-0.75
		T	0.45	0.05	-0.17	-0.12	2.90	-0.58	-0.46	-1.04
	NPA	B	0.72	0.05	-0.21	-0.17	2.22	-0.39	-0.30	-0.69
		T	0.84	0.01	-0.22	-0.21	2.76	-0.54	-0.41	-0.96

All calculations were performed using def2-TZVP basis sets and the functional B97-D (B) or TPSSh (T). For **5c** and **5e** identical results were obtained for both nitrosyl ligands.

**Table 2.21:** CDA analysis using AOMix-FO. All values are elementary charges.

	CT (Fe $\rightarrow$ NO) $_{\alpha}$	CT (Fe $\rightarrow$ NO) $_{\beta}$
<b>3</b>	-0.04	-0.03
<b>5a,b</b>	0.05	-0.10
<b>5c,e</b>	0.20	-0.07

All calculations were performed using def2-TZVP basis sets. The values displayed represent an average of the values obtained using the functionals B97-D and TPSSh. For **5c** and **5e** identical results were obtained for both nitrosyl ligands.

bonding interactions of the NO  $\pi^*$  orbitals with Fe  $d$  orbitals, are each occupied with two electrons and the remaining Fe  $d$  orbitals are each occupied with one unpaired electron. Yet this configuration accounts only for 50–60 % weight of the complete active space wave function. 35–40 % weight are distributed over different configurations, exciting electrons from the Fe–NO  $\pi$  bonding into the Fe–NO  $\pi$  antibonding orbitals. Especially for **5e**, there are many configurations possible; interestingly, the excitations of two electrons have a weight of 25 % altogether whereas the excitations of one electron sum up to only 12 %. This strong contribution of excited states is also reflected in the occupation numbers: the Fe–NO  $\pi$  bonding orbitals are occupied by 1.71 electrons, their antibonding counterparts are occupied by 0.28 electrons. The remaining 5–10 % weight are attributed to excitations from the Fe–NO  $\sigma$  bond or into the Fe  $d$  double-shells.

Again Mulliken population analyses were done. As shown in Table 2.22, the CASSCF calculation assigns a more positive charge to the iron atom than the DFT calculations do (Table 2.20). The charge on the nitrosyl ligand remains at 0 while the individual charges on oxygen and nitrogen become higher. The spin density on the nitrosyl ligand is reduced as compared to the DFT calculations, it now carries a  $\beta$  spin between  $-0.33$  and  $-0.55$ . The  $\alpha$  spin density on the iron atom is nearly identical for **3a** and **5a** (ca.  $+3.4$ ) but is reduced to  $+1.64$  for **5e**.

As a different approach to analyze the results of the CASSCF calculations, the orbitals of the active space were localized to yield 10 iron-centered orbitals and 3 nitrosyl-centered orbitals (6 nitrosyl-centered orbitals for **5e**). Now it is possible to determine the oxidation state of each configuration state function by simply summing up the occupied localized orbitals.<sup>[141,142]</sup> Table 2.23 gives an overview of the weights of each oxidation state. For **3a** and **5a**, the interpretation is fairly simple. With 66–70 %, the dominant oxidation state of the iron atom is  $+2$ . The oxidation state  $+3$  accounts for 21–25 %, the remaining 9 % correspond to the oxidation state  $+1$ . For **5e**, the interpretation becomes somewhat more complicated as both nitrosyl ligands interact with the iron atom and can take different oxidation states. Yet, due to symmetry, the interactions are identical for both nitrosyl ligands and can be summarized. With 52 %, the dominant oxidation state of the iron atom is again  $+2$  which is accomplished by one NO<sup>0</sup> and one NO<sup>-</sup> ligand, resulting in an average oxidation state of  $-0.5$  for the nitrosyl ligand. 29 % weight correspond to Fe<sup>I</sup>, mostly in combination with two NO<sup>0</sup> ligands. 16 % weight correspond to Fe<sup>III</sup> and two NO<sup>-</sup> ligands (15 %) or one NO<sup>0</sup> and one NO<sup>2-</sup> ligand (1 %). The remaining 3 % are allotted to Fe(0) with one NO<sup>0</sup> and one NO<sup>+</sup> ligand.

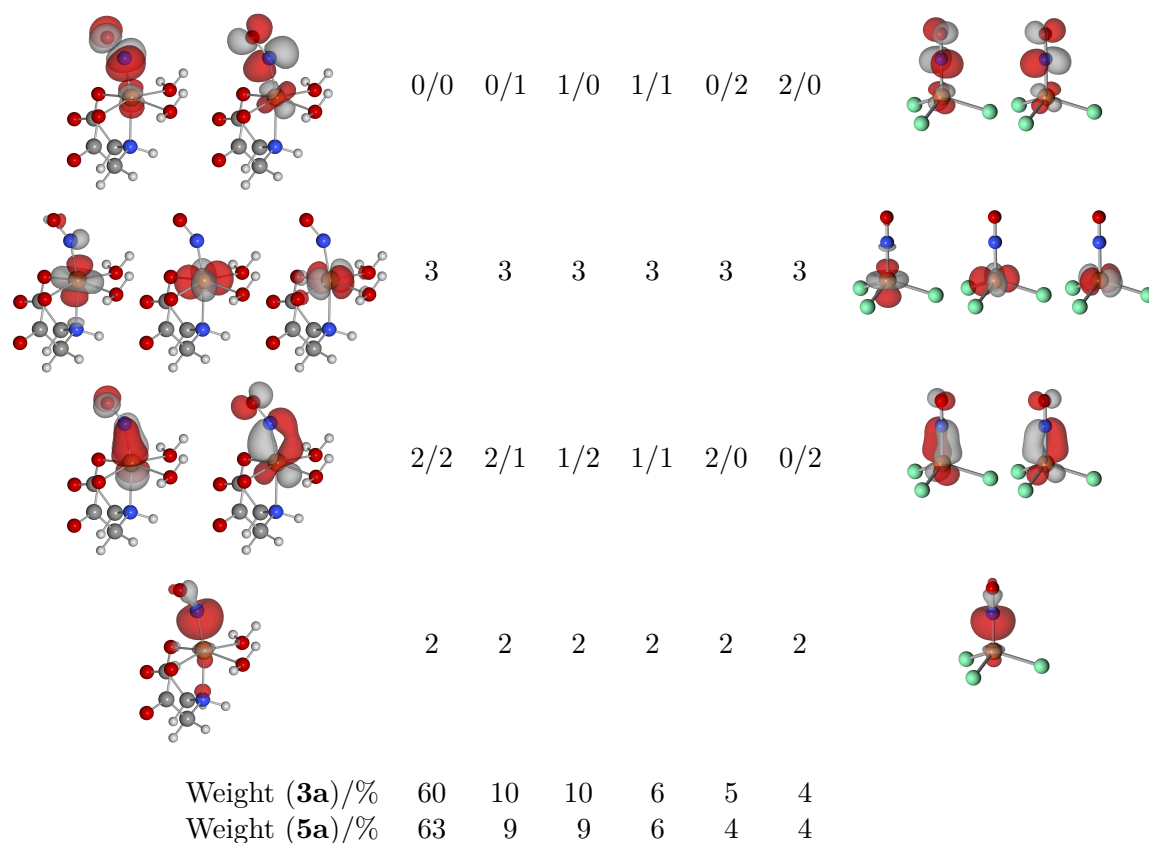


**Figure 2.29:** Active space in the CASSCF calculations of **3a** and **5a**. Given in the columns besides the different orbitals is the number of electrons in these orbitals for each configuration state function. The weight of each configuration state function is given below each column.

**Table 2.22:** Mulliken analysis on the CASSCF calculations of **3a**, **5a** and **5e**. All values are elementary charges.

		<b>3a</b>	<b>5a</b>	<b>5e</b>
Charge	Fe	1.12	1.04	0.94
	N	0.27	0.27	0.08
	O	-0.30	-0.24	-0.34
	NO	-0.03	0.03	-0.26
Spin	Fe	3.49	3.42	1.64
	N	-0.37	-0.33	-0.22
	O	-0.18	-0.18	-0.11
	NO	-0.55	-0.51	-0.33

All calculations were performed using def2-TZVP basis sets and COSMO (**5a,e**) or D-COSMO-RS (**3a**). For **5e** identical results were obtained for both nitrosyl ligands.

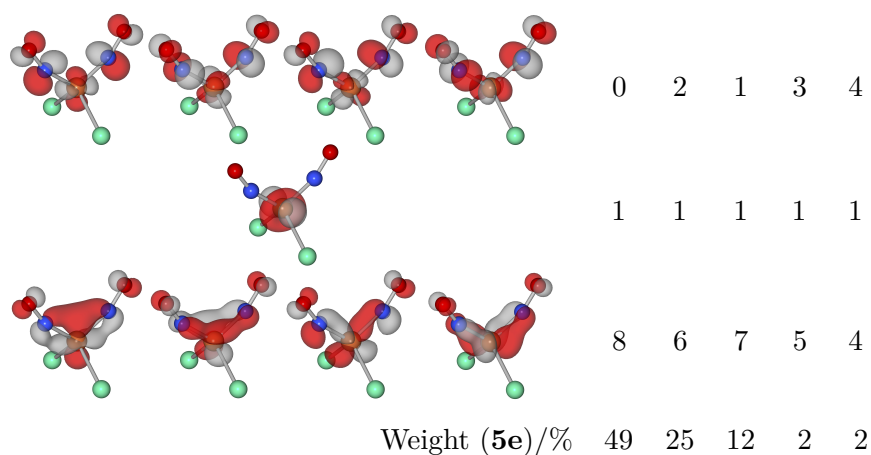


**Figure 2.30:** Active space in the CASSCF calculation of **5e**. Given in the columns besides the different orbitals is the number of electrons in these orbitals for each configuration state function. The weight of each configuration state function is given below each column. Configurations with the same electron count in each group of orbitals have been summarized.

**Table 2.23:** Weights of the different oxidation states in the CAS wave functions of **3a**, **5a** and **5e**, calculated from localized orbitals.

	<b>3a</b>	<b>5a</b>	<b>5e</b>
Fe <sup>I</sup> – NO <sup>+</sup>	9 %	9 %	
Fe <sup>II</sup> – NO <sup>0</sup>	66 %	70 %	
Fe <sup>III</sup> – NO <sup>-</sup>	25 %	21 %	
Fe <sup>0</sup> – NO <sup>0</sup> / NO <sup>+</sup>			3 %
Fe <sup>I</sup> – NO <sup>0</sup> / NO <sup>0</sup>			24 %
Fe <sup>I</sup> – NO <sup>-</sup> / NO <sup>+</sup>			5 %
Fe <sup>II</sup> – NO <sup>0</sup> / NO <sup>-</sup>			52 %
Fe <sup>III</sup> – NO <sup>-</sup> / NO <sup>-</sup>			15 %
Fe <sup>III</sup> – NO <sup>•</sup> / NO <sup>2-</sup>			1 %

### 2.8.5 TDDFT calculations

To gain better insight into the origin of the different absorption bands of the obtained complexes, their excitation energies were calculated by time-dependent DFT (TDDFT). The results with the best agreement to experimental data were obtained using the structure of calculations with the functional TPSSh and then calculating the excitations with the functional BP-86. Figure 2.31 shows a comparison of experimental spectra and calculated excitations.

The most simple UV-VIS spectrum is that of the pentaquanitrosyliron(2+) solution and the “brown FeSO<sub>4</sub>” (**1**), respectively. In the experiment three absorption bands can be identified at 330 nm, 451 nm and 584 nm. The TDDFT calculation is in very good agreement with these data and shows a strong excitation at 332 nm, a strong excitation at 441 nm and four weak excitations at 521 nm, 522 nm, 580 nm and 584 nm forming together an absorption band with a maximum around 550 nm. To all excitations, distinct orbital contributions can be assigned. Table 2.24 gives an overview of the TDDFT results.

For compounds **3** the analysis of the calculated TDDFT spectra becomes a lot more complicated. Between 20 and 30 excitations with a significant oscillator strength are calculated. Especially the region between 340 nm and 420 nm is made up of many excitations all of which have several orbital contributions. Yet a good agreement of experimental and calculated data can be achieved. In Table 2.24 the results for **3a** are shown.

For **5a** and **5b**, the calculated spectra are, again, very easy to analyze. More complicated is the spectrum of **5c**. The different excitations of  $\alpha$  electrons are especially hard to distinguish, as nearly every orbital features contributions from the iron center, the iodine ligands and the nitrosyl ligands. Nonetheless, an assignment is given in Table 2.24, taking into account only the most prominent contributions to each excitation.

## 2.9 The Fe–N–O bond angle

In most of the crystal structures **3** the nitrosyl-oxygen atoms feature very large atomic displacement parameters (ADP), indicating disorder. The question is, whether they are due to dynamic or static disorder. Bürgi *et al.*<sup>[143–146]</sup> suggest a temperature-dependent analysis of relevant ADPs to distinguish between dynamic and static disorder of corresponding atoms. For this purpose, two crystal structures **3e** and **3f** were measured at five different temperatures and the ADPs  $U_{11}$ ,  $U_{22}$  and  $U_{33}$  of O1 and N1 were plotted against the temperature (Figure 2.32). In the case of dynamic disorder they are expected to show a linear dependence on the temperature and an intercept of 0 Å<sup>2</sup> when extrapolating to 0 K.

**Table 2.24:** Results of the TDDFT calculations on **1**, **3a**, **5a** and **5c**.

Compound	$\lambda/\text{nm}$ exp./calc.	$\alpha$ electron density	$\beta$ electron density
<b>1</b>	584/550	Fe $d_{x^2-y^2, z^2} \rightarrow \text{NO } \pi^*$	—
	451/441	Fe $d_{xy, xz, yz} \rightarrow \text{NO } \pi^*$	Fe–NO $\pi \rightarrow \text{Fe–NO } \pi^*$
	330/332	—	H <sub>2</sub> O $\rightarrow \text{Fe } d_{xy}$
<b>3a</b>	694/758	Fe $d_{z^2} \rightarrow \text{NO } \pi^*$	Fe–NO $\pi \rightarrow \text{Fe } d_{xy}$
	618/575	Fe $d_{x^2-y^2} \rightarrow \text{NO } \pi^*$	Fe–NO $\pi \rightarrow \text{Fe–NO } \pi^*$
	459/453	Fe $d_{xz, yz, z^2} \rightarrow \text{NO } \pi^*$	Fe–NO $\pi \rightarrow \text{Fe–NO } \pi^*$
	416/365	ida $\rightarrow \text{NO } \pi^*$	ida + H <sub>2</sub> O $\rightarrow \text{Fe } d_{xy, x^2-y^2, z^2}$
	340/334	—	ida $\rightarrow \text{Fe } d_{xy, x^2-y^2}$
<b>5a</b>	692/710	—	Fe–NO $\pi \rightarrow \text{Fe } d_{xy, x^2-y^2}$
	669/535	—	Fe–NO $\pi \rightarrow \text{Fe–NO } \pi^* + \text{Fe } d_{z^2}$
	484/432	Cl $\rightarrow \text{NO } \pi^*$	Cl $\rightarrow \text{Fe } d_{xy, x^2-y^2}$
	370/360	Cl $\rightarrow \text{NO } \pi^*$	Cl $\rightarrow \text{Fe } d_{xy, x^2-y^2, z^2}$
	303/298	Cl $\rightarrow \text{NO } \pi^*$	Cl $\rightarrow \text{Fe } d_{xy, x^2-y^2, z^2}$
<b>5c</b>	762/827	—	Fe–NO $\pi \rightarrow \text{Fe } d_{z^2}$
	608/602	Fe $d_{z^2} \rightarrow \text{NO } \pi^*$	Fe–NO $\pi \rightarrow \text{Fe–NO } \pi^*$
	433/484	I $\rightarrow \text{NO } \pi^*$	I $\rightarrow \text{Fe } d_{z^2}$
	406/370	I $\rightarrow \text{NO } \pi^*$	I $\rightarrow \text{Fe–NO } \pi^* + \text{Fe } d_{z^2}$
	302/320	Fe $d_{xz, yz, y^2} \rightarrow \text{NO } \pi^*$	I + Fe $d_{xz} \rightarrow \text{Fe–NO } \pi^* + \text{Fe } d_{z^2}$

All calculations were performed using def2-TZVP basis sets. The structure of the compounds was calculated using the methods described above with functional TPSSh, the excitations were calculated using the functional BP-86.

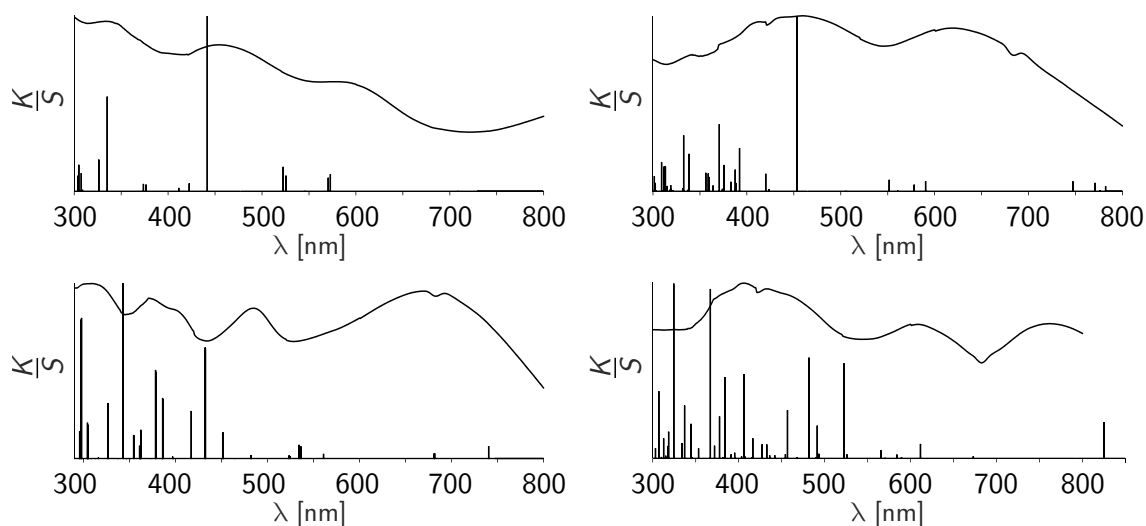


**Figure 2.31:** UV-VIS spectra from solid samples of **1** (top left), **3a** (top right), **5a** (bottom left) and **5c** (bottom right) together with calculated excitations using the TDDFT formalism.

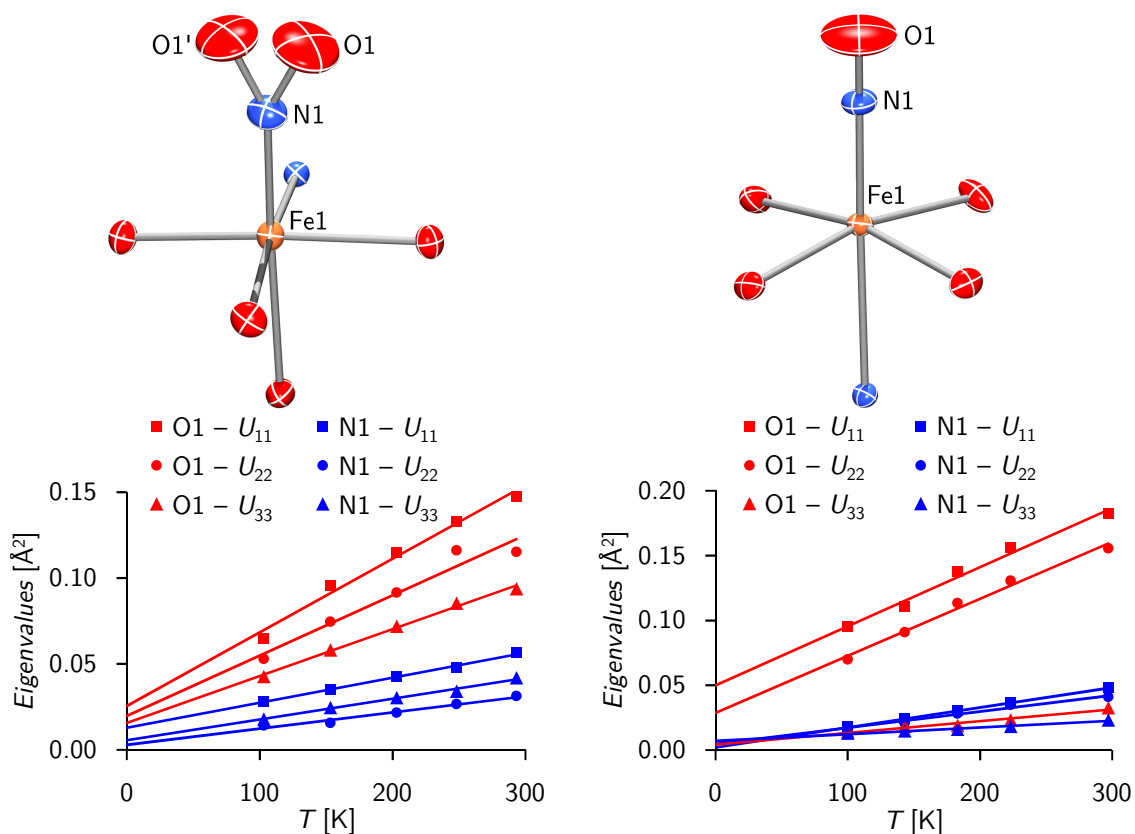


**Figure 2.32:** Plot of ADPs of O1 and N1 of **3e** (left) and **3f** (right) against the temperature. For O1 of **3e** the average of O1 and O1' was used.

According to literature<sup>[146]</sup>, an intercept significantly larger than  $0.005 \text{ \AA}^2$  indicates static disorder. It is obvious, that in both cases the oxygen atom is statically disordered. For **3e** the disorder is less dominant, probably because it had already been taken into account by splitting the position of the oxygen atom. The splitting of the position of the nitrogen atom was not possible, therefore it shows a significant intercept for  $U_{11}$ . For **3f**, only  $U_{11}$  and  $U_{22}$  show a significant intercept of  $0.05 \text{ \AA}^2$  and  $0.03 \text{ \AA}^2$  respectively,  $U_{33}$ , pointing in direction of the N–O bond shows no static disorder.

In order to get a better understanding of the Fe–N–O bond angle, DFT calculations were performed, constraining the angle to fixed values while optimizing all other coordinates. For **5e**, two calculations were done, constraining either one or both Fe–N–O angles. Figure 2.33 shows on its left side the Fe–N–O bending potential of **3a,d,f,i**, **5a** and **5e**. It becomes obvious that all compounds show a very flat bending potential. For  $180^\circ$  only **5e** shows a significant potential of  $12 \text{ kJ mol}^{-1}$  when constraining both Fe–N–O angles. When bending the angle, the potential stays below  $5 \text{ kJ mol}^{-1}$  until the angle reaches  $140^\circ$  to  $130^\circ$ . The only exception is again **5e** when constraining both angles. In addition to the constraint

structural optimizations, frequency analyses were done. Figure 2.33 shows on its right side a linear correlation of Fe–N–O angle and  $\nu(\text{NO})$  with a slope of approximately  $3 \text{ cm}^{-1}/^\circ$ . All compounds **3** are located on almost the same curve, for compounds **5a** and **5e** the curve has the same slope but a smaller intercept. This time the exception is **5e** with only one constraint angle; here the bending has only little effect on  $\nu(\text{NO})$ . MPA, and NPA analyses show no significant change of charge or spin population while bending the Fe–N–O moiety. The coupling constant  $J$  from broken symmetry calculations does not change between the Fe–N–O angles of  $180^\circ$  and  $140^\circ$  but decreases rapidly below an angle of  $140^\circ$ . Figure 2.34 shows the Walsh diagram of **3a** together with NPA analyses and the coupling constant  $J$ . At  $180^\circ$  the HOMO is a  $\sigma$  antibonding interaction between the Fe  $d_{z^2}$  orbital and the  $5\sigma$  orbital of NO. When bending the Fe–N–O angle to  $110^\circ$ , the HOMO is lowered in energy by 0.3 eV and becomes HOMO–2, a weak  $\sigma$  bonding interaction between the Fe  $d_{z^2}$  orbital and an NO  $\pi^*$  orbital. Meanwhile HOMO–1 and HOMO–2, being bonding  $\pi$  interactions of the NO  $\pi^*$  orbitals with the Fe  $d_{xz}$  and Fe  $d_{yz}$  orbitals, rise in energy by 0.5 eV. HOMO–1 also becomes a  $\sigma$  bonding interaction between the Fe  $d_{xz}$  orbital and an NO  $\pi^*$  orbital. HOMO–2 does not change at all except for the bending, it is now the HOMO.

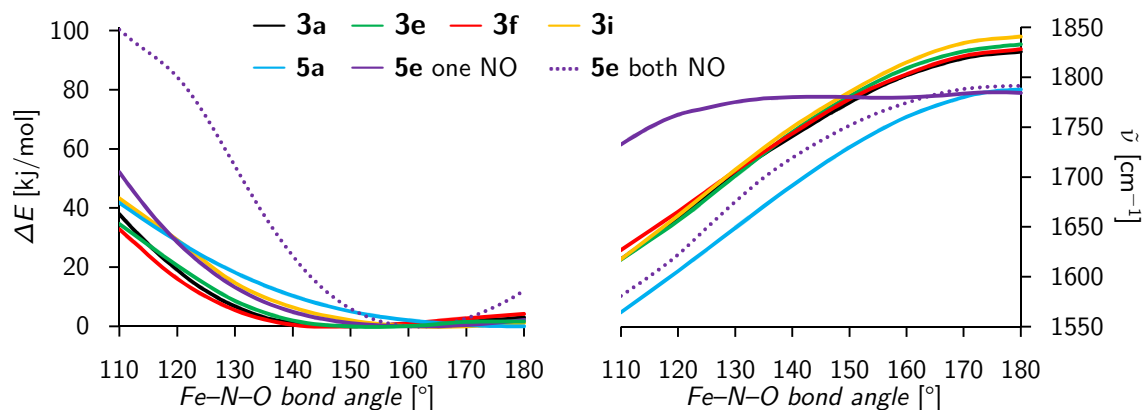


**Figure 2.33:** Left side: Fe–N–O bending potential of **3a,d,f,i**, **5a** and **5e**. Right side: Plot of  $\nu(\text{NO})$  against the Fe–N–O angle. Calculated using B97-D, def2-TZVP, D-COSMO-RS and dispersion correction (D3) (compounds **3** only).

## 2.10 Iron mono- and dinitrosyls and their corresponding nitrosyl-free compounds

For some  $\{\text{FeNO}\}^7$  compounds presented in this thesis the corresponding nitrosyl-free  $\text{Fe}^{\text{II}}$  complexes with an aqua ligand instead of the nitrosyl group could be synthesized. Others can be found in literature together with corresponding  $\text{Fe}^{\text{III}}$  complexes. To further investigate

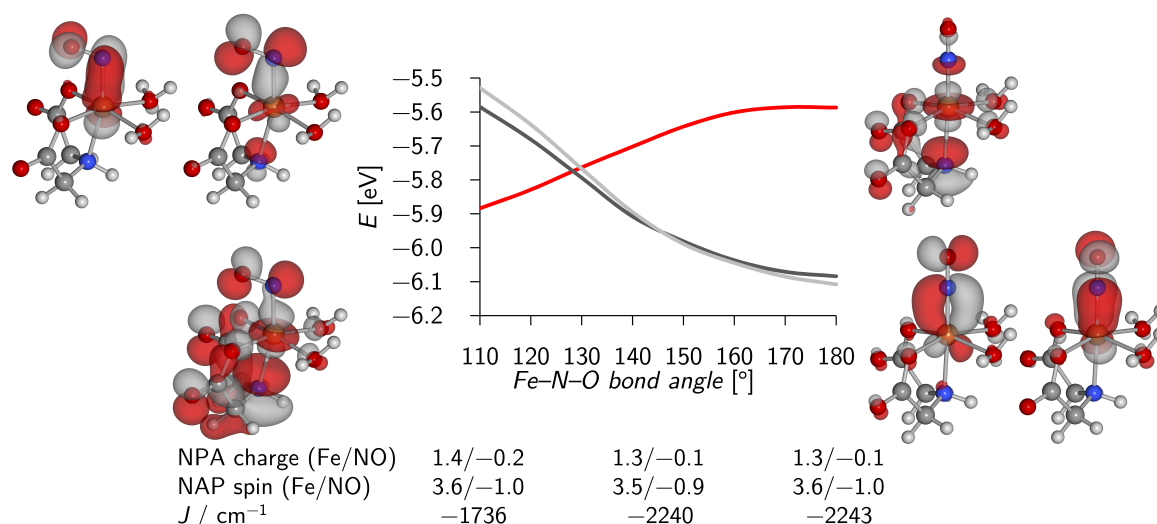


**Figure 2.34:** Walsh diagram of **3a**. Spin-up MOs in red, spin-down MOs in grey. Calculated using B97-D, def2-TZVP, D-COSMO-RS and dispersion correction (D3). Charge, spin and  $J$  are denoted for  $110^\circ$ ,  $144^\circ$  and  $180^\circ$ .

the oxidation state of the iron atom in the obtained  $\{\text{FeNO}\}^7$  and  $\{\text{Fe}(\text{NO})_2\}^9$  compounds, a comparison of these corresponding complexes with respect to their bond lengths, atomic charges and spin densities was made (see Table 2.25). Comparing the Fe–ligand bond lengths in the crystal structures, it becomes obvious, that the nitrosyl-iron compounds lie in between the  $\text{Fe}^{\text{II}}$  complexes and the  $\text{Fe}^{\text{III}}$  complexes but closer to the former. Yet only for the chlorido ferrates and the complexes with dipic as chelating ligand can a sound statement be made, as they feature an identical coordination sphere for the  $\text{Fe}^{\text{II}}$  and the  $\text{Fe}^{\text{III}}$  complexes. **3i** has nearly the same bond lengths as the corresponding  $\text{Fe}^{\text{II}}$  complex. **5a** resembles more the  $\text{Fe}^{\text{III}}$  ferrate while the dinitrosyl **5e** lies closer to the  $\text{Fe}^{\text{II}}$  ferrate. From the bond lengths calculated by DFT, the same conclusions can be drawn. Looking at the charges and spin densities on the iron atom, three facts stand out. Oxidizing an  $\text{Fe}^{\text{II}}$  complex has little effect on the charge of the iron atom when using MPA; using NPA, the charge rises by +0.3. The substitution with a nitrosyl ligand results in a less positive charge of the iron atom compared to the  $\text{Fe}^{\text{II}}$  complexes, thus a reduction of iron atom takes place. The spin density on the iron atom is lowered only a little by the nitrosyl ligand except for the dinitrosyl.

## 2.11 PLI measurements

The phenomenon of the photoinduced linkage isomerism (PLI) has already been discussed in the introduction (see page 3). So far, no PLI behavior has been detected for  $\{\text{FeNO}\}^7$

**Table 2.25:** Comparison of crystal structures (upper rows) and DFT results (lower rows) of  $\{\text{FeNO}\}^7$  compounds with nitrosyl-free  $\text{Fe}^{2+}$  and  $\text{Fe}^{3+}$  complexes. Distances in Å, charges and spins in elementary charges.

	Fe–OAc/Cl <sup>a</sup>		Charge(Fe)		Spin(Fe)	
	Fe–OH <sub>2</sub> /OR <sup>b</sup>		MPA	NPA	MPA	NPA
[Fe <sup>II</sup> (dhpida)(OH <sub>2</sub> ) <sub>2</sub> ] ( <b>4c</b> )	2.11	2.09				
	2.09	2.18	0.75	1.48	3.81	3.70
[Fe(dhpida)(NO)] ( <b>3c</b> )	2.05	2.10				
	2.05	2.13	0.58	1.37	3.76	3.66
[Fe <sup>III</sup> (dhpida)(OH <sub>2</sub> ) <sub>2</sub> ] <sup>+c</sup>	1.96	2.07	0.75	1.81	4.29	4.22
[Fe <sup>II</sup> (dipic)(OH <sub>2</sub> ) <sub>3</sub> ] ( <b>4i</b> )	2.16	2.12				
	2.14	2.18	0.76	1.52	3.84	3.73
[Fe(dipic)(NO)(OH <sub>2</sub> ) <sub>2</sub> ] ( <b>3i</b> )	2.12	2.11				
	2.11	2.15	0.58	1.39	3.78	3.69
[Fe <sup>III</sup> (dipic)(OH <sub>2</sub> ) <sub>3</sub> ] <sup>+ [147]</sup>	2.01	2.00				
	2.01	2.05	0.73	1.82	4.31	4.25
[Fe <sup>II</sup> (OH <sub>2</sub> ) <sub>2</sub> (oda)] <sub>n</sub> <sup>[148]</sup>	2.14	2.15				
	2.11	2.16	0.79	1.51	3.83	3.72
[Fe <sup>II</sup> (OH <sub>2</sub> ) <sub>3</sub> (oda)] <sup>c</sup>	2.12	2.16	0.82	1.51	3.83	3.73
[Fe(NO)(OH <sub>2</sub> ) <sub>2</sub> (oda)] ( <b>3d</b> )	2.07	2.08				
	2.05	2.15	0.62	1.41	3.78	3.69
[Fe <sup>III</sup> Cl(OH <sub>2</sub> ) <sub>2</sub> (oda)] <sup>[149]</sup>	2.00	2.03				
	2.00	2.10	0.73	1.65	4.23	4.21
[Fe <sup>III</sup> (OH <sub>2</sub> ) <sub>3</sub> (oda)] <sup>+c</sup>	1.96	2.07	0.79	1.82	4.30	4.25
[Fe <sup>II</sup> Cl <sub>4</sub> ] <sup>2- [150–153]</sup>	2.31					
	2.33		0.73	1.16	3.72	3.73
[FeCl <sub>2</sub> (NO) <sub>2</sub> ] <sup>-</sup> ( <b>5e</b> )	2.27					
	2.30		0.45	0.84	2.90	2.76
[FeCl <sub>3</sub> (NO)] <sup>-</sup> ( <b>5a</b> )	2.23					
	2.26		0.58	1.07	3.54	3.55
[Fe <sup>III</sup> Cl <sub>4</sub> ] <sup>- [153–156]</sup>	2.19					
	2.22		0.79	1.17	3.99	4.12

The values in the first two columns are an average of the two respective bond lengths in the complex. For the DFT calculations TPSSh, def2-TZVP, D-COSMO-RS (for the chlorido ferrates only COSMO) and dispersion correction (D3) were used.

<sup>a</sup> An average of all Fe–Cl bond lengths was taken. <sup>b</sup> Valid for compounds with dhpida.

<sup>c</sup> Only DFT data available.

compounds. Due to their stability against oxygen and moisture, the  $\{\text{FeNO}\}^7$  compounds presented in this thesis were promising candidates for the investigation of a possible PLI behavior. As these investigations require special equipment, they were performed by Dominik Schaniel at the *Institut Jean Barriol* in Nancy, France.

### 2.11.1 PLI of quartet- $\{\text{FeNO}\}^7$ compounds with aminocarboxylato ligands

Samples of **3a**, **3e** and **3f** were irradiated at 80 K with light of different wavelengths in the range of 325 nm to 660 nm. At the same time an IR spectrum was recorded and the  $\nu(\text{NO})$  stretching vibration band was monitored. Yet no PLI could be detected. Figure 2.35 shows the result of PLI investigations on **3e**. It is obvious that neither the  $\nu(\text{NO})$  stretching vibration band at  $1768\text{ cm}^{-1}$  changes in intensity nor a new band is formed.

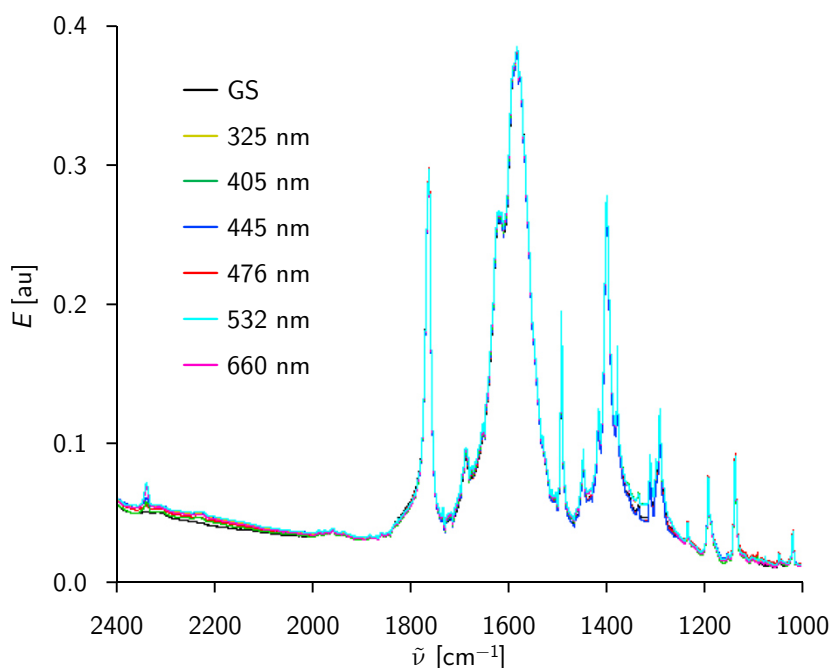


**Figure 2.35:** Plot of the IR spectrum of **3e** at 80 K under irradiation with light of different wavelengths.

### 2.11.2 PLI experiment on $\{\text{PPN}\}[\text{FeCl}_3(\text{NO})]$

The same experiments were performed at 9 K on  $(\text{PPN})\mathbf{5a}$ . Here a clear effect on the  $\nu(\text{NO})$  stretching vibration band is visible (see Figure 2.36). After irradiation with light of a wavelength of 635 nm, the  $\nu(\text{NO})$  stretching vibration band at  $1809\text{ cm}^{-1}$  is clearly less intensive, meanwhile a new band at  $1868\text{ cm}^{-1}$  is formed. Warming the sample to 40 K results

in a decay of the band at  $1868\text{ cm}^{-1}$ , the band at  $1809\text{ cm}^{-1}$  gains its former intensity. This is an indicator for a reversible process. When the sample is kept at 9 K after irradiation, a slow decay of the band at  $1868\text{ cm}^{-1}$  can be detected. After 30 minutes, it shows only 20% of its former intensity (see Figure 2.37).

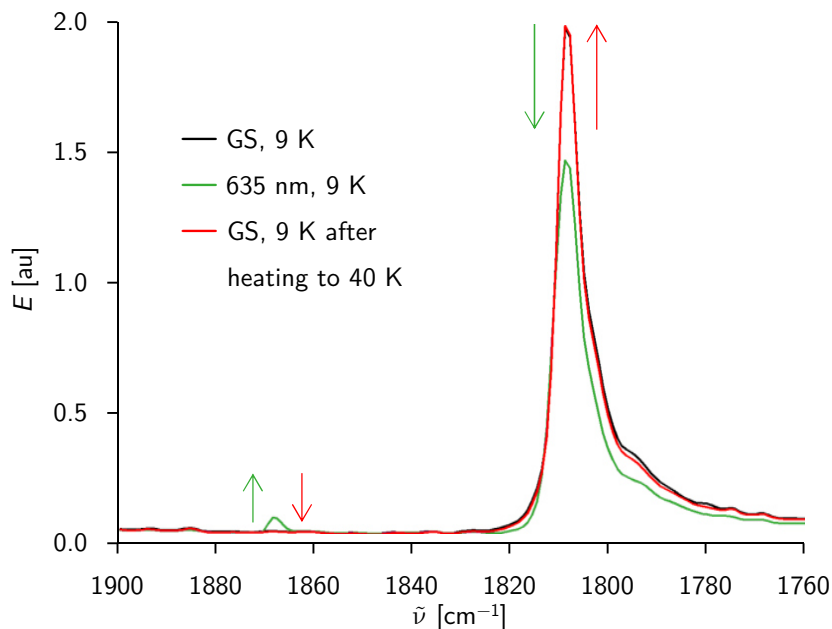


**Figure 2.36:** Plot of the IR spectrum of (PPN)**5a** at 9 K after irradiation with light of a wavelength of 635 nm and after heating to 40 K.

These results are somewhat surprising and were unexpected. The newly formed  $\nu(\text{NO})$  stretching vibration band at  $1868\text{ cm}^{-1}$  indicates that something other than a typical linkage isomerism has happened. The formation of an isonitrosyl or a side-on bound species usually results in a redshift of  $\nu(\text{NO})$ .<sup>[56–58]</sup> Here, however, a blueshift occurs, indicating a strengthening of the N–O bond. A possible explanation is the temporary transfer of one electron from the nitrosyl ligand to the  $(\text{PPN})^+$  cation. DFT calculations support this hypothesis. Figure 2.38 shows relevant MOs of **5a** at the ground state and after a 1-electron oxidation by removing one spin-down electron from the wave function, resulting in a quintet state. In doing so, the Fe–N–O angle is bent to  $129^\circ$  and the N–O bond length is shortened to  $1.13\text{ \AA}$ . Meanwhile the  $\nu(\text{NO})$  stretching vibration band is shifted to  $1871\text{ cm}^{-1}$  which is in very good agreement with the experimental value of  $1868\text{ cm}^{-1}$ . The HOMO changes from the known antibonding Fe–NO  $\sigma$  interaction to a Fe  $d_{x^2-y^2}$  orbital; HOMO–1 becomes the new LUMO, and HOMO–2 changes to a  $\sigma$  bonding interaction of the Fe  $d_{z^2}$  orbital with a NO  $\pi^*$  orbital.

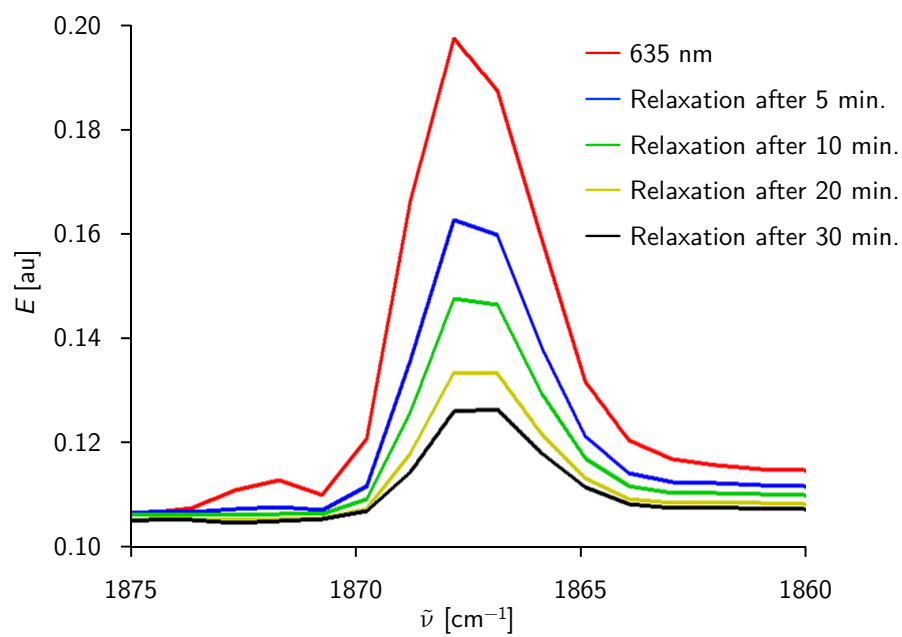


**Figure 2.37:** Plot of the IR spectrum of (PPN)5a at 9 K, after irradiation with light of a wavelength of 635 nm and after relaxation at 9 K for up to 30 minutes.

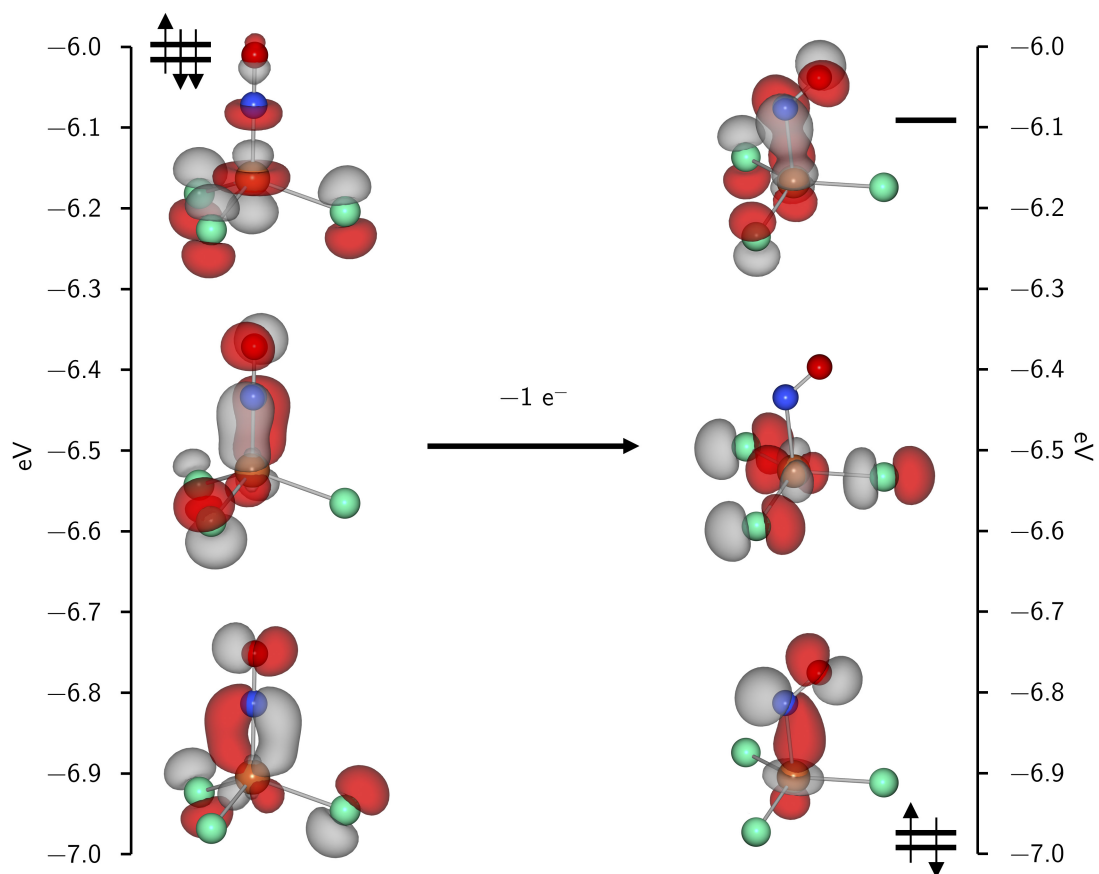


**Figure 2.38:** DFT calculation on the oxidation of **5a**. Calculated using BP-86, def2-TZVP and COSMO.



## 3 Discussion

### 3.1 Quartet- $\{\text{FeNO}\}^7$ compounds with aminocarboxylato ligands

During the research for this thesis nine octahedral quartet- $\{\text{FeNO}\}^7$  compounds were isolated in crystalline form and characterized by X-ray diffraction. They all feature a bent Fe–N–O moiety with an angle between  $148^\circ$  and  $171^\circ$ . The Fe–N bond lengths range between 176 pm and 180 pm, the N–O bond lengths range between 109 pm and 117 pm. Their  $\nu(\text{NO})$  stretching vibration band is found between  $1764\text{ cm}^{-1}$  and  $1814\text{ cm}^{-1}$  and their main UV-VIS absorption bands are located around 340 nm, 460 nm and 600 nm. With these experimental data the newly synthesized compounds match perfectly the crystalline quartet- $\{\text{FeNO}\}^7$  compounds known to literature: as of March, 2016, the Cambridge Structural Database listed 815 nitrosyl-iron compounds. 547 are MNICs but only 24 of them are quartet- $\{\text{FeNO}\}^7$  compounds with an octahedral coordination sphere.<sup>[42,61–78]</sup> Their Fe–N–O angles range between  $139^\circ$ <sup>[78]</sup> and  $174^\circ$ ,<sup>[73,77]</sup> the Fe–N bond lengths have values between 170 pm<sup>[63]</sup> and 182 pm,<sup>[42]</sup> their N–O bond lengths range between 110 pm<sup>[73]</sup> and 119 pm<sup>[70]</sup> and their  $\nu(\text{NO})$  stretching vibration bands are found between  $1685\text{ cm}^{-1}$ <sup>[71]</sup> and  $1831\text{ cm}^{-1}$ <sup>[77]</sup>. Besides all similarities, two aspects are unique about the new compounds **3**: they are the first crystalline nitrosyl-iron compounds with a  $(\text{NO}_4)$  coordination sphere and they are among the first crystalline nitrosyl-iron compounds with aqua ligands (so far only two heme  $\{\text{FeNO}\}^6$  structures have been published<sup>[157,158]</sup>). In 2001 Schnepf *et al.* published a study investigating  $\{\text{FeNO}\}^7$  complexes with aminocarboxylato ligands in aqueous solution.<sup>[79]</sup> Amongst others they also used the ligands **2a,b,d,i**. Their spectroscopic data is comparable to the results on crystalline samples but not identical. Their reported  $\nu(\text{NO})$  stretching vibration band for **3b** is  $1762\text{ cm}^{-1}$  which is  $20\text{ cm}^{-1}$  lower than the value for the crystalline compound while their result for **3a** matches perfectly ( $1769\text{ cm}^{-1}$  *vs.*  $1772\text{ cm}^{-1}$ ). Their reported UV-VIS absorption bands around 340 nm and 460 nm are in very good agreement with the crystalline data, but their bands around 600 nm are roughly 20 nm lower.

Some properties of the new compounds **3** stand out and deserve a closer look:

In all but one molecular structure the nitrosyl ligand coordinates *trans* to the nitrogen atom of the chelating ligand. The only exception is **3e** with *N*-phenyliminodiacetate as the ligand. In

addition, the different chelating ligands allow different coordination isomers. The tridentate ligands **2a**, **2f**, **2g** and **2h** coordinate facially while **2d** and **2e** coordinate meridionally. DFT calculations (see Table 2.18 on page 47) show that most possible coordination isomers lie energetically close to each other and that the crystallized isomers not always represent the global energetic minimum. In this context it is interesting to compare **3c** and **4c**: the ligand **2c** coordinates with both acetate groups *trans* to each other in **3c** and *cis* to each other in **4c**. All these results attest to the iron-aminocarboxylate system's great flexibility with respect to different coordination isomers. In solution most certainly a mixture of isomers is present. Which of them finally crystallizes is probably dependent on crystal-packing effects and the possibility to form strong hydrogen bond networks.

All equatorial ligands tilt away from the nitrosyl group. The mean NO–Fe–L<sub>eq</sub> angle for all compounds **3** is 97.4°. This observation can also be made for most other MNICs known to literature, amongst others for Fe-heme nitrosyls<sup>[159]</sup> or the nitroprusside anion.<sup>[160]</sup> Comparing **3i** with **4i** shows that while, in **3i**, the equatorial aqua ligands O91 and O92 tilt away from the nitrosyl group with 95.5° and 93.3° respectively (see page 24), they tilt towards the axial aqua ligand O93 in **4i** with 87.9° and 88.0° (see page 28). DFT calculations reveal the large orbital lobes of the Fe–NO  $\pi$  interactions as a possible reason for the tilting. Calculations on **3a** show that forcing the equatorial ligands in one plane costs 15 kJ mol<sup>-1</sup>.

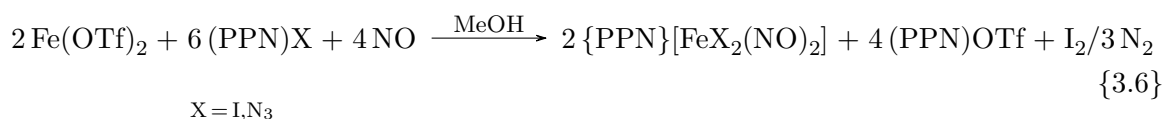
## 3.2 Halogenidonitrosylferrates

All crystalline halogenidonitrosylferrates described in this thesis have a tetrahedral coordination sphere. For dinitrosyl-iron compounds this is the usual coordination geometry; in March, 2016, the Cambridge Structural Database listed 209 corresponding entries. For mononitrosyl-iron compounds, however, only 11 crystalline monomeric compounds have been published so far, eight of which are of the type quartet- $\{\text{FeNO}\}$ <sup>7</sup>.<sup>[42,68,82,161–167]</sup> Compounds **5** have all been described long ago and recently in literature, yet sometimes with different cations.<sup>[42,82,88–104,106,107,109,112,168,169]</sup> Nonetheless, there are two reasons to discuss these compounds here. So far, for  $[\text{FeCl}_2(\text{NO})_2]^-$ , only disordered crystal structures have been published.<sup>[103,107]</sup> For all compounds **5** new syntheses have been developed.

The structures of  $[\text{FeCl}_3(\text{NO})]^-$  and  $[\text{FeBr}_3(\text{NO})]^-$  in crystals of (PPN)**5a** and (PPN)**5b** are nearly identical to published structures,<sup>[42,82,109]</sup> the different cationic environment does not seem to influence the geometry of the anions. For  $[\text{FeCl}_2(\text{NO})_2]^-$ , a comparison to literature data would not be reasonable as the published crystal structures exhibit strong disorder.<sup>[103,107]</sup> The structure of  $[\text{FeI}_2(\text{NO})_2]^-$  is very similar but not identical to published data,<sup>[104]</sup> probably due to the influence of the co-crystallized  $\text{I}_3^-$ . The coordination geometry

of all compounds **5** is nearly perfectly tetrahedral. The Fe–N–O angles are slightly bent with values between 161° and 171°. The Fe–N bond lengths range between 169 pm and 176 pm; the N–O bond lengths range between 109 pm and 117 pm. The  $\nu(\text{NO})$  stretching vibration band is found between 1772  $\text{cm}^{-1}$  and 1791  $\text{cm}^{-1}$  for **5a** and **5b**. For **5c** and **5e** the symmetric  $\nu(\text{NO})$  stretching vibration is found at 1762  $\text{cm}^{-1}$  and 1773  $\text{cm}^{-1}$  respectively, the antisymmetric vibrations are found at 1712  $\text{cm}^{-1}$  and 1697  $\text{cm}^{-1}$ . The main UV-VIS absorption bands are located around 315 nm, 375 nm, 490 nm, and 680 nm for **5a** and **5b** and at 406 nm, 433 nm, 608 nm, 762 nm for **5c**. All these results are in very good agreement with published data. Comparing compounds **5** with each other and with the octahedral complexes **3**, two facts stand out: there is no significant difference between compounds **5a**, **5b** and **3**, and the change of coordination geometry hardly influences the Fe–N–O moiety. In contrast, the addition of a second nitrosyl ligand results in somewhat shorter Fe–N and longer N–O bond lengths and a very different UV-VIS spectrum. By directly comparing **5a** to **5e** slightly longer Fe–Cl bond lengths can be observed for **5e**, probably due to the reduced Fe–N bond lengths.

Wilfer already developed a quite simple route towards **5a** and **5b** by slowly diffusing NO gas into a solution of  $\text{FeCl}_2$  or  $\text{FeBr}_2$  and  $\text{AsPh}_4\text{Cl}$  or  $\text{PPh}_4\text{Br}$  in methanol and half-concentrated hydrochloric or hydrobromic acid.<sup>[109]</sup> This method was now further simplified by using  $\text{FeOTf}_2$  and  $(\text{PPN})\text{Cl}$  or  $(\text{PPN})\text{Br}$  dissolved in pure methanol and by bubbling the NO gas directly through the solution. Thereby a nearly exclusively crystalline product was obtained in high yield (see reaction 3.5 on page 73). The application of this method to obtain the dinitrosyls **5c** and **5d** is remarkable. When using the PPN salts of iodide and azide, the formation of the respective mononitrosyl compounds was expected. The corresponding dinitrosyl compounds were, however, isolated. The formation of  $\text{I}_3^-$  proves, that iodide must have been oxidized during the reaction. The same probably happened to the azide ions, but the dinitrogen that probably formed was not detected. Obviously, the redox potential of the iodide and azide anions is sufficient to reduce the probably initially formed mononitrosyl compounds and to yield the respective dinitrosyl compounds (see reaction 3.6 on page 73). In contrast, Connelly and Gardner reported, that solutions of  $\text{FeCl}_2(\text{NO})_2$  or  $\text{FeBr}_2(\text{NO})_2$  decompose on standing to give the respective mononitrosyl compounds.<sup>[97]</sup>



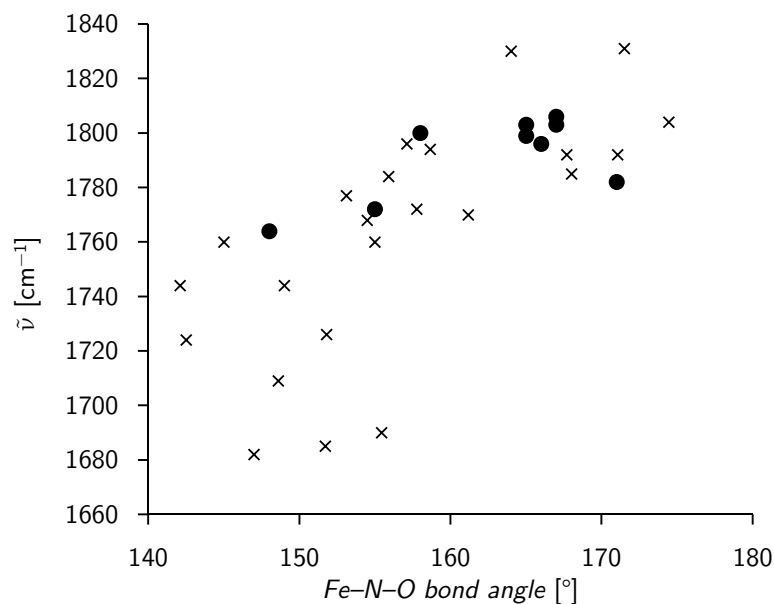


**Figure 3.1:** Plot of the Fe–N–O angle vs. the  $\nu(\text{NO})$  stretching vibration band of quartet- $\{\text{FeNO}\}^7$  compounds. Data from literature<sup>[42,61–64,66–71,73–78]</sup> is represented with crosses, data from this thesis with dots.

### 3.3 Structural correlations

It is quite obvious to assume a possible relation among the different bond lengths, angles and IR absorptions of the individual Fe–N–O moieties. Yet, the only correlation discernible is that of the Fe–N–O angle with the  $\nu(\text{NO})$  stretching vibration band which is illustrated in Figure 3.1, even though, it is not very distinct: the more acute the Fe–N–O angle is, the lower  $\nu(\text{NO})$  gets. From the DFT calculations using constraint Fe–N–O angles (see page 74), this correlation becomes more obvious. Here a slope of  $3 \text{ cm}^{-1}/^\circ$  can be observed. Similar correlations have already been published: Weber *et al.*<sup>[67]</sup> determined a slope of  $6 \text{ cm}^{-1}/^\circ$  for pentacoordinated  $\{\text{FeNO}\}^7$  compounds and Li *et al.*<sup>[77]</sup> calculated a slope of  $7 \text{ cm}^{-1}/^\circ$  for octahedral  $\{\text{FeNO}\}^7$  compounds. This value is more than twice as much as calculated here. However, Li *et al.* took into account only some data of quartet compounds but also included data of doublet compounds. Two reasons for this correlation should be discussed: (1) the better overlap of the NO  $\pi^*$  orbitals with the Fe  $d_{xz}$  and Fe  $d_{yz}$  orbitals for straight Fe–N–O moieties, allows a better electron donation from the nitrosyl to the iron atom, thereby strengthening the N–O bond; (2) in linear Fe–N–O moieties, the oscillation of the nitrogen atom is hindered by the iron atom and more energy is needed to stimulate the vibration. When the Fe–N–O angle becomes more acute, the nitrogen atom can oscillate freely and less energy is needed.

The parameters which influence the Fe–N–O angle in itself are more difficult to determine.

With angles between  $148^\circ$  (**3e**) and  $171^\circ$  (**3b**), compounds **3** cover nearly the full range determined for quartet- $\{\text{FeNO}\}^7$  compounds so far. Yet, the coordination sphere of the iron atom is nearly the same for all compounds. All but **3d** feature a  $(\text{NO}_4)$  coordination and in all but **3e** the nitrosyl ligand coordinates *trans* to the central hetero atom of the chelating ligand. The DFT calculations show three effects, affecting the Fe–N–O angle (see the Walsh diagram in Figure 2.34 on page 64): the  $\pi$  bonding interactions of the NO  $\pi^*$  orbitals with the Fe  $d_{xz}$  and Fe  $d_{yz}$  orbitals favor a linear bonding of the nitrosyl ligand, thus gaining the best orbital overlap. In contrast, the  $\sigma$  antibonding interaction of the NO lone pair with the Fe  $d_{z^2}$  orbital results in a bending of the NO ligand to avoid the antibonding interaction and to become, eventually, a  $\sigma$  bonding interaction. This antibonding interaction, however, is weak compared to the bonding  $\pi$  interaction (see the OPDOS on page 51). When bending the Fe–N–O bond, the third effect comes into play: one Fe–NO  $\pi$  bond becomes more and more a  $\sigma$  bond, making the bending less unfavorable for the  $\pi$  bonds. Due to these three effects, the DFT calculations show no distinct energetic minimum for most compounds **3** within the range of  $140^\circ$  to  $180^\circ$ . Experimentally, this becomes obvious in the large thermal ellipsoids of the nitrosyl-oxygen atoms. The exceptions are **3i** and the halogenidonitrosylferrates **5**. They show a more pronounced energetic minimum in the DFT calculations and smaller thermal ellipsoids on their nitrosyl-oxygen atoms.

In recent years Conradie and Ghosh published several DFT studies, concerning the Fe–N–O angle in  $\{\text{FeNO}\}^7$  compounds.<sup>[170–173]</sup> They concluded that the lack of a ligand *trans* to the nitrosyl group is responsible for linear Fe–N–O moieties. It results in a significant mixing of the Fe  $p_z$  orbital into the  $d_{z^2}$  based HOMO which in turn results in a weaker antibonding interaction with the NO lone pair and leads to a linear Fe–N–O angle. If a *trans* ligand is present, it has to be very weak (like an aqua ligand) in order to obtain a linear Fe–N–O moiety. For compounds **3** the *trans* ligand is usually a tertiary amine and the one compound with an aqua ligand *trans* to the NO (**3e**) features the most acute Fe–N–O bond angle. A mixing of the Fe  $p_z$  orbital into the HOMO is not detected for any of the obtained products. Not even for the tetrahedral mononitrosyl compounds **5a** and **5b**, which lack a *trans* ligand.

All these results show that it is very difficult to predict the Fe–N–O angle. The angle which is eventually characterized by X-ray diffraction is the result of subtle electronic effects, intermolecular interactions and crystal packing effects.

### 3.4 The oxidation state of Fe and NO

The probably most discussed issue in literature concerning quartet- $\{\text{FeNO}\}^7$  and doublet- $\{\text{Fe}(\text{NO})_2\}^9$  compounds is the oxidation state of the iron atom and the nitrosyl ligand.

**Table 3.1:** Comparison of experimental and calculated N–O bond lengths (in Å) and  $\nu(\text{NO})$  stretching vibration bands (in  $\text{cm}^{-1}$ ) of  $\{\text{FeNO}\}^7$  compounds, nitric oxide gas and nitric oxide ions.

	$\{\text{FeNO}\}^7$ <sup>a</sup>		${}^2\text{NO}^0$		${}^3\text{NO}^-$		${}^1\text{NO}^+$	
	Exp.	Calc. <sup>b</sup>	Exp.	Calc. <sup>b</sup>	Exp.	Calc. <sup>b</sup>	Exp.	Calc. <sup>b</sup>
$d(\text{NO})$	1.13	1.16	1.15 <sup>[13]</sup>	1.15	1.27 <sup>[194]</sup>	1.27	1.06 <sup>[12]</sup>	1.06
$\nu(\text{NO})$	1791	1799	1875	1900	1369 <sup>[195]</sup>	1383	2345 <sup>[195]</sup>	2418

<sup>a</sup> Average over all  $\{\text{FeNO}\}^7$  compounds, libration corrected. <sup>b</sup> B97-D, def2-TZVP, D-COSMO-RS, dispersion correction (D3).

Numerous theoretical and spectroscopic studies have been published. In early publications the quartet- $\{\text{FeNO}\}^7$  moiety was usually described as  $[\text{Fe}^+(S=3/2)\text{--NO}^+(S=0)]$ , especially for the brown ring and the Fe–EDTA–NO complex.<sup>[174,175]</sup> Soon the description  $[\text{Fe}^{3+}(S=5/2)\text{--NO}^-(S=1)]$  was established<sup>[34,43,65,66,70,71,130–133,176–181]</sup>, yet there are also many publications describing these nitrosyl-iron compounds as  $[\text{Fe}^{2+}(S=2)\text{--NO}^0(S=1/2)]$  instead.<sup>[171,182–188]</sup> Finally, there are also some publications stating that the oxidation state is something in between  $[\text{Fe}^{3+}\text{--NO}^-]$  and  $[\text{Fe}^{2+}\text{--NO}^0]$ .<sup>[142,189,190]</sup>

For doublet- $\{\text{Fe}(\text{NO})_2\}^9$  compounds the situation is equally complicated. They are described as  $[\text{Fe}^+(S=3/2)\text{--}(\text{NO}^0)_2(S=1)]$ <sup>[191,192]</sup>,  $[\text{Fe}^-(S=1/2)\text{--}(\text{NO}^+)_2(S=0)]$ <sup>[104]</sup>, resonance hybrids of  $[\text{Fe}^+(S=3/2)\text{--}(\text{NO}^0)_2(S=1)]$  and  $[\text{Fe}^{3+}(S=5/2)\text{--}(\text{NO}^-)_2(S=2)]$ <sup>[115,180]</sup> and resonance hybrids of  $[\text{Fe}^{2+}(S=2)\text{--}(\text{NO})_2^-(S=3/2)]$  and  $[\text{Fe}^{3+}(S=5/2)\text{--}(\text{NO}^-)_2(S=2)]$ .<sup>[75,193]</sup>

### 3.4.1 Spectroscopic evidence

Considering the spectroscopic data, iron–ligand bond lengths, N–O bond lengths and the  $\nu(\text{NO})$  stretching vibration bands can be consulted to make a statement with respect to the oxidation states. As pointed out in Section 2.10, the iron–ligand bond lengths of the nitrosyl-iron compounds lie in between those of corresponding  $\text{Fe}^{\text{II}}$  and  $\text{Fe}^{\text{III}}$  compounds. The experimental results are supported by DFT calculations. Thus an oxidation state of ca. +2.5 may be attributed to the iron atom. Metal–ligand bond lengths alone are not very significant to determine an oxidation state. Especially, if for comparison the nitrosyl ligand with its dominant  $\pi$  interactions is substituted with aqua or chlorido ligands. Still, a trend can be derived and the existence of an unambiguous  $\text{Fe}^{\text{II}}$  or  $\text{Fe}^{\text{III}}$  state can supposedly be denied.

Table 3.1 gives an overview of experimental and calculated N–O bond lengths and  $\nu(\text{NO})$  stretching vibration bands. From these data it is evident, that the nitrosyl ligands in the  $\{\text{FeNO}\}^7$  as well as  $\{\text{Fe}(\text{NO})_2\}^9$  compounds best resemble the neutral  $\text{NO}^0$ . The N–O bond

**Table 3.2:** Comparison of N–O bond lengths (in Å),  $\nu(\text{NO})$  stretching vibration bands (in  $\text{cm}^{-1}$ ) and the most common electronic description of different nitrosyl-iron compounds in literature.<sup>[14]</sup>

Compound	$d(\text{N-O})$	$\nu(\text{NO})$	electronic description
$(S = 1/2)\{\text{FeNO}\}^7$	1.17	1611 – 1690	$^1\text{Fe}^{2+}\text{-}^2\text{NO}^0$
$(S = 3/2)\{\text{FeNO}\}^7$	1.15	1682 – 1831	$^6\text{Fe}^{3+}\text{-}^3\text{NO}^-$
$(S = 0)\{\text{FeNO}\}^6$	1.14	1830 – 1937	$^1\text{Fe}^{2+}\text{-}^1\text{NO}^+$

lengths in these compounds are even a little bit shorter, than in  $\text{NO}^0$ , the  $\nu(\text{NO})$  stretching vibration bands are approximately  $100\text{ cm}^{-1}$  lower than in  $\text{NO}^0$ , hence shifted towards  $\text{NO}^-$ . To better classify these findings, it is important to compare them to published data. Most nitrosyl-iron compounds belong to one of three groups, shown in Table 3.2. It is obvious that, in contrast to the spectroscopic data, doublet- $\{\text{FeNO}\}^7$  compounds are usually described with a neutral  $\text{NO}^0$ , whereas quartet- $\{\text{FeNO}\}^7$  compounds which feature shorter N–O bond lengths and higher  $\nu(\text{NO})$  stretching vibration bands are rather described with a  $^3\text{NO}^-$ . In this context an assignment of oxidation states only on the basis of the N–O bond lengths and the  $\nu(\text{NO})$  stretching vibration bands does not seem appropriate, particularly if taking into account the strong dependence of the  $\nu(\text{NO})$  stretching vibration on the Fe–N–O angle as discussed above. Cheng *et al.* on the other hand, did a similar analysis with  $[\text{Fe}(\text{Me}_3\text{TACN})(\text{NO})(\text{N}_3)_2]$  ( $\text{Me}_3\text{TACN} = N,N',N''\text{-trimethyl-1,4,7-triazacyclononane}$ ). Finding that the N–O bond length and  $\nu(\text{NO})$  stretching vibration band in the complex are similar to that of  $\text{NO}^0$  they conclude that the nitrosyl in the complex is in the oxidation state 0.<sup>[187]</sup> On the whole, such an analysis may not be straightforward, still it gives some information regarding the strength of the N–O bond, and hence its electronic configuration.

### 3.4.2 Quantum-chemical evidence

Quantum-chemical calculations can be consulted to illuminate the electronic configuration of the quartet- $\{\text{FeNO}\}^7$  compounds. Subsequently the results presented in Section 2.8 will be discussed here.

The optimized geometries from DFT calculations are in good agreement with the crystal structures. To optimize the aminocarboxylate structures **3**, the application of the D-COSMO-RS model proves necessary as these complexes form strong intermolecular hydrogen-bond networks which considerably influence the Fe–O bond lengths. To optimize the halogenido ferrates **5**, the common COSMO model is sufficient to take into account the negative charge of the ferrates. The good agreement with IR and UV-VIS spectroscopy further confirms that a sufficient model of the studied complexes was established. To examine the electronic

configuration of the nitrosyl-iron compounds on the basis of DFT calculations, first the relevant orbitals should be analyzed. These are the five Fe  $d$  and the two NO  $\pi^*$  orbitals for both  $\alpha$  and  $\beta$  electrons. As evident from Figure 2.25 on page 52, the unoccupied orbitals of **3a** consist of five  $\beta$  orbitals with mainly Fe contributions and two  $\alpha$  orbitals with dominant NO contribution. This result is consistent with data published by Solomon and coworkers.<sup>[34,130–133]</sup> They state that, from these unoccupied orbitals, the conclusion can be drawn that two spin-down electrons reside on the NO ligand and five spin-up electrons on the Fe atom, hence the bonding should be described as  ${}^6\text{Fe}^{3+}-{}^3\text{NO}^-$ . A closer look at the occupied orbitals reveals, however, that the two orbitals carrying the spin-down electrons on the NO ligand (HOMO–1 and HOMO–2) are strongly delocalized onto the Fe atom and have a NO contribution of only 55 % but also a 40 % Fe contribution. Consequently, the bonding should rather be described as  $\text{Fe}^{2+}-\text{NO}^0$  with one half  $\beta$  electron residing in each NO  $\pi^*$  orbital and 1.5 electrons residing in the Fe  $d_{xz}$  orbital and in the Fe  $d_{yz}$  orbital respectively. This assignment is supported by the natural orbitals in Figure 2.26 on page 53 for **3a** and in Figure 2.27 on page 55 for **5e**. As they combine corresponding  $\alpha$  and  $\beta$  orbitals, there is no need to differentiate between occupied and corresponding unoccupied orbitals. The unpaired electrons residing on the Fe atom can easily be identified. The bonding and antibonding Fe  $d$ –NO  $\pi^*$  interactions show a dominant Fe contribution which sums up to 2.62 electrons *versus* 1.26 electrons on the NO ligand for **3a** and 4.86 electrons on Fe *versus* 1.47 electrons on each nitrosyl ligand for **5e**. Thus a slightly more negative charge is calculated for the nitrosyl ligands in **5e**, and they can be viewed as  $(\text{NO})_2^-$ .

In addition to analyzing relevant Fe and NO orbitals, several other methods are available to get useful information regarding the Fe–NO bonding. Tables 2.20 on page 56, 2.21 on page 56 and 2.25 on page 65 summarize the results of Mulliken population analyses (MPA),<sup>[137]</sup> natural population analysis (NPA)<sup>[138]</sup> and AOMix-FO charge decomposition analyses (CDA)<sup>[139,140]</sup> obtained for the different Fe–NO compounds as well as for the corresponding nitrosyl-free  $\text{Fe}^{\text{II}}$  and  $\text{Fe}^{\text{III}}$  complexes.

Both atomic population analyses assign a nearly neutral charge to the nitrosyl ligand. Even for the dinitrosyl complexes in which, formally, a  $\text{Cl}^-$  or  $\text{I}^-$  is replaced by a  $\text{NO}^-$  as compared to the corresponding mononitrosyl complexes, only a minor negative charge of  $-0.18$  is calculated for the nitrosyl ligand. The charges on the iron atom are best compared to those of corresponding nitrosyl-free  $\text{Fe}^{\text{II}}$  and  $\text{Fe}^{\text{III}}$  complexes. The results in Table 2.25 show that the iron atom in the Fe–NO compounds should be described as  $\text{Fe}^{\text{II}}$ . Its charges are even a bit lower than in the  $\text{Fe}^{\text{II}}$  complexes. Quite revealing is the comparison of  $[\text{FeCl}_3(\text{NO})]^-$  and  $[\text{FeCl}_2(\text{NO})_2]^-$ . The substitution of a  $\text{Cl}^-$  with a formal  $\text{NO}^-$  lowers the positive charge on the iron atom. Thus electron density is transferred from the nitrosyl ligand to the iron atom. The spin densities show a strong spin polarization. Depending on the functional,

the  $\beta$  spin on the nitrosyl ligand varies between  $-0.6$  and  $-1.1$ , equally distributed over both  $\pi$  orbitals; corresponding  $\alpha$  spin density is found on the iron atom. All these results indicate the presence of a  $\text{NO}^0$  antiferromagnetically coupled to a  $\text{Fe}^{2+}$  (or  $\text{Fe}^+$  for **5c** and **5e**). In fact the description as a covalent bond also seems appropriate, even more so if the coupling constant  $J$  of more than  $-2000\text{ cm}^{-1}$  is taken into account. According to this, the CDA analysis shows no significant charge transfer between the  $\text{NO}^0$  fragment and the  $\text{Fe}^{\text{II}}\text{L}$  fragment (L = all ligands but NO). Similar results and interpretations of DFT data were published in recent years by several authors.<sup>[171,184–188,191,192]</sup>

In Section 2.8.4 the results of CASSCF calculations are presented. They confirm, on the whole, the DFT results and are in good agreement with similar calculations presented in literature.<sup>[142,190]</sup> Mulliken analyses as well as the analysis of the localized active space show, that the most relevant description for both quartet- $\{\text{FeNO}\}^7$  and doublet- $\{\text{Fe}(\text{NO})_2\}^9$  compounds is  $\text{Fe}^{2+}$  antiferromagnetically coupled to  $\text{NO}^0$  or  $(\text{NO})_2^-$  respectively. The description of the dinitrosyl compounds with  $(\text{NO})_2^-$  explains their more negative charge, calculated for the nitrosyl ligands in these compounds and their longer N–O bond lengths. Configuration state functions with  $\text{Fe}^{3+}$  play only a minor role (25 % for **3**, 15 % for **5e**). Quite obviously  $\text{NO}^0$  is the preferred oxidation state for NO in these compounds. This is also evident from the fact that, for **5e**, 24 % weight are attributed to configuration state functions featuring  $\text{Fe}^+$  and two  $\text{NO}^0$  ligands.

In summary, all results – spectroscopic as well as computational – show that  $\text{Fe}^{2+}$  and  $\text{NO}^0$  are the dominating oxidation states found in the quartet- $\{\text{FeNO}\}^7$  and doublet- $\{\text{Fe}(\text{NO})_2\}^9$  compounds, discussed here. However, other oxidation states also have some relevance and importance and should not be ignored. Keeping this in mind, the probably best description was made by Rodriguez *et al.*: “We propose that it is more appropriate to regard iron and NO as integral parts of the  $\{\text{FeNO}\}^7$  unit where some valence electrons are shared to a large extent by the entire moiety.”<sup>[189]</sup>

### 3.5 PLI measurements

Upon irradiation, samples of the octahedral quartet- $\{\text{FeNO}\}^7$  compounds **3a**, **3e** and **3f** show no sign of a linkage isomerism. The tetrahedral compound **5a**, in contrast, shows a shift of the  $\nu(\text{NO})$  stretching vibration band to higher energy. This indicates a strengthening of the N–O bond which implies that the electron density in the N–O antibonding orbitals is reduced. This is possible by either a LMCT of one electron from a  $\text{NO } \pi^*$  orbital to the iron atom or by an oxidation. As the DFT and CASSCF calculations show, the electronic description of the Fe–N–O moiety is the same for the octahedral and tetrahedral quartet- $\{\text{FeNO}\}^7$  compounds.

According to this, it is unlikely that **5a** shows a NO-to-iron LMCT while compounds **3** do not. The oxidation of the Fe–N–O moiety, however, requires the presence of a redox partner, which compounds **3** are missing. **5a**, on the other hand, can transfer one electron from the NO  $\pi^*$  orbital to the (PPN)<sup>+</sup> cation. In summary, the oxidation of the ferrate **5a** explains the strengthening of the N–O bond and the shift of the  $\nu(\text{NO})$  stretching vibration band (also supported by DFT calculations, see page 69); the transfer of the electron to the (PPN)<sup>+</sup> cation explains why this behavior is not observed with the octahedral compounds **3**.

### 3.6 UV-VIS spectra and TDDFT

Except for the pentaquanitrosyliron(2+) solution and the “brown FeSO<sub>4</sub>”, all examined quartet-{FeNO}<sup>7</sup> compounds exhibit a dark green color. UV-VIS spectroscopy reveals absorption bands around 450 nm and 600–650 nm. In the region around 550 nm no absorptions are observed, hence the green color. For the “brown FeSO<sub>4</sub>”, the absorption band around 600 nm declines very quickly, red light is not absorbed which results in the more brownish color. The same is true for the dinitrosyl compounds which show, however, another absorption ranging into the near infrared. Common to all compounds are absorptions with higher energy between 300 nm and 400 nm. As spectra of corresponding nitrosyl-free compounds show no absorptions above 300 nm, the color is directly attributed to the effects of the nitrosyl ligand. Accordingly, TDDFT calculations show mainly excitations that involve the nitrosyl either as donor or as acceptor. For the octahedral complexes, the dominating excitation is found around 450 nm. It is composed of an iron to nitrosyl charge transfer for spin-up electrons and an excitation of spin-down electrons from the Fe–NO  $\pi$  bond into the Fe–NO  $\pi^*$  bond. In the UV region excitations from water or the chelating ligand to Fe and the nitrosyl are calculated. For nitrosyl-free compounds these LMCT excitations are found at a little higher energy and with less intensity.

For the tetrahedral mononitrosyls **5a** and **5b**, the same green color as for the octahedral compounds is observed. For the absorptions at low energy, similar excitations are calculated but for the absorption around 450 nm, which plays a significant role for the green color, the calculated excitations are quite different. For **5a**, they are dominated by chloride-to-iron and chloride-to-nitrosyl charge transfers. Considering this, it may just be a coincidence that the tetrahedral mononitrosyl compounds feature the same color as the octahedral ones. Compared to the dinitrosyl **5c**, it becomes apparent that the origin of the different absorptions is, more or less, the same for **5a** and **5c** and that only the excitation energies are different and the color changes from green to brown.

### 3.7 The brown ring

The reaction product of  $\text{Fe}^{\text{II}}$  salts and nitric oxide in aqueous solution is supposed to be  $[\text{Fe}(\text{NO})(\text{OH}_2)_5]^{2+}$  – the “brown ring”.<sup>[43]</sup> And while this assumption is by now more or less unquestioned, it has not yet been possible to crystallize the pentaaquanitrosyliron(2+) ion. During the research for this thesis, very often brown crystals of  $\text{FeSO}_4 \cdot 7 \text{H}_2\text{O}$  (**1**) were obtained. IR and UV-VIS spectra of these crystals showed absorptions identical to those of an aqueous  $[\text{Fe}(\text{NO})(\text{OH}_2)_5]^{2+}$  solution. By X-ray diffraction of similar crystals obtained by Kästele, small amounts of iron bound nitric oxide could be determined. These results indicate that a compound similar to  $[\text{Fe}(\text{NO})(\text{OH}_2)_5]^{2+}$  may have been captured in solid form and that one day it could be possible to crystallize the pentaaquanitrosyliron(2+) ion.



## 4 Summary

This thesis deals with the synthesis, crystallization, characterization and quantum-chemical analysis of quartet- $\{\text{FeNO}\}^7$  and doublet- $\{\text{Fe}(\text{NO})_2\}^9$  compounds.

Based on work of the van Eldik group<sup>[43,79–81]</sup>, nine crystalline quartet- $\{\text{FeNO}\}^7$  compounds with octahedral coordination sphere were synthesized and analyzed by X-Ray diffraction. They agree with the general formula  $[\text{Fe}(\text{L})(\text{NO})(\text{OH}_2)_n]$  (**3**) with  $n = 2$  for L = ida (**2a**), oda (**2d**), phida (**2e**), bnida (**2f**), brbnida (**2g**), pheida (**2h**) or dipic (**2i**);  $n = 1$  for L = heida (**2b**) and  $n = 0$  for L = dhpida (**2c**). They were synthesized by bubbling nitric oxide through an aqueous solution of iron(II) sulfate and the corresponding chelating ligand, followed by the diffusion of acetone into the resulting dark green solutions. The only exception was  $[\text{Fe}(\text{dhpida})(\text{NO})]$  (**3c**) which was obtained from iron(II) triflate and ethanol instead of water. All compounds **3** feature slightly bent Fe–N–O moieties with Fe–N–O angles between  $148^\circ$  and  $171^\circ$  and  $\nu(\text{NO})$  stretching vibration bands between  $1764\text{ cm}^{-1}$  and  $1814\text{ cm}^{-1}$ . Their main UV-VIS absorption bands are located around 340 nm, 460 nm and 600 nm. Their quartet ground state is confirmed by SQUID measurements. In all compounds **3**, the equatorial ligands tilt away from the nitrosyl ligand and with the exception of  $[\text{Fe}(\text{NO})(\text{phida})(\text{OH}_2)_2]$  (**3e**), the nitrosyl ligand coordinates *trans* to the central hetero atom of the chelating ligand. The Fe–N–O angle has a very weak bending potential which was obvious from the very large atomic displacement parameters of the nitrosyl-oxygen atoms and which was confirmed by DFT calculations. The reason for this flat potential is the interplay of the Fe–NO  $\pi$  bond on the one hand and the Fe–NO  $\sigma$  antibond on the other hand. The Fe–NO  $\pi$  bond prefers a straight Fe–N–O bond for maximum orbital overlap but tolerates also a bent Fe–N–O moiety. One of the Fe–NO  $\pi$  bonds then changes into a Fe–NO  $\sigma$  bond. The Fe–NO  $\sigma$  antibond prefers a strongly bent Fe–N–O bond to avoid the antibonding interaction. The Fe–N–O angle which was eventually characterized by X-ray diffraction is the result of subtle electronic effects, intermolecular interactions and crystal-packing effects and can hardly be predicted. Figure 4.1 shows  $[\text{Fe}(\text{ida})(\text{NO})(\text{OH}_2)_2]$  (**3a**) as a general example for compounds **3**.

Based on work started by Kohlschütter and Manchot<sup>[88–92]</sup> and continued by Connelly and Gardner<sup>[97]</sup> and later by Beck and coworkers<sup>[82]</sup>, new syntheses for the halogenidonitrosylferrates  $[\text{FeCl}_3(\text{NO})]^-$  (**5a**),  $[\text{FeBr}_3(\text{NO})]^-$  (**5b**),  $[\text{FeI}_2(\text{NO})_2]^-$  (**5c**),  $[\text{Fe}(\text{N}_3)_2(\text{NO})_2]^-$  (**5d**) and  $[\text{FeCl}_2(\text{NO})_2]^-$  (**5e**) were developed and disorder-free crystal structures of **5a**, **5b**, **5c** and **5e**

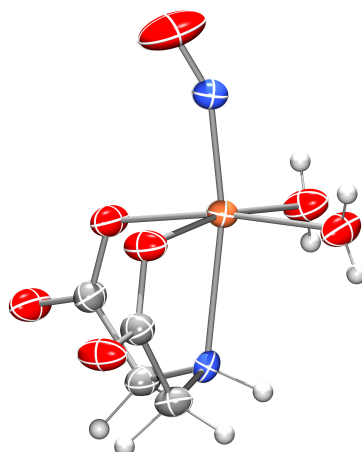


**Figure 4.1:** Plot of the complex  $[\text{Fe}(\text{ida})(\text{NO})(\text{OH}_2)_2]$  in crystals of **3a**.

were obtained. The syntheses were carried out by addition of the respective PPN salt (PPN = bis(triphenylphosphane)iminium) to a solution of iron(II) triflate in methanol, followed by the addition of nitric oxide. Using (PPN)Cl and (PPN)Br, the quartet- $\{\text{FeNO}\}^7$  compounds **5a** and **5b** were obtained, using (PPN)I and (PPN) $\text{N}_3$ , redox processes took place, yielding  $\text{I}_2$  and  $\text{N}_2$ , respectively, and the corresponding doublet- $\{\text{Fe}(\text{NO})_2\}^9$  compounds **5c** and **5d**.  $[\text{FeCl}_2(\text{NO})_2]^-$  (**5e**) was not accessible by this approach, therefore a different synthesis was developed using  $[\text{Fe}(\text{NO})_2(\text{ONO})_2]^-$  as a precursor which was again reacted with (PPN)Cl to yield **5e**. As the octahedral  $\{\text{FeNO}\}^7$  complexes, compounds **5** feature slightly bent Fe–N–O moieties with Fe–N–O angles between  $161^\circ$  and  $171^\circ$  and  $\nu(\text{NO})$  stretching vibration bands between  $1762\text{ cm}^{-1}$  and  $1791\text{ cm}^{-1}$ . Their main UV-VIS absorption bands are located around 315 nm, 375 nm, 490 nm and 680 nm for **5a** and **5b** and at 406 nm, 433 nm, 608 nm, 762 nm for **5c**.

Quantum-chemical calculations using DFT and CASSCF methods were performed to gain insight into the electronic configuration of the Fe–N–O moiety. Structural optimizations were done using the DFT functionals B97-D and TPSSh together with the basis set def2-TZVP and dispersion correction (D3). For compounds **5**, COSMO was used to account for the negative charge of the ferrates, for compounds **3**, the D-COSMO-RS model was used to simulate the intermolecular hydrogen bonds. For both, compounds **3** and **5**, a good description of the Fe–NO bond was achieved. The analysis of the different DFT results (population of selected orbitals, Mulliken and natural charges,  $\nu(\text{NO})$  stretching vibrations and N–O bond lengths) showed that the Fe–N–O moiety can best be described as  $\text{NO}^0$  antiferromagnetically coupled to a  $\text{Fe}^{2+}$  for the quartet- $\{\text{FeNO}\}^7$  compounds and as  $(\text{NO})_2^-$  antiferromagnetically coupled to a  $\text{Fe}^{2+}$  for the doublet- $\{\text{Fe}(\text{NO})_2\}^9$  compounds. These results were confirmed by CASSCF calculations which showed that configuration state functions with  $\text{Fe}^{\text{III}}$  play only a minor role (25 % for **3**, 15 % for **5e**) while configuration state functions with  $\text{Fe}^{\text{II}}$  account for up to

70% of the CAS wave function. These findings were also verified, using the spectroscopic data available: N–O bond lengths,  $\nu(\text{NO})$  stretching vibration bands and iron–ligand bond lengths of compounds **3** and **5** were compared with corresponding nitrosyl-free compounds as well as  $\text{NO}^-$ ,  $\text{NO}^0$  and  $\text{NO}^+$  to show that the best agreement was found with  $\text{NO}^0$  and nitrosyl-free  $\text{Fe}^{\text{II}}$  compounds.

Finally, PLI experiments (PLI = photoinduced linkage isomerism) were done to investigate a possible photoactivity of compounds **3** and **5**. While for compounds **3** no photoactivity was detected, **5a** showed promising yet unexpected results: upon irradiation with light of a wavelength of 635 nm at 9 K, the intensity of the  $\nu(\text{NO})$  stretching vibration band at  $1809\text{ cm}^{-1}$  lessened, while a new band at  $1868\text{ cm}^{-1}$  was formed. After warming to 40 K the band at  $1868\text{ cm}^{-1}$  disappeared, while the band at  $1809\text{ cm}^{-1}$  regained its original intensity. These results indicated that no typical linkage isomerism had occurred, as this would have resulted in the formation of a new absorption band at lower energy. Instead, using DFT calculations, the new absorption band was assigned to neutral  $[\text{FeCl}_3(\text{NO})]$  which may have formed by transferring one electron to the  $(\text{PPN})^+$  cation.



## 5 Experimental Part

### 5.1 Common working techniques

All reactions involving iron compounds were carried out under argon atmosphere using standard Schlenk techniques and degassed solvents. Pipettes, syringes and canulas, used for the dosage of solvents, were flushed three times with argon before usage.

Water used as solvent was degassed by refluxing while bubbling argon through it. Ethanol, methanol, acetone and DCM were degassed in the same way and subsequently dried and stored over a molecular sieve or (in the case of DCM) calcium chloride. THF and diethyl ether were distilled from sodium/benzophenone under nitrogen atmosphere and stored over sodium. All solvents were stored in Schlenk flasks under argon atmosphere.

Nitric oxide was purified by bubbling through a 4 M sodium hydroxide solution, excess nitric oxide was destroyed by bubbling through a saturated sulfamic acid solution.

### 5.2 Analytical methods

#### 5.2.1 NMR spectroscopy

NMR spectra were recorded on spectrometers of the types *Jeol Eclipse 270*, *Jeol Eclipse 400*, *Jeol Ex 400*, *Bruker 400* and *Bruker 400 TR*. The chemical shift  $\delta$  is given in ppm and refers to the solvent residual peak of the deuterated solvent. All  $^{13}\text{C}$ -NMR spectra were recorded broad band proton decoupled ( $^{13}\text{C}\{^1\text{H}\}$ -NMR). All spectra were interpreted using the software *MestReNova*.<sup>[196]</sup>

### 5.2.2 IR spectroscopy

IR spectra were recorded on a *Jasco FT/IR-460 Plus* spectrometer. Solid samples were recorded using an ATR diamond plate, aqueous solutions were recorded using a  $\text{CaF}_2$  cell. All spectra were interpreted using the software *Spectra Manager 2*.<sup>[197]</sup> All signals are given in wavenumbers ( $\text{cm}^{-1}$ ).

### 5.2.3 Mass spectrometry

EI and FAB spectra were measured on a *Jeol MStation 700*. EI samples were ionized at  $250^\circ\text{C}$  with an electron energy of 70 eV. FAB samples were ionized in a nitrobenzylalcohol or glycerine matrix, using 8 kV fast argon atoms. MALDI spectra were measured on a *Bruker Daltonics Autoflex II* using a nitrogen laser at 337 nm.

### 5.2.4 Elemental analysis

CHN analyses were performed on a *Elementar vario EL* and a *Elementar vario micro cube*. The halogen content was identified on a *Metrohm 888 Titrande*.

### 5.2.5 UV-VIS spectroscopy

UV-VIS spectra in solution were measured on a *Cary 50 Conc UV-Visible-Spectrophotometer* using silica glass cuvettes with a thickness of 1 cm. Obtained values were corrected by the absorption of cuvette and solvent. Solid samples were measured on a *Cary 500 Scan UV-Vis-NIR-Spectrophotometer* with *Labsphere DRA-CA-5500* photometer sphere. The diffuse reflection was measured and converted using the *Kubelka-Munk* function<sup>[198]</sup> to get data, comparable to absorption experiments.

$$\frac{K}{S} = \frac{(1 - R)^2}{2R} \quad (5.1)$$

( $R$  = remission;  $K$  = absorption coefficient;  $S$  = scattering coefficient)

### 5.2.6 X-Ray diffraction

Crystals were selected using a *Leica MZ6* polarization microscope. Suitable crystals were measured on single crystal diffractometers of the types *Bruker Nonius Kappa CCD*, *Bruker D8 Quest* and *Bruker D8 Venture* using  $\text{MoK}_\alpha$  irradiation. The structure solutions were carried

out by direct methods using *SHELXS-2014*.<sup>[199]</sup> The structures were refined by full-matrix least-squares calculations on  $F^2$  using *SHELXL-2014*<sup>[200]</sup> and *ShelXLc*.<sup>[201]</sup> Distances and angles were calculated using *Platon*.<sup>[202]</sup> For visualization the programs *ORTEP*<sup>[203]</sup> and *POV-Ray*<sup>[204]</sup> were used. Further details for every structure can be found in the appendix (Tables 6.1 – 6.6). The values given there are defined as follows:

$$R(F) = \frac{\sum ||F_o| - |F_c||}{\sum |F_o|} \quad (5.2)$$

$$R_{\text{int}} = \frac{\sum |F_o^2 - \langle F_o \rangle^2|}{\sum |F_o^2|} \quad (5.3)$$

$$wR(F^2) = \sqrt{\frac{\sum w(F_o^2 - F_c^2)^2}{\sum w(F_o^2)^2}} \quad (5.4)$$

$$S = \sqrt{\sum \frac{w(F_o^2 - F_c^2)^2}{N_{\text{hkl}} - N_{\text{parameter}}}} \quad (5.5)$$

The weighting factors  $w$  and  $P$  are define as:

$$w = \frac{1}{\sigma^2(F_o^2) + (0.02P)^2} \quad (5.6)$$

$$P = \frac{\max(F_o^2, 0) + 2F_c^2}{3} \quad (5.7)$$

In analogy to *SHELXL-2014*, the values of the parameter  $x$  and  $y$  were adopted to minimise the variance of  $w(F_c^2/F_o^2)$  for several intensity-ordered groups of reflexes. The coefficient  $U_{eq}$  is defined as:

$$U_{eq} = \frac{1}{3} \sum_{i=1}^3 \sum_{j=1}^3 U_{ij} a_i a_j a_i^* a_j^* \quad (5.8)$$

The value of  $shift/error_{\text{max}}$  is defined as the maximum parameter shift divided by the standard deviation in the last refinement cycle.

### 5.2.7 Magnetic Susceptibilities

Magnetic susceptibility data were collected with a Quantum Design MPMS XL-5 SQUID magnetometer over 10–300 K in the sweep mode. All samples were placed in gelatin capsules

held within plastic straws. The data were corrected for the diamagnetic magnetization of the ligands, which were estimated using Pascal's constants,<sup>[205]</sup> and for the sample holder.

### 5.3 Reagents and solvents

---

Name	Purity	Distributor
acetone	DAB	Merck
acetonitrile	99.8 %	Sigma-Aldrich
4-aminophenol	98 %	Aldrich
2-amino-1,3-propanediol	97 %	ABCR
aniline	99 %	Sigma-Aldrich
<i>N</i> -benzyliminodiacetic acid	98 %	Sigma
bis(triphenylphosphane)iminium chloride	97 %	Aldrich
4-bromobenzylamine	97 %	Acros
chelidamic acid	95 %	Sigma-Aldrich
chloroacetic acid	99 %	ABCR
dichloromethane	puriss.	Grüssing
diethyl ether	DAB	Merck
dipicolinic acid	99 %	Acros
ethanol	99.8 %	Fluka
ethyl bromoacetate	98 %	Acros
hydrochloric acid	37 wt. %	Merck
<i>N</i> -(2-hydroxyethyl)iminodiacetic acid	≥98.0 %	Aldrich
iminodiacetic acid	98 %	Aldrich
iron pentacarbonyl	>99.99 %	Aldrich
iron(II) sulfate heptahydrate	pa	Grüssing
iron(II) triflate · 3 CH <sub>3</sub> CN	–	[206]
methanol	99.8 %	Fluka
nitric oxide	99.5 %	Air Liquide
nitrosonium tetrafluoroborate	95 %	Aldrich
oxodiacetic acid	98 %	Aldrich
<i>n</i> -pentane	pure	Merck
petroleum ether	pure %	Merck
2-phenylethylamine	99 %	Acros
potassium bromide	zA	Grüssing
potassium carbonate	98 %	Grüssing
potassium hydroxide	99.99 %	Sigma-Aldrich

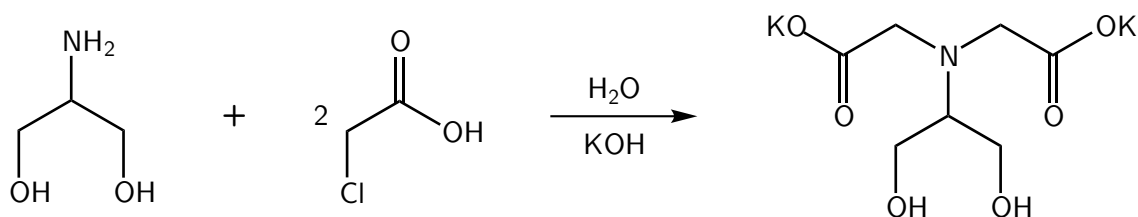
---

potassium iodide	98 %	Grüssing
sodium azide	puriss.	Grüssing
sodium hydroxide	99 %	Grüssing
sodium iodide	puriss. %	Grüssing
sodium nitrite	puriss.	Grüssing
tetraethylammonium bromide	98 %	ABCR
THF	puriss.	Grüssing
water	deionized	house installation

---

## 5.4 Synthesis of ligands and PPN salts

### 5.4.1 Dipotassium *N*-(1,3-dihydroxypropane-2-yl)iminodiacetate (**K<sub>2</sub>2c**)



**Literature:** A. J. Miralles, C. M. Silvernail (Ecolab Inc.), US 2009/0264677 A1, **2009**.

**Starting material:** Chloroacetic acid, potassium hydroxide, 2-amino-1,3-propanediol, ethanol, water, DCM, methanol.

**Procedure:** Chloroacetic acid (2.08 g, 22 mmol) was dissolved in a potassium hydroxide solution (5 M, 5 mL). The solution was refluxed and 2-amino-1,3-propanediol (0.91 g, 10 mmol) was added in small portions. More 5 M potassium hydroxide solution was added until a pH of 10–12 was reached. After refluxing for 4 h, the solution was cooled to 0 °C and 30 mL of ethanol were added. Immediately a white solid formed. The suspension was stored at 0 °C overnight and then filtrated. The filtrate was washed two times with 50 mL of DCM and the solvent was removed under reduced pressure. A yellow oil was obtained, which was dissolved in methanol and precipitated with an excess of DCM. The precipitate was dried under reduced pressure to give **K<sub>2</sub>2c** as a white powder.

**Yield:** 1.07 g (3.78 mmol, 38 %).

**Empirical formula:** C<sub>7</sub>H<sub>11</sub>K<sub>2</sub>NO<sub>6</sub>, 283.4 g mol<sup>-1</sup>.

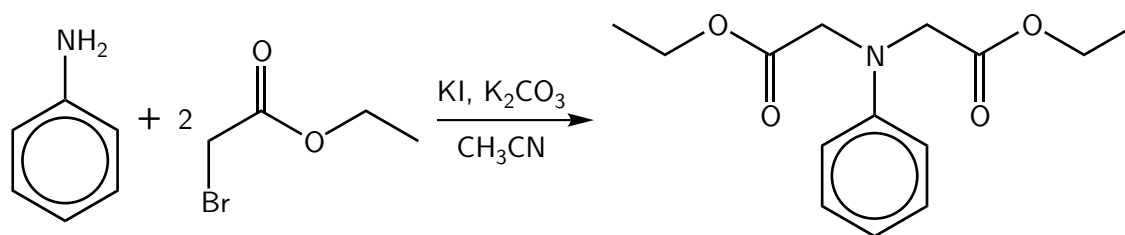
**<sup>1</sup>H-NMR** (400 MHz, D<sub>2</sub>O): δ = 3.33–3.21 (m, 8H), 2.88 (m, 1H) ppm.

**<sup>13</sup>C{<sup>1</sup>H}-NMR** (100 MHz, D<sub>2</sub>O): δ = 181.9, 66.2, 59.4, 54.0 ppm.

**MS** (FAB<sup>-</sup>): *m/z* (%) = 244.3 (23) [M - K]<sup>-</sup>, 206.4 (20) [M - 2K + H]<sup>-</sup>.

**MS** (FAB<sup>+</sup>): *m/z* (%) = 284.0 (3) [M + H]<sup>+</sup>, 39.0 (13) [K]<sup>+</sup>.

**IR** (solid, ATR):  $\tilde{\nu}$  = 3224 (br, w), 1579 (vs), 1421 (w), 1400 (s), 1325 (s), 1282 (w), 1262 (w), 1152 (w), 1134 (w), 1069 (w), 1041 (m), 1029 (s), 1015 (m), 991 (w), 974 (w), 918 (w), 882 (w), 743 (m), 715 (s), 682 (m) cm<sup>-1</sup>.

5.4.2 *N*-Phenyldiethyliminodiacetate

**Literature:** I. R. Gould, J. R. Lenhard, S. Farid, *J. Phys. Chem. A* **2004**, 10949–10956.

**Starting material:** Aniline, ethyl bromoacetate, potassium iodide, potassium carbonate, acetonitrile, DCM, water.

**Procedure:** Aniline (2.73 mL, 2.79 g, 30 mmol), ethyl bromoacetate (7.28 mL, 11.0 g, 66 mmol), potassium iodide (0.92 g, 5.5 mmol) and potassium carbonate (12 g, 87 mmol) were suspended in 60 mL of acetonitrile and refluxed for 6 days. After cooling to room temperature, undissolved components were removed by filtration. The filtrate was taken up in 100 mL of DCM, washed three times with 100 mL of saturated potassium carbonate solution and two times with 100 mL of water. The solvent was removed under reduced pressure and the crude product was distilled (115 °C, 0.001 mbar) to give *N*-phenyldiethyliminodiacetate as a yellow oil.

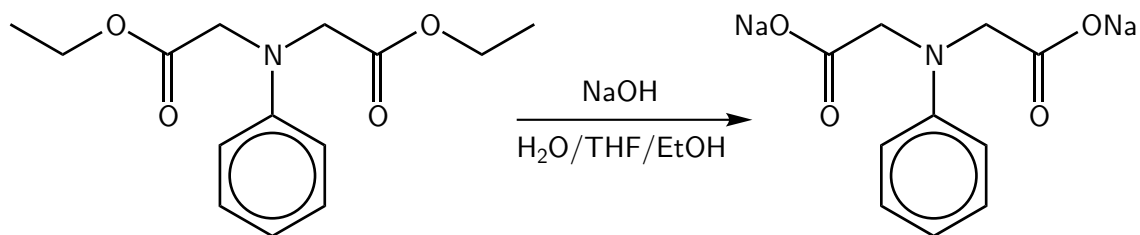
**Yield:** 3.40 g (13 mmol, 43 %).

**Empirical formula:** C<sub>14</sub>H<sub>19</sub>NO<sub>4</sub>, 265.3 g mol<sup>-1</sup>.

**<sup>1</sup>H-NMR** (400 MHz, D<sub>2</sub>O): δ = 7.21 (dd, *J* = 8.8, 7.3 Hz, 2H), 6.77 (tt, *J* = 7.3, 0.8 Hz, 1H), 6.61 (dd, *J* = 8.8, 0.8 Hz, 2H), 4.21 (q, *J* = 7.1 Hz, 4H), 4.13 (s, 4H), 1.27 (t, *J* = 7.1 Hz, 6H) ppm.

**<sup>13</sup>C{<sup>1</sup>H}-NMR** (100 MHz, D<sub>2</sub>O): δ = 171.25, 147.97, 129.39, 118.38, 113.07, 61.38, 53.61, 14.32 ppm.

**MS** (DEI+): *m/z* (%) = 265.1 (30) [M]<sup>+</sup>, 192.2 (100) [M - CO<sub>2</sub>C<sub>2</sub>H<sub>5</sub>]<sup>+</sup>.

5.4.3 Disodium *N*-phenyliminodiacetate (**Na<sub>2</sub>2e**)

**Literature:** I. R. Gould, J. R. Lenhard, S. Farid, *J. Phys. Chem. A* **2004**, 10949–10956.

**Starting material:** *N*-phenyldiethyliminodiacetate, sodium hydroxide, ethanol, THF, water.

**Procedure:** *N*-Phenyldiethyliminodiacetate (3.40 g, 13 mmol) and sodium hydroxide (1.00 g, 25 mmol) were refluxed in 3 mL of water, 3 mL of ethanol and 4 mL of THF for 5 h. After cooling in the refrigerator, **Na<sub>2</sub>2e** was obtained as a colorless solid by filtration and dried under reduced pressure.

**Yield:** 1.75 g (6.9 mmol, 53 %).

**Empirical formula:** C<sub>10</sub>H<sub>9</sub>NNa<sub>2</sub>O<sub>4</sub>, 253.1 g mol<sup>-1</sup>.

**<sup>1</sup>H-NMR** (400 MHz, D<sub>2</sub>O): δ = 7.26 (dd, *J* = 8.7, 7.4 Hz, 2H), 6.72 (tt, *J* = 7.4, 0.8 Hz, 1H), 6.54 (dd, *J* = 8.7, 0.8 Hz, 2H), 3.90 (s, 4H) ppm.

**<sup>13</sup>C{<sup>1</sup>H}-NMR** (100 MHz, D<sub>2</sub>O): δ = 179.80, 148.58, 129.36, 116.22, 111.48, 55.70 ppm.

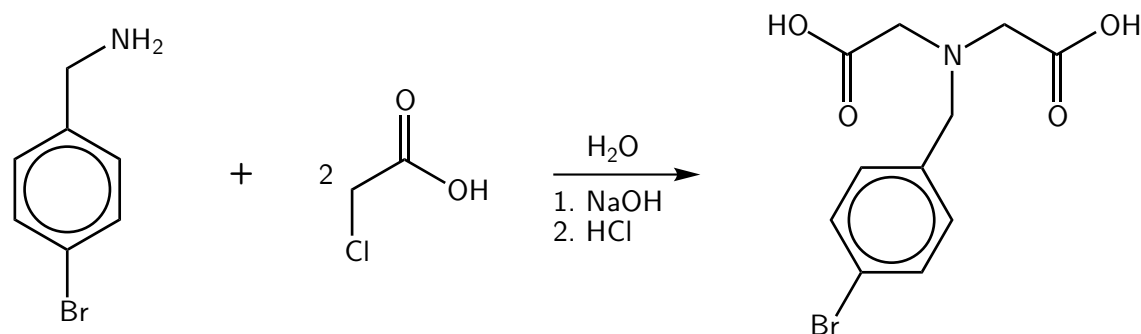
**Elemental analysis:** Calcd. (%): N 5.53, C 47.44, H 3.58.

Found (%): N 5.48, C 46.31, H 3.62.

**MS (FAB<sup>-</sup>):** *m/z* (%) = 230.0 (6) [M - Na]<sup>-</sup>, 208.2 (20) [M - 2Na + H]<sup>-</sup>.

**MS (FAB<sup>+</sup>):** *m/z* (%) = 23.0 (100) [Na]<sup>+</sup>.

**IR** (solid, ATR):  $\tilde{\nu}$  = 1587 (vs), 1500 (m), 1417 (s), 1335 (m), 1308 (w), 1208 (s), 1155 (w), 1079 (w), 1051 (w), 1032 (w), 989 (w), 955 (w), 940 (w), 914 (w), 876 (w), 841 (w), 750 (s), 723 (m), 688 (s) cm<sup>-1</sup>.

5.4.4 *N-p*-Bromobenzyliminodiacetic acid (**H<sub>2</sub>2g**)

**Literature:** N. Smrečki, B.-M. Kukovec, M. Đaković, Z. Popović, *Inorg. Chim. Acta*, **2013**, *400*, 122–129.

**Starting material:** Chloroacetic acid, sodium hydroxide, 4-bromobenzylamine, hydrochloric acid, water.

**Procedure:** Chloroacetic acid (4.73 g, 50.0 mmol) was dissolved in 20 mL of water, cooled to 5 °C and slowly neutralized with sodium hydroxide solution (5 M, 10 mL, 50 mmol) so that the temperature never reached 20 °C. 4-Bromobenzylamine (3.16 mL, 4.65 g, 25.0 mmol) was added and the reaction mixture was refluxed for 1 h while a sodium hydroxide solution (5 M, 10 mL, 50 mmol) was added dropwise. The mixture was refluxed for another hour, cooled to room temperature and acidified to pH 2 with 6 M hydrochloric acid. The mixture was stored in the refrigerator for one day to induce precipitation. **H<sub>2</sub>2g** was obtained as a white solid, filtered off, washed with a minimum amount of ice water and dried under reduced pressure.

**Yield:** 6.39 g (21.3 mmol, 85 %).

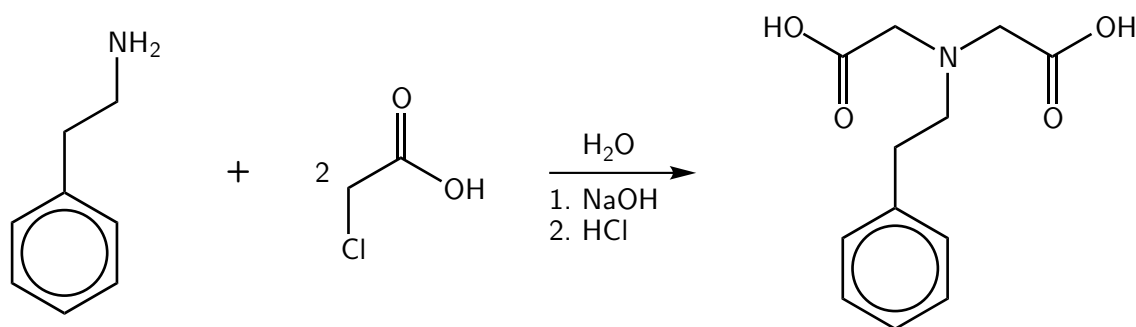
**Empirical formula:** C<sub>11</sub>H<sub>12</sub>BrNO<sub>4</sub>, 302.1 g mol<sup>-1</sup>.

**<sup>1</sup>H-NMR** (400 MHz, D<sub>2</sub>O): δ = 7.51 (d, *J* = 8.2 Hz, 2H), 7.30 (d, *J* = 8.1 Hz, 2H), 3.78 (s, 2H), 3.39 (s, 4H) ppm.

**<sup>13</sup>C{<sup>1</sup>H}-NMR** (100 MHz, D<sub>2</sub>O): δ = 172.3, 138.4, 131.1, 130.8, 120.1, 56.4, 53.7 ppm.

**MS (FAB<sup>-</sup>):** *m/z* (%) = 302.3/300.1 (99/100) [M - H]<sup>-</sup>, 244.0/241.9 (20/20) [M - CH<sub>2</sub>COOH]<sup>-</sup>, 222.2 (30) [M - Br]<sup>-</sup>, 162.8 (15) [M - Br - CH<sub>2</sub>COOH]<sup>-</sup>.

**MS (FAB<sup>+</sup>):** *m/z* (%) = 304.3/301.9 (99/100) [M + H]<sup>+</sup>.

5.4.5 *N*-Phenylethyliminodiacetic acid (**H<sub>2</sub>h**)

**Literature:** N. Smrečki, B.-M. Kukovec, M. Đaković, Z. Popović, *Inorg. Chim. Acta*, **2013**, *400*, 122–129.

**Starting material:** Chloroacetic acid, sodium hydroxide, 2-phenylethylamine, hydrochloric acid, water.

**Procedure:** Chloroacetic acid (4.73 g, 50.0 mmol) was dissolved in 20 mL of water, cooled to 5 °C and slowly neutralized with sodium hydroxide solution (5 M, 10 mL, 50 mmol) so that the temperature never reached 20 °C. 2-Phenylethylamine (3.19 mL, 3.03 g, 25.0 mmol) was added and the reaction mixture was refluxed for 1 h while a sodium hydroxide solution (5 M, 10 mL, 50 mmol) was added dropwise. The mixture was refluxed for another hour, cooled to room temperature and acidified to pH 2 with 6 M hydrochloric acid. The mixture was stored in the refrigerator for one day to induce precipitation. **H<sub>2</sub>h** was obtained as a white solid, filtered off, washed with a minimum amount of ice water and dried under reduced pressure.

**Yield:** 4.84 g (20.4 mmol, 82 %).

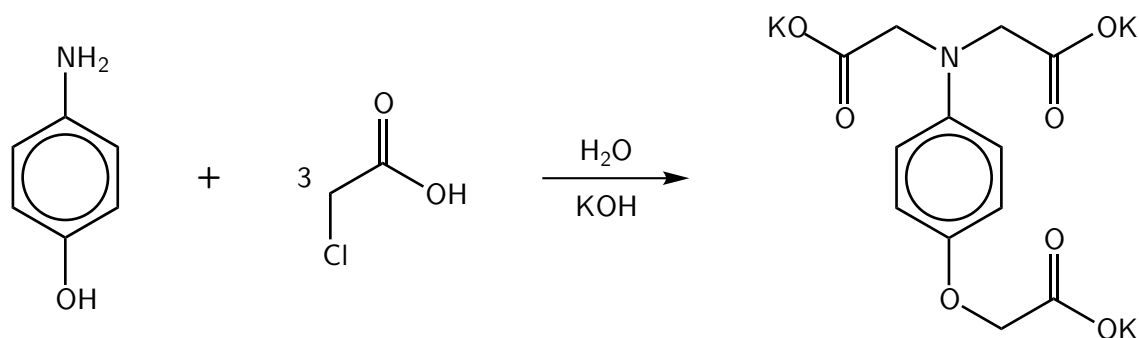
**Empirical formula:** C<sub>12</sub>H<sub>15</sub>NO<sub>4</sub>, 237.3 g mol<sup>-1</sup>.

**<sup>1</sup>H-NMR** (400 MHz, D<sub>2</sub>O): δ = 7.29–7.14 (m, 5H), 3.47 (s, 4H), 2.87 (dd, *J* = 9.8, 5.6 Hz, 2H), 2.71 (dd, *J* = 9.7, 5.6 Hz, 2H) ppm.

**<sup>13</sup>C{<sup>1</sup>H}-NMR** (100 MHz, D<sub>2</sub>O): δ = 172.5, 139.9, 128.6, 128.9, 125.9, 55.9, 54.7, 33.8 ppm.

**MS (FAB<sup>-</sup>):** *m/z* (%) = 473.5 (8) [2 M - H]<sup>-</sup>, 236.3 (100) [M - H]<sup>-</sup>, 178.0 (20) [M - CH<sub>2</sub>COOH]<sup>-</sup>.

**MS (FAB<sup>+</sup>):** *m/z* (%) = 475.5 (4) [2 M + H]<sup>+</sup>, 238.3 (100) [M + H]<sup>+</sup>, 180.3 (40) [M - CH<sub>2</sub>COOH + 2 H]<sup>+</sup>, 105.0 (20) [M - N(CH<sub>2</sub>COOH)]<sup>+</sup>.

5.4.6 Tripotassium *N*-[4-(carboxymethoxy)phenyl]iminodiacetate (**K<sub>3</sub>2k**)

**Literature:** A. J. Miralles, C. M. Silvernail (Ecolab Inc.), US 2009/0264677 A1, **2009**.

**Starting material:** Chloroacetic acid, potassium hydroxide, 4-aminophenol, ethanol, water, DCM, methanol.

**Procedure:** Chloroacetic acid (2.08 g, 22 mmol) was dissolved in a potassium hydroxide solution (5 M, 5 mL). The solution was refluxed and 4-aminophenol (1.09 g, 10 mmol) was added in small portions. More 5 M potassium hydroxide solution was added until a pH of 10–12 was reached. After refluxing for 4 h, the solution was cooled to 0 °C and 30 mL of ethanol was added. Immediately a white solid formed. The suspension was stored at 0 °C overnight and then filtrated. The filtrate was washed two times with 50 mL of DCM and the solvent was removed under reduced pressure. A yellow oil was obtained, which was dissolved in methanol and precipitated with an excess of DCM. The precipitate was dried under reduced pressure to give **K<sub>3</sub>2k** as a white powder.

**Yield:** 0.65 g (1.6 mmol, 22 %).

**Empirical formula:** C<sub>12</sub>H<sub>10</sub>K<sub>3</sub>NO<sub>7</sub>, 397.5 g mol<sup>-1</sup>.

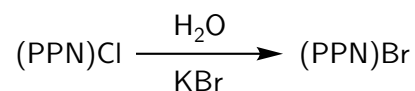
**<sup>1</sup>H-NMR** (400 MHz, D<sub>2</sub>O): δ = 6.79–6.45 (m, 4H), 4.75 (s, 4H), 3.85 (s, 2H) ppm.

**<sup>13</sup>C{<sup>1</sup>H}-NMR** (100 MHz, D<sub>2</sub>O): δ = 180.6, 180.5, 147.9, 143.3, 117.1, 113.6, 68.1, 56.9 ppm.

**MS (FAB-):** *m/z* (%) = 358.1 (100) [M - K]<sup>-</sup>, 320.2 (75) [M - 2K + H]<sup>-</sup>, 282.1 (30) [M - 3K + 2H]<sup>-</sup>.

**MS (FAB+):** *m/z* (%) = 397.9 (8) [M + H]<sup>+</sup>, 39.0 (13) [K]<sup>+</sup>.

**IR** (solid, ATR):  $\tilde{\nu}$  = 2909 (br, vw), 1580 (vs), 1514 (s), 1393 (s), 1296 (m), 1229 (m), 1071 (w), 1034 (w), 977 (w), 907 (w), 820 (w), 771 (w), 692 (w) cm<sup>-1</sup>.

**5.4.7 Bis(triphenylphosphane)iminium bromide, (PPN)Br**

**Literature:** A. Martinsen, J. Songstad, *Acta Chem. Scand.* **1977**, A 31, 645–650.

**Starting material:** Potassium bromide, bis(triphenylphosphane)iminium chloride, acetone, diethyl ether, water.

**Procedure:** (PPN)Cl (2 g, 3.48 mmol) was dissolved in 35 mL of water at 70 °C. Potassium bromide (10 g, 84.0 mmol) was dissolved in 20 mL of water at 70 °C and added slowly and under constant stirring to the hot (PPN)Cl solution. Immediately a white precipitate formed. The suspension was cooled to 0 °C for 2 h, filtered and washed with ice water. The residue was dried under reduced pressure and recrystallized from acetone/diethyl ether. (PPN)Br was obtained as a white powder.

**Yield:** 1.74 g (2.82 mmol, 81 %).

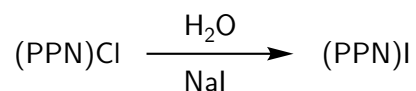
**Empirical formula:** C<sub>36</sub>H<sub>30</sub>BrNP<sub>2</sub>, 618.5 g mol<sup>-1</sup>.

**MS (FAB-):** *m/z* (%) = 78.9 (81) [Br]<sup>-</sup>.

**MS (FAB+):** *m/z* (%) = 538.2 (100) [M - Br]<sup>+</sup>, 384.1 (12) [M - 2 Ph - Br]<sup>+</sup>, 307.3 (31) [M - 3 Ph - Br]<sup>+</sup>.

**Elemental analysis:** Calcd. (%): N 2.26, C 69.91, H 4.89.

Found (%): N 2.17, C 67.12, H 5.06.

**5.4.8 Bis(triphenylphosphane)iminium iodide, (PPN)I**

**Literature:** A. Martinsen, J. Songstad, *Acta Chem. Scand.* **1977**, A 31, 645–650.

**Starting material:** Sodium iodide, bis(triphenylphosphane)iminium chloride, acetone, diethyl ether, water.

**Procedure:** (PPN)Cl (2 g, 3.48 mmol) was dissolved in 35 mL of water at 70 °C. Sodium iodide (10 g, 66.7 mmol) was dissolved in 20 mL of water at 70 °C and added slowly and under constant stirring to the hot (PPN)Cl solution. Immediately a white precipitate formed. The suspension was cooled to 0 °C for 2 h, filtered and washed with ice water. The residue was dried under reduced pressure and recrystallized from acetone/diethyl ether. (PPN)I was obtained as a white powder.

**Yield:** 1.83 g (2.75 mmol, 79 %).

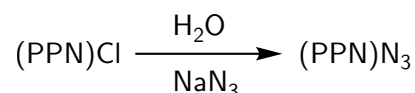
**Empirical formula:** C<sub>36</sub>H<sub>30</sub>INP<sub>2</sub>, 665.5 g mol<sup>-1</sup>.

**MS (FAB-):**  $m/z$  (%) = 127.1 (92) [Br]<sup>-</sup>.

**MS (FAB+):**  $m/z$  (%) = 538.1 (100) [M - I]<sup>+</sup>, 461.0 (18) [M - Ph - I]<sup>+</sup>, 384.3 (22) [M - 2 Ph - I]<sup>+</sup>, 307.1 (19) [M - 3 Ph - I]<sup>+</sup>.

**Elemental analysis:** Calcd. (%): N 2.10, C 64.97, H 4.54.

Found (%): N 1.95, C 59.95, H 4.55.

**5.4.9 Bis(triphenylphosphane)iminium azide, (PPN)N<sub>3</sub>**

**Literature:** A. Martinsen, J. Songstad, *Acta Chem. Scand.* **1977**, A 31, 645–650.

**Starting material:** Sodium azide, bis(triphenylphosphane)iminium chloride, acetone, diethyl ether, water.

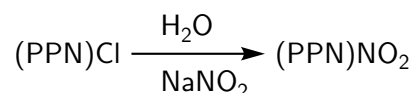
**Procedure:** (PPN)Cl (2 g, 3.48 mmol) was dissolved in 35 mL of water at 70 °C. Sodium azide (5 g, 76.9 mmol) was dissolved in 20 mL of water at 70 °C and added slowly and under constant stirring to the hot (PPN)Cl solution. Immediately a white precipitate formed. The suspension was cooled to 0 °C for 2 h, filtered and washed with ice water. The residue was dried under reduced pressure and recrystallized from acetone/diethyl ether. (PPN)N<sub>3</sub> was obtained as a white powder.

**Yield:** 1.72 g (2.96 mmol, 85 %).

**Empirical formula:** C<sub>36</sub>H<sub>30</sub>N<sub>4</sub>P<sub>2</sub>, 580.6 g mol<sup>-1</sup>.

**MS (FAB+):**  $m/z$  (%) = 538.4 (100) [M - N<sub>3</sub>]<sup>+</sup>, 461.1 (20) [M - Ph - N<sub>3</sub>]<sup>+</sup>, 384.5 (25) [M - 2 Ph - N<sub>3</sub>]<sup>+</sup>, 306.9 (17) [M - 3 Ph - N<sub>3</sub>]<sup>+</sup>.

**Elemental analysis:** Calcd. (%): N 9.65, C 74.47, H 5.21.  
Found (%): N 9.96, C 71.68, H 5.34.

**5.4.10 Bis(triphenylphosphane)iminium nitrite, (PPN)NO<sub>2</sub>**

**Literature:** A. Martinsen, J. Songstad, *Acta Chem. Scand.* **1977**, A 31, 645–650.

**Starting material:** Sodium nitrite, bis(triphenylphosphane)iminium chloride, acetone, diethyl ether, water.

**Procedure:** (PPN)Cl (2 g, 3.48 mmol) was dissolved in 35 mL of water at 70 °C. Sodium nitrite (5 g, 72.5 mmol) was dissolved in 20 mL of water at 70 °C and added slowly and under constant stirring to the hot (PPN)Cl solution. Immediately a white precipitate formed. The suspension was cooled to 0 °C for 2 h, filtered and washed with ice water. The residue was dried under reduced pressure and recrystallized from acetone/diethyl ether. (PPN)NO<sub>2</sub> was obtained as a white powder.

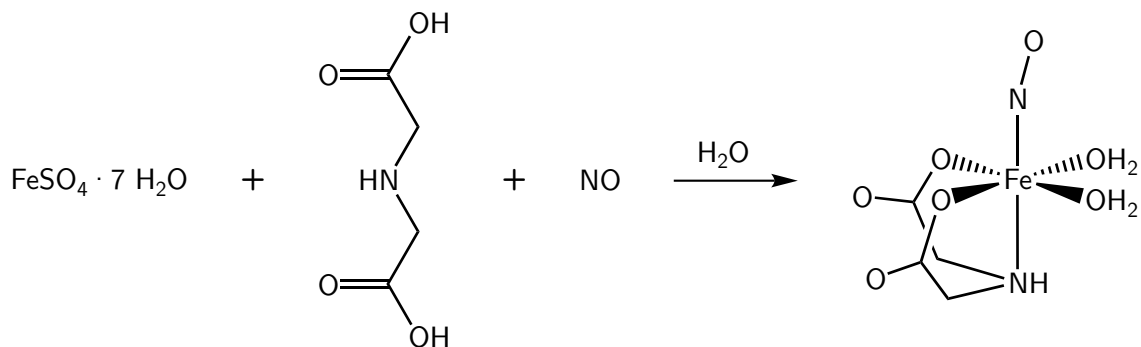
**Yield:** 1.61 g (2.75 mmol, 79 %).

**Empirical formula:** C<sub>36</sub>H<sub>30</sub>N<sub>2</sub>O<sub>2</sub>P<sub>2</sub>, 584.6 g mol<sup>-1</sup>.

**MS (FAB+):**  $m/z$  (%) = 538.4 (100) [M - NO<sub>2</sub>]<sup>+</sup>, 461.1 (20) [M - Ph - NO<sub>2</sub>]<sup>+</sup>, 384.5 (25) [M - 2 Ph - NO<sub>2</sub>]<sup>+</sup>, 306.9 (17) [M - 3 Ph - NO<sub>2</sub>]<sup>+</sup>.

## 5.5 Synthesis of quartet- $\{\text{FeNO}\}^7$ compounds with aminocarboxylato ligands

### 5.5.1 $[\text{Fe}(\text{ida})(\text{NO})(\text{OH}_2)_2]$ (**3a**)



**Starting material:** Iron(II) sulfate heptahydrate, iminodiacetic acid, nitric oxide, acetone, water.

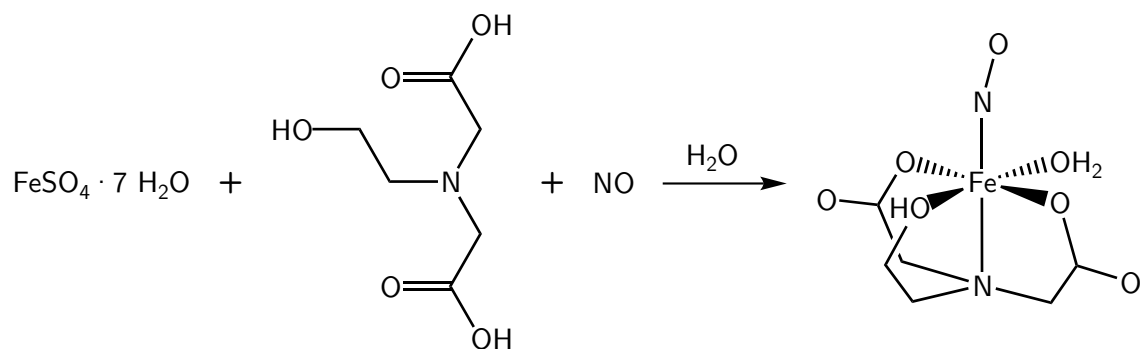
**Procedure:** In one chamber of a two-chamber Schlenk flask  $\text{FeSO}_4 \cdot 7 \text{H}_2\text{O}$  (278 mg, 1.0 mmol) and  $\text{H}_2\text{ida}$  (133 mg, 1.0 mmol) were dissolved in 5 mL of water, forming a colorless solution. Nitric oxide was bubbled through the solution for 10 min, turning it dark green. The gas phase of the Schlenk flask was flushed with argon and 5 mL of acetone were filled into the empty chamber of the Schlenk flask to induce crystallization. After one week, **3a** was obtained as green crystals.

**Yield:** 63 mg (0.25 mmol, 25 %).

**Empirical formula:**  $\text{C}_4\text{H}_9\text{FeN}_2\text{O}_7$ ,  $253.0 \text{ g mol}^{-1}$ .

**IR** (solid, ATR):  $\tilde{\nu} = 1772$  (s), 1566 (vs), 1454 (s), 1408 (s), 1338 (m), 1317 (m), 1256 (m), 1208 (w), 1143 (m), 950 (m), 922 (s), 797 (s), 723 (m), 659 (m)  $\text{cm}^{-1}$ .

**UV-VIS** (solid):  $\lambda = 340, 414, 459, 618, 692 \text{ nm}$ .

5.5.2  $[Fe(\text{heida})(NO)(OH_2)]$  (**3b**)

**Starting material:** Iron(II) sulfate heptahydrate, *N*-(2-hydroxyethyl)iminodiacetic acid, nitric oxide, acetone, water.

**Procedure:** In one chamber of a two-chamber Schlenk flask  $FeSO_4 \cdot 7 H_2O$  (278 mg, 1.0 mmol) and  $H_2\text{heida}$  (177 mg, 1.0 mmol) were dissolved in 5 mL of water, forming a colorless solution. Nitric oxide was bubbled through the solution for 10 min, turning it dark green. The gas phase of the Schlenk flask was flushed with argon and 5 mL of acetone were filled into the empty chamber of the Schlenk flask to induce crystallization. After three weeks, **3b** was obtained as green crystals.

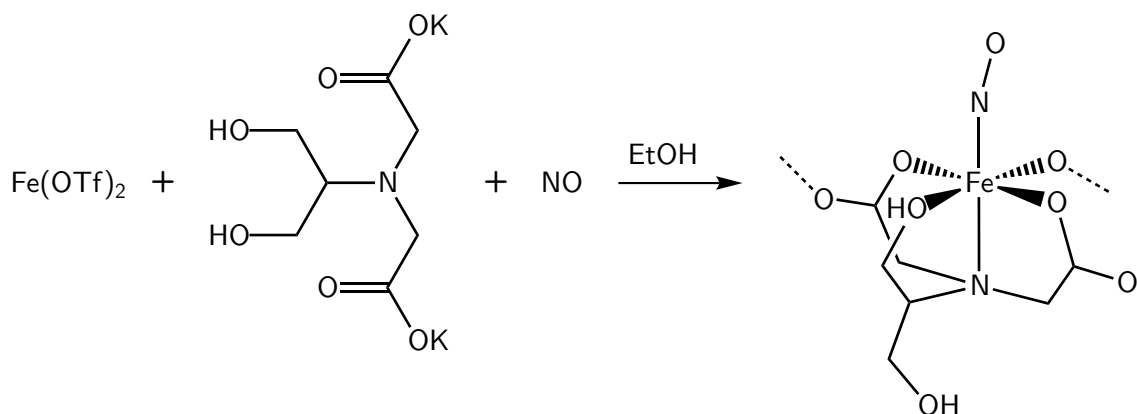
**Yield:** 75 mg (0.27 mmol, 27%).

**Empirical formula:**  $C_6H_{11}FeN_2O_7$ , 279.0 g mol<sup>-1</sup>.

**IR** (solid, ATR):  $\tilde{\nu} = 1782$  (m), 1555 (vs), 1480 (m), 1444 (m), 1428 (m), 1401 (s), 1388 (s), 1380 (s), 1351 (s), 1323 (m), 1300 (vs), 1264 (m), 1253 (m), 1221 (w), 1155 (w), 1108 (w), 1066 (m), 1055 (m), 998 (s), 973 (w), 921 (s), 883 (s), 839 (s), 812 (vs), 737 (s), 695 (m), 686 (m), 659 (m) cm<sup>-1</sup>.

**UV-VIS** (solid):  $\lambda = 341, 402, 457, 625, 691$  nm.

## 5.5.3 [Fe(dhpida)(NO)] (3c)



**Starting material:** Iron(II)triflate · 3 CH<sub>3</sub>CN, dipotassium *N*-(1,3-dihydroxypropane-2-yl)iminodiacetate, nitric oxide, ethanol, acetone.

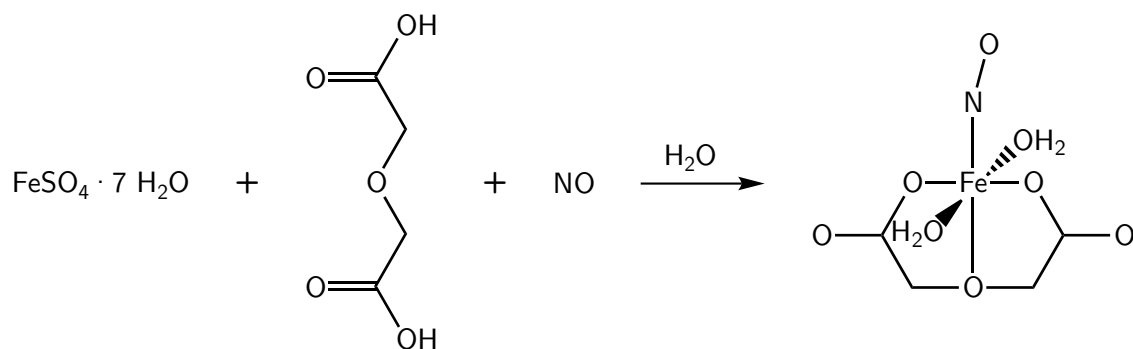
**Procedure:** In one chamber of a two-chamber Schlenk flask iron(II)triflate · 3 CH<sub>3</sub>CN (354 mg, 1.0 mmol) and K<sub>2</sub>dhpida (283 mg, 1.0 mmol) were dissolved in 5 mL of ethanol, forming a colorless solution. Nitric oxide was bubbled through the solution for 10 min, turning it dark green. The gas phase of the Schlenk flask was flushed with argon and 5 mL of acetone were filled into the empty chamber of the Schlenk flask to induce crystallization. After two week **3c** was obtained as green crystals.

**Yield:** 36 mg (0.12 mmol, 12%).

**Empirical formula:** C<sub>7</sub>H<sub>11</sub>FeN<sub>2</sub>O<sub>7</sub>, 291.0 g mol<sup>-1</sup>.

**IR** (solid, ATR):  $\tilde{\nu}$  = 1805 (w), 1789 (m), 1640 (s), 1589 (vs), 1555 (vs), 1407 (m), 1326 (m), 1303 (s), 1276 (s), 1252 (s), 1174 (m), 1146 (m), 1133 (m), 1101 (m), 1070 (s), 1055 (s), 1041 (s), 1013 (s), 1005 (s), 986 (m), 920 (s), 862 (w), 782 (s), 731 (s), 681 (w) cm<sup>-1</sup>.

**UV-VIS** (solid):  $\lambda$  = 341, 412, 457, 625, 690 nm.

5.5.4  $[Fe(NO)(OH_2)_2(oda)]$  (**3d**)

**Starting material:** Iron(II) sulfate heptahydrate, oxodiacetic acid, nitric oxide, acetone, water.

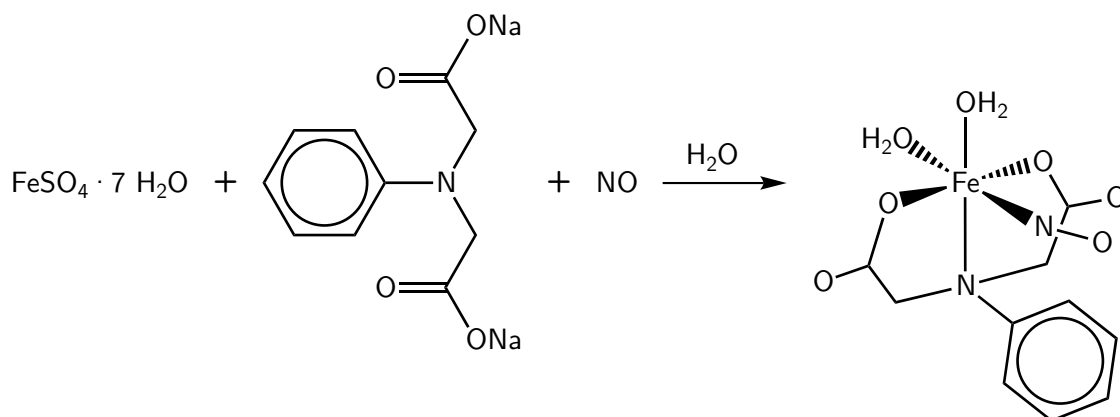
**Procedure:** In one chamber of a two-chamber Schlenk flask  $FeSO_4 \cdot 7 H_2O$  (278 mg, 1.0 mmol) and  $H_2oda$  (134 mg, 1.0 mmol) were dissolved in 5 mL of water, forming a colorless solution. Nitric oxide was bubbled through the solution for 10 min, turning it dark green. The gas phase of the Schlenk flask was flushed with argon and 5 mL of acetone were filled into the empty chamber of the Schlenk flask to induce crystallization. After two weeks, **3d** was obtained as green crystals.

**Yield:** 53 mg (0.21 mmol, 21 %).

**Empirical formula:**  $C_4H_8FeNO_8$ , 254.0  $g\ mol^{-1}$ .

**IR** (solid, ATR):  $\tilde{\nu} = 1799$  (m), 1557 (vs), 1467 (m), 1419 (vs), 1352 (m), 1305 (s), 1133 (s), 1034 (m), 933 (m), 806 (m), 796 (m), 729 (s), 677 (m)  $cm^{-1}$ .

**UV-VIS** (solid):  $\lambda = 340, 407, 459, 571, 693$  nm.

5.5.5  $[\text{Fe}(\text{NO})(\text{OH}_2)_2(\text{phida})] \cdot \text{H}_2\text{O}$  (**3e**)

**Starting material:** Iron(II) sulfate heptahydrate, disodium *N*-phenyliminodiacetate, nitric oxide, acetone, water.

**Procedure:** In one chamber of a two-chamber Schlenk flask  $\text{FeSO}_4 \cdot 7 \text{H}_2\text{O}$  (278 mg, 1.0 mmol) and  $\text{Na}_2\text{phida}$  (253 mg, 1.0 mmol) were dissolved in 5 mL of water, forming a colorless solution. Nitric oxide was bubbled through the solution for 10 min, turning it dark green. The gas phase of the Schlenk flask was flushed with argon and 5 mL of acetone were filled into the empty chamber of the Schlenk flask to induce crystallization. After one week **3e** was obtained as green crystals.

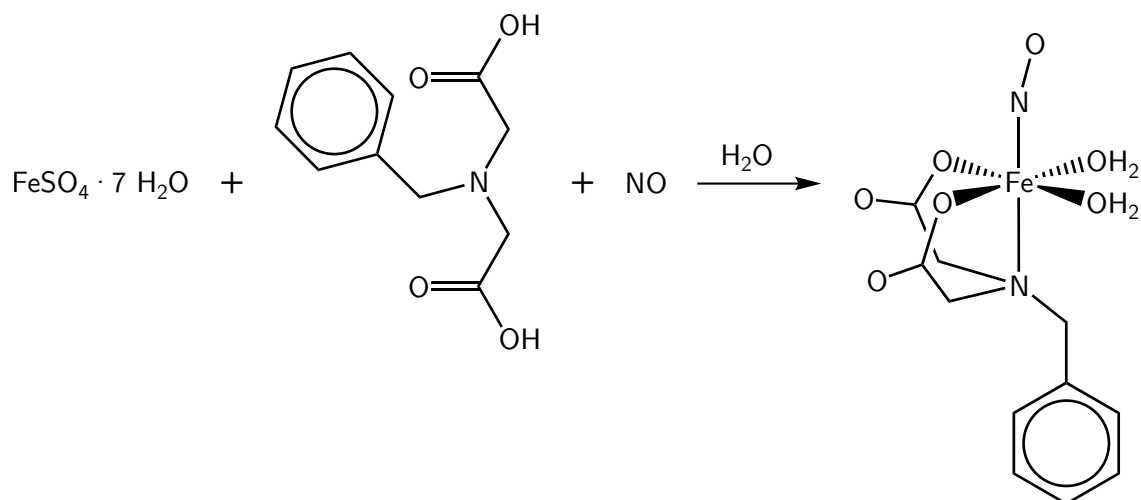
**Yield:** 140 mg (0.40 mmol, 40%).

**Empirical formula:**  $\text{C}_{10}\text{H}_{13}\text{FeN}_2\text{O}_7 \cdot \text{H}_2\text{O}$ ,  $347.0 \text{ g mol}^{-1}$ .

**Elemental analysis:** Calcd. (%): N 8.07, C 34.61, H 4.36.

Found (%): N 7.96, C 34.27, H 4.36.

**IR** (solid, ATR):  $\tilde{\nu} = 1763$  (s), 1680 (w), 1573 (vs), 1496 (s), 1454 (w), 1397 (s), 1295 (s), 1196 (m), 1143 (m), 1028 (w), 976 (m), 919 (m), 892 (w), 773 (s), 759 (s), 690 (vs)  $\text{cm}^{-1}$ .

5.5.6  $[Fe(bnida)(NO)(OH_2)_2]$  (**3f**)

**Starting material:** Iron(II) sulfate heptahydrate, *N*-benzyliminodiacetic acid, nitric oxide, acetone, water.

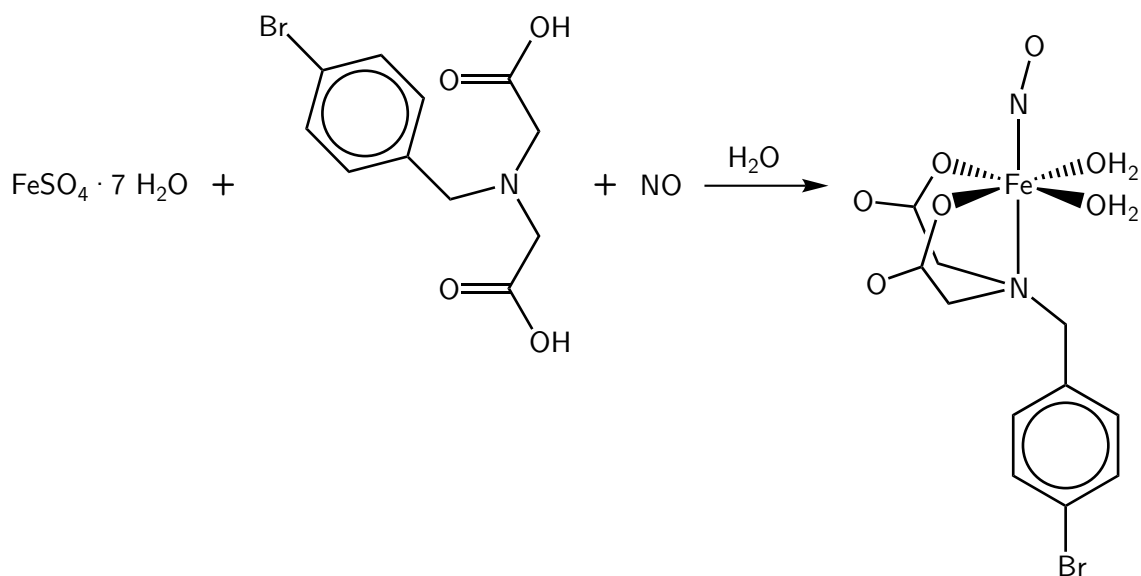
**Procedure:** In one chamber of a two-chamber Schlenk flask  $FeSO_4 \cdot 7 H_2O$  (278 mg, 1.0 mmol) and H<sub>2</sub>bnida (223 mg, 1.0 mmol) were dissolved in 5 mL of water, forming a colorless solution. Nitric oxide was bubbled through the solution for 10 min, turning it dark green. The gas phase of the Schlenk flask was flushed with argon and 5 mL of acetone were filled into the empty chamber of the Schlenk flask to induce crystallization. After four weeks, **3f** was obtained as green crystals.

**Yield:** 51 mg (0.15 mmol, 15%).

**Empirical formula:** C<sub>11</sub>H<sub>15</sub>FeN<sub>2</sub>O<sub>7</sub>, 343.0 g mol<sup>-1</sup>.

**IR** (solid, ATR):  $\tilde{\nu} = 1790$  (m), 1606 (s), 1494 (w), 1456 (w), 1394 (m), 1337 (m), 1219 (w), 1200 (w), 1090 (w), 1075 (m), 943 (m), 905 (m), 763 (s), 703 (s) cm<sup>-1</sup>.

**UV-VIS** (solid):  $\lambda = 341, 408, 459, 596, 692$  nm.

5.5.7 [Fe(brbnida)(NO)(OH<sub>2</sub>)<sub>2</sub>] (**3g**)

**Starting material:** Iron(II) sulfate heptahydrate, *N*-*p*-bromobenzyliminodiacetic acid, nitric oxide, acetone, water.

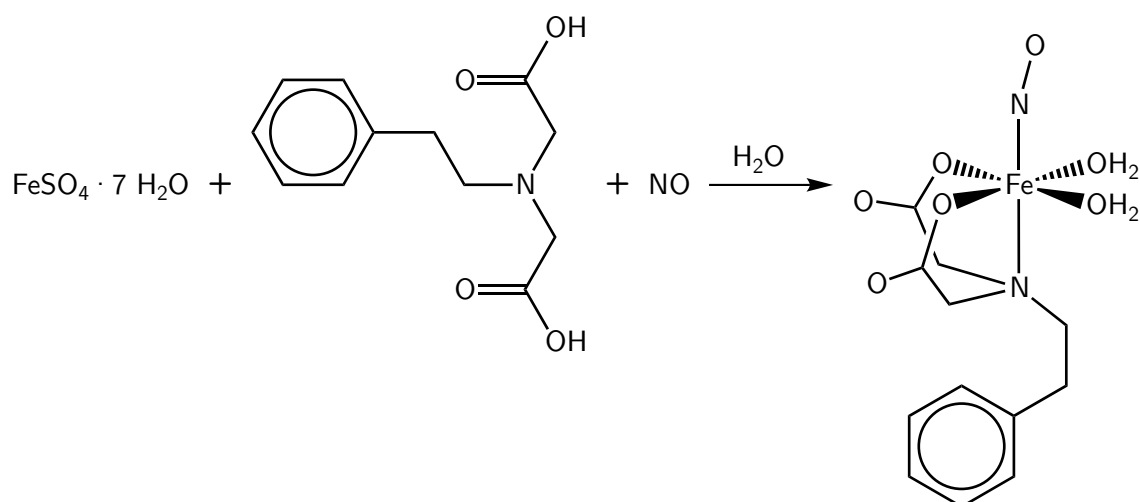
**Procedure:** In one chamber of a two-chamber Schlenk flask  $\text{FeSO}_4 \cdot 7 \text{H}_2\text{O}$  (278 mg, 1.0 mmol) and  $\text{H}_2\text{brbnida}$  (302 mg, 1.0 mmol) were dissolved in 5 mL of water, forming a colorless solution. Nitric oxide was bubbled through the solution for 10 min, turning it dark green. The gas phase of the Schlenk flask was flushed with argon and 5 mL of acetone were filled into the empty chamber of the Schlenk flask to induce crystallization. After one week **3g** was obtained as green crystals.

**Yield:** 55 mg (0.13 mmol, 13%).

**Empirical formula:**  $\text{C}_{11}\text{H}_{14}\text{BrFeN}_2\text{O}_7$ ,  $422.0 \text{ g mol}^{-1}$ .

**IR** (solid, ATR):  $\tilde{\nu} = 1800$  (m), 1604 (vs), 1486 (w), 1464 (w), 1438 (vw), 1398 (s), 1367 (m), 1342 (m), 1313 (w), 1292 (w), 1219 (w), 1089 (w), 1071 (w), 1011 (w), 975 (vw), 956 (vw), 938 (m), 910 (m), 850 (m), 797 (m), 766 (w), 748 (w),  $720 \text{ (m) cm}^{-1}$ .

**UV-VIS** (solid):  $\lambda = 371, 402, 459, 595, 691 \text{ nm}$ .

5.5.8  $[Fe(NO)(OH_2)_2(pheida)]$  (**3h**)

**Starting material:** Iron(II) sulfate heptahydrate, *N*-(2-phenylethyl)iminodiacetic acid, nitric oxide, acetone, water.

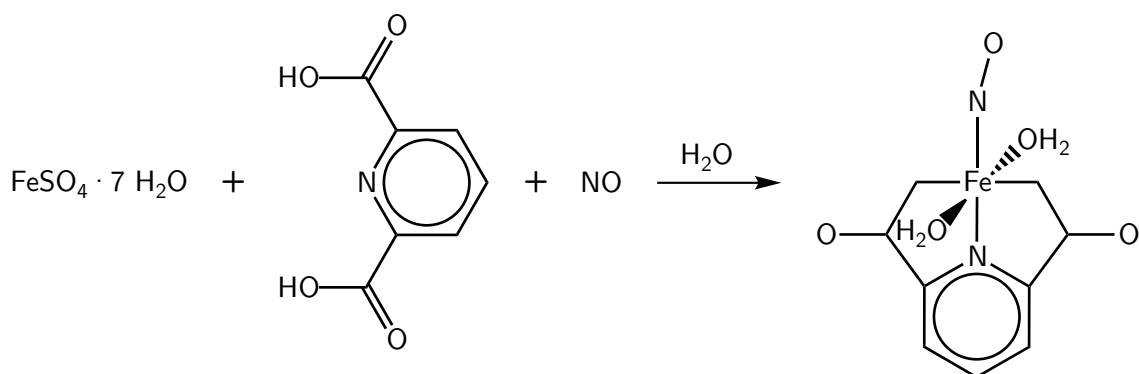
**Procedure:** In one chamber of a two-chamber Schlenk flask  $FeSO_4 \cdot 7 H_2O$  (278 mg, 1.0 mmol) and  $H_2pheida$  (237 mg, 1.0 mmol) were dissolved in 5 mL of water, forming a colorless solution. Nitric oxide was bubbled through the solution for 10 min, turning it dark green. The gas phase of the Schlenk flask was flushed with argon and 5 mL of acetone were filled into the empty chamber of the Schlenk flask to induce crystallization. After four weeks, **3a** was obtained as green crystals.

**Yield:** 32 mg (0.09 mmol, 9%).

**Empirical formula:**  $C_{12}H_{17}FeN_2O_7$ , 357.0 g mol<sup>-1</sup>.

**IR** (solid, ATR):  $\tilde{\nu} = 1814$  (m), 1793 (m), 1586 (vs), 1496 (w), 1469 (m), 1454 (w), 1436 (w), 1398 (vs), 1373 (s), 1346 (s), 1307 (m), 1250 (w), 1209 (w), 1110 (m), 1090 (w), 1071 (w), 1026 (w), 1012 (w), 980 (m), 953 (m), 906 (s), 830 (m), 812 (w), 745 (vs), 694 (vs) cm<sup>-1</sup>.

**UV-VIS** (solid):  $\lambda = 340, 420, 459, 596, 693$  nm.

5.5.9 [Fe(dipic)(NO)(OH<sub>2</sub>)<sub>2</sub>] (3i)

**Starting material:** Iron(II) sulfate heptahydrate, dipicolinic acid, nitric oxide, acetone, water.

**Procedure:** In one chamber of a two-chamber Schlenk flask  $\text{FeSO}_4 \cdot 7 \text{H}_2\text{O}$  (278 mg, 1.0 mmol) and  $\text{H}_2\text{dipic}$  (167 mg, 1.0 mmol) were dissolved in 5 mL of water, forming a red solution. Nitric oxide was bubbled through the solution for 10 min, turning it dark green. The gas phase of the Schlenk flask was flushed with argon and 5 mL of acetone were filled into the empty chamber of the Schlenk flask to induce crystallization. After one day **3i** was obtained as green crystals.

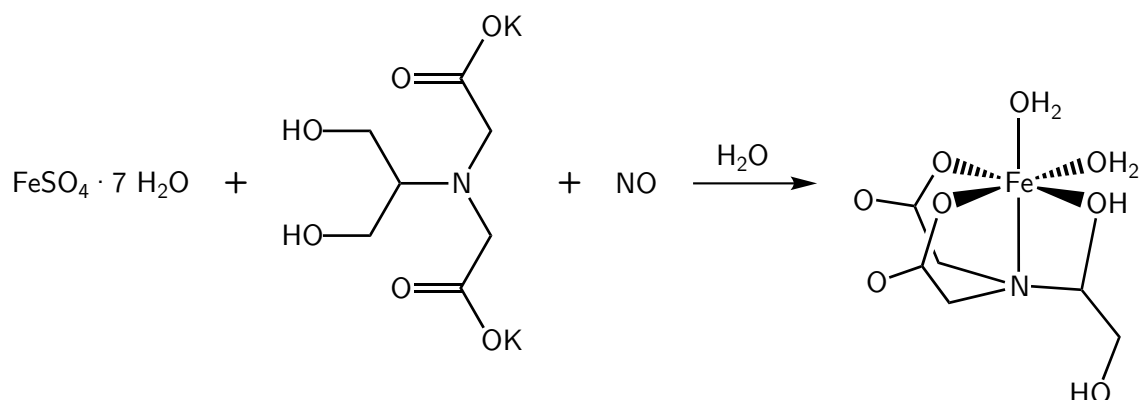
**Yield:** 109 mg (0.38 mmol, 38 %).

**Empirical formula:**  $\text{C}_7\text{H}_7\text{FeN}_2\text{O}_7$ , 287.0  $\text{g mol}^{-1}$ .

**IR** (solid, ATR):  $\tilde{\nu} = 1814$  (s), 1640 (s), 1607 (s), 1592 (s), 1574 (s), 1431 (m), 1375 (s), 1359 (s), 1278 (s), 1184 (m), 1154 (w), 1082 (m), 1036 (w), 1004 (w), 920 (s), 839 (w), 814 (w), 769 (vs), 750 (vs), 688 (vs), 668 (vs)  $\text{cm}^{-1}$ .

## 5.6 Synthesis of iron(II) aminocarboxylates

### 5.6.1 $[\text{Fe}(\text{dhpida})(\text{OH}_2)_2] \cdot 2\text{H}_2\text{O}$ (**4c**)



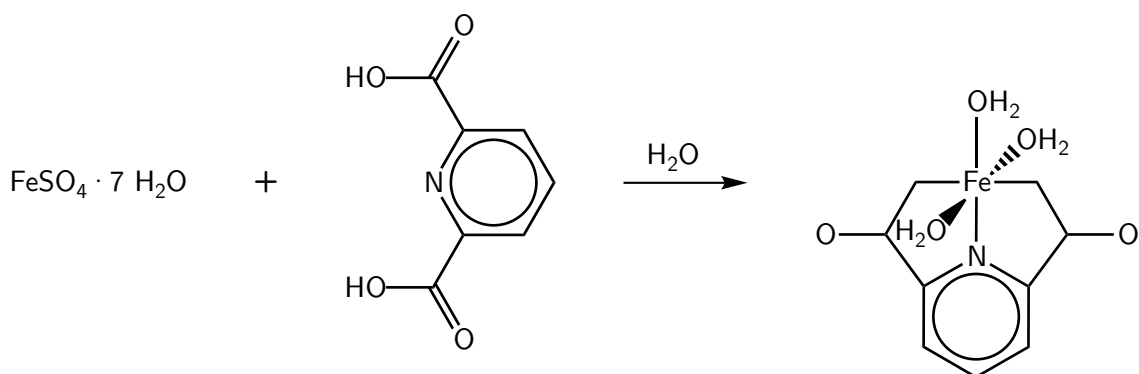
**Starting material:** Iron(II) sulfate heptahydrate, dipotassium *N*-(1,3-dihydroxypropane-2-yl)iminodiacetate, nitric oxide, acetone, water.

**Procedure:** In one chamber of a two-chamber Schlenk flask  $\text{FeSO}_4 \cdot 7\text{H}_2\text{O}$  (278 mg, 1.0 mmol) and  $\text{K}_2\text{dhpida}$  (283 mg, 1.0 mmol) were dissolved in 5 mL of water, forming a colorless solution. Nitric oxide was bubbled through the solution for 10 min, turning it dark green. The gas phase of the Schlenk flask was flushed with argon and 5 mL of acetone were filled into the empty chamber of the Schlenk flask to induce crystallization. After three weeks, **4c** was obtained as colorless crystals.

**Yield:** 83 mg (0.25 mmol, 25 %).

**Empirical formula:**  $\text{C}_7\text{H}_{15}\text{FeNO}_8 \cdot 2\text{H}_2\text{O}$ , 333.1  $\text{g mol}^{-1}$ .

**IR** (solid, ATR):  $\tilde{\nu} = 2540$  (m), 2311 (m), 1632 (s), 1581 (vs), 1544 (vs), 1399 (m), 1318 (m), 12095 (s), 1260 (s), 1244 (s), 1168 (m), 1131 (m), 1125 (m), 1095 (m), 1058 (s), 1048 (s), 1035 (s), 1003 (s), 999 (s), 990 (m), 925 (s), 870 (w), 775 (s), 740 (s), 723 (m) 681 (w)  $\text{cm}^{-1}$ .

5.6.2 [Fe(dipic)(OH<sub>2</sub>)<sub>3</sub>] · 2 H<sub>2</sub>O (4i)

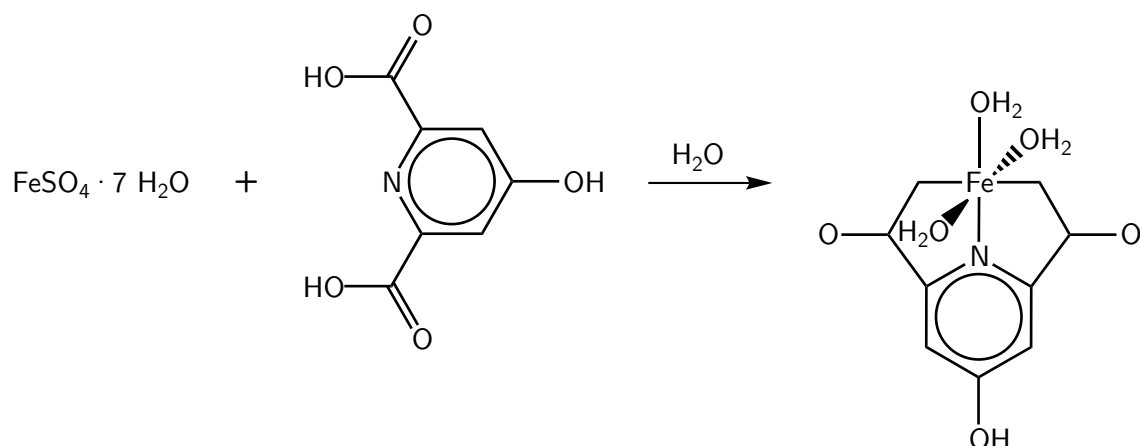
**Starting material:** Iron(II) sulfate heptahydrate, dipicolinic acid, acetone, water.

**Procedure:** In one chamber of a two-chamber Schlenk flask  $\text{FeSO}_4 \cdot 7\text{H}_2\text{O}$  (67 mg, 0.24 mmol) and  $\text{H}_2\text{dipic}$  (40 mg, 0.24 mmol) were dissolved in 5 mL of water, forming a red solution. 3 mL of acetone were filled into the second chamber of the Schlenk flask to induce crystallization. After five days **4i** was obtained as red crystals.

**Yield:** 60 mg (0.19 mmol, 81 %).

**Empirical formula:**  $\text{C}_7\text{H}_9\text{FeNO}_7 \cdot 2 \text{H}_2\text{O}$ , 311.0 g mol<sup>-1</sup>.

**IR** (solid, ATR):  $\tilde{\nu} = 2527$  (m), 2360 (m), 2183 (w), 1682 (s), 1612 (s), 1591 (s), 1570 (m), 1424 (m), 1387 (s), 1373 (s), 1351 (s), 1266 (m), 1232 (m), 1187 (m), 1163 (m), 1081 (s), 1028 (s), 997 (s), 925 (m), 866 (w), 851 (w), 819 (w), 774 (m), 758 (s), 750 (s), 715 (vs), 688 (s) cm<sup>-1</sup>.

5.6.3  $[\text{Fe}(\text{ca})(\text{OH}_2)_3] \cdot 0.5 \text{H}_2\text{O}$  (**4j**)

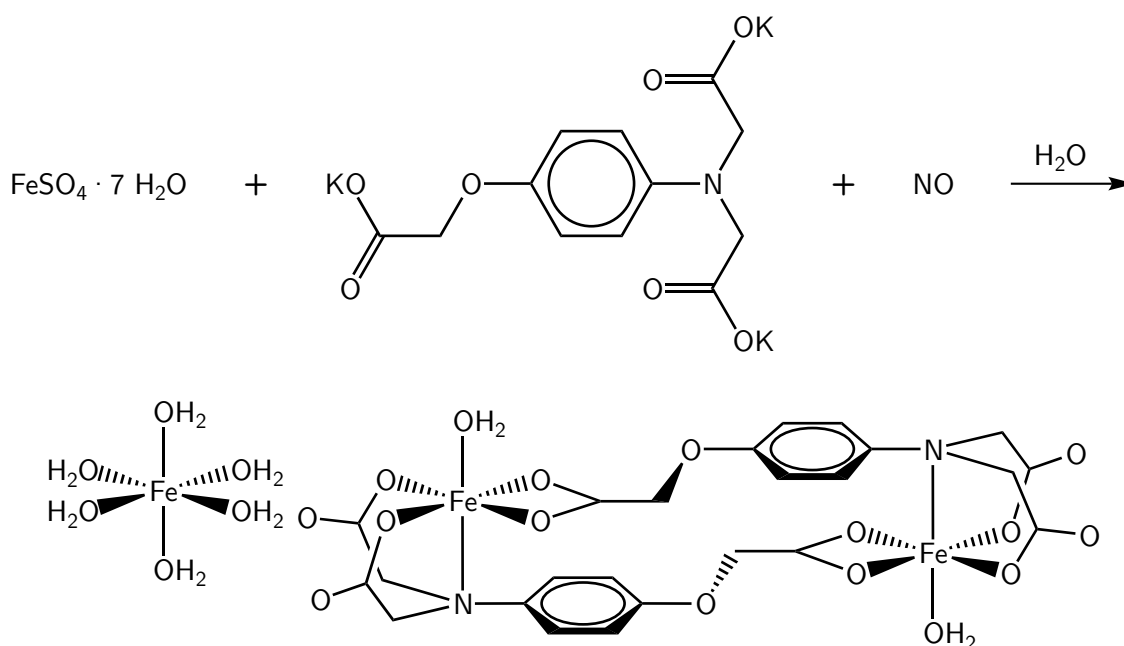
**Starting material:** Iron(II) sulfate heptahydrate, chelidamic acid, acetone, water.

**Procedure:** In one chamber of a two-chamber Schlenk flask  $\text{FeSO}_4 \cdot 7 \text{H}_2\text{O}$  (76 mg, 0.27 mmol) and  $\text{H}_2\text{ca}$  (50 mg, 0.27 mmol) were dissolved in 4 mL of water, forming a red solution. 4 mL of acetone were filled into the second chamber of the Schlenk flask to induce crystallization. After five weeks, **4j** was obtained as orange crystals.

**Yield:** 44 mg (0.19 mmol, 54 %).

**Empirical formula:**  $\text{C}_7\text{H}_9\text{FeNO}_8 \cdot 0.5 \text{H}_2\text{O}$ ,  $300.0 \text{ g mol}^{-1}$ .

**IR** (solid, ATR):  $\tilde{\nu} = 3327$  (s), 2965 (w), 2742 (w), 2606 (w), 1680 (s), 1610 (vs), 1402 (vs), 1339 (s), 1242 (m), 1130 (m), 1013 (s), 938 (w), 898 (m), 810 (s), 762 (m), 712 (s), 678 (w)  $\text{cm}^{-1}$ .

5.6.4  $[\text{Fe}_3(\text{cpida})_2(\text{OH}_2)_8] \cdot 2\text{H}_2\text{O}$  (**4k**)

**Starting material:** Iron(II) sulfate heptahydrate, tripotassium *N*-[4-(carboxymethoxy)phenyl]iminodiacetate, nitric oxide, acetone, water.

**Procedure:** In one chamber of a two-chamber Schlenk flask  $\text{FeSO}_4 \cdot 7\text{H}_2\text{O}$  (417 mg, 1.5 mmol) and  $\text{K}_3\text{cpida}$  (398 mg, 1.0 mmol) were dissolved in 5 mL of water, forming a colorless solution. Nitric oxide was bubbled through the solution for 10 min, turning it dark green. The gas phase of the Schlenk flask was flushed with argon and 5 mL of degassed acetone were filled into the empty chamber of the Schlenk flask to induce crystallization. After six months **4k** was obtained as light brown crystals.

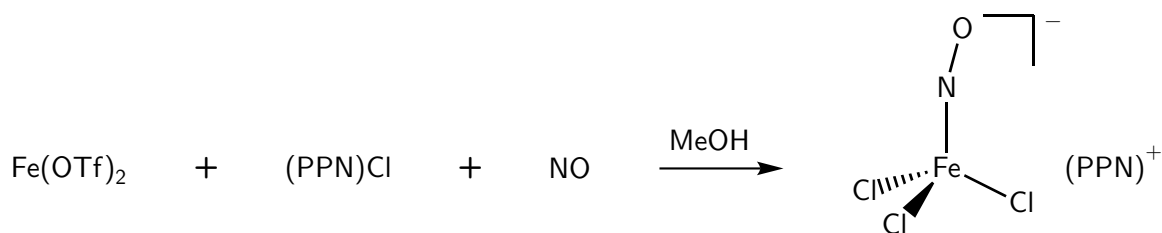
**Yield:** 103 mg (0.11 mmol, 23 %).

**Empirical formula:**  $\text{C}_{24}\text{H}_{36}\text{Fe}_3\text{N}_2\text{O}_{22} \cdot 2\text{H}_2\text{O}$ ,  $908.1 \text{ g mol}^{-1}$ .

**IR** (solid, ATR):  $\tilde{\nu} = 3415$  (s), 1616 (vs), 1565 (m), 1512 (w), 1410 (m), 1331 (w), 1238 (m), 1187 (w), 1144 (w), 1061 (w), 917 (w), 811 (m), 705 (w), 660 (w)  $\text{cm}^{-1}$ .

## 5.7 Synthesis of halogenidonitrosylferrates

### 5.7.1 {PPN}[FeCl<sub>3</sub>(NO)] ((PPN)5a)



**Starting material:** Iron(II)triflate · 3 CH<sub>3</sub>CN, bis(triphenylphosphane)iminium chloride, nitric oxide, methanol.

**Procedure:** Iron(II)triflate · 3 CH<sub>3</sub>CN (131 mg, 0.3 mmol) and (PPN)Cl (517 mg, 0.9 mmol) were dissolved in 5 mL of methanol. Nitric oxide was bubbled through the solution for 5 min. Immediately green crystals of (PPN)5a formed which were filtrated and dried under reduced pressure.

**Yield:** 177 mg (0.24 mmol, 81 %).

**Empirical formula:** C<sub>36</sub>H<sub>30</sub>Cl<sub>3</sub>FeN<sub>2</sub>OP<sub>2</sub>, 730.8 g mol<sup>-1</sup>.

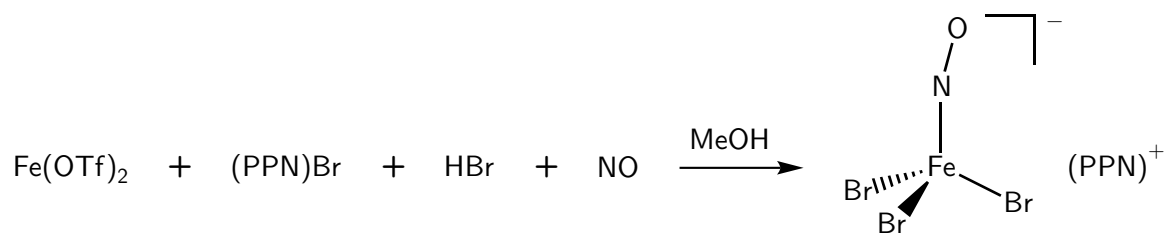
**Elemental analysis:** Calcd. (%): N 3.83, C 59.17, H 4.14.  
Found (%): N 3.46, C 58.94, H 4.34.

**MS (FAB-):**  $m/z$  (%) = 191.0 (30) [FeCl<sub>3</sub>(NO)]<sup>-</sup>, 161.0 (70) [FeCl<sub>3</sub>]<sup>-</sup>.

**MS (FAB+):**  $m/z$  (%) = 538.7 (100) [M - FeCl<sub>3</sub>(NO)]<sup>+</sup>, 460.0 (30) [M - Ph - FeCl<sub>3</sub>(NO)]<sup>+</sup>, 384.5 (40) [M - 2 Ph - FeCl<sub>3</sub>(NO)]<sup>+</sup>, 307.0 (20) [M - 3 Ph - FeCl<sub>3</sub>(NO)]<sup>+</sup>, 262.4 (20) [PPh<sub>3</sub>]<sup>+</sup>.

**IR (solid, ATR):**  $\tilde{\nu}$  = 2360 (m), 2341 (m), 1792 (m), 1588 (w), 1482 (w), 1437 (m), 1265 (m), 1239 (s), 1180 (m), 1113 (s), 1074 (w), 1030 (m), 998 (m), 797 (w), 764 (w), 746 (s), 721 (vs), 689 (vs), 668 (s) cm<sup>-1</sup>.

**UV-VIS (solid):**  $\lambda$  = 309, 371, 485, 670, 692 nm.

5.7.2 {PPN}[FeBr<sub>3</sub>(NO)] ((PPN)5b)

**Starting material:** Iron(II)triflate · 3 CH<sub>3</sub>CN, bis(triphenylphosphane)iminium bromide, hydrobromic acid, nitric oxide, methanol.

**Procedure:** Iron(II)triflate · 3 CH<sub>3</sub>CN (131 mg, 0.3 mmol), (PPN)Br (186 mg, 0.3 mmol) and hydrobromic acid (2 M, 300 µL, 0.6 mmol) were dissolved in 5 mL of methanol. Nitric oxide was bubbled through the solution for 5 min. After five weeks, green crystals of (PPN)5b formed which were filtrated and dried under reduced pressure.

**Yield:** 131 mg (0.15 mmol, 51 %).

**Empirical formula:** C<sub>36</sub>H<sub>30</sub>Br<sub>3</sub>FeN<sub>2</sub>OP<sub>2</sub>, 864.2 g mol<sup>-1</sup>.

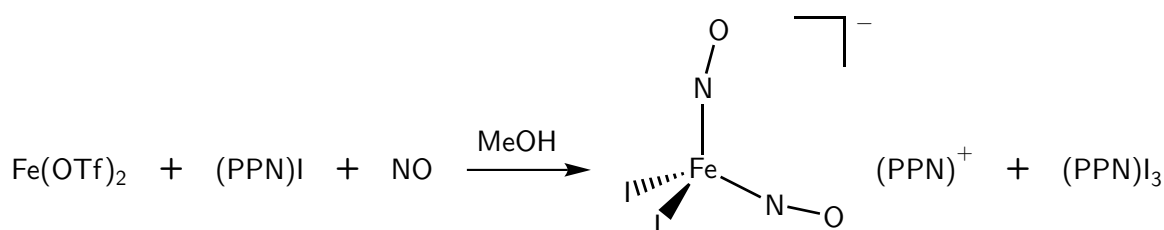
**Elemental analysis:** Calcd. (%): N 3.24, C 50.04, H 3.50.  
Found (%): N 2.12, C 53.03, H 4.23.

**MS (FAB-):**  $m/z$  (%) = 325.0 (4) [FeBr<sub>3</sub>(NO)]<sup>-</sup>, 295.0 (5) [FeBr<sub>3</sub>]<sup>-</sup>.

**MS (FAB+):**  $m/z$  (%) = 538.6 (100) [M - FeBr<sub>3</sub>(NO)]<sup>+</sup>, 460.0 (15) [M - Ph - FeBr<sub>3</sub>(NO)]<sup>+</sup>, 384.1 (18) [M - 2 Ph - FeBr<sub>3</sub>(NO)]<sup>+</sup>.

**IR (solid, ATR):**  $\tilde{\nu}$  = 2360 (w), 2342 (w), 1772 (m), 1588 (w), 1482 (w), 1438 (m), 1262 (vs), 1227 (m), 1182 (m), 1149 (m), 1112 (s), 1031 (s), 997 (m), 798 (w), 762 (w), 743 (m), 721 (vs), 689 (vs) cm<sup>-1</sup>.

**UV-VIS (solid):**  $\lambda$  = 326, 382, 500, 673, 696 nm.

5.7.3  $\{ \{ \text{PPN} \} [\text{Fe}_2(\text{NO})_2] \} \{ \{ \text{PPN} \} [\text{I}_3] \} ((\text{PPN})_2\text{5c}(\text{I}_3))$ 

**Starting material:** Iron(II)triflate  $\cdot$  3 CH<sub>3</sub>CN, bis(triphenylphosphane)iminium iodide, nitric oxide, methanol.

**Procedure:** Iron(II)triflate  $\cdot$  3 CH<sub>3</sub>CN (131 mg, 0.3 mmol) and (PPN)I (599 mg, 0.9 mmol) were dissolved in 5 mL of methanol. Nitric oxide was bubbled through the solution for 5 min. After two weeks, brown crystals of bis(triphenylphosphane)iminium diiodidodinitrosylferrate(I)-triiodide formed which were filtrated and dried under reduced pressure.

**Yield:** 121 mg (0.07 mmol, 22 %).

**Empirical formula:** C<sub>72</sub>H<sub>60</sub>FeI<sub>5</sub>N<sub>4</sub>O<sub>2</sub>P<sub>4</sub>, 1827.6 g mol<sup>-1</sup>.

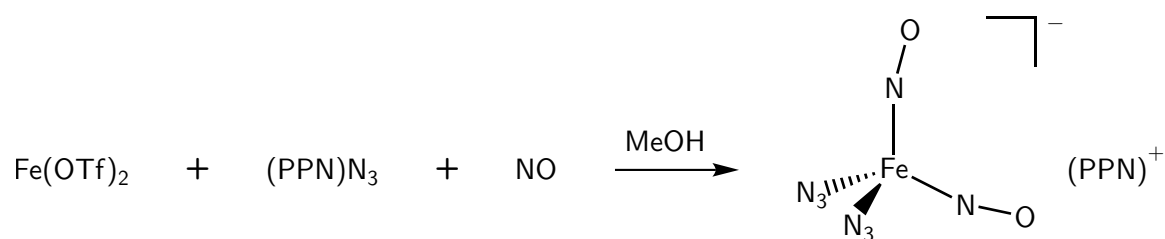
**Elemental analysis:** Calcd. (%): N 3.07, C 47.32, H 3.31.  
Found (%): N 3.49, C 47.52, H 3.34.

**MS (FAB-):**  $m/z$  (%) = 381.0 (10) [I<sub>3</sub>]<sup>-</sup>, 370.2 (65) [FeI<sub>2</sub>(NO)<sub>2</sub>]<sup>-</sup>, 340.1 (30) [FeI<sub>2</sub>(NO)]<sup>-</sup>, 243.1 (5) [FeI(NO)<sub>2</sub>]<sup>-</sup>, 127.1 (30) [I]<sup>-</sup>.

**MS (FAB+):**  $m/z$  (%) = 538.7 (100) [M - FeI<sub>2</sub>(NO)<sub>2</sub>]<sup>+</sup>, 460.0 (20) [M - Ph - FeI<sub>2</sub>(NO)<sub>2</sub>]<sup>+</sup>, 384.5 (30) [M - 2 Ph - FeI<sub>2</sub>(NO)<sub>2</sub>]<sup>+</sup>, 307.5 (15) [M - 3 Ph - FeI<sub>2</sub>(NO)<sub>2</sub>]<sup>+</sup>, 262.0 (10) [PPh<sub>3</sub>]<sup>+</sup>.

**IR (solid, ATR):**  $\tilde{\nu}$  = 1762 (m), 1712 (s), 1588 (w), 1482 (w), 1436 (s), 1256 (ws, br), 1183 (m), 1158 (m), 1113 (s), 1032 (m), 997 (m), 743 (m), 722 (vs), 689 (vs), 654 (m) cm<sup>-1</sup>.

**UV-VIS (solid):**  $\lambda$  = 302, 406, 433, 608, 762 nm.

5.7.4 {PPN}[Fe(N<sub>3</sub>)<sub>2</sub>(NO)<sub>2</sub>] ((PPN)5d)

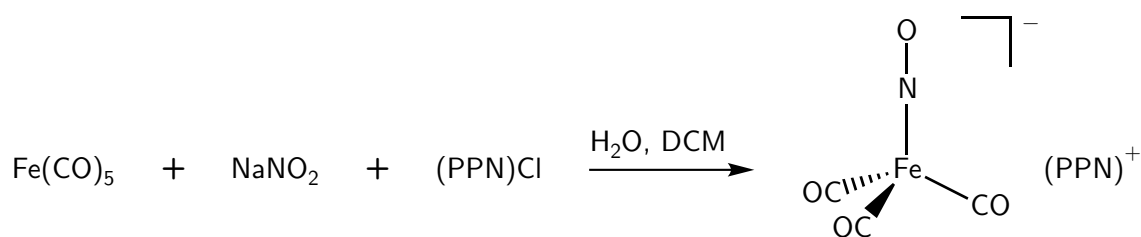
**Starting material:** Iron(II)triflate · 3 CH<sub>3</sub>CN, bis(triphenylphosphane)iminium azide, nitric oxide, methanol.

**Procedure:** Iron(II)triflate · 3 CH<sub>3</sub>CN (131 mg, 0.3 mmol) and (PPN)N<sub>3</sub> (523 mg, 0.9 mmol) were dissolved in 5 mL of methanol. Nitric oxide was bubbled through the solution for 5 min. After two weeks, a red powder of (PPN)5d formed which was filtrated and dried under reduced pressure.

**Yield:** 66 mg (0.09 mmol, 30 %).

**Empirical formula:** C<sub>36</sub>H<sub>30</sub>FeN<sub>9</sub>O<sub>2</sub>P<sub>2</sub>, 738.5 g mol<sup>-1</sup>.

**IR** (solid, ATR):  $\tilde{\nu} = 2953$  (w), 2921 (m), 2851 (w), 2360 (w), 2342 (w), 2061 (w), 2035 (w), 1757 (w), 1698 (w), 1588 (w), 1438 (m), 1377 (w), 1261 (vs), 1226 (s), 1183 (m), 1149 (m), 1112 (s), 1031 (s), 997 (m), 798 (w), 763 (m), 744 (m), 721 (vs), 689 (vs) cm<sup>-1</sup>.

5.7.5 {PPN}[Fe(CO)<sub>3</sub>(NO)]

**Literature:** M. Holzwarth, A. Dieskau, M. Tabassam, B. Plietker, *Angew. Chem. Int. Ed.* **2009**, *48*, 7251–7255.

**Starting material:** Bis(triphenylphosphane)iminium chloride, sodium nitrite, iron pentacarbonyl, DCM, water, acetone, petroleum ether.

**Procedure:** Sodium nitrite (1.0 g, 15.0 mmol) was dissolved in 5 mL of degassed water and added to (PPN)Cl (8.61 g, 15 mmol) in 40 mL of DCM. Iron pentacarbonyl (2.03 mL, 15.0 mmol) was added and the mixture was stirred vigorously for 1 h. The organic phase was separated, washed two times with 10 mL of water, dried over magnesium sulfate and the solvent was removed under reduced pressure. A brown solid was obtained, which was dissolved in 10 mL of acetone, precipitated with an excess of petroleum ether and filtrated. Bis(triphenylphosphane)iminium tricarbonylnitrosylferrate was obtained as a yellow powder.

**Yield:** 7.33 g (10.3 mmol, 69 %).

**Empirical formula:** C<sub>39</sub>H<sub>30</sub>FeN<sub>2</sub>O<sub>4</sub>P<sub>2</sub>, 708.5 g mol<sup>-1</sup>.

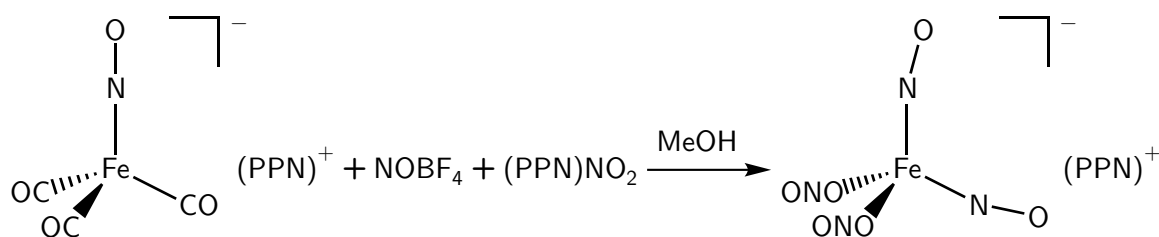
**Elemental analysis:** Calcd. (%): N 3.95, C 66.12, H 4.27.

Found (%): N 4.09, C 65.73, H 4.22.

**MS (FAB-):** *m/z* (%) = 170.0 (100) [Fe(CO)<sub>3</sub>(NO)]<sup>-</sup>.

**MS (FAB+):** *m/z* (%) = 538.3 (100) [C<sub>36</sub>H<sub>30</sub>NP<sub>2</sub>]<sup>+</sup>.

**IR (solid, ATR):**  $\tilde{\nu}$  = 1977 (m), 1864 (vs), 1763 (w), 1698 (w), 1646 (vs), 1587 (w), 1483 (w), 1436 (s), 1262 (s), 1184 (m), 1111 (vs), 997 (m), 793 (w), 721 (vs), 688 (vs) cm<sup>-1</sup>.

5.7.6 {PPN}[Fe(NO)<sub>2</sub>(ONO)<sub>2</sub>]

**Literature:** M.-C. Tsai *et al.*, *Inorg. Chem.* **2009**, *48*, 9579–9591.

**Starting material:** Bis(triphenylphosphane)iminium tricarbonylnitrosylferrate, nitrosonium tetrafluoroborate, bis(triphenylphosphane)iminium nitrite, THF, *n*-pentane, diethyl ether.

**Procedure:** Bis(triphenylphosphane)iminium tricarbonylnitrosylferrate (354 mg, 0.5 mmol) and nitrosonium tetrafluoroborate (117 mg, 1.0 mmol) were dissolved in 5 mL of THF at 0 °C and stirred for 5 min. Bis(triphenylphosphane)iminium nitrite was added and the mixture was stirred for 30 min at room temperature. The mixture was filtrated over celite, and *n*-pentane was added to the filtrate to precipitate bis(triphenylphosphane)iminium dinitritodinitrosylferrate as a brown solid.

**Yield:** 90 mg (0.12 mmol, 24 %).

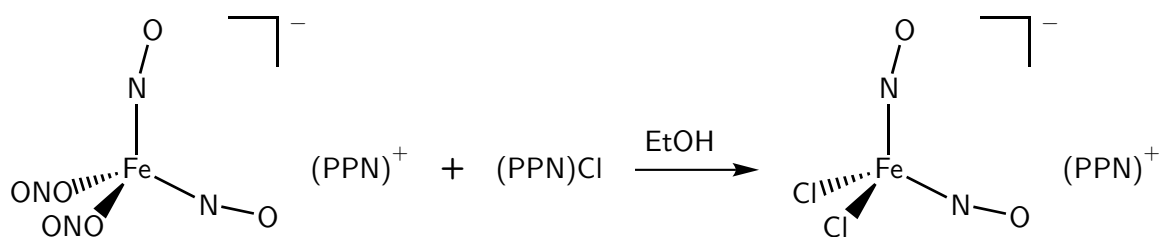
**Empirical formula:** C<sub>36</sub>H<sub>30</sub>FeN<sub>5</sub>O<sub>6</sub>P<sub>2</sub>, 746.5 g mol<sup>−1</sup>.

**Elemental analysis:** Calcd. (%): N 9.38, C 57.93, H 4.05.  
Found (%): N 7.00, C 58.38, H 4.21.

**MS (FAB−):** *m/z* (%) = 207.9 (100) [Fe(ONO)<sub>2</sub>(NO)<sub>2</sub>]<sup>−</sup>.

**MS (FAB+):** *m/z* (%) = 538.2 (100) [C<sub>36</sub>H<sub>30</sub>NP<sub>2</sub>]<sup>+</sup>.

**IR (solid, ATR):**  $\tilde{\nu}$  = 1873 (w), 1778 (m), 1703 (vs), 1653 (w), 1482 (w), 1437 (s), 1248 (vs), 1182 (m), 1111 (vs), 1062 (s), 996 (s), 800 (m) cm<sup>−1</sup>.

5.7.7 {PPN}[FeCl<sub>2</sub>(NO)<sub>2</sub>] ((PPN)5e)

**Starting material:** Bis(triphenylphosphane)iminium dinitritodinitrosylferrate, bis(triphenylphosphane)iminium chloride, ethanol, petroleum ether.

**Procedure:** Bis(triphenylphosphane)iminium dinitritodinitrosylferrate (142 mg, 0.2 mmol) and bis(triphenylphosphane)iminium chloride (230 mg, 0.4 mmol) were suspended in 15 mL of ethanol, stirred for 30 min at 75 °C and filtrated. The diffusion of petroleum ether into the filtrate at 4 °C gave brown crystals of (PPN)5e after 5 days.

**Yield:** 55 mg (0.08 mmol, 38 %).

**Empirical formula:** C<sub>36</sub>H<sub>30</sub>Cl<sub>2</sub>FeN<sub>3</sub>O<sub>2</sub>P<sub>2</sub>, 725.4 g mol<sup>-1</sup>.

**MS (FAB-):**  $m/z$  (%) = 186.1 (40) [FeCl<sub>2</sub>(NO)<sub>2</sub>]<sup>-</sup>.

**MS (FAB+):**  $m/z$  (%) = 538.5 (100) [C<sub>36</sub>H<sub>30</sub>NP<sub>2</sub>]<sup>+</sup>.

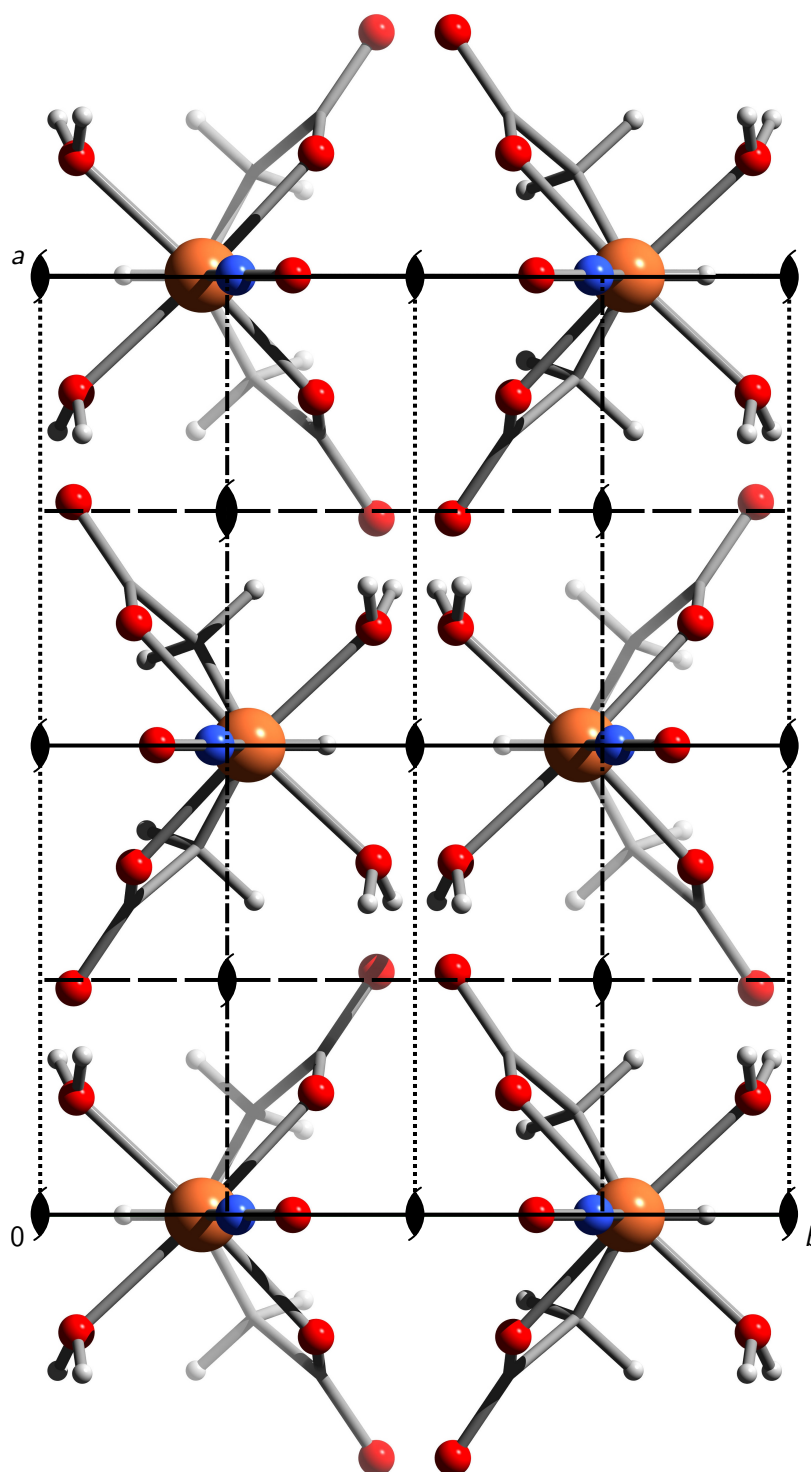
**IR (solid, ATR):**  $\tilde{\nu}$  = 1773 (m), 1697 (s), 1587 (w), 1481 (w), 1437 (s), 1282 (m), 1247 (s), 1181 (m), 1111 (vs), 1050 (m), 997 (s), 799 (w), 742 (m), 721 (vs), 689 (vs) cm<sup>-1</sup>.

## 5.8 Computational methods

All quantum-chemical calculations at the DFT level were done with the program system *Turbomole*<sup>[207,208]</sup>. Initial geometries were taken either from crystal-structure analyses or set up using *TmoleX*.<sup>[209,210]</sup> Wave functions were calculated at the multipole-accelerated RI-DFT level<sup>[211,212]</sup> using *def2-TZVP* basis sets<sup>[118,213,214]</sup> and the functionals BP-86,<sup>[116,117]</sup> B97-D<sup>[127]</sup> and TPSSH.<sup>[122,123,126]</sup> Dispersion correction was applied, using *Grimme's* DFT-D3<sup>[128]</sup> with BJ-damping<sup>[129]</sup>. COSMO<sup>[119]</sup> was used to take into account the negative charge of the nitrosyl ferrates and D-COSMO-RS<sup>[120,121]</sup> was used to simulate hydrogen-bond networks. Frequency analyses were done numerically, excited states were calculated using the TD-DFT formalism.<sup>[215,216]</sup> CASSCF calculations were done with the *ORCA* program system.<sup>[217]</sup>

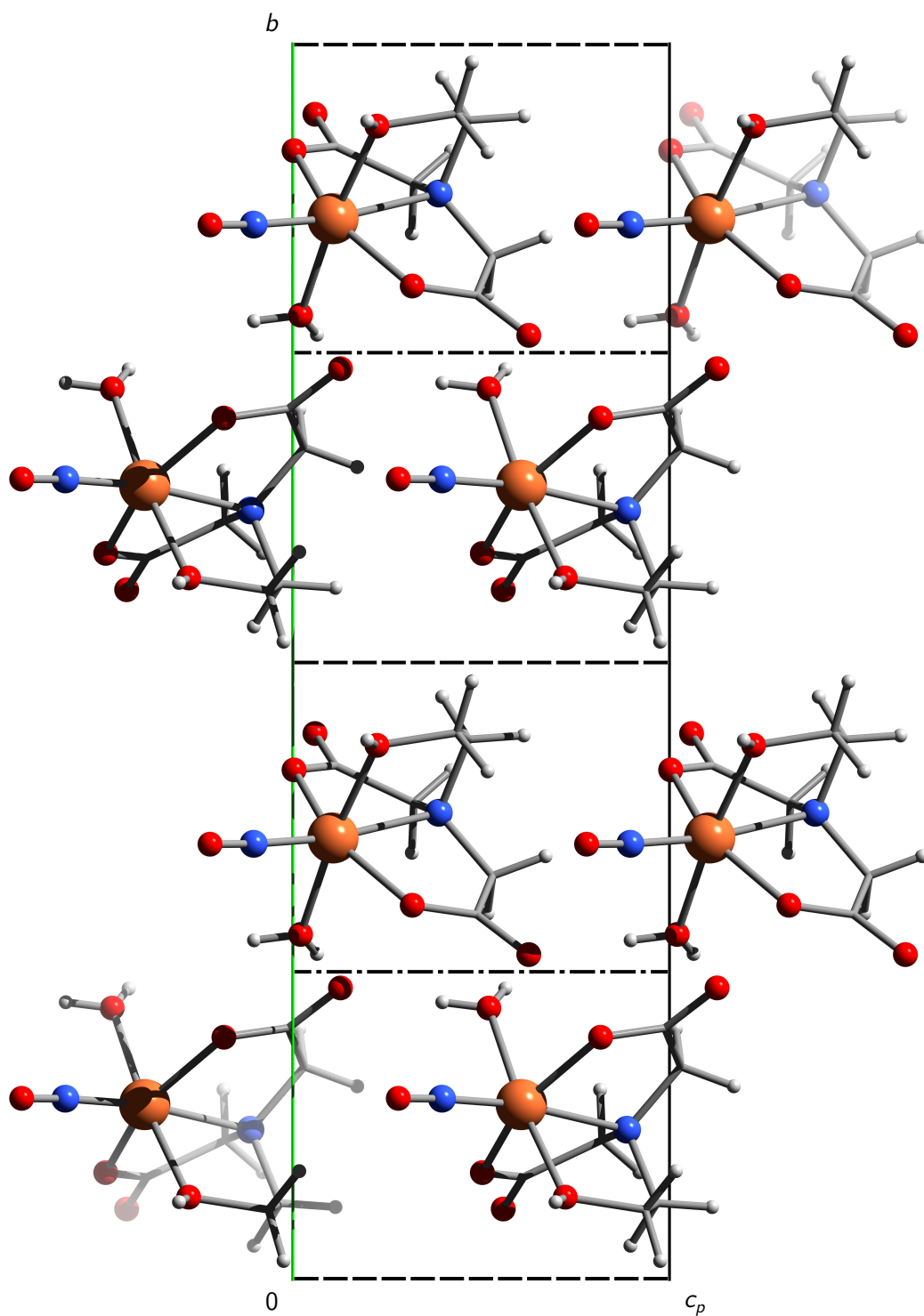
# 6 Appendix

## 6.1 Packing diagrams of the crystal structures



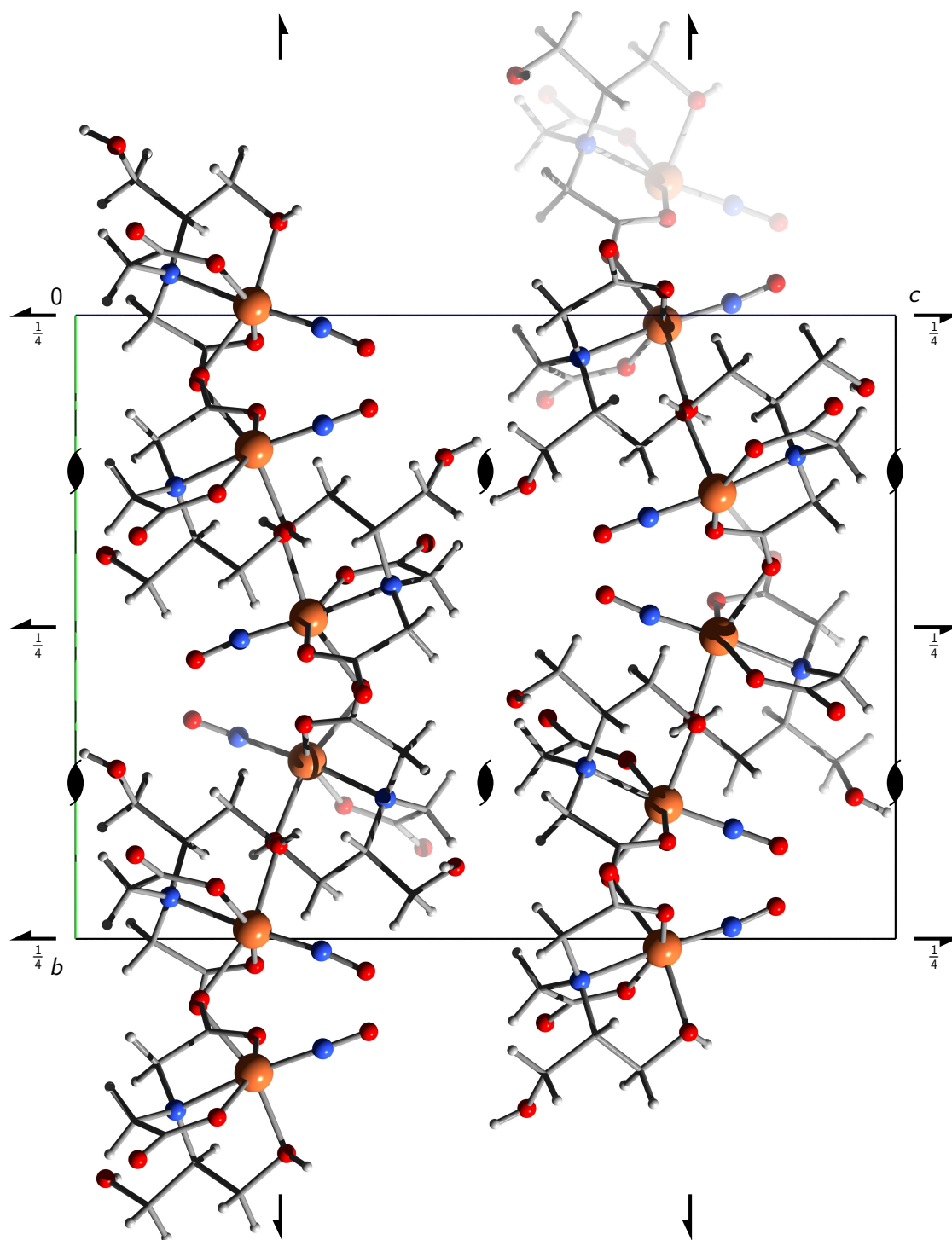
**Figure 6.1:**

Packing diagram of **3a** in the orthorhombic space group  $Cmc2_1$  with view along  $[001]$ . The symmetry elements of the space group  $Cmc2_1$  are overlaid. Atoms: carbon (grey, wireframe), hydrogen (white), iron (orange), nitrogen (blue), oxygen (red).



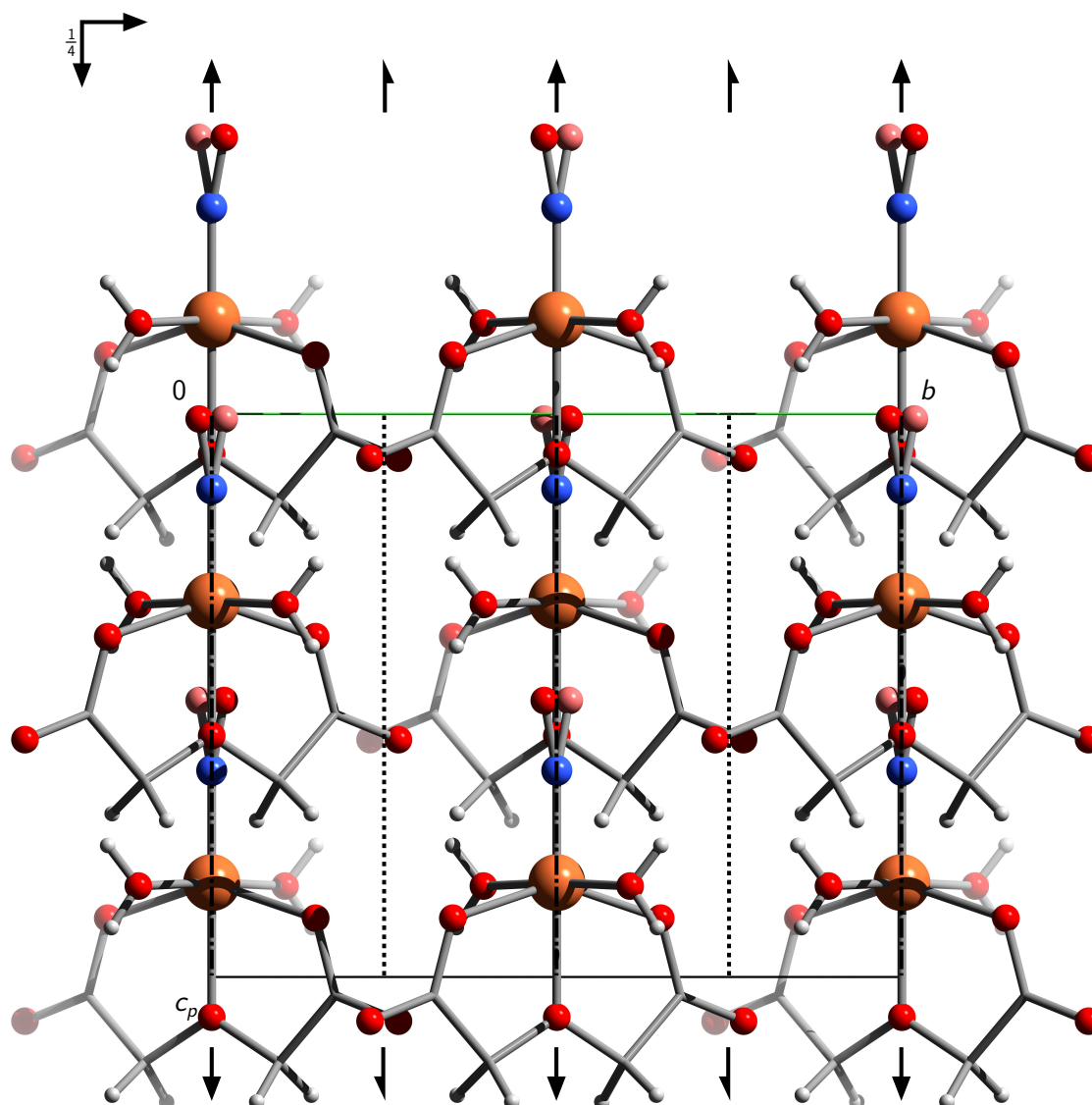
**Figure 6.2:**

Packing diagram of **3b** in the monoclinic space group  $Cc$  with view along  $[100]$ . The symmetry elements of the space group  $Cc$  are overlaid. Atoms: carbon (grey, wireframe), hydrogen (white), iron (orange), nitrogen (blue), oxygen (red).

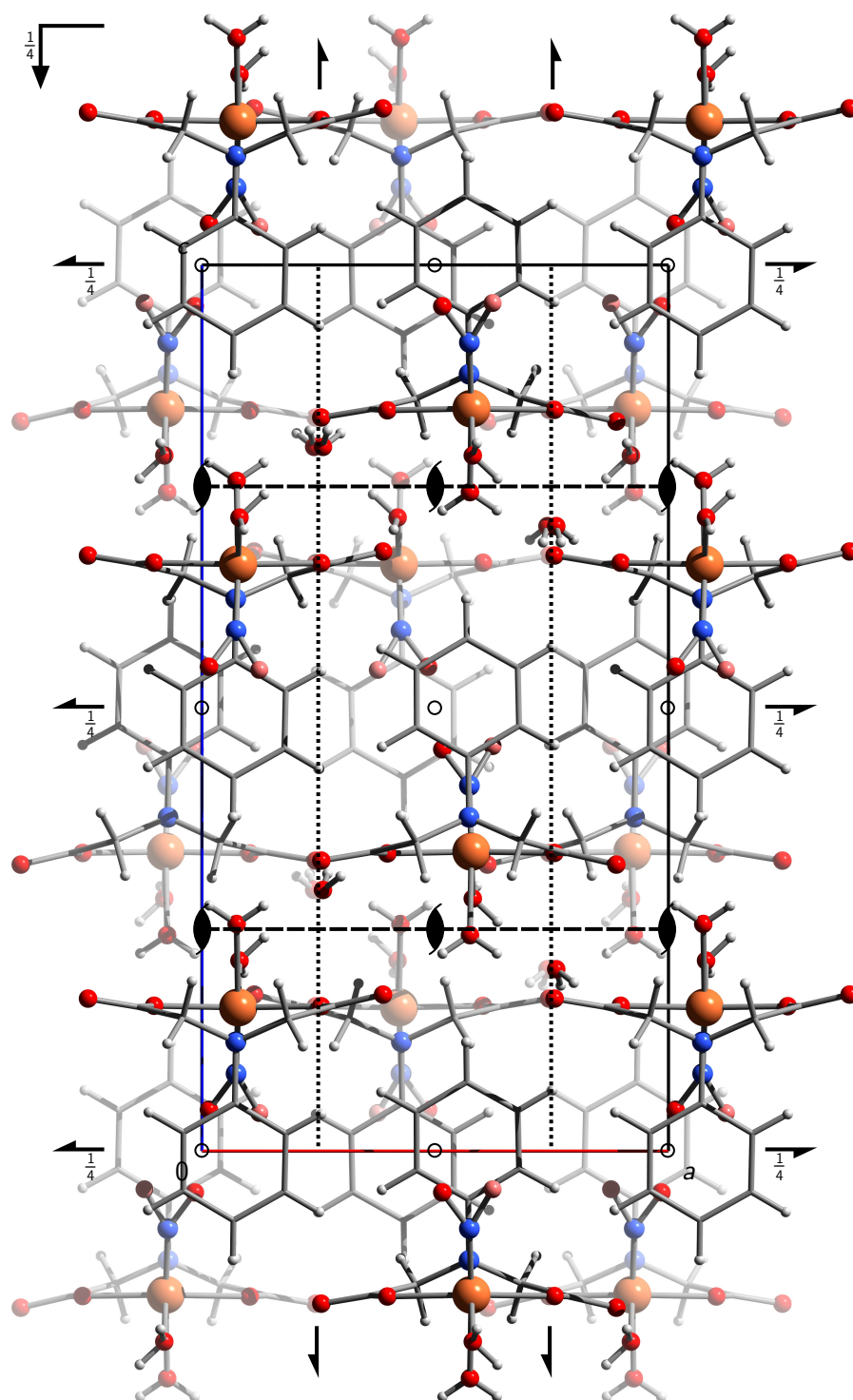


**Figure 6.3:**

Packing diagram of **3c** in the orthorhombic space group  $P2_12_12_1$  with view along  $[\bar{1}00]$ . The symmetry elements of the space group  $P2_12_12_1$  are overlaid. Atoms: carbon (grey, wireframe), hydrogen (white), iron (orange), nitrogen (blue), oxygen (red).

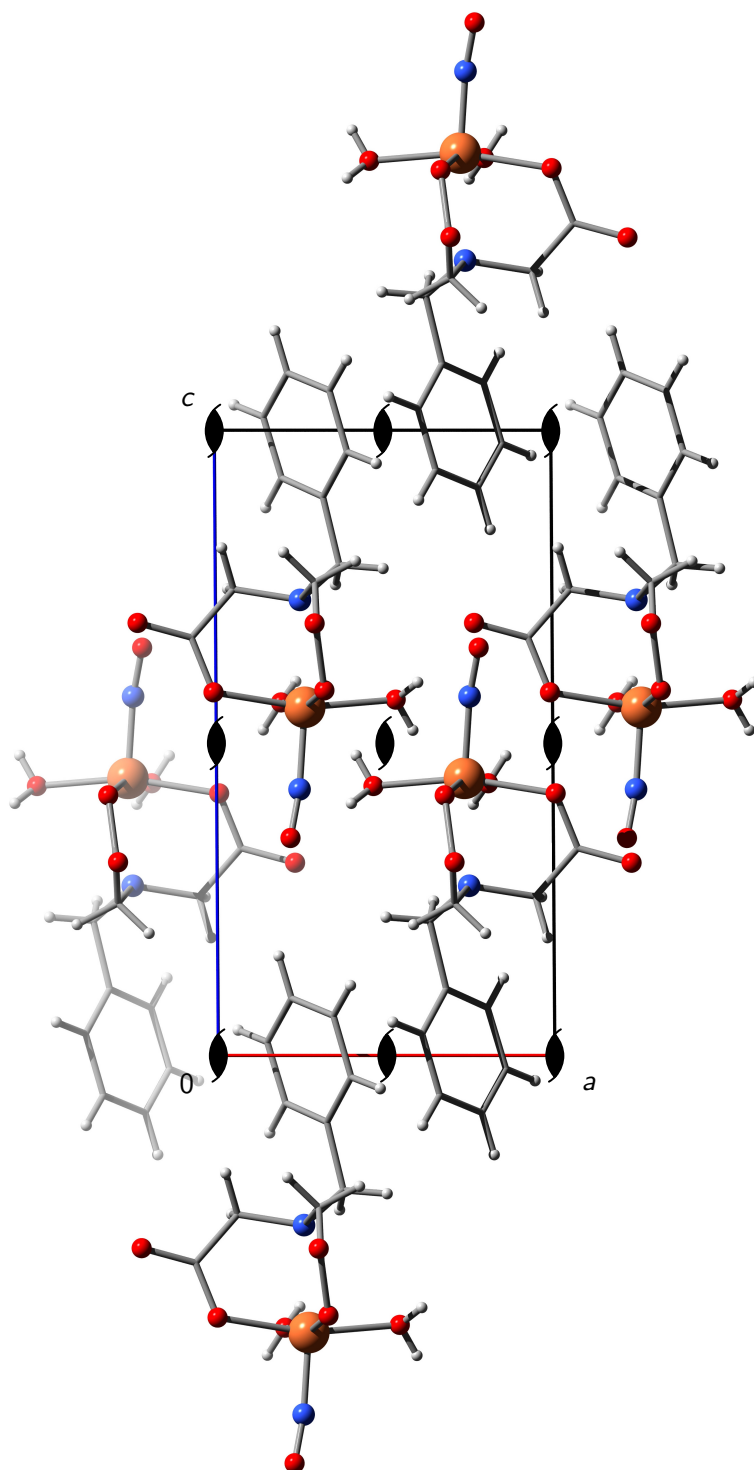


**Figure 6.4:** Packing diagram of **3d** in the orthorhombic space group *Aba2* with view along  $[100]$ . The symmetry elements of the space group *Aba2* are overlaid. Atoms: carbon (grey, wireframe), hydrogen (white), iron (orange), nitrogen (blue), oxygen (red).



**Figure 6.5:**

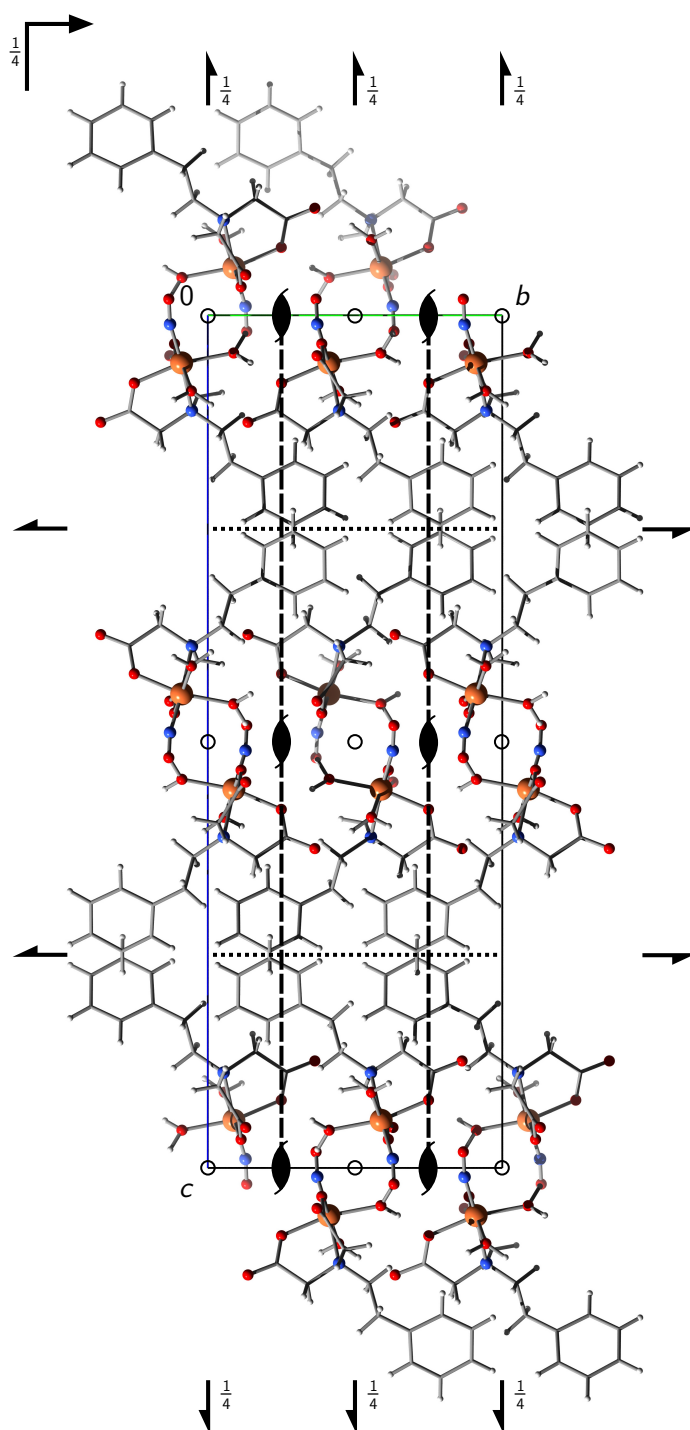
Packing diagram of **3e** in the orthorhombic space group  $Pbca$  with view along  $[010]$ . The symmetry elements of the space group  $Pbca$  are overlaid. Atoms: carbon (grey, wireframe), hydrogen (white), iron (orange), nitrogen (blue), oxygen (red).



**Figure 6.6:**

Packing diagram of **3f** in the monoclinic space group  $P2_1$  with view along  $[010]$ . The symmetry elements of the space group  $P2_1$  are overlaid. Atoms: carbon (grey, wireframe), hydrogen (white), iron (orange), nitrogen (blue), oxygen (red).



**Figure 6.8:**

Packing diagram of **3h** in the orthorhombic space group *Pbca* with view along [100]. The symmetry elements of the space group *Pbca* are overlaid. Atoms: carbon (grey, wireframe), hydrogen (white), iron (orange), nitrogen (blue), oxygen (red).

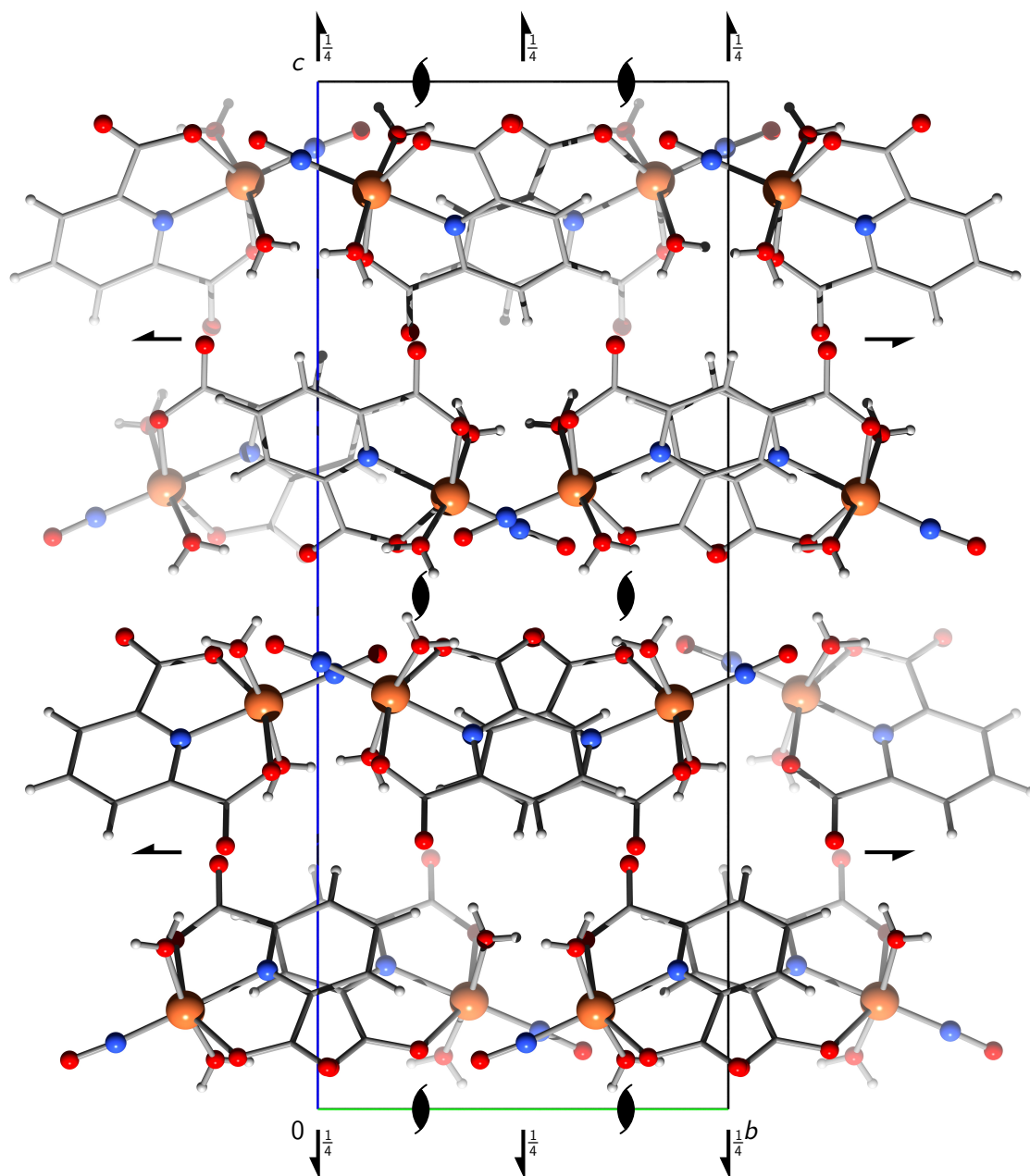


**Figure 6.9:**

Packing diagram of **3i** in the orthorhombic space group  $P2_12_12_1$  with view along  $[\bar{1}00]$ . The symmetry elements of the space group  $P2_12_12_1$  are overlaid. Atoms: carbon (grey, wireframe), hydrogen (white), iron (orange), nitrogen (blue), oxygen (red).

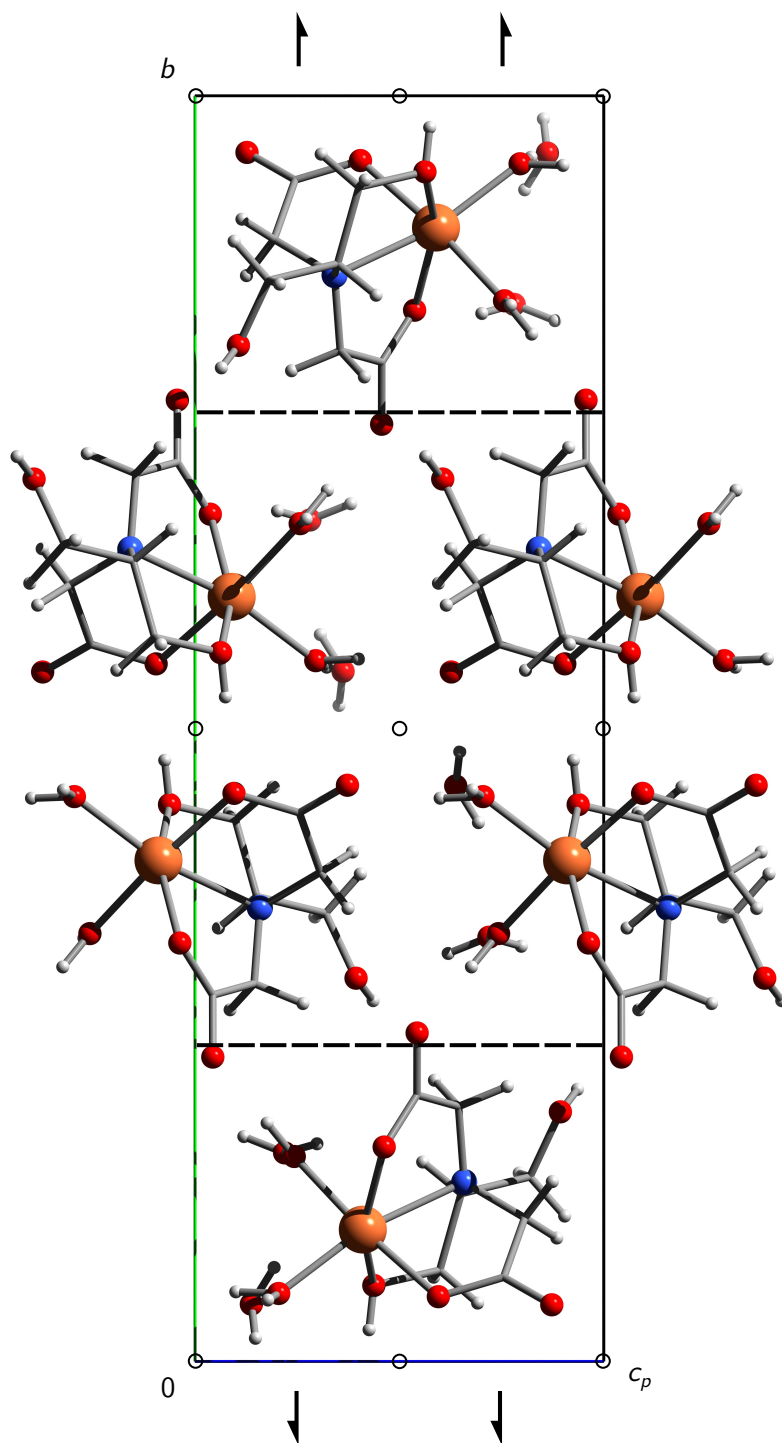


**Figure 6.10:**

Packing diagram of **4c** in the monoclinic space group  $P2_1/c$  with view along  $[100]$ . The symmetry elements of the space group  $P2_1/c$  are overlaid. Atoms: carbon (grey, wireframe), hydrogen (white), iron (orange), nitrogen (blue), oxygen (red).

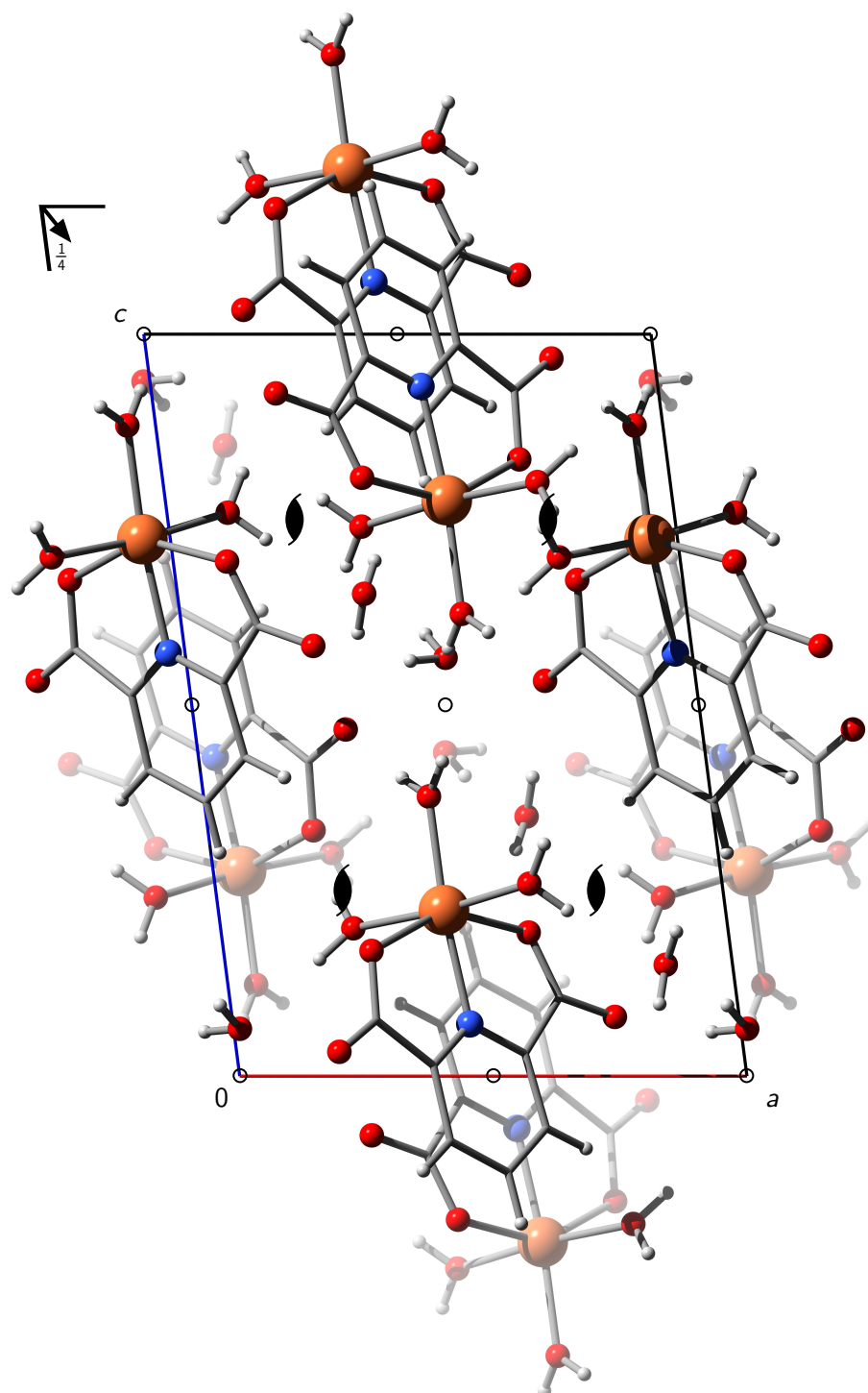


**Figure 6.11:**

Packing diagram of **4i** in the monoclinic space group  $P2_1/n$  with view along  $[0\bar{1}0]$ . The symmetry elements of the space group  $P2_1/n$  are overlaid. Atoms: carbon (grey, wireframe), hydrogen (white), iron (orange), nitrogen (blue), oxygen (red).

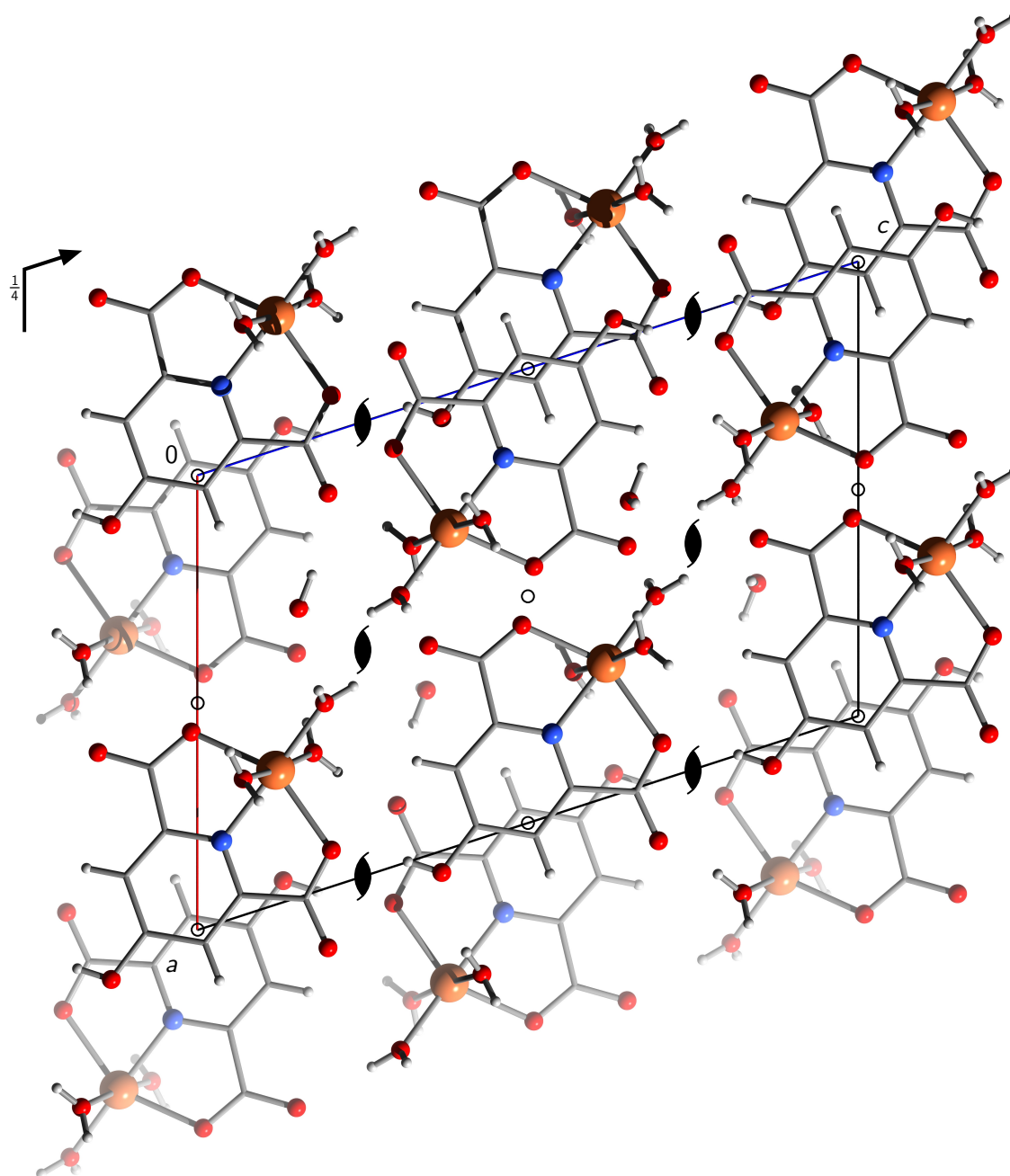


**Figure 6.12:**

Packing diagram of **4j** in the monoclinic space group  $P2_1/c$  with view along  $[010]$ . The symmetry elements of the space group  $P2_1/c$  are overlaid. Atoms: carbon (grey, wireframe), hydrogen (white), iron (orange), nitrogen (blue), oxygen (red).

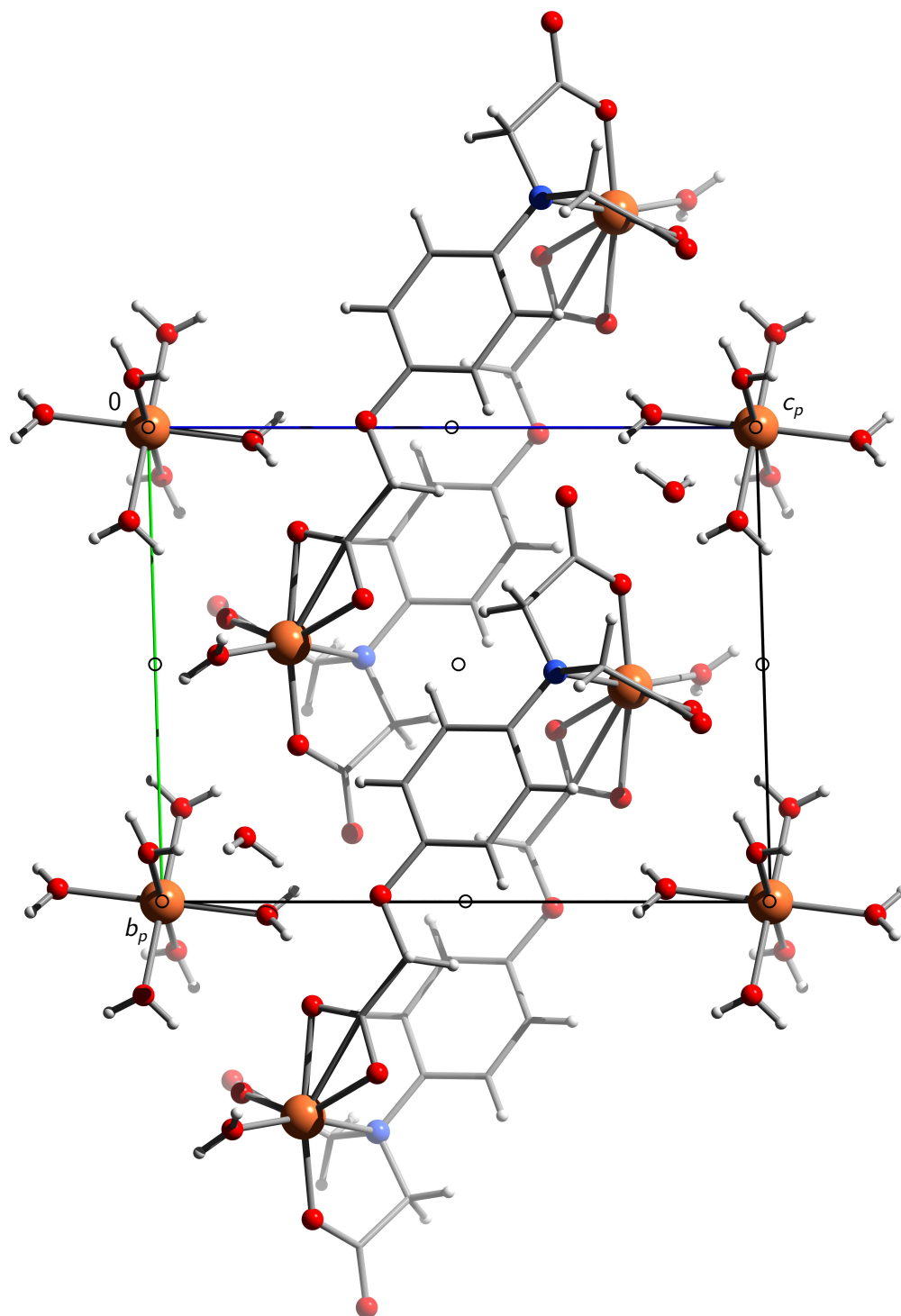


**Figure 6.13:**

Packing diagram of **4k** in the triclinic space group  $P\bar{1}$  with view along  $[\bar{1}00]$ . The symmetry elements of the space group  $P\bar{1}$  are overlaid. Atoms: carbon (grey, wireframe), hydrogen (white), iron (orange), nitrogen (blue), oxygen (red).

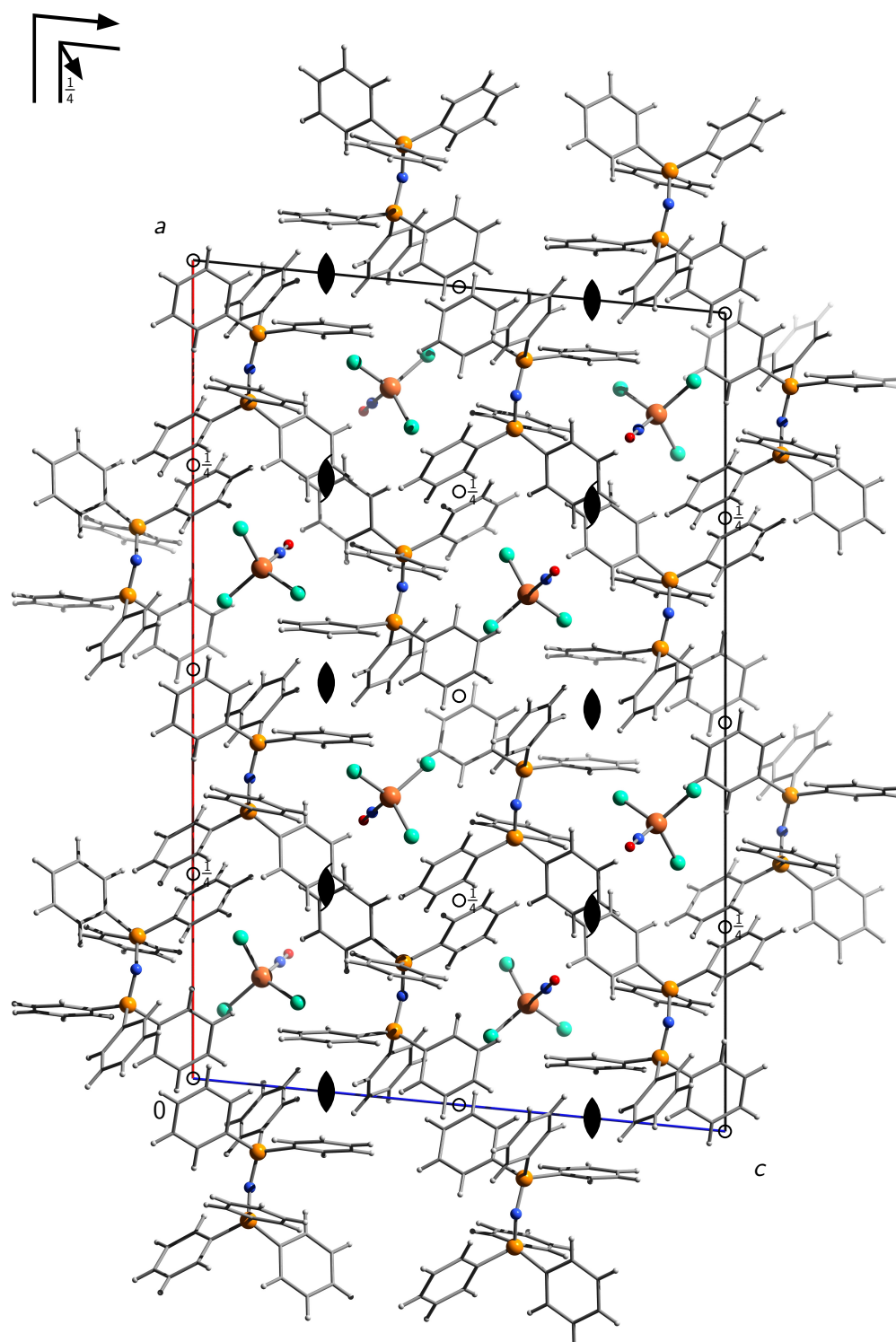


**Figure 6.14:**

Packing diagram of **5a** in the monoclinic space group  $C2/c$  with view along  $[0\bar{1}0]$ . The symmetry elements of the space group  $C2/c$  are overlaid. Atoms: carbon (grey, wireframe), hydrogen (white), chlorine (turquoise), iron (orange), nitrogen (blue), oxygen (red), phosphorus (yellow).

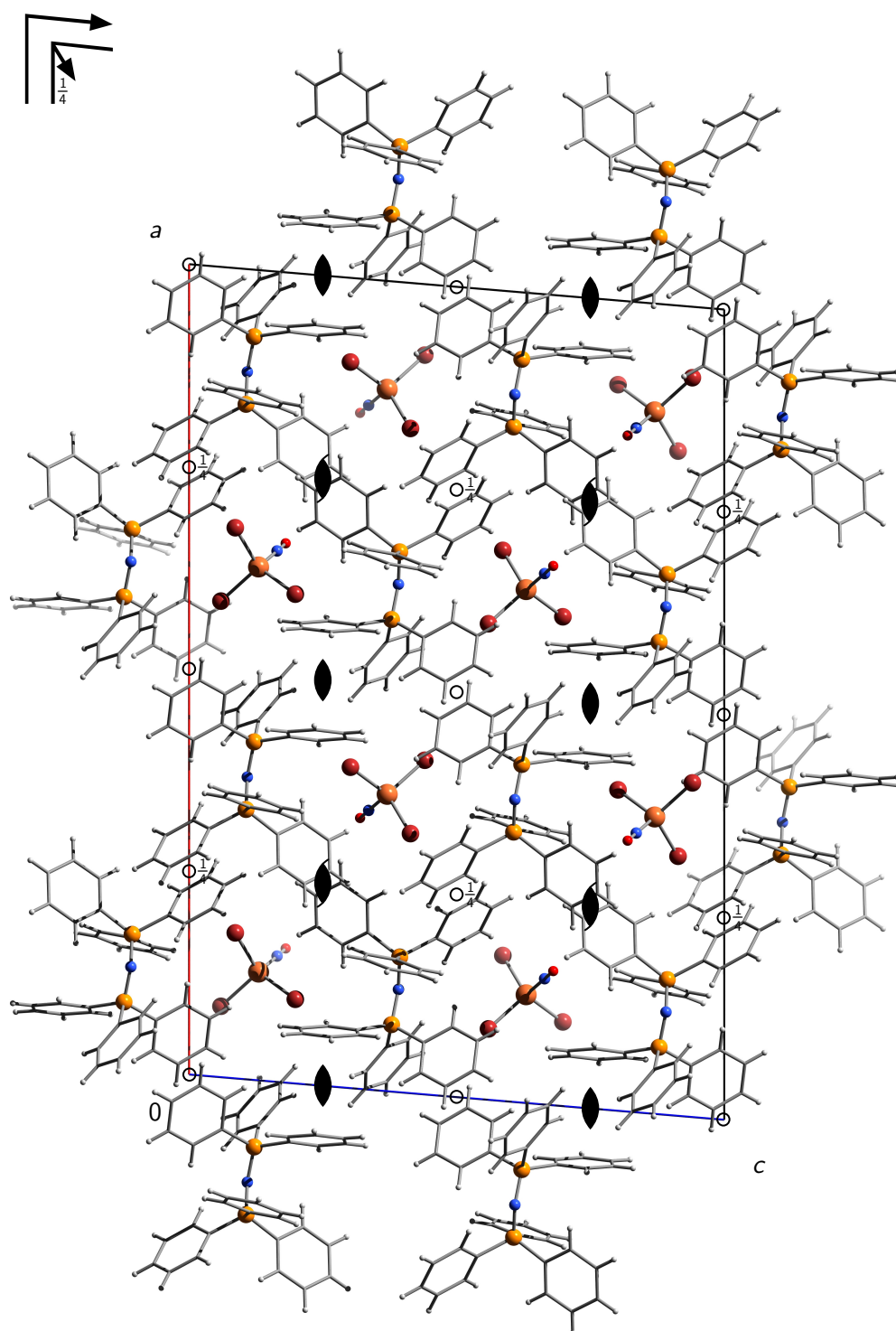


**Figure 6.15:**

Packing diagram of **5b** in the monoclinic space group  $C2/c$  with view along  $[0\bar{1}0]$ . The symmetry elements of the space group  $C2/c$  are overlaid. Atoms: carbon (grey, wireframe), hydrogen (white), bromine (brown), iron (orange), nitrogen (blue), oxygen (red), phosphorus (yellow).

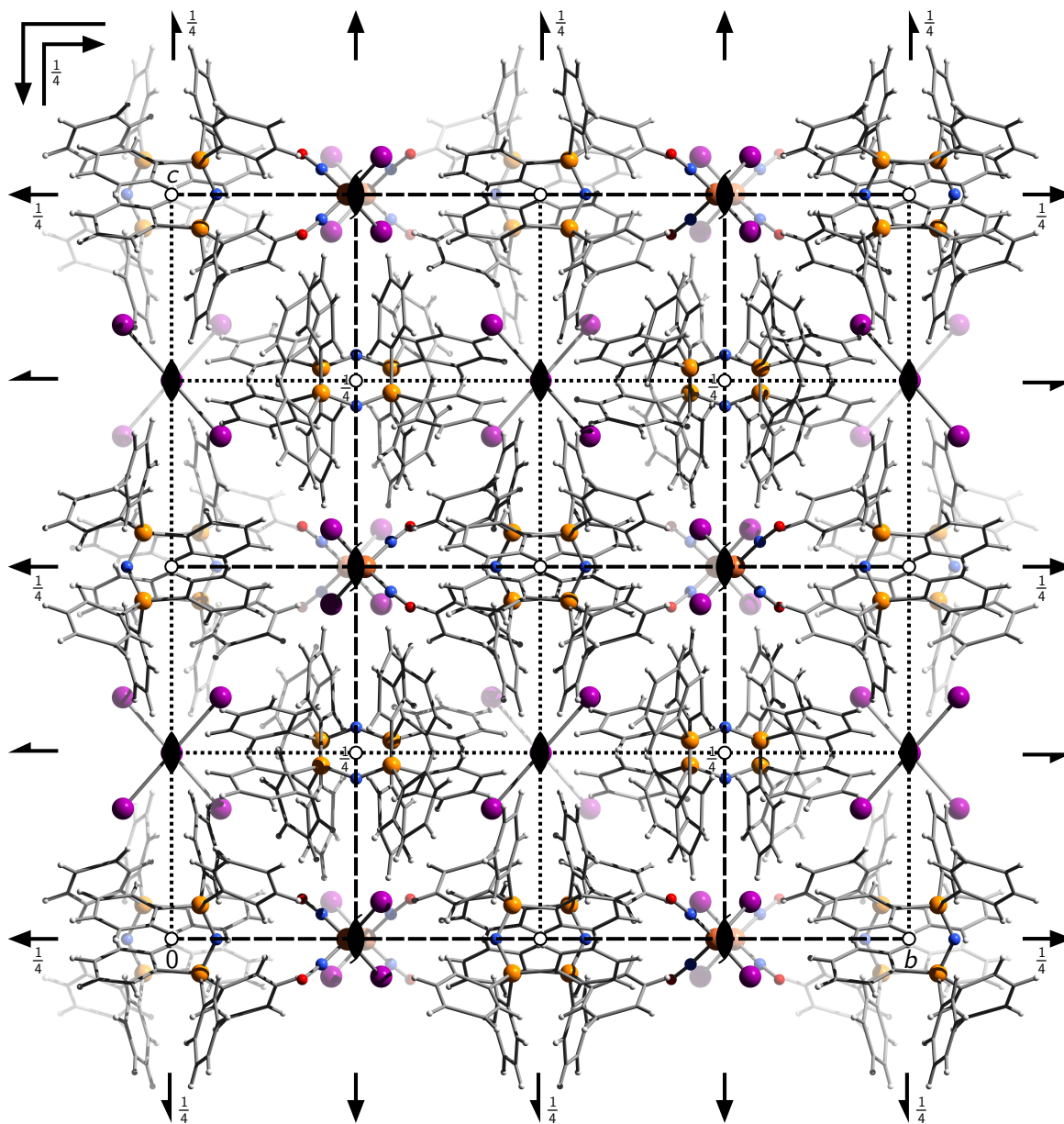


**Figure 6.16:**

Packing diagram of **5c** in the orthorhombic space group *Ibca* with view along  $[\bar{1}00]$ . The symmetry elements of the space group *Ibca* are overlaid. Atoms: carbon (grey, wireframe), hydrogen (white), iodine (purple), iron (orange), nitrogen (blue), oxygen (red), phosphorus (yellow).

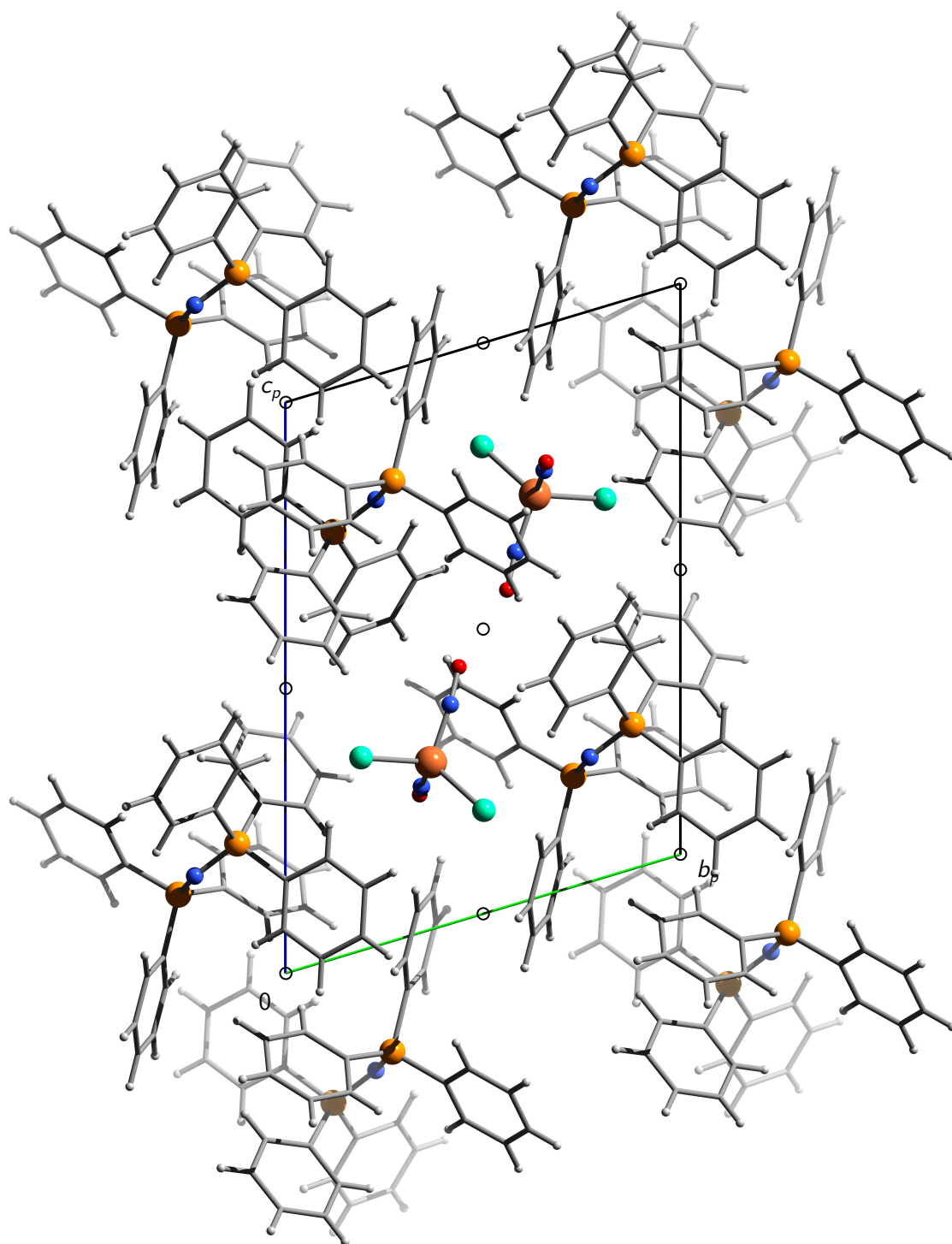


**Figure 6.17:**

Packing diagram of **5e** in the triclinic space group  $P\bar{1}$  with view along  $[\bar{1}00]$ . The symmetry elements of the space group  $P\bar{1}$  are overlaid. Atoms: carbon (grey, wireframe), hydrogen (white), chlorine (turquoise), iron (orange), nitrogen (blue), oxygen (red), phosphorus (yellow).

## 6.2 Crystallographic tables

**Table 6.1:** Crystallographic data of [Fe(ida)(NO)(OH<sub>2</sub>)<sub>2</sub>] (**3a**), [Fe(heida)(NO)(OH<sub>2</sub>)] (**3b**) and [Fe(dhpida)(NO)] (**3c**).

	<b>3a</b>	<b>3b</b>	<b>3c</b>
empirical formula	C <sub>4</sub> H <sub>9</sub> FeN <sub>2</sub> O <sub>7</sub>	C <sub>6</sub> H <sub>11</sub> FeN <sub>2</sub> O <sub>7</sub>	C <sub>14</sub> H <sub>22</sub> Fe <sub>2</sub> N <sub>4</sub> O <sub>14</sub>
$M_r$ /g mol <sup>-1</sup>	252.98	279.02	582.05
color	black	green	green
habitus	rod	platelet	rod
crystal system	orthorhombic	monoclinic	orthorhombic
space group	<i>Cmc</i> 2 <sub>1</sub>	<i>Cc</i>	<i>P</i> 2 <sub>1</sub> 2 <sub>1</sub> 2 <sub>1</sub>
$a/\text{Å}$	11.2905(7)	7.0472(2)	7.8786(10)
$b/\text{Å}$	9.0840(5)	21.7450(8)	14.3701(19)
$c/\text{Å}$	8.6720(4)	6.7771(3)	18.945(2)
$\alpha/^\circ$	90	90	90
$\beta/^\circ$	90	103.451(2)	90
$\gamma/^\circ$	90	90	90
$V/\text{Å}^3$	889.43(8)	1010.04(7)	2144.9(5)
$Z$	4	4	4
$\rho_{\text{calc}}/\text{g cm}^{-3}$	1.889	1.835	1.802
$\mu/\text{mm}^{-1}$	1.713	1.518	1.434
crystal size/mm	0.13 × 0.04 × 0.03	0.19 × 0.10 × 0.02	0.10 × 0.02 × 0.01
$T/\text{K}$	173(2)	173(2)	100(2)
diffractometer	KappaCCD	KappaCCD	Bruker D8 Venture
radiation	MoK $\alpha$	MoK $\alpha$	MoK $\alpha$
anode	rotating anode	rotating anode	rotating anode
rated input/kW	3.025	3.025	2.5
$\theta$ -range/ $^\circ$	3.609–27.475	3.615–27.806	2.800–25.07
reflexes for metric	1795	2207	1767
absorption correction	—	—	multi-scan
transmission factors	—	—	0.6372–0.7452
reflexes measured	3373	3829	24174
independent reflexes	1069	2109	3774
$R_{\text{int}}$	0.0316	0.0690	0.1559
mean $\sigma(I)/I$	0.0294	0.1191	0.1053
reflexes with $I \geq 2\sigma(I)$	1012	1959	2645
$x, y$ (weighting scheme)	0.0269, 0.5542	0.0224, 0.5526	0.0620, 2.6011
hydrogen refinement	<sup>a</sup>	<sup>a</sup>	<sup>a</sup>
Flack parameter	−0.017(12)	0.013(19)	0.49(5) <sup>b</sup>
parameters	77	154	172
restraints	4	5	0
$R(F_{\text{obs}})$	0.0247	0.0356	0.0608
$R_w(F^2)$	0.0590	0.0560	0.1358
$S$	1.102	1.084	1.021
shift/error <sub>max</sub>	0.001	0.001	0.001
max. electron density/e $\text{Å}^{-3}$	0.301	0.221	1.585
min. electron density/e $\text{Å}^{-3}$	−0.298	−0.268	−0.639
measurement code	pn395	pn307	tv103

<sup>a</sup> Coordinates of hydrogen atoms bonded to aqua ligands were refined freely, all other hydrogen atoms were calculated in idealized positions, riding on their parent atoms.  $U_{\text{iso}}$  was always coupled to the parent atom. <sup>b</sup> Inversion twin.

**Table 6.2:** Crystallographic data of [Fe(NO)(OH<sub>2</sub>)<sub>2</sub>(oda)] (**3d**), [Fe(NO)(OH<sub>2</sub>)(phida)] · H<sub>2</sub>O (**3e**) and [Fe(bnida)(NO)(OH<sub>2</sub>)] (**3f**).

	<b>3d</b>	<b>3e</b>	<b>3f</b>
empirical formula	C <sub>4</sub> H <sub>8</sub> FeNO <sub>8</sub>	C <sub>10</sub> H <sub>15</sub> FeN <sub>2</sub> O <sub>8</sub>	C <sub>11</sub> H <sub>15</sub> FeN <sub>2</sub> O <sub>7</sub>
$M_r$ /g mol <sup>-1</sup>	253.96	347.09	343.10
color	black	brown	green
habitus	block	block	platelet
crystal system	orthorhombic	orthorhombic	monoclinic
space group	<i>Aba2</i>	<i>Pbca</i>	<i>P2</i> <sub>1</sub>
$a/\text{Å}$	8.8713(8)	10.9870(4)	7.2791(3)
$b/\text{Å}$	10.8750(7)	12.7756(5)	7.5111(4)
$c/\text{Å}$	8.8860(6)	20.9357(8)	13.4960(7)
$\alpha/^\circ$	90	90	90
$\beta/^\circ$	90	90	90.376(3)
$\gamma/^\circ$	90	90	90
$V/\text{Å}^3$	857.28(11)	2938.63(19)	737.87(6)
$Z$	4	8	2
$\rho_{\text{calc}}/\text{g cm}^{-3}$	1.968	1.569	1.544
$\mu/\text{mm}^{-1}$	1.783	1.065	1.055
crystal size/mm	0.13 × 0.11 × 0.09	0.32 × 0.26 × 0.18	0.14 × 0.07 × 0.02
$T/\text{K}$	100(2)	103(2)	173(2)
diffractometer	Bruker D8 Venture	Oxford XCalibur	KappaCCD
radiation	MoK $\alpha$	MoK $\alpha$	MoK $\alpha$
anode	rotating anode	fine-focus sealed tube	rotating anode
rated input/kW	2.5	2.00	3.025
$\theta$ -range/ $^\circ$	3.747–28.31	4.181–27.421	3.898–24.075
reflexes for metric	119	2851	2172
absorption correction	multi-scan	multi-scan	—
transmission factors	0.6959–0.7457	0.9682–1.0000	—
reflexes measured	15676	8670	4140
independent reflexes	1079	3356	2149
$R_{\text{int}}$	0.0311	0.0268	0.0213
mean $\sigma(I)/I$	0.0155	0.0316	0.0319
reflexes with $I \geq 2\sigma(I)$	1069	2710	2088
$x, y$ (weighting scheme)	0.0183, 0.3161	0.0393, 0.5100	0.0199, 0.1932
hydrogen refinement	<sup>a</sup>	<sup>a</sup>	<sup>a</sup>
Flack parameter	0.01(2)	—	0.007(10)
parameters	78	219	203
restraints	4	9	7
$R(F_{\text{obs}})$	0.0137	0.0308	0.0209
$R_w(F^2)$	0.0386	0.0842	0.0533
$S$	1.177	1.062	1.111
shift/error <sub>max</sub>	0.001	0.001	0.001
max. electron density/e $\text{Å}^{-3}$	0.286	0.443	0.202
min. electron density/e $\text{Å}^{-3}$	-0.158	-0.310	-0.225
measurement code	rv102	qo098	qn035

<sup>a</sup> Coordinates of hydrogen atoms bonded to aqua ligands were refined freely, all other hydrogen atoms were calculated in idealized positions, riding on their parent atoms.  $U_{\text{iso}}$  was always coupled to the parent atom.

**Table 6.3:** Crystallographic data of [Fe(bnbrid)(NO)(OH<sub>2</sub>)<sub>2</sub>] (**3g**), [Fe(NO)(OH<sub>2</sub>)(pheida)] (**3h**) and [Fe(dipic)(NO)(OH<sub>2</sub>)] (**3i**).

	<b>3g</b>	<b>3h</b>	<b>3i</b>
empirical formula	C <sub>11</sub> H <sub>14</sub> BrFeN <sub>2</sub> O <sub>7</sub>	C <sub>12</sub> H <sub>17</sub> FeN <sub>2</sub> O <sub>7</sub>	C <sub>7</sub> H <sub>7</sub> FeN <sub>2</sub> O <sub>7</sub>
$M_r$ /g mol <sup>-1</sup>	422.00	357.12	287.00
color	brown	brown	dark green
habitus	Platelet	rod	platelet
crystal system	monoclinic	orthorhombic	orthorhombic
space group	<i>P2</i> <sub>1</sub>	<i>Pbca</i>	<i>P2</i> <sub>1</sub> <i>2</i> <sub>1</sub> <i>2</i> <sub>1</sub>
$a/\text{Å}$	7.1492(5)	7.811(3)	8.7779(3)
$b/\text{Å}$	7.4128(5)	11.533(5)	9.4177(3)
$c/\text{Å}$	14.9927(9)	33.326(14)	23.6244(9)
$\alpha/^\circ$	90	90	90
$\beta/^\circ$	95.911(2)	90	90
$\gamma/^\circ$	90	90	90
$V/\text{Å}^3$	790.32(9)	3002(2)	1952.97(12)
$Z$	2	8	8
$\rho_{\text{calc}}/\text{g cm}^{-3}$	1.773	1.580	1.952
$\mu/\text{mm}^{-1}$	3.516	1.041	1.574
crystal size/mm	0.10 × 0.05 × 0.01	0.17 × 0.03 × 0.02	0.20 × 0.10 × 0.01
$T/\text{K}$	173(2)	173(2)	100(2)
diffractometer	Bruker D8 Venture	Bruker D8 Venture	Bruker D8 Venture
radiation	MoK $\alpha$	MoK $\alpha$	MoK $\alpha$
anode	rotating anode	rotating anode	rotating anode
rated input/kW	2.5	2.5	2.5
$\theta$ -range/ $^\circ$	2.864–27.08	3.209–21.96	3.173–27.17
reflexes for metric	7868	125	9923
absorption correction	multi-scan	multi-scan	multi-scan
transmission factors	0.6611–0.7455	0.7282–0.8618	0.7075–0.7455
reflexes measured	5519	5969	70533
independent reflexes	1945	1732	4338
$R_{\text{int}}$	0.0610	0.0874	0.0450
mean $\sigma(I)/I$	0.0330	0.1152	0.0183
reflexes with $I \geq 2\sigma(I)$	1817	1104	4014
$x, y$ (weighting scheme)	0.0188, 0.7525	0.0655, 96.6731	0.0255, 0.7280
hydrogen refinement	<sup>a</sup>	<sup>a</sup>	<sup>a</sup>
Flack parameter	0.074(14)	–	0.443(13) <sup>b</sup>
parameters	214	187	333
restraints	7	6	12
$R(F_{\text{obs}})$	0.0301	0.1127	0.0207
$R_w(F^2)$	0.0581	0.2745	0.0489
$S$	1.064	1.175	1.069
shift/error <sub>max</sub>	0.001	0.001	0.001
max. electron density/e $\text{Å}^{-3}$	0.389	1.874	0.357
min. electron density/e $\text{Å}^{-3}$	–0.354	–0.916	–0.209
measurement code	sv088	rv451	sv152

<sup>a</sup> Coordinates of hydrogen atoms bonded to aqua ligands were refined freely, all other hydrogen atoms were calculated in idealized positions, riding on their parent atoms.  $U_{\text{iso}}$  was always coupled to the parent atom. <sup>b</sup> Inversion twin.

**Table 6.4:** Crystallographic data of  $[\text{Fe}(\text{dhpida})(\text{OH}_2)_2] \cdot 2 \text{H}_2\text{O}$  (**4c**),  $[\text{Fe}(\text{dipic})(\text{OH}_2)_3] \cdot 2 \text{H}_2\text{O}$  (**4i**) and  $[\text{Fe}(\text{ca})(\text{OH}_2)_3] \cdot 0.5 \text{H}_2\text{O}$  (**4j**).

	<b>4c</b>	<b>4i</b>	<b>4j</b>
empirical formula	$\text{C}_7\text{H}_{19}\text{FeNO}_{10}$	$\text{C}_7\text{H}_{13}\text{FeNO}_9$	$\text{C}_{14}\text{H}_{20}\text{Fe}_2\text{N}_2\text{O}_{17}$
$M_r/\text{g mol}^{-1}$	333.08	311.03	600.02
color	green	red	light brown
habitus	block	block	block
crystal system	monoclinic	monoclinic	monoclinic
space group	$P2_1/c$	$P2_1/n$	$P2_1/c$
$a/\text{\AA}$	7.0539(3)	8.9944(3)	10.4396(4)
$b/\text{\AA}$	23.7513(10)	9.9117(4)	6.6518(3)
$c/\text{\AA}$	7.8881(3)	13.3023(5)	15.9924(7)
$\alpha/^\circ$	90	90	90
$\beta/^\circ$	104.4786(12)	97.3460(10)	107.8940(10)
$\gamma/^\circ$	90	90	90
$V/\text{\AA}^3$	1279.59(9)	1176.16(8)	1056.83(8)
$Z$	4	4	2
$\rho_{\text{calc}}/\text{g cm}^{-3}$	1.729	1.757	1.886
$\mu/\text{mm}^{-1}$	1.228	1.323	1.466
crystal size/mm	$0.21 \times 0.12 \times 0.11$	$0.16 \times 0.14 \times 0.12$	$1.00 \times 0.60 \times 0.50$
$T/\text{K}$	200(2)	173(2)	100(2)
diffractometer	Bruker D8 Quest	Bruker D8 Venture	Bruker D8 Venture
radiation	MoK $\alpha$	MoK $\alpha$	MoK $\alpha$
anode	micro focus source	rotating anode	rotating anode
rated input/kW	50	2.5	2.5
$\theta$ -range/ $^\circ$	3.103–27.51	3.072–27.18	3.342–27.22
reflexes for metric	124	9963	9892
absorption correction	multi-scan	multi-scan	multi-scan
transmission factors	0.7075–0.7456	0.7196–0.7455	0.7068–0.7455
reflexes measured	24577	46895	46041
independent reflexes	2798	2599	2335
$R_{\text{int}}$	0.0255	0.0245	0.0244
mean $\sigma(I)/I$	0.0158	0.0083	0.0126
reflexes with $I \geq 2\sigma(I)$	2616	2482	2294
$x, y$ (weighting scheme)	0.0380, 1.3154	0.0245, 0.6195	0.0218, 1.9467
hydrogen refinement	<sup>a</sup>	<sup>a</sup>	<sup>a</sup>
Flack parameter	—	—	—
parameters	199	194	189
restraints	12	15	12
$R(F_{\text{obs}})$	0.0332	0.0189	0.0300
$R_w(F^2)$	0.0852	0.0508	0.0783
$S$	1.173	1.076	1.275
shift/error <sub>max</sub>	0.001	0.001	0.001
max. electron density/ $\text{e \AA}^{-3}$	1.013	0.391	0.452
min. electron density/ $\text{e \AA}^{-3}$	−0.324	−0.236	−0.486
measurement code	qq082	sv215	tv030

<sup>a</sup> Coordinates of hydrogen atoms bonded to aqua ligands were refined freely, all other hydrogen atoms were calculated in idealized positions, riding on their parent atoms.  $U_{\text{iso}}$  was always coupled to the parent atom.

**Table 6.5:** Crystallographic data of  $[\text{Fe}_3(\text{cpida})_2(\text{OH}_2)_8] \cdot 2 \text{H}_2\text{O}$  (**4k**),  $\{\text{PPN}\}[\text{FeCl}_3(\text{NO})]$  (**5a**) and  $\{\text{PPN}\}[\text{FeBr}_3(\text{NO})]$  (**5b**).

	<b>4k</b>	<b>5a</b>	<b>5b</b>
empirical formula	$\text{C}_{24}\text{H}_{40}\text{Fe}_3\text{N}_2\text{O}_{24}$	$\text{C}_{36}\text{H}_{30}\text{Cl}_3\text{FeN}_2\text{OP}_2$	$\text{C}_{36}\text{H}_{30}\text{Br}_3\text{FeN}_2\text{OP}_2$
$M_r/\text{g mol}^{-1}$	908.13	730.76	864.14
color	brown	green	brown
habitus	platelet	needle	platelet
crystal system	triclinic	monoclinic	monoclinic
space group	$P\bar{1}$	$C2/c$	$C2/c$
$a/\text{\AA}$	7.6891(4)	34.4349(10)	34.6432(13)
$b/\text{\AA}$	9.6802(5)	8.9952(3)	8.9595(3)
$c/\text{\AA}$	12.4555(6)	22.4458(7)	22.9056(9)
$\alpha/^\circ$	84.905(3)	90	90
$\beta/^\circ$	75.007(3)	95.6917(10)	94.8470(12)
$\gamma/^\circ$	76.529(2)	90	90
$V/\text{\AA}^3$	870.49(8)	6918.3(4)	7084.1(5)
$Z$	1	8	8
$\rho_{\text{calc}}/\text{g cm}^{-3}$	1.732	1.403	1.620
$\mu/\text{mm}^{-1}$	1.331	0.792	3.932
crystal size/mm	$0.10 \times 0.08 \times 0.04$	$0.20 \times 0.01 \times 0.01$	$0.08 \times 0.05 \times 0.02$
$T/\text{K}$	100(2)	173(2)	173(2)
diffractometer	Bruker D8 Venture	Bruker D8 Venture	Bruker D8 Venture
radiation	MoK $\alpha$	MoK $\alpha$	MoK $\alpha$
anode	rotating anode	rotating anode	rotating anode
rated input/kW	2.5	2.5	2.5
$\theta$ -range/ $^\circ$	3.151–26.39	2.341–26.45	2.495–30.60
reflexes for metric	9923	9869	9916
absorption correction	multi-scan	multi-scan	multi-scan
transmission factors	0.6830–0.7454	0.7231–0.7454	0.6454–0.7461
reflexes measured	40733	135034	133354
independent reflexes	3563	7093	10857
$R_{\text{int}}$	0.0271	0.0801	0.0389
mean $\sigma(I)/I$	0.0186	0.0258	0.0199
reflexes with $I \geq 2\sigma(I)$	3208	5713	9425
$x, y$ (weighting scheme)	0.0238, 0.8316	0.0344, 8.9307	0.0290, 51.3833
hydrogen refinement	<sup>a</sup>	<sup>a</sup>	<sup>a</sup>
Flack parameter	—	—	—
parameters	272	406	406
restraints	15	0	0
$R(F_{\text{obs}})$	0.0235	0.0333	0.0400
$R_w(F^2)$	0.0593	0.0777	0.1060
$S$	1.048	1.031	1.147
shift/error <sub>max</sub>	0.001	0.001	0.001
max. electron density/ $e \text{\AA}^{-3}$	0.434	0.481	0.902
min. electron density/ $e \text{\AA}^{-3}$	−0.230	−0.476	−1.036
measurement code	tv066	sv198	tv137

<sup>a</sup> Coordinates of hydrogen atoms bonded to aqua ligands were refined freely, all other hydrogen atoms were calculated in idealized positions, riding on their parent atoms.  $U_{\text{iso}}$  was always coupled to the parent atom.

**Table 6.6:** Crystallographic data of  $\{\{\text{PPN}\}[\text{FeI}_2(\text{NO})_2]\}\{\{\text{PPN}\}[\text{I}_3]\}$  (**5c**) and  $\{\{\text{PPN}\}[\text{FeCl}_2(\text{NO})_2]\}$  (**5e**).

	<b>5c</b>	<b>5e</b>
empirical formula	$\text{C}_{72}\text{H}_{60}\text{FeI}_5\text{N}_4\text{O}_2\text{P}_4$	$\text{C}_{36}\text{H}_{30}\text{Cl}_2\text{FeN}_3\text{O}_2\text{P}_2$
$M_r/\text{g mol}^{-1}$	1827.47	725.32
color	red	orange
habitus	needle	platelet
crystal system	orthorhombic	triclinic
space group	<i>Ibca</i>	$P\bar{1}$
$a/\text{\AA}$	16.6144(9)	9.8240(2)
$b/\text{\AA}$	29.2101(15)	11.4411(2)
$c/\text{\AA}$	29.5421(16)	16.1360(4)
$\alpha/^\circ$	90	73.1010(10)
$\beta/^\circ$	90	79.405(2)
$\gamma/^\circ$	90	87.749(2)
$V/\text{\AA}^3$	14337.0(13)	1705.55(6)
$Z$	8	2
$\rho_{\text{calc}}/\text{g cm}^{-3}$	1.693	1.412
$\mu/\text{mm}^{-1}$	2.499	0.730
crystal size/mm	$0.60 \times 0.10 \times 0.10$	$0.15 \times 0.08 \times 0.03$
$T/\text{K}$	173(2)	200(2)
diffractometer	Bruker D8 Venture	KappaCCD
radiation	MoK $\alpha$	MoK $\alpha$
anode	rotating anode	rotating anode
rated input/kW	2.5	3.025
$\theta$ -range/ $^\circ$	2.452–23.33	3.211–27.788
reflexes for metric	9928	7714
absorption correction	multi-scan	—
transmission factors	0.6581–0.7453	—
reflexes measured	69371	14994
independent reflexes	5178	7952
$R_{\text{int}}$	0.0740	0.0379
mean $\sigma(I)/I$	0.0292	0.0556
reflexes with $I \geq 2\sigma(I)$	4165	5642
$x, y$ (weighting scheme)	0.2000, —	0.0415, 0.4315
hydrogen refinement	<sup>a</sup>	<sup>a</sup>
Flack parameter	—	—
parameters	399	415
restraints	0	0
$R(F_{\text{obs}})$	0.1721 <sup>b</sup>	0.0419
$R_w(F^2)$	0.5277 <sup>b</sup>	0.1033
$S$	2.516 <sup>b</sup>	1.060
shift/error <sub>max</sub>	0.263 <sup>b</sup>	0.001
max. electron density/ $\text{e \AA}^{-3}$	5.629 <sup>b</sup>	0.291
min. electron density/ $\text{e \AA}^{-3}$	−6.843 <sup>b</sup>	−0.321
measurement code	sv238	qn151

<sup>a</sup> Coordinates of hydrogen atoms were calculated in idealized positions, riding on their parent atoms.  $U_{\text{iso}}$  was coupled to the parent atom. <sup>b</sup> The structure refinement was repeated with crystals of better quality by *In-Iam* (measurement code tv029).



## 7 Bibliography

- [1] D. E. Koshland, Jr., *Science* **1992**, *258*, 1861, DOI: 10.1126/science.1470903.
- [2] E. Culotta, D. E. Koshland, Jr., *Science* **1992**, *258*, 1862–1865, DOI: 10.1126/science.1361684.
- [3] P. Brimblecombe, D. H. Stedman, *Nature* **1982**, *298*, 460–462, DOI: 10.1038/298460a0.
- [4] H. Ohshima, H. Bartsch, *Mutat. Res. Fundam. Mol. Mech. Mutagen.* **1994**, *305*, 253–264, DOI: 10.1016/0027-5107(94)90245-3.
- [5] D. A. Wink, Y. Vodovotz, J. Laval, F. Laval, M. W. Dewhirst, J. B. Mitchell, *Carcinogenesis* **1998**, *19*, 711–721, DOI: 10.1093/carcin/19.5.711.
- [6] H. Johnston, *Science* **1971**, *173*, 517–522, DOI: 10.1126/science.173.3996.517.
- [7] P. J. Crutzen, *Q. J. R. Meteorolog. Soc.* **1970**, *96*, 320–325, DOI: 10.1002/qj.49709640815.
- [8] A. R. Ravishankara, J. S. Daniel, R. W. Portmann, *Science* **2009**, *326*, 123–125, DOI: 10.1126/science.1176985.
- [9] J. F. Kerwin, Jr., J. R. Lancaster, Jr., P. L. Feldman, *J. Med. Chem.* **1995**, *38*, 4343–4362, DOI: 10.1021/jm00022a001.
- [10] J. Loscalzo, G. Welch, *Prog. Cardiovasc. Dis.* **1995**, *38*, 87–104, DOI: 10.1016/s0033-0620(05)80001-5.
- [11] C. Bogdan, *Nat. Immunol.* **2001**, *2*, 907–916, DOI: 10.1038/ni1001-907.
- [12] A. F. Holleman, E. Wiberg, N. Wiberg, *Lehrbuch der Anorganischen Chemie*, 102nd ed., Walter de Gruyter, Berlin · New York, **2007**, pp. 707–712, DOI: 10.1515/9783110177701.b.651.
- [13] F. J. Lovas, E. Tiemann, *J. Phys. Chem. Ref. Data* **1974**, *3*, 609–769, DOI: 10.1063/1.3253146.
- [14] J. A. McCleverty, *Chem. Rev.* **2004**, *104*, 403–418, DOI: 10.1021/cr020623q.
- [15] F. Roncaroli, M. Videla, L. D. Slep, J. A. Olabe, *Coord. Chem. Rev.* **2007**, *251*, 1903–1930, DOI: 10.1016/j.ccr.2007.04.012.

- [16] J. Enemark, R. Feltham, *Coord. Chem. Rev.* **1974**, *13*, 339–406, DOI: 10.1016/s0010-8545(00)80259-3.
- [17] C. E. Cooper, *Biochim. Biophys. Acta Bioenerg.* **1999**, *1411*, 290–309, DOI: 10.1016/s0005-2728(99)00021-3.
- [18] A. R. Butler, I. L. Megson, *Chem. Rev.* **2002**, *102*, 1155–1166, DOI: 10.1021/cr000076d.
- [19] A. F. Vanin, *Nitric Oxide* **2009**, *21*, 1–13, DOI: 10.1016/j.niox.2009.03.005.
- [20] D. J. Stuehr, *Annu. Rev. Pharmacol. Toxicol.* **1997**, *37*, 339–359, DOI: 10.1146/annurev.pharmtox.37.1.339.
- [21] T. L. Poulos, H. Li, C. Raman, *Curr. Opin. Chem. Biol.* **1999**, *3*, 131–137, DOI: 10.1016/s1367-5931(99)80024-6.
- [22] H. Li, T. L. Poulos, *J. Inorg. Biochem.* **2005**, *99*, 293–305, DOI: 10.1016/j.jinorgbio.2004.10.016.
- [23] I. M. Wasser, S. de Vries, P. Moënne-Loccoz, I. Schröder, K. D. Karlin, *Chem. Rev.* **2002**, *102*, 1201–1234, DOI: 10.1021/cr0006627.
- [24] S. R. Poock, E. R. Leach, J. W. B. Moir, J. A. Cole, D. J. Richardson, *J. Biol. Chem.* **2002**, *277*, 23664–23669, DOI: 10.1074/jbc.m200731200.
- [25] R. Silaghi-Dumitrescu, E. D. Coulter, A. Das, L. G. Ljungdahl, G. N. L. Jameson, B. H. Huynh, D. M. Kurtz, Jr., *Biochemistry* **2003**, *42*, 2806–2815, DOI: 10.1021/bi027253k.
- [26] H. Corker, R. K. Poole, *J. Biol. Chem.* **2003**, *278*, 31584–31592, DOI: 10.1074/jbc.m303282200.
- [27] R. Silaghi-Dumitrescu, D. M. Kurtz, Jr., L. G. Ljungdahl, W. N. Lanzilotta, *Biochemistry* **2005**, *44*, PMID: 15850383, 6492–6501, DOI: 10.1021/bi0473049.
- [28] T. Hayashi, J. D. Caranto, H. Matsumura, D. M. Kurtz, Jr., P. Moënne-Loccoz, *J. Am. Chem. Soc.* **2012**, *134*, 6878–6884, DOI: 10.1021/ja301812p.
- [29] J. Ribeiro, J. Hazzard, R. Nussenzveig, D. Champagne, F. Walker, *Science* **1993**, *260*, 539–541, DOI: 10.1126/science.8386393.
- [30] E. M. Maes, S. A. Roberts, A. Weichsel, W. R. Montfort, *Biochemistry* **2005**, *44*, 12690–12699, DOI: 10.1021/bi0506573.
- [31] S. Moncada, R. M. Palmer, E. A. Higgs, *Pharmacol. Rev.* **1991**, *43*, 109–142.
- [32] D. S. Bredt, S. H. Snyder, *Annu. Rev. Biochem.* **1994**, *63*, 175–195, DOI: 10.1146/annurev.bi.63.070194.001135.
- [33] A. M. Orville, V. J. Chen, A. Kriauciunas, M. R. Harpel, B. G. Fox, E. Munck, J. D. Lipscomb, *Biochemistry* **1992**, *31*, 4602–4612, DOI: 10.1021/bi00134a010.

- 
- [34] C. A. Brown, M. A. Pavlosky, T. E. Westre, Y. Zhang, B. Hedman, K. O. Hodgson, E. I. Solomon, *J. Am. Chem. Soc.* **1995**, *117*, 715–732, DOI: 10.1021/ja00107a015.
- [35] T. W. Hayton, W. S. McNeil, B. O. Patrick, P. Legzdins, *J. Am. Chem. Soc.* **2003**, *125*, 12935–12944, DOI: 10.1021/ja036887r.
- [36] W. Beck, T. M. Klapötke, P. Mayer, *Z. Anorg. Allg. Chem.* **2006**, *632*, 417–420, DOI: 10.1002/zaac.200500415.
- [37] C.-H. Hsieh, M. Y. Darensbourg, *J. Am. Chem. Soc.* **2010**, *132*, 14118–14125, DOI: 10.1021/ja104135x.
- [38] Z.-S. Lin, T.-W. Chiou, K.-Y. Liu, C.-C. Hsieh, J.-S. K. Yu, W.-F. Liaw, *Inorg. Chem.* **2012**, *51*, 10092–10094, DOI: 10.1021/ic3018437.
- [39] T. W. Hayton, P. Legzdins, W. B. Sharp, *Chem. Rev.* **2002**, *102*, 935–992, DOI: 10.1021/cr000074t.
- [40] Å. Wennmalm, B. Lanne, A.-S. Petersson, *Anal. Biochem.* **1990**, *187*, 359–363, DOI: 10.1016/0003-2697(90)90470-t.
- [41] K. M. Skodje, M.-Y. Kwon, S. W. Chung, E. Kim, *Chem. Sci.* **2014**, *5*, 2374–2378, DOI: 10.1039/c3sc53319k.
- [42] E. Victor, S. Kim, S. J. Lippard, *Inorg. Chem.* **2014**, *53*, 12809–12821, DOI: 10.1021/ic501765g.
- [43] A. Wanat, T. Schnepf, G. Stochel, R. Van Eldik, E. Bill, K. Wieghardt, *Inorg. Chem.* **2002**, *41*, 4–10, DOI: 10.1021/ic010628q.
- [44] H. Zöllner, T. Woike, W. Krasser, S. Haussühl, *Z. Kristallogr.* **1989**, *188*, 139–154, DOI: 10.1524/zkri.1989.188.14.139.
- [45] H. Zöllner, W. Krasser, T. Woike, S. Haussühl, *Chem. Phys. Lett.* **1989**, *161*, 497–501, DOI: 10.1016/0009-2614(89)87027-7.
- [46] D. V. Fomitchev, I. Novozhilova, P. Coppens, *Tetrahedron* **2000**, *56*, 6813–6820, DOI: 10.1016/S0040-4020(00)00503-2.
- [47] P. Coppens, I. Novozhilova, A. Kovalevsky, *Chem. Rev.* **2002**, *102*, 861–884, DOI: 10.1021/cr000031c.
- [48] U. Hauser, V. Oestreich, H. D. Rohrweck, *Z. Phys. A: At. Nucl.* **1977**, *280*, 17–25, DOI: 10.1007/bf01438104.
- [49] P. Coppens, D. V. Fomitchev, M. D. Carducci, K. Culp, *J. Chem. Soc. Dalton Trans.* **1998**, 865–872, DOI: 10.1039/a708604k.
- [50] P. Gütllich, Y. Garcia, T. Woike, *Coord. Chem. Rev.* **2001**, *219-221*, 839–879, DOI: 10.1016/S0010-8545(01)00381-2.
-

- [51] C. L. Conrado, J. L. Bourassa, C. Egler, S. Weckslar, P. C. Ford, *Inorg. Chem.* **2003**, *42*, 2288–2293, DOI: 10.1021/ic020309e.
- [52] T. E. Bitterwolf, *Inorg. Chem. Commun.* **2004**, *7*, 956–959, DOI: 10.1016/j.inoche.2004.06.009.
- [53] J. Lee, A. Y. Kovalevsky, I. V. Novozhilova, K. a. Bagley, P. Coppens, G. B. Richter-Addo, *J. Am. Chem. Soc.* **2004**, *126*, 7180–7181, DOI: 10.1021/ja0488986.
- [54] T. E. Bitterwolf, *Coord. Chem. Rev.* **2006**, *250*, 1196–1207, DOI: 10.1016/j.ccr.2005.12.016.
- [55] T. E. Bitterwolf, *Coord. Chem. Rev.* **2006**, *250*, 388–413, DOI: 10.1016/j.ccr.2005.10.019.
- [56] A. Zangl, P. Klüfers, D. Schaniel, T. Woike, *Inorg. Chem. Commun.* **2009**, *12*, 1064–1066, DOI: 10.1016/j.inoche.2009.08.021.
- [57] A. Zangl, P. Klüfers, D. Schaniel, T. Woike, *Dalton Trans.* **2009**, *2009*, 1034–1045, DOI: 10.1039/b812246f.
- [58] M. S. Lynch, M. Cheng, B. E. Van Kuiken, M. Khalil, *J. Am. Chem. Soc.* **2011**, *133*, 5255–5262, DOI: 10.1021/ja110881n.
- [59] N. Casaretto, S. Pillet, E.-E. Bendeif, D. Schaniel, A. K. E. Gallien, P. Klüfers, T. Woike, *Acta Crystallogr. Sect. B: Struct. Sci* **2015**, *71*, 788–797, DOI: 10.1107/s2052520615018132.
- [60] N. Casaretto, S. Pillet, E.-E. Bendeif, D. Schaniel, A. K. E. Gallien, P. Klüfers, T. Woike, *IUCrJ* **2015**, *2*, 35–44, DOI: 10.1107/s2052252514023598.
- [61] K. Pohl, K. Wieghardt, B. Nuber, J. Weiss, *J. Chem. Soc. Dalton Trans.* **1987**, 187–192, DOI: 10.1039/dt9870000187.
- [62] C. R. Randall, Y. Zang, A. E. True, L. Que, Jr., J. M. Charnock, C. D. Garner, Y. Fujishima, C. J. Schofield, J. E. Baldwin, *Biochemistry* **1993**, *32*, 6664–6673, DOI: 10.1021/bi00077a020.
- [63] Y.-M. Chiou, L. Que, Jr., *Inorg. Chem.* **1995**, *34*, 3270–3278, DOI: 10.1021/ic00116a020.
- [64] A. L. Feig, M. T. Bautista, S. J. Lippard, *Inorg. Chem.* **1996**, *35*, 6892–6898, DOI: 10.1021/ic960552b.
- [65] C. Hauser, T. Glaser, E. Bill, T. Weyhermüller, K. Wieghardt, *J. Am. Chem. Soc.* **2000**, *122*, 4352–4365, DOI: 10.1021/ja994161i.
- [66] M. Li, D. Bonnet, E. Bill, F. Neese, T. Weyhermüller, Thomas, N. Blum, D. Sellmann, K. Wieghardt, *Inorg. Chem.* **2002**, *41*, 3444–3456, DOI: 10.1021/ic011243a.

- 
- [67] B. Weber, H. Görls, M. Rudolph, E.-G. Jäger, *Inorg. Chim. Acta* **2002**, *337*, 247–265, DOI: 10.1016/S0020-1693(02)01114-3.
- [68] D. P. Klein, V. G. Young, Jr., W. B. Tolman, L. Que, Jr., *Inorg. Chem.* **2006**, *45*, 8006–8008, DOI: 10.1021/ic0610740.
- [69] F.-T. Tsai, P.-L. Chen, W.-F. Liaw, *J. Am. Chem. Soc.* **2010**, *132*, 5290–5299, DOI: 10.1021/ja100849r.
- [70] T. C. Berto, M. B. Hoffman, Y. Murata, K. B. Landenberger, E. E. Alp, J. Zhao, N. Lehnert, *J. Am. Chem. Soc.* **2011**, *133*, 16714–16717, DOI: 10.1021/ja111693f.
- [71] G. Villar-Acevedo, E. Nam, S. Fitch, J. Benedict, J. Freudenthal, W. Kaminsky, J. a. Kovacs, *J. Am. Chem. Soc.* **2011**, *133*, 1419–1427, DOI: 10.1021/ja107551u.
- [72] H. Park, M. M. Bittner, J. S. Baus, S. V. Lindeman, A. T. Fiedler, *Inorg. Chem.* **2012**, *51*, 10279–10289, DOI: 10.1021/ic3012712.
- [73] A. Majumdar, S. J. Lippard, *Inorg. Chem.* **2013**, *52*, 13292–13294, DOI: 10.1021/ic4019508.
- [74] F.-T. Tsai, Y.-C. Lee, M.-H. Chiang, W.-F. Liaw, *Inorg. Chem.* **2013**, *52*, 464–473, DOI: 10.1021/ic3023437.
- [75] C.-C. Tsou, F.-T. Tsai, H.-Y. Chen, I.-J. Hsu, W.-F. Liaw, *Inorg. Chem.* **2013**, *52*, 1631–1639, DOI: 10.1021/ic302537d.
- [76] S. Zheng, T. C. Berto, E. W. Dahl, M. B. Hoffman, A. L. Speelman, N. Lehnert, *J. Am. Chem. Soc.* **2013**, *135*, 4902–4905, DOI: 10.1021/ja309782m.
- [77] J. Li, A. Banerjee, P. L. Pawlak, W. W. Brennessel, F. A. Chavez, *Inorg. Chem.* **2014**, *53*, 5414–5416, DOI: 10.1021/ic500558j.
- [78] E. Victor, M. A. Minier, S. J. Lippard, *Eur. J. Inorg. Chem.* **2014**, *2014*, 5640–5645, DOI: 10.1002/ejic.201402543.
- [79] T. Schnepf, S. Finkler, A. Czap, R. van Eldik, M. Heus, P. Nieuwenhuizen, C. Wreesmann, W. Abma, *Eur. J. Inorg. Chem.* **2001**, *2001*, 491–501, DOI: 10.1002/1099-0682(200102)2001:2<491::AID-EJIC491>3.0.CO;2-2.
- [80] T. Schnepf, A. Wanat, G. Stochel, S. Goldstein, D. Meyerstein, R. van Eldik, *Eur. J. Inorg. Chem.* **2001**, *2001*, 2317–2325, DOI: 10.1002/1099-0682(200109)2001:9<2317::AID-EJIC2317>3.0.CO;2-F.
- [81] T. Schnepf, A. Wanat, G. Stochel, R. Van Eldik, *Inorg. Chem.* **2002**, *41*, 2565–2573, DOI: 10.1021/ic011220w.
- [82] M. Steimann, U. Nagel, R. Grenz, W. Beck, *J. Organomet. Chem.* **1983**, *247*, 171–174, DOI: 10.1016/S0022-328X(00)98752-7.
-

- [83] I. R. Gould, J. R. Lenhard, S. Farid, *J. Phys. Chem. A* **2004**, *108*, 10949–10956, DOI: 10.1021/jp040536x.
- [84] N. Smrečki, B.-M. Kukovec, M. Đaković, Z. Popović, *Inorg. Chim. Acta* **2013**, *400*, 122–129, DOI: 10.1016/j.ica.2013.02.017.
- [85] A. J. Miralles, C. M. Silvernail, US 2009/0264677 A1, **2009**.
- [86] P. Laine, A. Gourdon, J.-P. Launay, *Inorg. Chem.* **1995**, *34*, 5129–5137, DOI: 10.1021/ic00125a009.
- [87] C.-B. Liu, H.-L. Wen, Y.-N. Gong, X.-M. Liu, S.-S. Tan, *Z. Anorg. Allg. Chem.* **2011**, *637*, 122–129, DOI: 10.1002/zaac.201000228.
- [88] V. Kohlschütter, M. Kutscheroff, *Ber. Dtsch. Chem. Ges.* **1904**, *37*, 3044–3052, DOI: 10.1002/cber.19040370389.
- [89] W. Manchot, K. Zechentmayer, *Justus Liebigs Ann. Chem.* **1906**, *350*, 368–389, DOI: 10.1002/jlac.19063500307.
- [90] W. Manchot, F. Huttner, *Justus Liebigs Ann. Chem.* **1910**, *372*, 153–178, DOI: 10.1002/jlac.19103720202.
- [91] V. Kohlschütter, P. Sazanoff, *Ber. Dtsch. Chem. Ges.* **1911**, *44*, 1423–1432, DOI: 10.1002/cber.19110440233.
- [92] W. Manchot, *Ber. Dtsch. Chem. Ges.* **1914**, *47*, 1601–1614, DOI: 10.1002/cber.19140470244.
- [93] I. Bellucci, *Gazz. Chim. Ital.* **1914**, *44*, 384–389.
- [94] W. E. Silverthorn, R. D. Feltham, *Inorg. Chem.* **1967**, *6*, 1662–1666, DOI: 10.1021/ic50055a011.
- [95] L. Burlamacchi, G. Martini, E. Tiezzi, *Inorg. Chem.* **1969**, *8*, 2021–2025, DOI: 10.1021/ic50079a047.
- [96] D. Gwost, K. G. Caulton, *Inorg. Chem.* **1973**, *12*, 2095–2099, DOI: 10.1021/ic50127a030.
- [97] N. G. Connelly, C. Gardner, *J. Chem. Soc. Dalton Trans.* **1976**, *1976*, 1525–1527, DOI: 10.1039/dt9760001525.
- [98] D. Ballivet-Tkatchenko, M. Riveccie, N. El Murr, *J. Am. Chem. Soc.* **1979**, *101*, 2763–2765, DOI: 10.1021/ja00504a062.
- [99] W. Beck, R. Grenz, F. Götzfried, E. Vilsmaier, *Chem. Ber.* **1981**, *114*, 3184–3187, DOI: 10.1002/cber.19811140926.
- [100] A. R. Butler, C. Glidewell, A. R. Hyde, J. C. Walton, *Polyhedron* **1985**, *4*, 303–306, DOI: 10.1016/S0277-5387(00)84503-9.

- 
- [101] S. Brownstein, B. Irish, *Polyhedron* **1988**, *7*, 97–101, DOI: 10.1016/S0277-5387(00)80454-4.
- [102] C. Glidewell, I. L. Johnson, *Polyhedron* **1988**, *7*, 1371–1375, DOI: 10.1016/S0277-5387(00)80387-3.
- [103] H. L. K. Wah, M. Postel, F. Tomi, L. Mordenti, *New J. Chem.* **1991**, *15*, 629–633.
- [104] T. R. Bryar, D. R. Eaton, *Can. J. Chem.* **1992**, *70*, 1917–1926, DOI: 10.1139/v92-240.
- [105] F. Bohr, H. Chermette, M. F. Ruiz-López, *Int. J. Quantum Chem.* **1994**, *52*, 1039–1049, DOI: 10.1002/qua.560520429.
- [106] C. T. Tran, E. Kim, *Inorg. Chem.* **2012**, *51*, 10086–10088, DOI: 10.1021/ic301676f.
- [107] H. Akutsu, J.-i. Yamada, S. Nakatsuji, S. S. Turner, *X-Ray Struct. Anal. Online* **2014**, *30*, 49–50, DOI: 10.2116/xraystruct.30.49.
- [108] K.-Y. Liu, J.-S. K. Yu, *Inorg. Chem.* **2014**, *53*, 10785–10787, DOI: 10.1021/ic501116t.
- [109] C. Wilfer, MA thesis, Ludwig-Maximilians-Universität München, **2011**.
- [110] H.-C. Böttcher, *Private Communication*, Ludwig-Maximilians-Universität München, **2014**.
- [111] A. In-Iam, *Private Communication*, Ludwig-Maximilians-Universität München, **2015**.
- [112] M.-L. Tsai, C.-H. Hsieh, W.-F. Liaw, *Inorg. Chem.* **2007**, *46*, 5110–5117, DOI: 10.1021/ic0702567.
- [113] D. Ballivet-Tkatchenko, C. Billard, A. Revillon, *J. Polym. Sci. Polym. Chem. Ed.* **1981**, *19*, 1697–1706, DOI: 10.1002/pol.1981.170190710.
- [114] M. Holzwarth, A. Dieskau, M. Tabassam, B. Plietker, *Angew. Chem. Int. Ed.* **2009**, *48*, 7251–7255, DOI: 10.1002/anie.200901930.
- [115] M.-C. Tsai, F.-T. Tsai, T.-T. Lu, M.-L. Tsai, Y.-C. Wei, I.-J. Hsu, J.-F. Lee, W.-F. Liaw, *Inorg. Chem.* **2009**, *48*, 9579–9591, DOI: 10.1021/ic901675p.
- [116] A. D. Becke, *Phys. Rev. A: At. Mol. Opt. Phys.* **1988**, *38*, 3098–3100, DOI: 10.1103/physreva.38.3098.
- [117] J. P. Perdew, *Phys. Rev. B: Condens. Matter Mater. Phys.* **1986**, *33*, 8822–8824, DOI: 10.1103/physrevb.33.8822.
- [118] F. Weigend, R. Ahlrichs, *Phys. Chem. Chem. Phys.* **2005**, *7*, 3297–3305, DOI: 10.1039/b508541a.
- [119] A. Klamt, G. Schüürmann, *J. Chem. Soc. Perkin Trans. 2* **1993**, 799–805, DOI: 10.1039/p29930000799.
-

- [120] S. Sinnecker, A. Rajendran, A. Klamt, M. Diedenhofen, F. Neese, *J. Phys. Chem. A* **2006**, *110*, 2235–2245, DOI: 10.1021/jp056016z.
- [121] A. Klamt, M. Diedenhofen, *J. Phys. Chem. A* **2015**, *119*, 5439–5445, DOI: 10.1021/jp511158y.
- [122] J. P. Perdew, Y. Wang, *Phys. Rev. B: Condens. Matter Mater. Phys.* **1992**, *45*, 13244–13249, DOI: 10.1103/physrevb.45.13244.
- [123] J. Tao, J. P. Perdew, V. N. Staroverov, G. E. Scuseria, *Phys. Rev. Lett.* **2003**, *91*, 1464011–1464014, DOI: 10.1103/physrevlett.91.146401.
- [124] C. Lee, W. Yang, R. G. Parr, *Phys. Rev. B: Condens. Matter Mater. Phys.* **1988**, *37*, 785–789, DOI: 10.1103/physrevb.37.785.
- [125] A. D. Becke, *J. Chem. Phys.* **1993**, *98*, 5648–5652, DOI: 10.1063/1.464913.
- [126] V. N. Staroverov, G. E. Scuseria, J. Tao, J. P. Perdew, *J. Chem. Phys.* **2003**, *119*, 12129–12137, DOI: 10.1063/1.1626543.
- [127] S. Grimme, *J. Comput. Chem.* **2006**, *27*, 1787–1799, DOI: 10.1002/jcc.20495.
- [128] S. Grimme, J. Antony, S. Ehrlich, H. Krieg, *J. Chem. Phys.* **2010**, *132*, 15410401–15410419, DOI: 10.1063/1.3382344.
- [129] S. Grimme, S. Ehrlich, L. Goerigk, *J. Comput. Chem.* **2011**, *32*, 1456–1465, DOI: 10.1002/jcc.21759.
- [130] G. Schenk, M. Y. M. Pau, E. I. Solomon, *J. Am. Chem. Soc.* **2004**, *126*, 505–515, DOI: 10.1021/ja036715u.
- [131] C. D. Brown, M. L. Neidig, M. B. Neibergall, J. D. Lipscomb, E. I. Solomon, *J. Am. Chem. Soc.* **2007**, *129*, 7427–7438, DOI: 10.1021/ja071364v.
- [132] A. R. Diebold, C. D. Brown-Marshall, M. L. Neidig, J. M. Brownlee, G. R. Moran, E. I. Solomon, *J. Am. Chem. Soc.* **2011**, *133*, 18148–18160, DOI: 10.1021/ja202549q.
- [133] N. Sun, L. V. Liu, A. Dey, G. Villar-Acevedo, J. a. Kovacs, M. Y. Darensbourg, K. O. Hodgson, B. Hedman, E. I. Solomon, *Inorg. Chem.* **2011**, *50*, 427–436, DOI: 10.1021/ic1006378.
- [134] L. Noodleman, *J. Chem. Phys.* **1981**, *74*, 5737–5743, DOI: 10.1063/1.440939.
- [135] L. Noodleman, E. R. Davidson, *Chem. Phys.* **1986**, *109*, 131–143, DOI: 10.1016/0301-0104(86)80192-6.
- [136] T. Soda, Y. Kitagawa, T. Onishi, Y. Takano, Y. Shigeta, H. Nagao, Y. Yoshioka, K. Yamaguchi, *Chem. Phys. Lett.* **2000**, *319*, 223–230, DOI: 10.1016/s0009-2614(00)00166-4.
- [137] R. S. Mulliken, *J. Chem. Phys.* **1955**, *23*, 1833–1840, DOI: 10.1063/1.1740588.

- 
- [138] A. E. Reed, R. B. Weinstock, F. Weinhold, *J. Chem. Phys.* **1985**, *83*, 735–746, DOI: 10.1063/1.449486.
- [139] S. I. Gorelsky, *AOMix 2.8: Program for Molecular Orbital Analysis*, **1997–2013**.
- [140] S. I. Gorelsky, A. B. P. Lever, *J. Organomet. Chem.* **2001**, *635*, 187–196, DOI: 10.1016/s0022-328x(01)01079-8.
- [141] B. O. Roos, V. Veryazov, J. Conradie, P. R. Taylor, A. Ghosh, *J. Phys. Chem. B* **2008**, *112*, 14099–14102, DOI: 10.1021/jp807734x.
- [142] M. Radón, E. Broclawik, K. Pierloot, *J. Phys. Chem. B* **2010**, *114*, 1518–1528, DOI: 10.1021/jp910220r.
- [143] H.-B. Bürgi, M. Förtsch, *J. Mol. Struct.* **1999**, *485-486*, 457–463, DOI: 10.1016/S0022-2860(99)00055-1.
- [144] H. B. Bürgi, *Annu. Rev. Phys. Chem.* **2000**, *51*, 275–296, DOI: 10.1146/annurev.physchem.51.1.275.
- [145] H.-B. Bürgi, S. C. Capelli, *Helv. Chim. Acta* **2003**, *86*, 1625–1640, DOI: 10.1002/hlca.200390138.
- [146] S. Smeets, P. Parois, H.-B. Bürgi, M. Lutz, *Acta Crystallogr. Sect. B: Struct. Sci* **2011**, *67*, 53–62, DOI: 10.1107/S01087681110054571.
- [147] K. A. Abboud, C. Xu, R. S. Drago, *Acta Crystallogr. Sect. C: Cryst. Struct. Commun.* **1998**, *54*, 1270–1273, DOI: 10.1107/s0108270198000183.
- [148] A. Grirrane, A. Pastor, C. Mealli, A. Ienco, P. Rosa, R. Prado-Gotor, A. Galindo, *Inorg. Chim. Acta* **2004**, *357*, 4215–4219, DOI: 10.1016/j.ica.2004.05.033.
- [149] A. K. Powell, J. M. Charnock, A. C. Flood, C. D. Garner, M. J. Ware, W. Clegg, *J. Chem. Soc. Dalton Trans.* **1992**, 203–207, DOI: 10.1039/dt9920000203.
- [150] N. Kuwamura, R. Kato, K. Kitano, M. Hirotsu, T. Nishioka, H. Hashimoto, I. Kinoshita, *Dalton Trans.* **2010**, *39*, 9988–9993, DOI: 10.1039/c0dt00615g.
- [151] J. D. Nobbs, A. K. Tomov, R. Cariou, V. C. Gibson, A. J. P. White, G. J. P. Britovsek, *Dalton Trans.* **2012**, *41*, 5949–5964, DOI: 10.1039/c2dt30324h.
- [152] K. Cheaib, D. Martel, N. Clément, F. Eckes, S. Kouaho, G. Rogez, S. Dagonne, M. Kurmoo, S. Choua, R. Welter, *Dalton Trans.* **2013**, *42*, 1406–1416, DOI: 10.1039/C2DT32310A.
- [153] L. P. Wu, Y. Yamagiwa, I. Ino, K. Sugimoto, T. Kuroda-Sowa, T. Kamikawa, M. Munakata, *Polyhedron* **1999**, *18*, 2047–2053, DOI: 10.1016/s0277-5387(99)00083-2.
- [154] B. M. Krieger, H. Y. Lee, T. J. Emge, J. F. Wishart, E. W. Castner, Jr., *Phys. Chem. Chem. Phys.* **2010**, *12*, 8919–8925, DOI: 10.1039/b920652n.
-

- [155] G. J. Reiss, *Z. Kristallogr. - New Cryst. Struct.* **2013**, *228*, 407–409, DOI: 10.1524/ncrs.2013.0187.
- [156] M. Lutz, Y. Huang, M.-E. Moret, R. J. M. Klein Gebbink, *Acta Crystallogr. Sect. C: Struct. Chem.* **2014**, *70*, 470–476, DOI: 10.1107/s2053229614007955.
- [157] W. R. Scheidt, Y. J. Lee, K. Hatano, *J. Am. Chem. Soc.* **1984**, *106*, 3191–3198, DOI: 10.1021/ja00323a022.
- [158] N. Xu, D. R. Powell, G. B. Richter-Addo, *Angew. Chem. Int. Ed.* **2011**, *50*, 9694–9696, DOI: 10.1002/anie.201103329.
- [159] N. J. Silvernail, J. W. Pavlik, B. C. Noll, C. E. Schulz, W. R. Scheidt, *Inorg. Chem.* **2008**, *47*, 912–920, DOI: 10.1021/ic701700p.
- [160] E. Wenger, S. Dahaoui, P. Alle, P. Parois, C. Palin, C. Lecomte, D. Schaniel, *Acta Crystallogr. Sect. B: Struct. Sci* **2014**, *70*, 783–791, DOI: 10.1107/s2052520614017338.
- [161] M. Di Vaira, C. A. Ghilardi, L. Sacconi, *Inorg. Chem.* **1976**, *15*, 1555–1561, DOI: 10.1021/ic50161a018.
- [162] K. H. Pannell, Y.-S. Chen, K. Belknap, C. C. Wu, I. Bernal, M. W. Creswick, H. N. Huang, *Inorg. Chem.* **1983**, *22*, 418–427, DOI: 10.1021/ic00145a011.
- [163] L. M. Clarkson, W. Clegg, D. C. R. Hockless, N. C. Norman, *Acta Crystallogr. Sect. C: Cryst. Struct. Commun.* **1992**, *48*, 236–239, DOI: 10.1107/s0108270191010405.
- [164] S. L. Stokes, W. M. Davis, A. L. Odom, C. C. Cummins, *Organometallics* **1996**, *15*, 4521–4530, DOI: 10.1021/om960455q.
- [165] T. C. Harrop, D. Song, S. J. Lippard, *J. Am. Chem. Soc.* **2006**, *128*, 3528–3529, DOI: 10.1021/ja060186n.
- [166] T.-T. Lu, S.-J. Chiou, C.-Y. Chen, W.-F. Liaw, *Inorg. Chem.* **2006**, *45*, 8799–8806, DOI: 10.1021/ic061439g.
- [167] Z. J. Tonzetich, F. Héroguel, L. H. Do, S. J. Lippard, *Inorg. Chem.* **2011**, *50*, 1570–1579, DOI: 10.1021/ic102300d.
- [168] H. Kalyvas, D. Coucouvanis, *Polyhedron* **2007**, *26*, 4765–4778, DOI: 10.1016/j.poly.2007.06.015.
- [169] S. Begel, R. Puchta, J. Sutter, F. W. Heinemann, L. Dahlenburg, R. v. Eldik, *Inorg. Chem.* **2015**, *54*, 6763–6775, DOI: 10.1021/acs.inorgchem.5b00595.
- [170] J. Conradie, A. Ghosh, *J. Inorg. Biochem.* **2006**, *100*, 2069–2073, DOI: 10.1016/j.jinorgbio.2006.09.016.
- [171] J. Conradie, D. a. Quarless, H.-F. Hsu, T. C. Harrop, S. J. Lippard, S. a. Koch, A. Ghosh, *J. Am. Chem. Soc.* **2007**, *129*, 10446–10456, DOI: 10.1021/ja0719982.

- 
- [172] J. Conradie, K. H. Hopmann, A. Ghosh, *J. Phys. Chem. B* **2010**, *114*, 8517–8524, DOI: 10.1021/jp101847y.
- [173] J. Conradie, A. Ghosh, *Inorg. Chem.* **2011**, *50*, 4223–4225, DOI: 10.1021/ic102388c.
- [174] W. P. Griffith, J. Lewis, G. Wilkinson, *J. Chem. Soc.* **1958**, 3993–3998, DOI: 10.1039/jr9580003993.
- [175] H. B. Gray, I. Bernal, E. Billig, *J. Am. Chem. Soc.* **1962**, *84*, 3404–3405, DOI: 10.1021/ja00876a037.
- [176] A. Earnshaw, E. A. King, L. F. Larkworthy, *J. Chem. Soc. A* **1969**, 2459–2463, DOI: 10.1039/j19690002459.
- [177] H. Twilfer, F.-H. Bernhardt, K. Gersonde, *Eur. J. Biochem.* **1985**, *147*, 171–176, DOI: 10.1111/j.1432-1033.1985.tb08733.x.
- [178] Y. Zhang, M. A. Pavlosky, C. A. Brown, T. E. Westre, B. Hedman, K. O. Hodgson, E. I. Solomon, *J. Am. Chem. Soc.* **1992**, *114*, 9189–9191, DOI: 10.1021/ja00049a062.
- [179] T. A. Jackson, E. Yikilmaz, A.-F. Miller, T. C. Brunold, *J. Am. Chem. Soc.* **2003**, *125*, 8348–8363, DOI: 10.1021/ja029523s.
- [180] K. H. Hopmann, A. Ghosh, L. Noodleman, *Inorg. Chem.* **2009**, *48*, 9155–9165, DOI: 10.1021/ic9008784.
- [181] S. Ye, J. C. Price, E. W. Barr, M. T. Green, J. M. Bollinger, C. Krebs, F. Neese, *J. Am. Chem. Soc.* **2010**, *132*, 4739–4751, DOI: 10.1021/ja909715g.
- [182] J. C. Salerno, J. N. Siedow, *Biochim. Biophys. Acta Protein Struct.* **1979**, *579*, 246–251, DOI: 10.1016/0005-2795(79)90104-1.
- [183] D. M. Arciero, J. D. Lipscomb, B. H. Huynh, T. A. Kent, M. Eckard, *J. Biol. Chem.* **1983**, *258*, 14981–14991.
- [184] Y. Zhang, E. Oldfield, *J. Phys. Chem. A* **2003**, *107*, 4147–4150, DOI: 10.1021/jp030222u.
- [185] H.-Y. Cheng, S. Chang, P.-Y. Tsai, *J. Phys. Chem. A* **2004**, *108*, 358–361, DOI: 10.1021/jp031136x.
- [186] Y. Zhang, E. Oldfield, *J. Am. Chem. Soc.* **2004**, *126*, 9494–9495, DOI: 10.1021/ja0401242.
- [187] H.-Y. Cheng, S. Chang, *Int. J. Quantum Chem.* **2005**, *105*, 511–517, DOI: 10.1002/qua.20734.
- [188] S. Chakraborty, J. Reed, M. Ross, M. J. Nilges, I. D. Petrik, S. Ghosh, S. Hammes-Schiffer, J. T. Sage, Y. Zhang, C. E. Schulz, Y. Lu, *Angew. Chem. Int. Ed.* **2014**, *53*, 2417–2421, DOI: 10.1002/anie.201308431.
-

- [189] J. H. Rodriguez, Y.-M. Xia, P. G. Debrunner, *J. Am. Chem. Soc.* **1999**, *121*, 7846–7863, DOI: 10.1021/ja990129c.
- [190] E. Broclawik, A. Stepniewski, M. Radoń, *J. Inorg. Biochem.* **2014**, *136*, 147–153, DOI: 10.1016/j.jinorgbio.2014.01.010.
- [191] M.-L. Tsai, C.-C. Chen, I.-J. Hsu, S.-C. Ke, C.-H. Hsieh, K.-A. Chiang, G.-H. Lee, Y. Wang, J.-M. Chen, J.-F. Lee, W.-F. Liaw, *Inorg. Chem.* **2004**, *43*, 5159–5167, DOI: 10.1021/ic0494915.
- [192] R. J. Dai, S. C. Ke, *J. Phys. Chem. B* **2007**, *111*, 2335–2346, DOI: 10.1021/jp066964f.
- [193] S. Ye, F. Neese, *J. Am. Chem. Soc.* **2010**, *132*, 3646–3647, DOI: 10.1021/ja9091616.
- [194] D. Teillet-Billy, F. Fiquet-Fayard, *J. Phys. B: At. Mol. Phys.* **1977**, *10*, L111–L117, DOI: 10.1088/0022-3700/10/4/006.
- [195] M. E. Jacox, W. E. Thompson, *J. Chem. Phys.* **1990**, *93*, 7609–7621, DOI: 10.1063/1.459392.
- [196] Mestrelab Research S.L., *MestReNova 8.1.1-11591*, Santiago de Compostela, ESP, **2013**.
- [197] JASCO Corporation, *Spectra Manager 2.07.00*, **2002–2008**.
- [198] G. Kortüm, *Reflexionsspektroskopie*, Springer, Berlin · New York, **1969**, pp. 725–727, DOI: 10.1515/9783110177701.b.651.
- [199] G. M. Sheldrick, *Acta Crystallogr. Sect. A: Found. Crystallogr.* **2008**, *64*, 112–122, DOI: 10.1107/s0108767307043930.
- [200] G. M. Sheldrick, *Acta Crystallogr. Sect. C: Struct. Chem.* **2015**, *71*, 3–8, DOI: 10.1107/s2053229614024218.
- [201] C. B. Hübschle, G. M. Sheldrick, B. Dittrich, *J. Appl. Cryst.* **2011**, *44*, 1281–1284, DOI: 10.1107/s0021889811043202.
- [202] A. L. Spek, *Acta Crystallogr. Sect. D: Biol. Crystallogr.* **2009**, *65*, 148–155, DOI: 10.1107/s090744490804362x.
- [203] L. J. Farrugia, *J. Appl. Cryst.* **2012**, *45*, 849–854, DOI: 10.1107/s0021889812029111.
- [204] Persistence of Vision Pty. Ltd., *Persistence of Vision Raytracer (Version 3.7)*, Williamstown, VIC, AUS, **1991–2013**.
- [205] G. A. Bain, J. F. Berry, *J. Chem. Educ.* **2008**, *85*, 532–536, DOI: 10.1021/ed085p532.
- [206] S. Hong, H. So, H. Yoon, K.-B. Cho, Y.-M. Lee, S. Fukuzumi, W. Nam, *Dalton Trans.* **2013**, *42*, 7842–7845, DOI: 10.1039/c3dt50750e.

- [207] *TURBOMOLE V6.6 2014*, a development of University of Karlsruhe and Forschungszentrum Karlsruhe GmbH, 1989-2007, TURBOMOLE GmbH, since 2007; available from <http://www.turbomole.com>.
- [208] R. Ahlrichs, M. Bär, M. Häser, H. Horn, C. Kölmel, *Chem. Phys. Lett.* **1989**, *162*, 165–169, DOI: 10.1016/0009-2614(89)85118-8.
- [209] COSMOlogic GmbH & Co. KG, *TmoleX 4.0.1*, Leverkusen, GER, **2014**.
- [210] C. Steffen, K. Thomas, U. Huniar, A. Hellweg, O. Rubner, A. Schroer, *J. Comput. Chem.* **2010**, 2967–2970, DOI: 10.1002/jcc.21576.
- [211] O. Treutler, R. Ahlrichs, *J. Chem. Phys.* **1995**, *102*, 346–354, DOI: 10.1063/1.469408.
- [212] M. Sierka, A. Hogekamp, R. Ahlrichs, *J. Chem. Phys.* **2003**, *118*, 9136–9148, DOI: 10.1063/1.1567253.
- [213] K. Eichkorn, F. Weigend, O. Treutler, R. Ahlrichs, *Theor. Chem. Acc.* **1997**, *97*, 119–124, DOI: 10.1007/s002140050244.
- [214] F. Weigend, *Phys. Chem. Chem. Phys.* **2006**, *8*, 1057–1065, DOI: 10.1039/b515623h.
- [215] R. Bauernschmitt, R. Ahlrichs, *Chem. Phys. Lett.* **1996**, *256*, 454–464, DOI: 10.1016/0009-2614(96)00440-x.
- [216] F. Furche, R. Ahlrichs, *J. Chem. Phys.* **2002**, *117*, 7433–7447, DOI: 10.1063/1.1508368.
- [217] F. Neese, *Wiley Interdiscip. Rev.: Comput. Mol. Sci.* **2012**, *2*, 73–78, DOI: 10.1002/wcms.81.



# Danksagung

Prof. Dr. Peter Klüfers danke ich für die interessante Themenstellung, den großen wissenschaftlichen Freiraum und die hervorragenden Arbeitsbedingungen.

Prof. Dr. Hans-Christian Böttcher danke ich für die Erstellung des Zweitgutachtens für die vorliegende Arbeit, sowie seine zahlreichen Tipps zu den diversen PPN-Salzen.

Für Ihre Mitwirkung in der Promotionskommission danke ich Prof. Dr. Konstantin Karaghiosoff, Prof. Dr. Christian Ochsenfeld, Prof. Dr. Wolfgang Beck und Prof. Dr. Ingo-Peter Lorenz.

Lida Holowatyj-den Toom danke ich für ihre Hilfe bei allen organisatorischen Dingen, das Korrekturlesen der vorliegenden Arbeit und ihre herzliche und hilfsbereite Art.

Helen Funk und Bianca Aas danke ich für das sorgfältige Korrekturlesen dieser Arbeit.

Sandra Albrecht, Anja Belz, Anna Gallien, Leonie Lindner, Peter Mayer, Johanna Schulten und Christine Sturm danke ich für die vielen Stunden im kalten Röntgenraum zum Messen meiner Kristalle. Tobias Mayer danke ich für die geduldige Einführung ins Lösen von Kristallstrukturen.

Xaver Wurzenberger danke ich für die Einführung in die DFT Rechnung und seine stete Hilfsbereitschaft bei sämtlichen Linuxproblemen.

Christine Neumann danke ich für den steten Nachschub an Schlenkgefäßen und anderen Glasgeräten, sowie ihre vielen hilfreichen Tipps zu Arbeitstechniken aller Art. Sandra Albrecht danke ich für zahlreiche Chemikalienbestellungen.

Meinen Bachelor- und F-Praktikanten Claudia Kleinlein, Philipp Leippe, Maria Mertens, Andreas Baumann, Nadine Berger, Jens Oetken und Johannes Maschita danke ich für ihre fleißige und sorgfältige Mitarbeit.

Dem gesamten Arbeitskreis Klüfers und insbesondere dem P-Saal danke ich für die schöne gemeinsame Zeit, die gute Atmosphäre und viele Abende in der Kaffeeküche.

Helen und meiner Familie danke ich für die jahrelange Unterstützung während meines Studiums und meiner Promotion. Vielen Dank für Alles!